A QUANTUM ELECTRODYNAMICAL APPROACH TO NONLINEAR AND STRUCTURED LIGHT INTERACTIONS WITH MATTER

A thesis submitted by:

MATHEW D. WILLIAMS

as part of the requirements for the degree of PhD in the

School of Chemistry

University of East Anglia

NORWICH NR4 7TJ

September 2016

ABSTRACT

This thesis employs molecular quantum electrodynamical theory to analyse the interactions between light and matter for four main processes. The first to be considered is Raman scattering, where the effect of the electrodynamic environment for the centre of spectroscopic interest is considered. This is achieved by engaging a retarded dipole-dipole interaction between the centre and a neighbouring molecule. Physically, this is explained by a virtual photon between the pair of centres. The results predict characteristic new lines on the Raman spectrum, for the species, arising from the engagement of selection rules not limited to those of a two-photon process.

The second process, is hyper-Rayleigh scattering, in which a single multipolar coupling is considered in place of the more familiar electric dipole. This modification to the theory subverts the standard selection rules for a three-photon process, which can allow for second-harmonic emission to be generated by a centre of high symmetry, such as a centrosymmetric molecule.

The third process offers another means of subverting the standard selection rules for second-harmonic generation, namely by incorporating six-wave mixing. First, the general mechanism is developed and pertinent results are expressed for the widely-deployed depolarisation ratio. Following this, structured light is considered and by utilising orbital angular momentum (OAM) conservation arguments, the pair of harmonic photons are found to display quantum entanglement. Moreover, the relative magnitudes of the possible emissions are found to correspond directly to that of the binomial coefficients.

This thesis concludes with a family of novel structures capable of directly generating OAM light. This work exploits symmetry characteristics for a delocalised excitonic structure that can allow for a more complex multipolar emission than that of any isolated centres. The phase of the exciton is shown to display an azimuthal phase progression, a vortex feature most commonly associated with Laguerre-Gaussian light.

PUBLICATIONS

XVIII. M. D. Williams, D. S. Bradshaw, and D. L. Andrews, "Symmetry analysis of Raman scattering mediated by neighboring molecules," J. Chem. Phys. **145**, 184301 (2016).

XVII. M. D. Williams, D. S. Bradshaw, and D. L. Andrews, "Raman scattering mediated by neighboring molecules," J. Chem. Phys. **144**, 174304 (2016).

XVI. M. D. Williams, D. S. Bradshaw, and D. L. Andrews, "On the emergence of Raman signals characterizing multicenter nanoscale interactions," Proc. SPIE **9884**, 98840N (2016).

XV. K.A. Forbes, M. D. Williams and D. L. Andrews, "Quantum theory for the nanoscale propagation of light through stacked thin film layers," Proc. SPIE **9884**, 988434 (2016).

XIV. M. D. Williams, D. S. Bradshaw, and D. L. Andrews, "Quantum issues with structured light," Proc. SPIE **9764**, 976407 (2016).

XIII. J. M. Leeder, D. S. Bradshaw, M. D. Williams, and D. L. Andrews, "Developments in the Photonic Theory of Fluorescence," in Reviews in Fluorescence 2015, C. D. Geddes, ed. (Springer International Publishing, 2016), pp. 235.

XII. M. D. Williams, J. S. Ford, and D. L. Andrews, "Hyper-Rayleigh scattering in centrosymmetric systems," J. Chem. Phys. **143**, 124301 (2015).

XI. R. Liu, D. B. Phillips, F. Li, M. D. Williams, D. L. Andrews, and M. J. Padgett, "Discrete emitters as a source of orbital angular momentum," J. Opt. **17**, 045608 (2015). [*Collaboration & IOP Select*]

X. M. D. Williams, J. S. Ford, and D. L. Andrews, "Mechanisms universally permitting hyper-Rayleigh scattering," Proc. SPIE **9347**, 934711 (2015).

IX. D. L. Andrews, M. D. Williams, D. S. Bradshaw, R. Lui, D. B. Phillips, S. Franke-Arnold, and M. J. Padgett, "Nanoarrays for the generation of complex optical wave-forms," Proc. SPIE **9160**, 91601L (2014). [*Collaboration*]

VIII. M. D. Williams, D. S. Bradshaw, and D. L. Andrews, "Principles of vortex light generation from electronically excited nanoscale arrays," Proc. SPIE **9126**, 91260F (2014).

VII. M. D. Williams, M. M. Coles, D. S. Bradshaw, and D. L. Andrews, "Direct generation of optical vortices," Phys. Rev. A **89**, 033837 (2014).

VI. M. D. Williams, M. M. Coles, D. S. Bradshaw, and D. L. Andrews, "Optical vortex mode generation by nanoarrays with a tailored geometry," Proc. SPIE **8999**, 89990Q (2014).

V. M. M. Coles, M. D. Williams, and D. L. Andrews, "Optical vortices in six-wave mixing," Proc. SPIE **8999**, 89990Y (2014).

IV. M. D. Williams, M. M. Coles, K. Saadi, D. S. Bradshaw, and D. L. Andrews, "Optical vortex generation from molecular chromophore arrays," Phys. Rev. Lett. **111**, 153603 (2013).

III. M. M. Coles, M. D. Williams, K. Saadi, D. S. Bradshaw, and D. L. Andrews, "Chiral nanoemitter array: A launchpad for optical vortices," Laser & Photon. Rev. **7**, 1088 (2013). [*Issue front cover*]

II. D. L. Andrews, M. M. Coles, M. D. Williams, and D. S. Bradshaw, "Expanded horizons for generating and exploring optical angular momentum in vortex structures," Proc. SPIE **8813**, 88130Y (2013).

I. M. M. Coles, M. D. Williams, and D. L. Andrews, "Second harmonic generation in isotropic media: six-wave mixing of optical vortices," Opt. Express **21**, 12783 (2013).

ACKNOWLEDGEMENTS

Firstly, I would like to express my gratitude for the supervision and guidance Prof. David L. Andrews has consistently provided me throughout my PhD research; I cannot imagine a better mentor to have had throughout this endeavour.

I thank my co-authors and group members for the many fruitful conversations: Dr Matt M. Coles, Dr Jack S. Ford, Kayn A. Forbes, Dr Jamie M. Leeder. But most of all to Dr David S. Bradshaw for offering your time and insights throughout this research and thesis.

I thank the University of East Anglia for funding this research.

Last but by no means least, I would like to thank my parents. Not just for the care and attention you so readily give out. But also for the sacrifices you make to provide the best for us all.

CONTENTS

LIST OF FIGURES

LIST OF TABLES

LIST OF ABBREVIATIONS

Abbreviated form	Unabbreviated form
DR	depolarisation ratio
E1	electric dipole
E2	electric quadrupole
E*n*	electric multipole
HRS	hyper-Rayleigh scattering
LG	Laguerre-Gaussian
M1	magnetic dipole
M*n*	magnetic multipole
MQED	molecular quantum electrodynamics
OAM	orbital angular momentum
QED	quantum electrodynamics
RR	reversal ratio
SAM	spin angular momentum
SHG	second harmonic generation
V-tensor	retarded dipole-dipole interaction

LIST OF SYMBOLS

Symbol	Significance
$A_{l,p}$	normalisation constant
$\mathbf{a}$	vector potential
$\hat{a}$	annihilation operator
$\hat{a}^{\dagger}$	creation operator
$\boldsymbol{\alpha}$	polarizability
α	vibrational excited state
	conical emission angle
$\mathbf{b}$	magnetic field
β_T^n	bulk isothermal compressibility
d	molecular diameter
$\mathbf{d}^{\perp}$	microscopic transverse displacement field operator
δ_{ij}	Kronecker delta
E	energy
e_{α}	optical centre charge
$\boldsymbol{\mathcal{E}}$	electric field
ε_{ijk}	Levi-Civita
$f_{l,p}$	radial distribution function
$f_p^{(n)}$	permutations of field vectors
$g_q^{(n)}$	permutations of molecular responses
$g^{(n)}$	degree of n^{th} order coherence
$G\bar{G}^{\mathrm{T}}$	gramian matrix
γ_r	decay constant for a state r
H	Hamiltonian
η	polarisation
I_0	beam irradiance
I'	radiant intensity

$I^{(n)}$	rotational average of n^{th} order
$\mathbf{J}$	total angular momentum
$\boldsymbol{J}$	response tensor involving an M1 transition
$\boldsymbol{K}$	response tensor involving an E2 transition
$\mathbf{k}$	wave vector
$\mathbf{L}$	orbital angular momentum
l	topological charge
λ	wavelength
M	matrix element
$\mathbf{m}$	magnetic transition dipole moment
$m_{pq}^{(n)}$	weighting tensor for rotational average
$\boldsymbol{\mu}$	transition dipole moment
N	number of scatterers
n_{ω}	refractive index at frequency, ω
n	order of process
	rank of rotational average
	number of emitters
ξ	optical centres
$\boldsymbol{P}$	polarisation tensor
P	number of parameters in irreducible tensors
P_s	spatial parity transformation
P_t	temporal parity transformation
$\mathbf{p}_{e_\alpha}$	momentum operator
$\mathbf{Q}$	transition quadrupole moment
Q	vibrational coordinate
$\mathbf{q}_{\alpha(\xi)}$	position vector
$\mathbf{R}_{\xi}$	position vector for ξ
ρ_F	density of states
$\rho_{\perp}$	depolarisation ratio
$\mathbf{S}$	spin angular momentum

$\mathcal{S}$	Poynting vector
T	temperature
$\mathbf{T}$	Cartesian tensor
t	time
$\boldsymbol{T}_w$	collection of molecular responses
U	neighbour interaction energy
u	general field amplitude
$\mathbf{V}$	retarded dipole-dipole interaction
V	quantised volume
	retarded interaction potential
$V(\xi)$	intramolecular Coulomb potential
ϕ	scalar potential
χ	optical susceptibility
$\mathbf{\Psi}$	wavefunction
$\mathrm{d}\Omega$	solid angle
ω	frequency

Consistent with convention, bold face indicates a vector quality, italics for variables, overbars for complex conjugates and circumflex accents for unit vectors throughout. Note, that also following with convention operators are inferred under quantum mechanical principles and not marked with a circumflex accent to avoid confusion with the unit vectors. All of $\{i, j, k, l, m, n\}$ are reserved for use as Cartesian indices and $\{\lambda, \mu, \nu, \pi, \rho, \sigma\}$ for their corresponding laboratory reference frame. In order to avoid conflict Roman "i" will denote a mathematically imaginary component.

1

FUNDAMENTAL THEORY

1.1 INTRODUCTION

Life on earth was progenerated by the sun: a mere segment of its vast reservoir of energy was the spark and nurturer of life. This energy takes the form of electromagnetic radiation and not only shapes the world around us, but also enables us to marvel at the beauty of the natural world. The complexity and mysticism of the dynamical system that has been created is a projection of the fundamental laws which governs it; unsurprisingly people are fascinated by what the nature of light truly is. For something that has been and still is so pivotal to our development there is still a substantial portion of uncertainty over our understanding of what light is and how much we can reasonably know about it.

Light-matter interaction events are ubiquitous in nature. There are countless quanta of light flashing in and out of existence: interacting with our seas, skies and ourselves. By further understanding that which is around us we can gain insights to what is pervasive throughout the universe. Consider a blink of our eye, taking just a few hundred milliseconds, light is capable of traversing a distance comparable to the diameter of Saturn: an order of magnitude larger than that of the Earth. Of course, light does not travel so swiftly everywhere, with substances impeding its progress. The property that defines the extent that light slows within a material is known as the refractive index. This aspect has a complex quantity, the more often considered real part of it is the portion relating to the modulation of lights phase velocity; that is the speed to which the light can convey information and induces electric field oscillations in the media it is traversing. This will be referred to at the tail end of this work.

With the light traversing such vast distances in a literal blink of an eye it is hard to know what the expected number of quanta of light in a given volume is likely to be. A back of the envelope calculation can help with this. The mean number of photons, m_p, of a given mode is related to the wavelength of light, λ, the volume considered, V_m, as well as a selection of fundamental values: the maximum speed of light, Planck's and Avogadro's constant, c, h and N_A, respectively. The ensuing relation is $m_p = \lambda I V_m / hc^2 N_A$. From this, it is possible to discern the chances that a quanta of light will encounter a molecule of a given volume.

As a first example, if we consider a day of sunlight, which by definition is a time in which the ground irradiance is in excess of 120 Wm^{-2} [1] and on a peak sunny day can approach tenfold that amount. Considering one of the most abundant molecules on the surface, water, it follows that one can expect to find 1 quanta of light of an average visible wavelength of about 500 nm in about 3×10^{16} molecules, with the upper limit of solar irradiance reducing the order of magnitude by one. If we now shift our focus to lasers, they are capable of surpassing daylight by some 20-orders of magnitude [2] at such extreme levels one could expect to find thousands of quanta of light per molecule. Under such high intensities of light, nonlinear processes become increasingly likely to occur and are of particular relevance to chapters 3 and 4 of this work. However, such lasers are beyond the remit of commercial laboratory lasers and would generate fields that would be comparable to the field strength of the molecules themselves and therefore beyond the remit of the perturbation methods introduced in §1.3 [3].

Dimensions and geometry of all constituents engaged in a process must be considered and can be collected into three classes of scattering. The most studied class is also the one that is most observed in nature: specifically, where the wavelengths of electromagnetic radiation are much greater than that of the diameter of the molecule(s) engaged in a given process. For example, most molecules will have a diameter in the region of 1 nm, and the spectral composition of light observed on earth is heavily weighted to the region of visible light with wavelengths, λ = 380-760 nm. Many commercial lasers also operate in this region, as well as into the infrared region, up to and beyond 1500 nm. In §1.4 we will consider a number of different mechanism to which a photon can be scattered under this regime.

Light can engage with matter in a vast number of ways, the lowest number of interactions are seen in a single-photon absorption and spontaneous emission. The latter is a hallmark of quantum electrodynamical (QED) theory, with preceding theoretical treatments incapable of capturing this insight. However, the majority of interest to us and indeed the subject of this thesis is light which is scattered by matter. To date quantum theory offers the most accurate insight into what occurs at a fundamental level and as such that is what is used throughout this work. A quantum depiction for light is the only instance to which a photon is a legitimate concept.

1.2 UNDERLYING THEORY

Quantum electrodynamics is a fully covariant theory that is compatible with relativity and particularly excels when dealing with particles approaching the universal speed limit, such as free electrons. However, when regarding coupling between radiation and modest energy perturbations (as is the case in this body of work) a noncovariant formulation can more readily be deployed, dubbed molecular quantum electrodynamics (MQED) [3] and still retains the retardation features of its parent theory [4]. Moreover, for reasons more extensive than purely consistency, all matter engaged by light is also considered in a quantum sense. Hence, molecular quantum electrodynamics is reasonably deployed. A key feature is that both the molecular and radiation components are regarded on an equal footing. Figure 1 selects one closed dynamical process and breaks this down into the matter and radiation transitions.

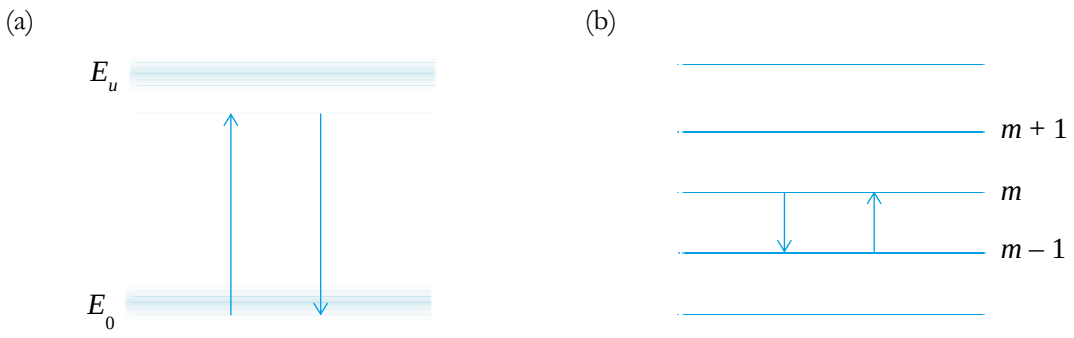

Figure 1: A quantum representation of: (a) a molecule undergoing an electronic transition from a ground state E_0 to a virtual excited state $E_0 + \hbar ck$ before relaxing back to its ground state; (b) a radiation transition utilising ladder operators to demote the radiation state to $m-1$ and subsequently promoted back to m.

The Hamiltonian under multipolar formalism is composed of three distinct components,

$$H = H_{\text{rad}} + \sum_{\xi} H_{\text{mat}}(\xi) + \sum_{\xi} H_{\text{int}}(\xi) \ , \tag{1.2.1}$$

the radiation field, intrinsic matter component and their associated interactions, respectively. The first summations are required to span the full set of normal nonrelativistic Schrödinger operators for each optical centre (ξ) and the second for the corresponding interactions engaged in the process. The selected formalism freely permits this interaction to engage with any term in the expansion for the interaction Hamiltonian. Notice that none of the terms relate to instantaneous intermolecular interactions, which are present in the interaction Hamiltonian for semi-classical theory. Under MQED all interactions that are longitudinal in character, with respect to intermolecular vector, emerge from a formulation in which only fields transverse to the wave vectors are deployed [3].

Mathematically each of the panels in Figure 1 require the respective Hamiltonian to invoke operations to change state. Figure 1(a) engages the interaction Hamiltonian and (b) engages the radiation vector potential. In each instance, there are a Hermitian conjugate pair of creation and annihilation operators:

$$a_{\mathbf{k}}^{(\eta)} \left| m(\mathbf{k},\eta) \right\rangle = \sqrt{m} \left| (m-1)(\mathbf{k},\eta) \right\rangle \ , \tag{1.2.2}$$

$$a_{\mathbf{k}}^{\dagger\,(\eta)} \left| m(\mathbf{k},\eta) \right\rangle = \sqrt{m+1} \left| (m+1)(\mathbf{k},\eta) \right\rangle \ , \tag{1.2.3}$$

associated with each event. The former operates on eigenstates of H_{rad} with mode occupation number (m) and reduces the number of photons in mode $(\mathbf{k},\eta)$, while the latter increases the number of photons in the same mode. The factors present on the right-hand-side ensure correct normalisation of the wave function.

The selected solution for Maxwell's equations are gauge invariant, explicitly there exists a set of vector $(\mathbf{a})$ and scalar (ϕ) potentials that deliver the same electric $(\mathbf{e})$ and magnetic $(\mathbf{b})$ observable fields under any given Gauge transformation. It is possible to decompose the vector potential into a sum of two components which have $\nabla \times \mathbf{a} = 0$ and $\nabla \cdot \mathbf{a} = 0$, this corresponds

to the longitudinal $\left(\mathbf{a}^{\parallel}\right)$ and transverse $\left(\mathbf{a}^{\perp}\right)$ fields respectively. Here, we select the Coulomb gauge, defined by $\nabla\cdot\mathbf{a}=0$, under which the static and dynamic interactions can be separated, this corresponds to the basis of the separation of particles from the interactions with the radiation field.

Now, we can consider the transverse vector potential, summed over all radiation modes $\left(\mathbf{k},\eta\right)$ and under SI convention this is,

$$\mathbf{a}^{\perp}\left(\mathbf{r},t\right)=\sum_{\mathbf{k},\eta}\sqrt{\frac{\hbar}{2c\varepsilon_0 kV}}\left[\mathbf{e}_{\mathbf{k}}^{(\eta)}a_{\mathbf{k}}^{(\eta)}\mathrm{e}^{\mathrm{i}\mathbf{k}\cdot\mathbf{r}}-\bar{\mathbf{e}}_{\mathbf{k}}^{(\eta)}a_{\mathbf{k}}^{\dagger(\eta)}\mathrm{e}^{-\mathrm{i}\mathbf{k}\cdot\mathbf{r}}\right], \tag{1.2.4}$$

where V is the quantisation volume, ε_0 is the vacuum electric susceptibility, $\mathbf{e}$ is the unit polarisation vector for the radiation mode of polarisation η and wavevector $\mathbf{k}$. All polarisation vectors are permitted to be complex, in order to accommodate left- and right- handed modes. The overbar indicates a complex conjugate.

From the vector potential, the microscopic transverse displacement electric and magnetic field operators can be obtained, $\mathbf{d}^{\perp}$ and $\mathbf{b}^{\perp}$, respectively. The former is obtainable by this relation;

$$\mathbf{d}^{\perp}(\mathbf{r},t)=-\varepsilon_0\frac{\partial\mathbf{a}^{\perp}\left(\mathbf{r},t\right)}{\partial t}, \tag{1.2.5}$$

which is,

$$\mathbf{d}^{\perp}(\mathbf{r},t)=\mathrm{i}\sum_{\mathbf{k},\eta}\sqrt{\frac{\varepsilon_0\hbar ck}{2V}}\left[\mathbf{e}_{\mathbf{k}}^{(\eta)}a_{\mathbf{k}}^{(\eta)}\mathrm{e}^{\mathrm{i}\mathbf{k}\cdot\mathbf{r}}-\bar{\mathbf{e}}_{\mathbf{k}}^{(\eta)}a_{\mathbf{k}}^{\dagger(\eta)}\mathrm{e}^{-\mathrm{i}\mathbf{k}\cdot\mathbf{r}}\right]. \tag{1.2.6}$$

As stated by Maxwell II [5], $\nabla\cdot\mathbf{b}=0$ and as such the magnetic field is purely transverse $\left(\mathbf{b}=\mathbf{b}^{\perp}\right)$, hence we can write;

$$\mathbf{b}\left(\mathbf{r},t\right)=\nabla\times\mathbf{a}^{\perp}\left(\mathbf{r},t\right). \tag{1.2.7}$$

Evaluating this, we now have:

$$\mathbf{b}\left(\mathbf{r},t\right)=\mathrm{i}\sum_{\mathbf{k},\eta}\sqrt{\frac{\hbar k}{2c\varepsilon_0 V}}\left[\mathbf{b}_{\mathbf{k}}^{(\eta)}a_{\mathbf{k}}^{(\eta)}\mathrm{e}^{\mathrm{i}\mathbf{k}\cdot\mathbf{r}}-\bar{\mathbf{b}}_{\mathbf{k}}^{(\eta)}a_{\mathbf{k}}^{\dagger(\eta)}\mathrm{e}^{-\mathrm{i}\mathbf{k}\cdot\mathbf{r}}\right], \tag{1.2.8}$$

Note that all occurrences of magnetic permeability $\left(\mu_0\right)$ have been suppressed in favour of c and ε_0 such that $\mu_0 = c^{-2}\varepsilon_0^{-1}$. The complex unit vector $\mathbf{b}_{\mathbf{k}}^{(\eta)}$ is defined as,

$$\mathbf{b}_{\mathbf{k}}^{(\eta)} = \hat{\mathbf{k}} \times \mathbf{e}_{\mathbf{k}}^{(\eta)} \ . \tag{1.2.9}$$

Where $\{\mathbf{e}, \mathbf{b}, \mathbf{k}\}$ form a right-handed triad of orthogonal vectors. There are a number of permissible polarisations of light, of particular interest are spin polarisations, of which there are two helicities that of left and right handedness:

$$\mathbf{e}_{\mathbf{k}}^{(\mathrm{L})} = \frac{1}{\sqrt{2}}\left(\hat{\mathbf{i}} + \mathrm{i}\hat{\mathbf{j}}\right) , \tag{1.2.10}$$

$$\mathbf{e}_{\mathbf{k}}^{(\mathrm{R})} = \frac{1}{\sqrt{2}}\left(\hat{\mathbf{i}} - \mathrm{i}\hat{\mathbf{j}}\right) , \tag{1.2.11}$$

respectively. This is a property known as spin angular momentum (SAM), with each circularly polarised photon capable of conveying $\hbar$ of either handedness per photon, where $\hbar = h/2\pi$ is the reduced Planck's constant. Linear polarisations can be cast as linear combinations of these spin states. Utilising equation (1.2.9) similar equations can be expressed for the magnetic polarisations:

$$\mathbf{b}_{\mathbf{k}}^{(\mathrm{L})} = -\frac{\mathrm{i}}{\sqrt{2}}\left(\hat{\mathbf{i}} + \mathrm{i}\hat{\mathbf{j}}\right) , \tag{1.2.12}$$

$$\mathbf{b}_{\mathbf{k}}^{(\mathrm{R})} = \frac{\mathrm{i}}{\sqrt{2}}\left(\hat{\mathbf{i}} - \mathrm{i}\hat{\mathbf{j}}\right) , \tag{1.2.13}$$

See complement 1A for a discussion on the parity transformations of equations (1.2.4), (1.2.6) and (1.2.8).

Now we are equipped to unravel the first term in equation (1.2.1);

$$H_{\mathrm{rad}} = \frac{1}{2}\int\left[\varepsilon_0^{-1}\mathbf{d}^{\perp 2}\left(\mathbf{r}\right) + c^2\varepsilon_0\mathbf{b}^2\left(\mathbf{r}\right)\right]\mathrm{d}^3\mathbf{r} \ . \tag{1.2.14}$$

SCT does not accommodate a term associated with the radiation field and as such is considered as a fixed agent. In many cases, this is deemed satisfactory, such as in cases where the field strength is sufficiently strong that any influence matter has on it is small. However, there are a

few cases that this is not the case. It is the quantised treatment of the radiation field that accurately describes the lifting of degeneracy between two of atomic hydrogen's energy levels $\left({}^2S_{1/2} \text{ and } {}^2P_{1/2}\right)$, namely the Lamb shift [6]. Two further cases were QED exceeds classical techniques is the presence of electron's magnetic moment [7]; and the occurrence of a force between a pair of conducting plates or a plate and a polarisable atom, Casimir effect and Casimir-Polder force respectively [8, 9]. These effects are better seen by incorporating the field operators into equation (1.2.14), which displays the photon annihilation and creation operators directly and holds a term that is associated with vacuum fluctuations:

$$H_{\text{rad}} = \sum_{\mathbf{k},\eta} \left(a_{\mathbf{k}}^{\dagger(\eta)} a_{\mathbf{k}}^{(\eta)} + \frac{1}{2} \right) \hbar c k \ , \tag{1.2.15}$$

that arises from the non-commutativity of the two creation and annihilation operators for any given radiation mode. The second term that appears in the parentheses of the above equation, is the zero-point energy in the electromagnetic field is analogous to that seen in matter.

To complete the definitions of the terms in equation (1.2.1), the full expression for the interaction Hamiltonian can be expressed as an expansion [10], the leading contributions are from these three terms:

$$H_{\text{int}}(\xi) = -\varepsilon_0^{-1} \mu_i(\xi) d_i^{\perp}\left(\mathbf{R}_\xi\right) - \varepsilon_0^{-1} Q_{ij}(\xi) \nabla_i d_j^{\perp}\left(\mathbf{R}_\xi\right) - m_i(\xi) b_i\left(\mathbf{R}_\xi\right) - \ldots \ . \tag{1.2.16}$$

Here $\mu_i(\xi)$, $Q_{ij}(\xi)$, $m_i(\xi)$ are the electric dipole (E1), electric quadrupole (E2) and magnetic dipole (M1) operators respectively, associated with a molecule a ξ located at position $\mathbf{R}_\xi$. The product of two operators with Latin subscripts is evaluated under the implied Einstein summation convention [11]: the product of respective pairs of x, y and z components are taken and then summed. Explicit expressions for the components of the leading molecular multipoles are as follows;

$$\mu_i(\xi) = \sum_{\alpha(\xi)} e_\alpha \left(\mathbf{q}_{\alpha(\xi)} - \mathbf{R}_\xi \right)_i \ , \tag{1.2.17}$$

$$Q_{ij}(\xi) = \frac{1}{2} \sum_{\alpha(\xi)} e_\alpha \left[\left(\mathbf{q}_{\alpha(\xi)} - \mathbf{R}_\xi \right)_i \left(\mathbf{q}_{\alpha(\xi)} - \mathbf{R}_\xi \right)_j - \frac{1}{3} \left| \mathbf{q}_{\alpha(\xi)} - \mathbf{R}_\xi \right| \delta_{ij} \right] \ , \tag{1.2.18}$$

$$m_i(\xi) = \frac{1}{2}\sum e_\alpha \left[\left(\mathbf{q}_{\alpha(\xi)} - \mathbf{R}_\xi \right) \times \dot{\mathbf{q}}_{\alpha(\xi)} \right]_i \ . \tag{1.2.19}$$

Again, these summations are across all optical centres of charge, e_α and position vector, $\mathbf{q}_{\alpha(\xi)}$.

In the majority of instances, the electric dipole transition moments are the greatest contributor to the interaction Hamiltonian, however, with increasing intensities the series of corrective terms can become significant. As a guide, the first corrections to the electric dipole approximation, explicitly the electric quadrupole and magnetic dipole can be expected to be smaller than the leading term by a factor equal to the fine structure constant.

For completeness, the final term in equation (1.2.1),

$$H_{\text{mat}} = -\frac{1}{2m}\sum_{e_\alpha} \mathbf{p}_{e_\alpha}^2(\xi) + V(\xi) \ , \tag{1.2.20}$$

where $\mathbf{p}_{e_\alpha}$ is the momentum operator for the charge associated with optical centre ξ and $V(\xi)$ is the intramolecular Coulomb potential.

1.3 PERTURBATION THEORY

We now have a prescribed Hamiltonian H, to deliver the initial state $|I\rangle$ for a system at a given time t_0, equation (1.2.1), an obvious next step is to attempt to find the final state $|F\rangle$ of the same system at a later time t_1. Unfortunately, due to the inherently delicate nature of quantum systems, any attempt to measure a system introduces an interaction and as such alters the system states; we must therefore consider alternative theoretical options. The time evolution for any quantum system is governed by the time-dependant Schrödinger equation,

$$i\hbar \frac{\partial \Psi(t)}{\partial t} = H\Psi(t) \ , \tag{1.3.1}$$

where $\Psi(t)$ is the wavefunction for the system. This method for perturbing the initial state is valid so long as the irradiance of the light considered is much less than the Coulombic fields within the matter. As a rough guide, the current lasers of 10^{20} Wm^{-2} are just reaching the levels

of that to which an atomic hydrogens electron experiences in its ground state. As such time-dependant perturbation theory is applicable to MQED.

First taking the Hamiltonian and separating into the time independent terms and those that may hold a time dependence:

$$H(t) = H_0 + H'(t) \ , \tag{1.3.2}$$

where $H_0 = H_{\text{mat}} + H_{\text{rad}}$.

$$i\hbar \frac{\partial \Psi(t)}{\partial t} = \left[H_0 + H'(t) \right] \Psi(t) \ . \tag{1.3.3}$$

Utilising the interaction picture, which permits operators and states to hold a level of time dependence we can use a known solution to this equation,

$$\Psi(t) = \sum_i a_i(t) \psi_0^{(I)} \mathrm{e}^{-\mathrm{i}E_0^{(i)} t/\hbar} \ . \tag{1.3.4}$$

Substituting in, this produces the exact result:

$$\frac{\partial a_F(t)}{\partial t} = -\frac{\mathrm{i}}{\hbar} \sum_i a_i \langle F | H'(t) | I \rangle \mathrm{e}^{-\mathrm{i}\left[E_0^{(F)} - E_0^{(I)}\right] t/\hbar} \ . \tag{1.3.5}$$

Here $\langle F | H' | I \rangle = H'_{fi}$,

$$a_F(t) \approx a_F(0) - \frac{\mathrm{i}}{\hbar} \sum_i a_i(0) \int_0^t H'_{FI}(t) \mathrm{e}^{-\mathrm{i}\left[E_0^{(F)} - E_0^{(I)}\right] t/\hbar} . \mathrm{d}t \ . \tag{1.3.6}$$

Importantly, at $t = 0$ the system will be in state I, which is in agreement with what was set up at the beginning. Now, if $F \neq I$,

$$a_F(t) = -\frac{\mathrm{i}}{\hbar} \int_0^t H'_{FI}(t) \mathrm{e}^{\mathrm{i}\left[E_0^{(F)} - E_0^{(I)}\right] t/\hbar} . \mathrm{d}t \ . \tag{1.3.7}$$

Matrix element, $H'_{FI}(t)$ causes transitions from i to a continuum of states f, assuming H'_{FI} is independent of time,

$$a_F(t) = H'_{FI}(t)\frac{e^{-i\left[E_0^{(F)}-E_0^{(I)}\right]t/\hbar}-1}{E_0^{(F)}-E_0^{(I)}} \ . \tag{1.3.8}$$

It is of interest to square this expression,

$$\left|a_F(t)\right|^2 = 4\left|H'_{FI}\right|^2 \frac{\sin^2\left(\left[E_0^{(F)}-E_0^{(I)}\right]t/2\hbar\right)}{\left[E_0^{(F)}-E_0^{(I)}\right]^2} \ . \tag{1.3.9}$$

A plot of the above equation for a given time, delivers the probability of finding the optical centre in a state F, which is proportional to t^2. Probability of a transition to one state F is the sum of all transition probabilities,

$$P(t) = \sum_{F\neq I}\left|a_F(t)\right|^2 = 4\left|H'_{FI}\right|^2 \sum \frac{\sin^2\left(\left[E_0^{(F)}-E_0^{(I)}\right]t/2\hbar\right)}{\left[E_0^{(F)}-E_0^{(I)}\right]^2} \ , \tag{1.3.10}$$

If we now integrate over the continuum of states,

$$P(t) = 4\left|H'_{FI}\right|^2 \rho_F \int_{-\infty}^{\infty} \frac{\sin^2\left(\left[E_0^{(F)}-E_0^{(I)}\right]t/2\hbar\right)}{\left[E_0^{(F)}-E_0^{(I)}\right]^2} .\mathrm{d}\left[E_0^{(F)}-E_0^{(I)}\right] \ , \tag{1.3.11}$$

where ρ_F is the number of final states F, close in energy to the initial state, E_I per unit energy interval $\hbar ck$. We are left with a compact expression for the probability of a transition from a state I to F,

$$P(t) = t\frac{2\pi}{\hbar}\left|H'_{FI}\right|^2 \rho_F \ . \tag{1.3.12}$$

Hence, the rate of transition can be expressed as;

$$\Gamma = \frac{2\pi}{\hbar}\left|H'_{FI}\right|^2 \rho_F \ . \tag{1.3.13}$$

This is a rate expression for a single transition H'_{FI}. Similar derivations can be made for processes involving any number of interactions. Once obtained, they can be assembled to form a general series applicable to any process, called the matrix element:

$$
\begin{aligned}
M_{FI} = & \langle F \mid H_{\text{int}} \mid I \rangle \\
& + \sum_{R \neq I,F} \frac{\langle F \mid H_{\text{int}} \mid R \rangle \langle R \mid H_{\text{int}} \mid I \rangle}{(E_I - E_R)} \\
& + \sum_{R,S \neq I,F} \frac{\langle F \mid H_{\text{int}} \mid S \rangle \langle S \mid H_{\text{int}} \mid R \rangle \langle R \mid H_{\text{int}} \mid I \rangle}{(E_I - E_S)(E_I - E_R)} \\
& + \sum_{R,S,T \neq I,F} \frac{\langle F \mid H_{\text{int}} \mid T \rangle \langle T \mid H_{\text{int}} \mid S \rangle \langle S \mid H_{\text{int}} \mid R \rangle \langle R \mid H_{\text{int}} \mid I \rangle}{(E_I - E_T)(E_I - E_S)(E_I - E_R)} + \ldots \ .
\end{aligned} \tag{1.3.14}
$$

Here, $\{R,S,T,\ldots\}$ correspond to indeterminable intermediary states in a process, of which all possible pathways must be summed over to deliver the overall rate of the process. Each interaction event connecting two states engages the interaction Hamiltonian, equation (1.2.16), the number of interactions, n, occurring in an instant of time corresponds to the order of a given process. This can be fed directly into the expression for rate:

$$\Gamma = \frac{2\pi}{\hbar} |M_{FI}|^2 \rho_F \ , \tag{1.3.15}$$

which was originally formulated by Dirac and later dubbed golden rule no.2, by Fermi [12].

1.4 PROCESSES

1.4A RAYLEIGH SCATTERING

To begin, let us expand the example displayed in Figure 1, this is the simplest form of scattering event known as Rayleigh scattering. Here an incident photon of wavevector and polarisation is scattered into a radiation mode $(\mathbf{k}', \eta')$. This is the form of scattering arguably most observed and familiar to us and is the one responsible for the azure colour of the sky. Rayleigh scattering is a concerted process of single-photon annihilation and creation by an optical centre. With no possibility of measurement during the course of such a process, each interaction occurs in an indeterminate order, therefore, all possibilities must be included in the summation for the overall rate of the process. A commonly deployed diagrammatic method to display all interaction permutations are Feynman diagrams [13], whereby you consider the evolution of the Hamiltonian system of states with time.

Figure 2(a) is representative of looking left-to-right for each panel in Figure 1. Figure 2(b) takes a little more consideration, it is indeed equivalent to the time-inverse of Figure 1(a), however in (b) the mode will first be promoted a level before returning to the median level. For this process, the energy and momentum of the centre are both conserved and therefore it is elastic, $|\mathbf{k}| = |\mathbf{k}'|$. However, the emergent radiation mode is different to that of incident mode and hence it is not a parametric process, $\mathbf{k} \neq \mathbf{k}'$.

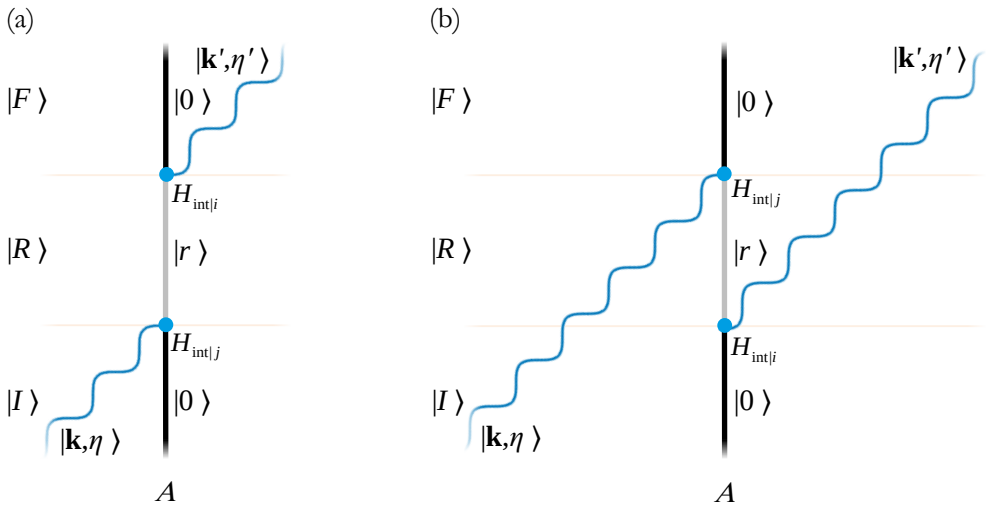

Figure 2: A pair of Feynman diagrams depicting both the photon annihilation and creation events at a world line for an optical centre, A. Read from the bottom up: (a) depicts a centre in its ground state, 0, annihilating a photon at vertex j, at which time it enters an intermediary state, r, before subsequently relaxing and creating a photon at vertex i and returns the centre to its ground state; (b) is the time inverse of the left panel, moreover all matter and radiation states are equivalent.

Before we proceed with the calculation for the rate of Rayleigh scattering, it must be stated that the regarded process is assumed to dominate the optical response of the interrogated medium with each optical centre distinct, electrically neutral and in their ground state. Selecting the $n = 2$ instance of equation (1.3.14), with one intermediary state (R), the matrix element that delivers the leading contribution to the rate is:

$$M_{FI}^{(E1^2)} = \frac{\hbar c\sqrt{kk'n}}{2\varepsilon_0 V}\bar{e}_i' e_j \sum_r \left\{ \frac{\mu_i^{0r|A}\mu_j^{r0|A}}{\left[E_{r0}^A - \hbar ck\right]} + \frac{\mu_j^{0r|A}\mu_i^{r0|A}}{\left[E_{r0}^A + \hbar ck\right]} \right\}. \qquad (1.4.1)$$

The two terms held in the summation correspond with Figure 2(a) and (b) respectively. The shorthand: $E_{r0}^{A} \equiv E_{r}^{A} - E_{0}^{A}$ will be used throughout. Any variable with a prime associated with it indicates that it is attributed to a scattered photon. Each numerator denotes invokes a pair of electric dipole transitions to modify the state of the optical centre, explicitly,

$$\mu_{i}^{0r|A}\mu_{j}^{r0|A} = \langle 0|\mu_{i}^{A}|r\rangle\langle r|\mu_{j}^{A}|0\rangle \ . \tag{1.4.2}$$

When present, an electric dipole transition is the most significant contributor in the interaction Hamiltonian, equation (1.2.16), as such it is common to restrict the engagement to just this first term, this is referred to as the electric dipole approximation. The subscript associated with the transition dipole moment refers to the Cartesian laboratory frame. In the denominator $E_{r0}^{A} = E_{r}^{A} - E_{0}^{A}$ and gives the collective energy of the system at each stage and pivotally this holds information relative to those observed and the initiation of the process. A useful relation known as the completeness relation is,

$$\sum_{r} |\psi_{R}\rangle\langle\psi_{R}| \equiv 1 \ . \tag{1.4.3}$$

The summation in equation (1.4.1) is defined as the intrinsic molecular polarizability, which is unique for each process. In the case of Rayleigh scattering,

$$\alpha_{ij}^{00|A} = \sum_{r}\left\{\frac{\mu_{i}^{0r|A}\mu_{j}^{r0|A}}{\left[E_{r0}^{A} - \hbar ck\right]} + \frac{\mu_{j}^{0r|A}\mu_{i}^{r0|A}}{\left[E_{r0}^{A} + \hbar ck\right]}\right\} , \tag{1.4.4}$$

and hence the contracted form of the matrix element can be expressed as,

$$M_{FI}^{(\mathrm{E1}^2)} = -\frac{\hbar c\sqrt{kk'n}}{2\varepsilon_{0}V}\bar{e}_{i}'e_{j}\alpha_{ij}^{00|A} \ . \tag{1.4.5}$$

At this juncture, it is necessary to interrogate the system for any intrinsic symmetries that may be present in the response tensors. These can arise for a number of reasons and are discussed in complement 1B. Using equation (1.3.15), the rate of single-centre solid-phase Rayleigh scattering can be cast as,

$$\Gamma = \frac{\pi\hbar c^{2}kk'n}{2\varepsilon_{0}^{2}V^{2}}\left|\bar{e}_{i}'e_{j}\alpha_{ij}^{00|A}\right|^{2}\rho_{F} \ . \tag{1.4.6}$$

If we consider non-forward scattering, it is of more interest to consider the distribution of emission from the centre over all 4π sr. This can be obtained by using the relation,

$$\rho_F = \frac{k'^2 \, \mathrm{d}\Omega' V}{(2\pi)^3 \hbar c} \,, \tag{1.4.7}$$

to obtain the differential scattering cross section for this process:

$$\mathrm{d}\Gamma = \frac{ckk'^3 n \mathrm{d}\Omega'}{16\varepsilon_0^2 \pi^2 V} \bar{e}_i' e_j e_k' \bar{e}_l \alpha_{ij}^{00|A} \bar{\alpha}_{kl}^{00|A} \,, \tag{1.4.8}$$

which is the transition probability per second per unit solid angle $\mathrm{d}\Omega'$ around $\mathbf{k}'$ per unit incident photon number flux per unit area. This can be fed into,

$$I' = \hbar c k' \frac{\mathrm{d}\Gamma}{\mathrm{d}\Omega'} \,, \tag{1.4.9}$$

This is known as the radiant intensity I', which is defined by the energy radiated of directionality and polarisation of that of the scattered photon, per unit solid angle $\mathrm{d}\Omega'$ per unit time.

$$I' = \frac{N I_0 k'^4}{16\varepsilon_0^2 \pi^2} \bar{e}_i' e_j e_k' \bar{e}_l \alpha_{ij}^{00|A} \bar{\alpha}_{kl}^{00|A} \,. \tag{1.4.10}$$

where,

$$I_0 = \frac{n\hbar c^2 k}{V} \,, \tag{1.4.11}$$

is the beam irradiance. Also, note the introduction of N in equation (1.4.10), this is the sum of independent scattering rates. Up until that point, the term associated with the phase factor had been partitioned and a discussion on how N arises, appears in complement 1C. This is a crucial a step, before considering any molecular motion, termed a rotational average, indicated by chevron brackets. Complement 1D discusses this in more detail, but the salient result is equation (1D.10), which defines the isotropic rotation tensor for a 4th rank process, $I_{ijkl;\lambda\mu\nu\pi}^{(4)}$, and can be applied to equation (1.4.10).

$$\langle I' \rangle = \left(\frac{k'^2}{4\pi\varepsilon_0} \right)^2 N I_0 \bar{e}_i' e_j e_k' \bar{e}_l I_{ijkl;\lambda\mu\nu\pi}^{(4)} \alpha_{\lambda\mu}^{00|A} \bar{\alpha}_{\nu\pi}^{00|A} \,. \tag{1.4.12}$$

As an incoherent process the rotational average cannot be carried out on the matrix element, and as a result requires a rotational average of twice the order of the process. The final result is cast below:

$$\langle I' \rangle = \frac{NI_0 k'^4}{480\varepsilon_0^2 \pi^2} \begin{pmatrix} \left|(\bar{\mathbf{e}}' \cdot \mathbf{e})\right|^2 \\ (\bar{\mathbf{e}}' \cdot \mathbf{e}')(\mathbf{e} \cdot \bar{\mathbf{e}}) \\ \left|(\mathbf{e} \cdot \mathbf{e}')\right|^2 \end{pmatrix}^{\mathrm{T}} \begin{pmatrix} 4 & -1 & -1 \\ -1 & 4 & -1 \\ -1 & -1 & 4 \end{pmatrix} \begin{pmatrix} \alpha_{\lambda\lambda}^{00|A} \bar{\alpha}_{\nu\nu}^{00|A} \\ \alpha_{\lambda\mu}^{00|A} \bar{\alpha}_{\lambda\mu}^{00|A} \\ \alpha_{\lambda\mu}^{00|A} \bar{\alpha}_{\mu\lambda}^{00|A} \end{pmatrix}. \tag{1.4.13}$$

The field vector products, displayed in the first tensor, can be evaluated in accordance with complement 1E.

Rayleigh scattering requires merely the presence of one incident photon per scattering event and therefore its rate has a linear dependence on the intensity of light: the remit of so-called linear optics and is the most probable form of non-resonant interaction that can occur in a given molecular volume. See complement 1F for relevant information on resonance processes. Next, we will consider a second two-photon scattering process.

1.4B RAMAN SCATTERING

Like Rayleigh scattering, Raman scattering is a two-photon process involving the concurrent annihilation and creation of a photon. The difference here is that the molecular state relaxes to its ground electronic state, but not of a same vibrational level. In Figure 1, this corresponds to the series of levels each of the electronic energy levels are split into. Interrogating this figure, it can be seen that there are occupiable levels of a higher and lower energy than that of the ground vibrational state. The scattered photon will also differ in energy, $\hbar ck'$, from that of the annihilated photon, $\hbar ck$, evidently this can have two variations, where $\hbar ck' < \hbar ck$ and $\hbar ck' > \hbar ck$. In the former instance the optical centre is promoted to a higher vibrational energy level than its initial state, this is referred to as Stokes scattering. The latter, in which the optical centre is demoted to a lower vibrational energy level than its initial state, this is referred to as anti-Stokes scattering. There are alternate forms for Raman scattering involving electric or vibrational energy levels, these employ the same framework as introduced here.

Raman scattering requires a vibration transition this is the next term in the familiar Born-Oppenheimer expansion (see complement 1G). As can be expected for a non-leading term of an expansion the resulting rate terms are smaller in magnitude than those associated with the polarisability itself, as is apparent from the relative weakness of Raman compared to Rayleigh scattering. The resemblance to the prior process is echoed in the form the rate expression takes, with a few key distinctions. Raman scattering is a nonparametric scattering process, the optical centre does not adhere to energy conservation throughout the process and the same is true for the radiation. As such, this is also both an inelastic process with regard to the matter and incoherent with regard to the radiation.

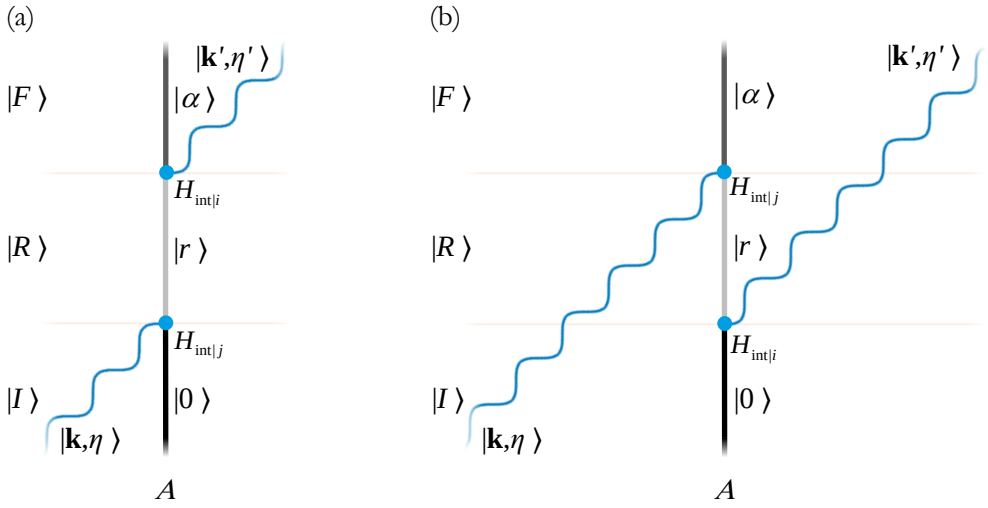

Figure 3: A pair of Feynman diagrams depicting both the photon annihilation and creation events at a world line for an optical centre, A. Read from the bottom up: (a) depicts a centre in its ground state, 0, annihilating a photon at vertex j, at which time it enters an intermediary state, r, before subsequently relaxing and creating a photon at vertex i and relaxes to a different vibrational energy state, α; (b) is the time inverse of the left panel, moreover all matter and radiation states are equivalent.

The ensuing matrix element is,

$$M_{FI}^{(\mathrm{E1}^2)} = -\frac{\hbar c\sqrt{kk'n}}{2\varepsilon_0 V}\bar{e}_i' e_j \alpha_{ij}^{\alpha 0|A} \quad , \tag{1.4.14}$$

where the molecular response is now,

$$\alpha_{ij}^{\alpha 0|A} = \sum_r \left\{ \frac{\mu_i^{\alpha r|A}\mu_j^{r0|A}}{\left[E_{r0}^A - \hbar ck\right]} + \frac{\mu_j^{\alpha r|A}\mu_i^{r0|A}}{\left[E_{r\alpha}^A + \hbar ck\right]} \right\} . \tag{1.4.15}$$

In which, energy conservation has been deployed:

$$E_\alpha - E_0 = \hbar ck - \hbar ck' \ , \tag{1.4.16}$$

which allows us to cast the full result in a form that depends solely on the magnitude of the wavevector, and hence the frequency of the input beam. The result is closely related to that of Rayleigh scattering, as can be expected from only a minor change to the molecular state progression. This is also seen in the rate for single-centre solid-phase Raman scattering,

$$\Gamma = \frac{\pi\hbar c^2 kk' n}{2\varepsilon_0^2 V^2}\left|\bar{e}_i' e_j \alpha_{ij}^{\alpha 0|A}\right|^2 \rho_F \ . \tag{1.4.17}$$

As can be expected from this, the rotational average of the subsequent radiant intensity for an ensemble of molecules takes the same following form,

$$\left\langle I' \right\rangle = \left(\frac{k'^2}{4\pi\varepsilon_0}\right)^2 N I_0 \bar{e}_i' e_j e_k' \bar{e}_l I^{(4)}_{ijkl;\lambda\mu\nu\pi} \alpha_{\lambda\mu}^{\alpha 0|A} \bar{\alpha}_{\nu\pi}^{\alpha 0|A} \ . \tag{1.4.18}$$

Again, this is another incoherent process, the 4th order rotational average is engaged. The final result is cast below:

$$\left\langle I' \right\rangle = \frac{N I_0 k'^4}{480\varepsilon_0^2 \pi^2}\begin{pmatrix} \left|(\bar{\mathbf{e}}'\cdot\mathbf{e})\right|^2 \\ (\bar{\mathbf{e}}'\cdot\mathbf{e}')(\mathbf{e}\cdot\bar{\mathbf{e}}) \\ \left|(\mathbf{e}\cdot\mathbf{e}')\right|^2 \end{pmatrix}^{\mathrm{T}} \begin{pmatrix} 4 & -1 & -1 \\ -1 & 4 & -1 \\ -1 & -1 & 4 \end{pmatrix} \begin{pmatrix} \alpha_{\lambda\lambda}^{\alpha 0|A}\bar{\alpha}_{\nu\nu}^{\alpha 0|A} \\ \alpha_{\lambda\mu}^{\alpha 0|A}\bar{\alpha}_{\lambda\mu}^{\alpha 0|A} \\ \alpha_{\lambda\mu}^{\alpha 0|A}\bar{\alpha}_{\mu\lambda}^{\alpha 0|A} \end{pmatrix} . \tag{1.4.19}$$

So far, in §1.4A and §1.4B, we have considered two-photon processes, next we will consider the effect of a second photon simultaneously interacting with the centre.

1.4C SECOND-HARMONIC GENERATION

By increasing the intensity, and consequently the number of photons simultaneously traversing an optically nonlinear medium, mechanisms involving more instantaneous interaction events become more noticeable in the output signal. Primarily through the involvement of a second photon annihilation, such a process has a nonlinear dependence on the beam intensity and is therefore known as a nonlinear optical process.

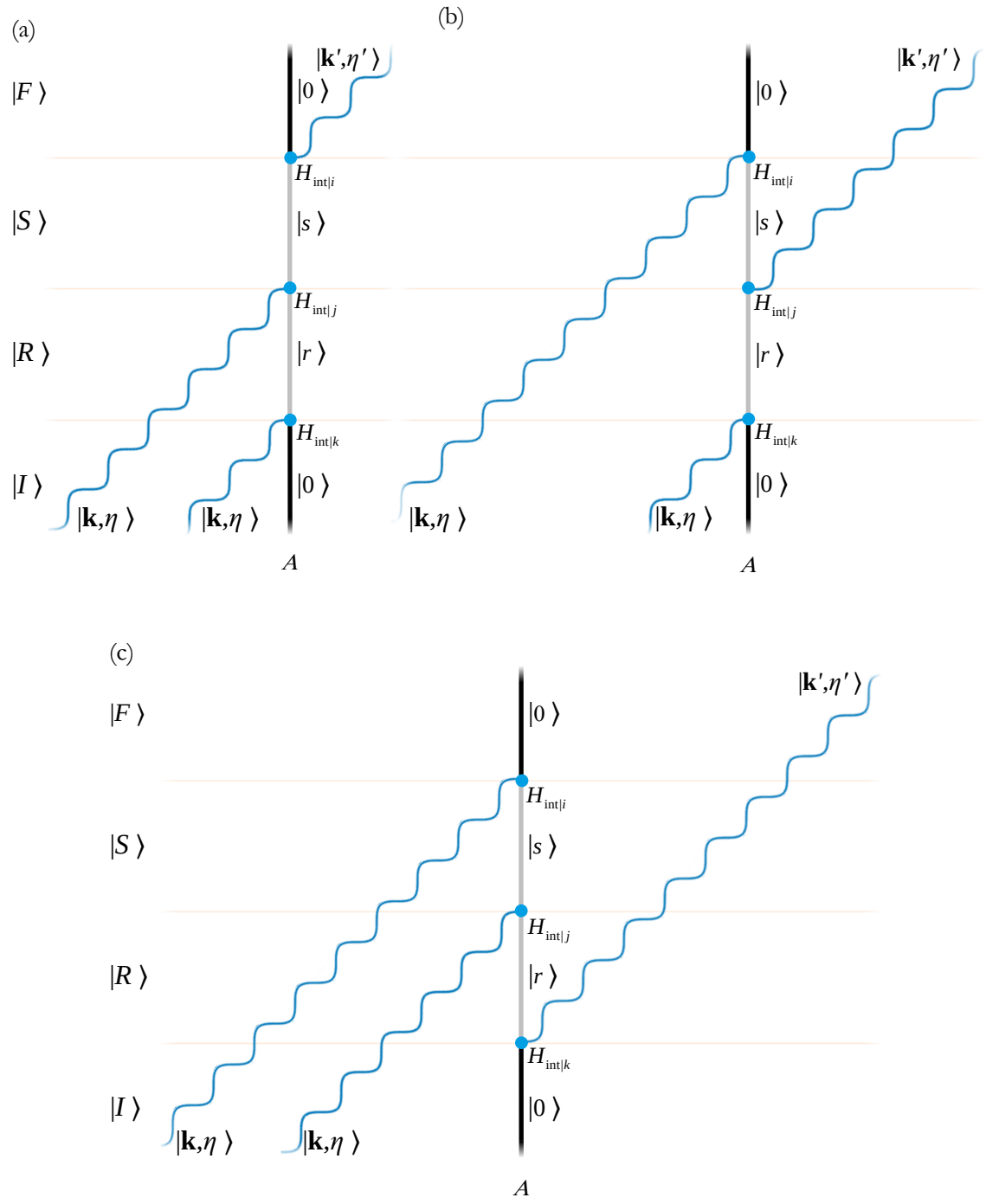

Figure 4: Three Feynman diagram representations for the distinct time-orderings associated with second-harmonic generation: (a) the photon annihilation operators j and k precede the photon creation i; (b) the creation event straddles the two annihilation events; (c) the creation event precedes both the annihilation events. In all cases the scatterer begins and completes the process in its ground state 0 traversing two intermediary states, r and s. Moreover, the emitted photon conveys the energy sum of the two annihilated photons: $\hbar ck' = \hbar ck + \hbar ck$, in each schematic.

For a process returns molecules to their ground state this case accommodates two possibilities – the generation of sum-frequency or second-harmonic output. Both are primarily considered to involve E1[3] mechanisms. The latter form of interaction, widely employed in condensed phase media that support collective, coherent forward scattering of monochromatic light, is generally known as second harmonic generation (SHG). In such a case, the total energy and momentum for both the molecule and radiation are conserved and as such is a parametric process that will be introduced. To begin, the more general case of,

$$2|\mathbf{k}| = |\mathbf{k}'| \ . \tag{1.4.20}$$

For three events, there are six achievable orders. Figure 4 displays three out of the six, each of the three displayed have a partner diagram in which the two incident photons are interchanged. The reason that they can both be encapsulated in one diagram is that both radiation modes are identical and therefore indistinguishable. All time orderings can be collectively represented by the state sequence method [14], which is based on the Hasse combinatorial diagram [15]. Figure 5 displays a tabulated variant on this method, which aids the reader to regard all unique pathways connecting the initial to the final state. This can be obvious in processes such as these, however it can prove invaluable when considering other, more complex mechanisms, such as the six-photon considered in chapter 4.

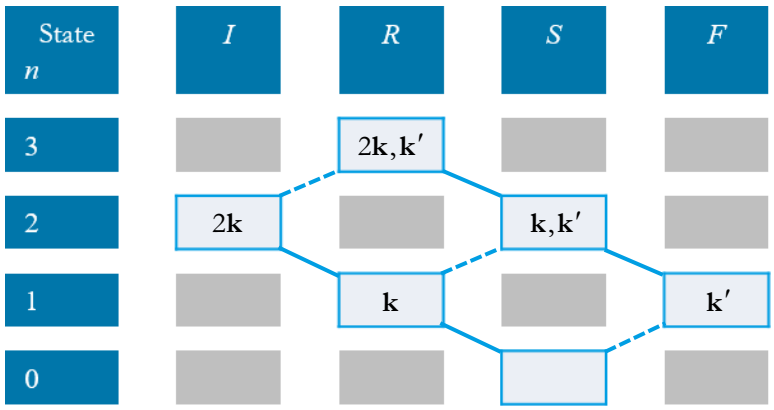

Figure 5: A tabular state sequence diagram depicts all the pathways for SHG, with each row representing a state of consecutive photon occupying number, n. Columns denote successive system states that each time-ordering progress through. Any pair of radiation states linked by a line represent interactions between the molecule and the radiation mode. The inclined dashed lines represent a photon creation event, while the declining solid lines represent a photon annihilation event.

The matrix element for this system is,

$$M_{FI}^{(\mathrm{E1})^3} = -\frac{\mathrm{i}}{2}\left(\frac{\hbar ck}{\varepsilon_0 V}\right)^{3/2}\sqrt{n(n-1)}\bar{e}_i' e_j e_k \beta_{ijk} \ , \tag{1.4.21}$$

with a hyperpolarisability tensor defined as,

$$\beta_{ijk} = \sum_{r,s}\left\{\frac{\mu_i^{0s}\mu_j^{sr}\mu_k^{r0}}{\left[E_{r0}-2\hbar ck\right]\left[E_{s0}-\hbar ck\right]} + \frac{\mu_j^{0s}\mu_i^{sr}\mu_k^{r0}}{\left[E_{r0}+\hbar ck\right]\left[E_{s0}-\hbar ck\right]} + \frac{\mu_j^{0s}\mu_k^{sr}\mu_i^{r0}}{\left[E_{r0}+\hbar ck\right]\left[E_{s0}+2\hbar ck\right]}\right\} . \tag{1.4.22}$$

At this juncture, it is worth commenting on the summation. In the previous subsection, it was introduced that each electronic energy level is subdivided into a series of vibrational levels. These sublevels are all summed over for each and every molecular response tensor. Although, this has been largely overlooked, in the case of hyperpolarisability tensors, extensive studies of its applications have been carried out [16, 17].

The second-harmonic generation rate expression takes the following form,

$$\Gamma = \frac{\pi\hbar^2 c^3 k^3}{2\varepsilon_0^3 V^3} n(n-1)\left|\bar{e}_i' e_j e_k \beta_{ijk}\right|^2 \rho_F \ . \tag{1.4.23}$$

Equation (1.4.7) incorporating equation (1.4.20) can now be substituted in to deliver the differential scattering cross section,

$$\mathrm{d}\Gamma = \frac{\hbar c^2 k^5 \mathrm{d}\Omega}{2^2 \varepsilon_0^3 \pi^2 V^2} n(n-1)\left|\bar{e}_i' e_j e_k \beta_{ijk}\right|^2 . \tag{1.4.24}$$

As with the previous subsections, we can use (1.4.9) with the wavevector relation, equation (1.4.20), to deliver the radiant intensity,

$$I' = \frac{\hbar^2 c^3 k^6 \mathrm{d}\Omega}{2\varepsilon_0^3 \pi^2 V^2} n(n-1)\left|\bar{e}_i' e_j e_k \beta_{ijk}\right|^2 . \tag{1.4.25}$$

At this point, we must first consider the degree of second order coherence,

$$g^{(2)} = \frac{\langle n(n-1)\rangle}{\langle n\rangle^2} \ , \tag{1.4.26}$$

before utilising a modified form of equation (1.4.11), relating to the mean input mode,

$$\bar{I}_0 = \frac{\langle n\rangle \hbar c^2 k}{V} \ . \tag{1.4.27}$$

We are then able to introduce the mean beam irradiance and in turn deliver an expression for the radiant intensity of second-harmonic generation in terms of physical observables,

$$I' = \frac{g^{(2)} k^4 \bar{I}_0^2}{2c\varepsilon_0^3 \pi^2} \left| \bar{e}_i' e_j e_k \beta_{ijk} \right|^2 . \tag{1.4.28}$$

This is the single-centre result for solid state materials. In order to obtain a result that is applicable to fluid media, we must apply a rotationally average to allow for a range of orientations, the coherent form of this result is of particular interest,

$$\langle I' \rangle = \frac{g^{(2)} k^4 \bar{I}_0^2}{72c\varepsilon_0^3 \pi^2} \left| \varepsilon_{ijk} \bar{e}_i' e_j e_k \varepsilon_{\lambda\mu\nu} \beta_{\lambda\mu\nu} \right|^2 \ , \tag{1.4.29}$$

this is the result for coherent scattering. The contraction of the field vectors with the Levi-Civita tensor: $\varepsilon_{ijk} \bar{e}_i' e_j e_k = 0$. This is consistent with experiment and theory, in which randomly oriented dipoles are forbidden to produce even order harmonics to all levels of multipole approximation [18, 19]. A weak incoherent contribution does persist, which will be discussed in chapter 3.

All calculations throughout this work assume a molecule to be in its ground electronic and vibrational state for the initial – and often the final – state. Under standard conditions, the population of these states will far outweigh those of excited states and as such it is these levels in which the processes will invariably involve. Any instance of the ground state can readily be exchanged for an excited state and an appropriate transition response tensor found. There are results to show that if you first utilise a population inversion stage, to increase the occupancy of excited states, before carrying out a nonlinear process, an enhancement can be seen in the output

by an order in magnitude, or more [20]. Another method for enhancement is that of incorporating resonance effects, which will be discussed in complement 1F.

1.5 MULTICENTRE INTERACTIONS

All the processes considered in §1.4 only took into consideration the cases where a lone centre carried out the entirety of a process. However, it is conceivable that the local environment can have an electrodynamic influence on the process. Here, we will consider a nearest neighbouring centre, B coupling with the prior introduced centre of interest A. The possibility of additional interactions will be shown to modify the symmetry of the system in which scattering occurs and thus allow transitions to occur that were previously thought to be forbidden. This is particularly of interest in the case of optical centres of high symmetries, such as centrosymmetric media. In such media, it is widely known that for odd-photon numbered processes, the parity of the states must be conserved from a process in order for it to be allowed. However, the presence of a neighbouring molecule may be capable of reducing the symmetry of a centre, represented as an additional interaction linking the evolution of the centrosymmetric centre to that of its neighbour.

The method for accommodating an electronic coupling between two centres, and thus elicit such an effect as mentioned above, is by accommodating a number of virtual photon exchanges between A and B, thereby entwining the evolution of each centres world-line [21-23]. Virtual photons are inherently transverse, unobservable and capable of subverting energy conservation for time scales spanned by a process; this is achieved by borrowing the requisite energy from the vacuum and returning it before the process completes and does not invalidate the energy-time uncertainty principle $\Delta E \Delta t \geq \hbar/2$.

All terms present in the interaction Hamiltonian, equation (1.2.16), are only capable of operating on exactly one molecular and one radiative state. As such a further operator is required to mediate the interaction between two molecules:

$$V_{ij}(k,\mathbf{R}) = \frac{\mathrm{e}^{\mathrm{i}kR}}{4\pi\varepsilon_0 R^3}\left\{\left(\delta_{ij} - 3\hat{R}_i\hat{R}_j\right) - \mathrm{i}kR\left(\delta_{ij} - 3\hat{R}_i\hat{R}_j\right) - (kR)^2\left(\delta_{ij} - \hat{R}_i\hat{R}_j\right)\right\} . \quad (1.5.1)$$

This is known as the retarded dipole-dipole interaction and in this form, is limited in application to E1 transition (V-tensor). It emerges following the sum over all virtual photon wavevectors and polarisations. In actuality, the detail for all processes differ, however, it can be proven to be the general form applicable to all (E1) permitted processes. The equation above has three familiar prefactors: the phase factor (see complement 1B), Coulomb's constant as well as cubic dependence on the inter-centre distance, R. By inspecting the respective distance dependences present in each of the terms, it is immediately apparent that as you approach the limit $kR \to 0$, the Coulombic term will dominate, this is referred to as the near-zone and often it is useful to consider the near-field approximation alone:

$$V_{ij}(0;\mathbf{R}) = \frac{1}{4\pi\varepsilon_0 R^3}\left(\delta_{ij} - 3\hat{R}_i\hat{R}_j\right) , \quad (1.5.2)$$

Similarly, the far-field limit can also be taken, in which the final term in equation (1.5.1) dominates, analogous to that of the inverse square law. However, this work is interested in single-centre and nearest neighbour coupling and as such the retarded dipole-dipole coupling is cast in near-field approximation.

1.6 OPTICAL ANGULAR MOMENTUM

1.6A SPIN ANGULAR MOMENTUM

It has already been mentioned that light has the property of spin polarisation, this is a form of optical angular momentum known as spin angular momentum. This is a property that is not limited to a collective beam segment, but observable on a single photon level. Each photon is in fact capable of conveying not only angular momentum associated with the polarisation, but a further component associated with the field distribution [1]. Both components are found in the optical angular momentum operator [24], which is often presented as:

$$\mathbf{J} = \varepsilon_0 \int \mathbf{r} \times \left\{\mathbf{e}(\mathbf{r},t) \times \mathbf{b}(\mathbf{r},t)\right\} . \mathrm{d}^3\mathbf{r} , \quad (1.6.1)$$

The integrand encapsulates the vector product of the electric and magnetic fields and can be recast as the sum of two angular momentum operators;

$$\mathbf{S} = \varepsilon_0 \int \{\mathbf{e}(\mathbf{r},t) \times \mathbf{a}(\mathbf{r},t)\}.\mathrm{d}^3\mathbf{r} \ , \tag{1.6.2}$$

$$\mathbf{L} = \varepsilon_0 \int e_i(\mathbf{r},t)\{\mathbf{r} \times \nabla\} a_i(\mathbf{r},t).\mathrm{d}^3\mathbf{r} \ . \tag{1.6.3}$$

the SAM and orbital angular momentum (OAM), respectively. From here, it is useful to consider the SAM operator as a mode expansion, similar in form to equation (1.2.15):

$$\mathbf{S}_{\mathrm{rad}} = \mathrm{i}\hbar \sum_{\mathbf{k},\eta,\eta'} \left(a_{\mathbf{k}}^{\dagger(\eta')} a_{\mathbf{k}}^{(\eta)} + \frac{1}{2}\delta_{\eta\eta'} \right) \left(\mathbf{e}_{\mathbf{k}}^{(\eta)} \times \bar{\mathbf{e}}_{\mathbf{k}}^{(\eta')} \right) \ , \tag{1.6.4}$$

the two operators support the pair of eigenstates for circular polarisation, displayed as equations (1.2.10) and (1.2.11). The spin angular momentum operator reduces to:

$$\mathbf{S}_{\mathrm{rad}} = \hbar \sum_{\mathbf{k}} \left(a_{\mathbf{k}}^{\dagger(\mathrm{L})} a_{\mathbf{k}}^{(\mathrm{L})} - a_{\mathbf{k}}^{\dagger(\mathrm{R})} a_{\mathbf{k}}^{(\mathrm{R})} \right) \ , \tag{1.6.5}$$

which restricts the spin states to either $\pm\hbar$ per photon, the sign indicative of the handedness of the circulation.

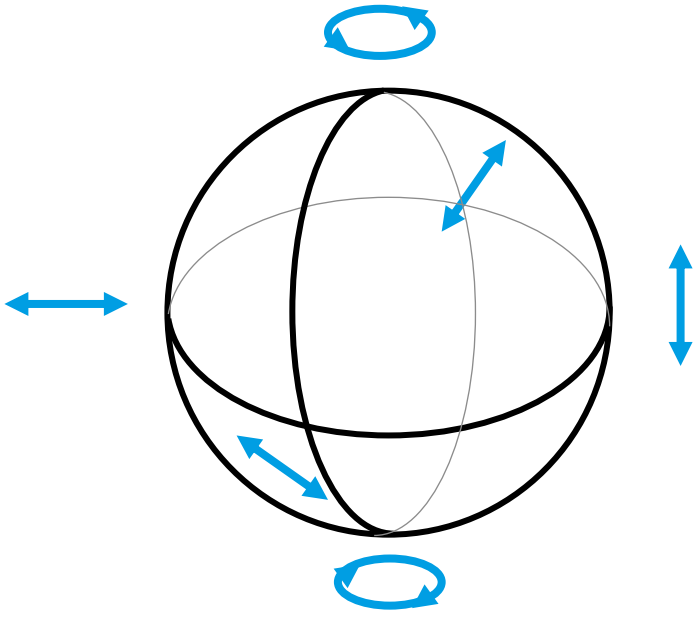

Figure 6: Poincaré sphere, the two poles representing the two pure eigenstates of spin polarisations. Linear superpositions of these will form all other polarisations: the linear modes line up around the equator and elliptical the remaining regions are dedicated to elliptical polarisations.

1.6B ORBITAL ANGULAR MOMENTUM

Up until now, we have covered two properties associated with each photon, spin and wavevector, these are known as degrees of freedom. Next we will consider the OAM of a photon, introduced as a second distinct angular momentum quality each photon can accommodate, seen in equation (1.6.3). This will be shown to provide new degrees of freedom and also display increased variability in the values accessible to these degrees of freedom.

In order to do this, we must first consider the source-free Maxwell equations in paraxial form;

$$\nabla_{\perp}^{2} u + 2ik\frac{\partial}{\partial z}u = 0 \ , \tag{1.6.6}$$

where $\nabla_{\perp}^{2} = \left(\partial^2/\partial x^2 + \partial^2/\partial y^2\right)$ is the transverse Laplacian operator acting on a transverse field, of amplitude $u(x,y,z)$. Under this regime all ray angles are assumed to be less than the small angle approximation *i.e.* $\theta < 12^{o}$. Considering the dimensions associated with rays of light, paraxial optics often employs cylindrical polar coordinates and so takes the form of;

$$\left[\frac{1}{r}\frac{\partial}{\partial r} + \frac{\partial^2}{\partial r^2} + \frac{1}{r}\frac{\partial^2}{\partial \phi^2} + 2ik\frac{\partial}{\partial z}\right]u_{l,p}(r,\phi,z) = 0 \ , \tag{1.6.7}$$

where z is along the propagation axis, r is the radial displacement in the transverse plane and ϕ the azimuthal projection onto the transverse plane. There are several solutions to these equations, the most widely studied amplitude distribution is for Laguerre-Gaussian (LG) light;

$$u_{l,p}^{LG}(r,\phi,z) = \frac{C_{|l|}^{p}}{w(z)}\left(\frac{\sqrt{2}r}{w(z)}\right)^{|l|} e^{\frac{-r^2}{w^2(z)}} L_{|l|}^{p}\left(\frac{2r^2}{w^2(z)}\right) e^{-il\phi} e^{-i(2p+|l|+1)\arctan\left(\frac{z}{z_R}\right)} e^{-\frac{ikr^2 z}{2\left(z^2+z_R^2\right)}} \ , \tag{1.6.8}$$

where, $C_{|l|}^{p}$ is the normalisation constant for light of topological charge $\pm l$ and radial index p [25], $w(z)$ is the greatest r for which the field amplitude falls to e^{-2} of maximal value, the penultimate exponential represents the Gouy phase and z_R is the Rayleigh range. The terms have been separated into meaningful segments to aid with simplification.

A Rayleigh range of several metres can be achieved in experimental setups, hence $z_R \gg z$, this then allows us to say $w(z) \to w_0$, which becomes the Gaussian beam-waist, the final pair of

exponentials in equation (1.6.8) tend to 1 as their exponents tend to 0. Selecting the radial distribution u to be independent of z, this is now expressible as,

$$u_{l,p}^{LG}(r,\phi) = f_{l,p}(r)\mathrm{e}^{-\mathrm{i}l\phi} \ , \tag{1.6.9}$$

where,

$$f_{l,p}(r) = \frac{C_{|l|}^{p}}{w_0}\left[\frac{\sqrt{2}r}{w_0}\right]^{|l|} \mathrm{e}^{\frac{-r^2}{w_0^2}} L_{|l|}^{p}\left(\frac{2r^2}{w_0^2}\right) . \tag{1.6.10}$$

$L_{|l|}^{p}$ is the associated Laguerre polynomial solutions of indices l and p, see complement 1H. Multiplying the vector potential by the radial distribution, equations (1.2.4) and (1.6.9) respectively, we can now re-express this and the derivative fields for LG modes:

$$\mathbf{a}^{\perp}(\mathbf{r},t) = \sum_{\mathbf{k},\eta,l,p}\sqrt{\frac{\hbar}{2c\varepsilon_0 kV}}\left[\mathbf{e}_{\mathbf{k},l,p}^{(\eta)}a_{\mathbf{k},l,p}^{(\eta)}f_{l,p}(r)\mathrm{e}^{\mathrm{i}(\mathbf{k}.\mathbf{r}-l\phi)} - \overline{\mathbf{e}}_{\mathbf{k},l,p}^{(\eta)}a_{\mathbf{k},l,p}^{\dagger(\eta)}\overline{f}_{l,p}(r)\mathrm{e}^{-\mathrm{i}(\mathbf{k}.\mathbf{r}-l\phi)}\right] , \tag{1.6.11}$$

$$\mathbf{d}^{\perp}(\mathbf{r},t) = \mathrm{i}\sum_{\mathbf{k},\eta,l,p}\sqrt{\frac{\varepsilon_0\hbar ck}{2V}}\left[\mathbf{e}_{\mathbf{k},l,p}^{(\eta)}a_{\mathbf{k},l,p}^{(\eta)}f_{l,p}(r)\mathrm{e}^{\mathrm{i}(\mathbf{k}.\mathbf{r}-l\phi)} - \overline{\mathbf{e}}_{\mathbf{k},l,p}^{(\eta)}a_{\mathbf{k},l,p}^{\dagger(\eta)}\overline{f}_{l,p}(r)\mathrm{e}^{-\mathrm{i}(\mathbf{k}.\mathbf{r}-l\phi)}\right] , \tag{1.6.12}$$

$$\mathbf{b}(\mathbf{r},t) = \mathrm{i}\sum_{\mathbf{k},\eta,l,p}\sqrt{\frac{\hbar k}{2c\varepsilon_0 V}}\left[\mathbf{b}_{\mathbf{k},l,p}^{(\eta)}a_{\mathbf{k},l,p}^{(\eta)}f_{l,p}(r)\mathrm{e}^{\mathrm{i}(\mathbf{k}.\mathbf{r}-l\phi)} - \overline{\mathbf{b}}_{\mathbf{k},l,p}^{(\eta)}a_{\mathbf{k},l,p}^{\dagger(\eta)}\overline{f}_{l,p}(r)\mathrm{e}^{-\mathrm{i}(\mathbf{k}.\mathbf{r}-l\phi)}\right] . \tag{1.6.13}$$

At this point, it is worth emphasising that OAM associated with a photon is not limited to a single unit of two handedness, but can take any value from the real integer set, $l \in \mathbb{Z}$ and corresponds to $\pm l\hbar$ per photon.

Each mode is orthogonal subject to the following integral;

$$\int_0^{\infty} f_{l,p}(r)\, f_{l,p'}(r) r.\mathrm{d}r = A_{l,p}^2 w_0^2 \delta_{pp'} \ , \tag{1.6.14}$$

where $A_{l,p}$ is a normalisation constant, in the case of LG modes it is commonly chosen to be, $A_{l,p} = 1/2$ for all combinations of indices l and p. This orthogonality quality, should permit the complete separation of each mode from all others present in a beam. Unfortunately, so far incomplete modal orthogonality for different l values is evident in the results of most experiments [26, 27]. Imperfections are also apparent in recent experiments on the

multiplication of OAM values [28]. These imperfections could be arising from experimental error; however, a fundamental limit of quantum character associated with the photon number and phase uncertainty relation [3], may also be a factor. If all modes were achievably separable, the impact on data communication technologies would be revolutionary. With such wide-ranging degrees of freedom, far surpassing that of current binary infrastructure.

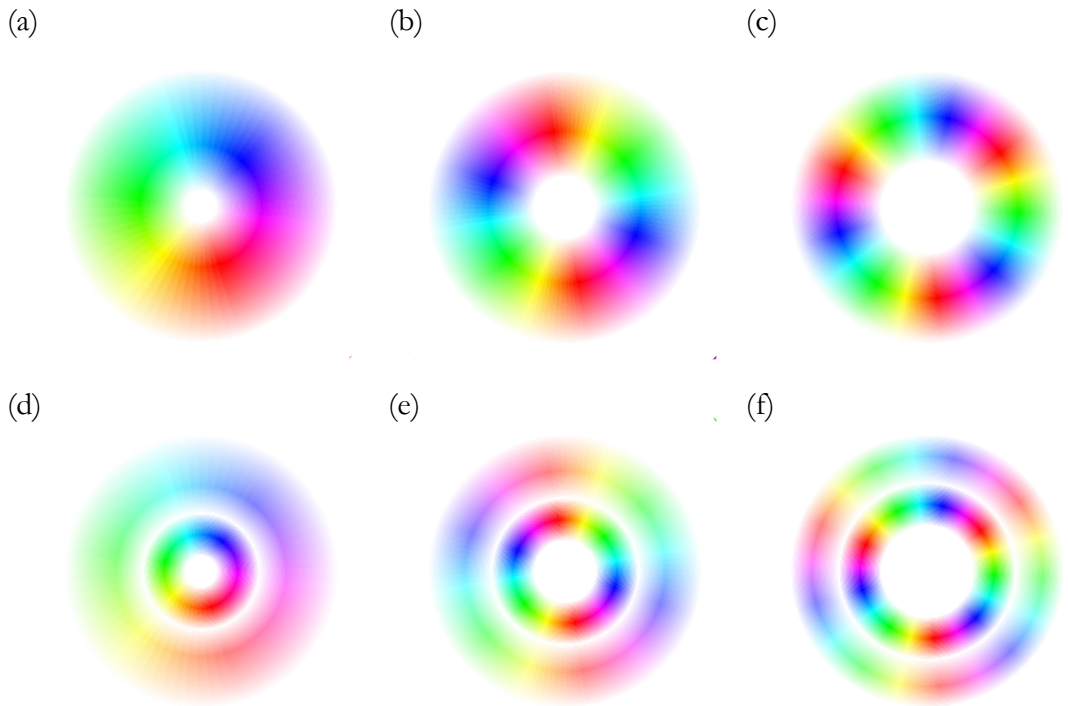

Figure 7: A series of simulations depicting the phase progression of increasing topological charge from left-to-right for the first two values for the radial index, explicitly: (a) $l=1, p=0$; (b) $l=2, p=0$; (c) $l=3, p=0$; (d) $l=1, p=1$; (e) $l=2, p=1$; (f) $l=3, p=1$. The phase cycles through $2\pi l$ [c] the intensity distribution has been overlaid, where white represents zero-intensity in each case.

OAM beams are not limited in application to information communication technology. They have proven their worth in optical manipulations, [29-33], where the capacity to exert a far greater torque than a regular circularly polarized beam has earned the technique the name 'optical spanners (wrench)' [34-37]. There are also numerous methods utilizing structured light in imaging applications and edge contrast enhancement [38], for example.

Here, a set of orthogonal LG solutions for the paraxial source-free Maxwell equations are expressed. Hermite-Gaussian are closely related and are formable from LG modes and vice-versa [39], for a given solution they both form their own special case of Ince-Gaussian modes. Many other forms of wavefront modification can be deployed to produce these modes, for example by passage through pitch-fork holograms [40, 41], *q*-plates [42], hyperbolic metamaterials [43], spiral phase plates [44]. The most widely deployed by virtue of its dynamic control modification are spatial light modulators [45, 46]. In the final chapter, a theoretical method for the direct generation of OAM light will be explored.

1.6C POYNTING VECTOR

It is well known that light has a momentum quality to it, this is most commonly associated with radiation pressure, such as the force exerted on an irradiated surface. Initially, the radiation pressure was thought to be exerted solely in the direction of propagation, this is shown by considering the radiation flux, $\mathcal{S}$, known as the Poynting vector:

$$\mathcal{S} = c^2 \varepsilon_0^2 \mathbf{d}^{\perp}(\mathbf{r},t) \times \mathbf{b}(\mathbf{r},t) \ , \tag{1.6.15}$$

is the microscopic source-free form. Evidently the cross product of two transverse vectors will deliver a vector in the wavevector direction. However, light with a nonzero topological charge twists the transverse wavefront for the beam, likened to the wobble seen in a spinning plate. Now, the cross product of the field vectors, shifts off of the direction of propagation forming a corkscrew around the beam axis as it evolves over time: the Poynting vector therefore displays an azimuthal component [47]. This is supported by the intensity depicted in Figure 7, where the maximal intensities lies just away from the core of the beam and leaves a singular axis down the centre. The phase maps seen in that figure circulate as the beam evolves, selecting one colour, contours of constant phase can be drawn, as displayed in Figure 8.

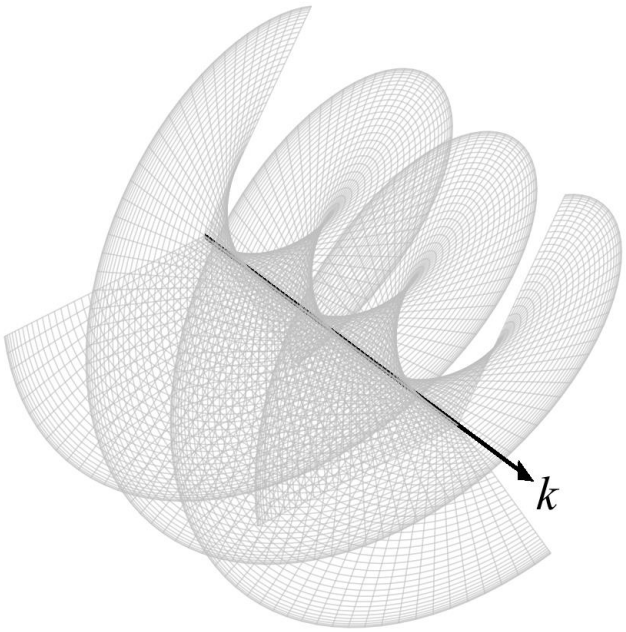

Figure 8: Procession in wavefront for an LG beam with $l = 3$ over the course of three wavelengths, depicted as three interleaved helices, each representing a surface of constant phase.

1.7 TIMELINE OF MILESTONES

A timeline has been laid out in Table 1, marking the key contributions to the fields that were required to carry out this research. Any work that occurred after the first journals were produced has been included, in this case, the first entry is Newton. Prior to this there were many wide-ranging ideas, in particular, the field of optics was largely bifurcated until the recognition of the dual wave-particle nature for light was acknowledged at the turn of the 20th century.

Table 1: A timeline of key contributions that have led to the current field of research.

Year	Contributors	Description
1687	Newton	The basis for Newtonian mechanics was produced [48].
1811	Lagrange	The birth of Lagrangian mechanics: a means of describing a system by then energies exchanged within it [49].
1820	Oersted	Showed that electric current was capable of deflecting magnets [50].
1832	Faraday	Demonstrated that moving magnets generated electric current [51].

1833	Hamilton	The inception of Hamiltonian mechanics: a reformulation on Lagrangian mechanics, often synonymised with the total energy of a system [52].
1865	Maxwell	A dynamical theory for electromagnetic fields was assembled, following key contributions from Ampere, Coulomb, Faraday, Franklin and Planck [5].
1884	Poynting	Derived the energy flux density for an electromagnetic field, which is now named after him [53].
1888	Hertz	Optics became integrated with electromagnetism [54].
1901	Lebedev	First experimental confirmation of Maxwell's theory for electromagnetism [55].
1901	Planck	It was suggested that electromagnetic radiation could take the form of discrete packets of energy, in the course of his work on black-body radiation [56].
1905	Einstein	An explanation for the photoelectric effect was presented, in which the concept of discrete units of electromagnetic wave-packets was introduced [57].
1905	Einstein	In the same year a first attempt at the theory governing relativistic effects was produced [58].
1909	Einstein	Work on radiation fluctuations was the start of a statistical description for photons [59].
1909	Taylor	A low intensity form of two the double-slit experiment was performed, almost reducing it down to the single photon level [60].
1909	Poynting	A light beam was first suggested to be capable of conveying angular momentum [61].
1916	Einstein	Eleven years after the inception of relativity, a theory applicable to particles and their interactions was published, known as general relativity [11].
1918	Noether	Several hallmark conservation theories were established, relating to momenta and energy [62].

1925	Laporte Meggers	Set out transition parity constraints for particles with an inversion symmetry element [63].
1926	Lewis	The term "photon" was coined [64].
1926	Schrödinger	The evolution of states of a system were cast under quantum theory [65].
1927	Dirac	Dirac equation: reformulated Schrödinger's wave equation to accommodate relativistic effects and in turn predicted the existence of antimatter. He was later awarded the Nobel prize in 1933 [66].
1930	Oppenheimer	Subsequent to Dirac's contribution, the possible existence of a positron was determined [67].
1932	Fermi	Named the now famous "golden rule no.2" and displayed the computability of any light-matter interaction [12].
1932	Darwin	Light was suggested to be capable of generating quantities of torque in excess of that generated by the single unit attributed to spin [68].
1936	Beth	Light conveyance of angular momentum was first observed, by a circularly polarised beam and its reflection imparting a torque onto a half-waveplate [69].
1937	Bloch Nordsieck	Limitations of computations in excess of first order perturbation theory for light and charged particles demonstrated [70].
1939	Weisskopf	Independently demonstrated computational limitations, that weren't overcome until developments were made in relativistic QED [71].
1946	Gabor	The origin of holographic techniques, a widely deployed method of wavefront modification [72].
1946	Tomonaga	Formulation of relativistic quantum field theory, one of three to earn a share in the 1965 Nobel prize in Physics [73].
1947	Lamb Retherford	A discrepancy in magnitude of two energy levels $\left({}^2S_{1/2} \text{ and } {}^2P_{1/2}\right)$ of atomic Hydrogen were detected [6].
1947	Bethe	Performed the first calculation that accounted for the shift measured in atomic Hydrogen [74].

1948	Feynman	The inception of quantum electrodynamical is often attributed to this work, earning him a share of the 1965 Nobel prize in Physics. He also introduced the common diagrammatic scheme to analyse processes [13].
1948	Schwinger	A third researcher to contribute to the inception of quantum electrodynamical formulation, which later earned him a share in the joint 1965 Nobel prize in Physics [75].
1948	Schwinger	Applied quantum electrodynamic theory to prove the existence of an electrons magnetic moment [6].
1948	Casimir Polder	Both the Casimir effect and Casimir-Polder force [8, 9].
1949	Dyson	Combined the radiation theories of Feynman, Schwinger and Tomonaga [76].
1959	Power Zienau	Established the nonrelativistic formulation for molecular quantum electrodynamics [77].
1959	Wigner	Application for group theory to explain spectroscopic selection rules [78].
1960	Maiman	The first operational laser pulse was fired [79].
1961	Franken, *et al.* Terhune, *et al.*	A first two independent experimental demonstrations of a nonlinear optical process, second-harmonic generation, were made [80, 81].
1963	Glauber	Non-classical statistical explanation of light states [82].
1974	Nye Berry	The roots of singular optics can be traced back to here, when the theory for three interfering waves resulted in a point of indeterminate phase [83].
1983 -93	Power Thiru.	A series of papers were released and are widely considered as the cornerstone of molecular quantum electrodynamics [84-88].
1990	Andrews	The incorporation of irreducible Cartesian tensors calculus to molecular symmetry characterisation [89].
1990	Bazhenov, *et al.*	Experimental identification of laser light with a singular axis [40].

1992	Allen, *et al.*	Laser light with a Laguerre-Gaussian intensity distribution is found to convey a well-defined orbital angular momentum [90].
1993	Basisitiy, *et al.*	The first identification of a nonlinear optical process with singular beams, a second-harmonic emission [91].
1996	Dholakia, *et al.*	An analysis of second-harmonic generation with Laguerre-Gaussian light was presented [92].
1997	Bouwmeester, *et al.*	The first experimental evidence for the teleportation of photon states [93].
2002	Romero, *et al.*	The complete formulation for singular light was laid out under QED theory [94].

COMPLEMENT 1A: PARITY CONSIDERATIONS

This complement will provide an additional insight into the nature of the vector potential, equation (1.2.4) as well as its derivative fields, equations (1.2.6) and (1.2.8). First consideration, the vector potential is intrinsically Hermitian. There are two forms of parity transformation, both of which are of interest and to be investigated here: space-inversion and time-inversion. The former is obtainable by a spatial parity transformation, P_s, for all of the spatial coordinates, resulting in a reversal in sign of **r**, **e** and **k**:

$$\mathbf{a}^{\perp}(\mathbf{r}) \xrightarrow{P_s} \sum_{\mathbf{k},\eta} \sqrt{\frac{\hbar}{2\varepsilon_0 ckV}} \left[-\mathbf{e}_{-\mathbf{k}}^{(\eta)} a_{-\mathbf{k}}^{(\eta)} \mathrm{e}^{\mathrm{i}(-\mathbf{k})\cdot(-\mathbf{r})} + \overline{\mathbf{e}}_{-\mathbf{k}}^{(\eta)} a_{-\mathbf{k}}^{\dagger(\eta)} \mathrm{e}^{-\mathrm{i}(-\mathbf{k})\cdot(-\mathbf{r})} \right], \tag{1A.1}$$

and thereby produces a reversal in the sign of the overall vector.

With regard to time-inversion, P_t, this operation reverses the sign of **k** and takes the complex conjugate of all numbers;

$$\mathbf{a}^{\perp}(\mathbf{r}) \xrightarrow{P_t} \sum_{\mathbf{k},\eta} \sqrt{\frac{\hbar}{2\varepsilon_0 ckV}} \left[\overline{\mathbf{e}}_{-\mathbf{k}}^{(\eta)} a_{-\mathbf{k}}^{(\eta)} \mathrm{e}^{\mathrm{i}(-\mathbf{k})\cdot\mathbf{r}} - \mathbf{e}_{-\mathbf{k}}^{(\eta)} a_{-\mathbf{k}}^{\dagger(\eta)} \mathrm{e}^{-\mathrm{i}(-\mathbf{k})\cdot\mathbf{r}} \right]. \tag{1A.2}$$

Since the sum over the dummy variable **k** covers all space, it encapsulates the region pertaining to $-\mathbf{k}$. Furthermore, by deploying the relation $\overline{e}_{-\mathbf{k}}^{(\eta)} = -e_{\mathbf{k}}^{(\eta)}$, we can discern that the vector potential is also of odd parity in time.

The expressions for the derivative fields, like their parent equation, are both Hermitian. The methods for obtaining each of the expressions can give away the ensuing parity for each of them. Firstly, the displacement field operator,

$$\mathbf{d}^{\perp}(\mathbf{r}) \xrightarrow{P_s} \mathrm{i} \sum_{\mathbf{k},\eta} \sqrt{\frac{\varepsilon_0 \hbar ck}{2V}} \left[-\mathbf{e}_{-\mathbf{k}}^{(\eta)} a_{-\mathbf{k}}^{(\eta)} \mathrm{e}^{\mathrm{i}(-\mathbf{k})\cdot(-\mathbf{r})} + \overline{\mathbf{e}}_{-\mathbf{k}}^{(\eta)} a_{-\mathbf{k}}^{\dagger(\eta)} \mathrm{e}^{-\mathrm{i}(-\mathbf{k})\cdot(-\mathbf{r})} \right], \tag{1A.3}$$

$$\mathbf{d}^{\perp}(\mathbf{r}) \xrightarrow{P_t} \mathrm{i} \sum_{\mathbf{k},\eta} \sqrt{\frac{\varepsilon_0 \hbar ck}{2V}} \left[\overline{\mathbf{e}}_{-\mathbf{k}}^{(\eta)} a_{-\mathbf{k}}^{(\eta)} \mathrm{e}^{\mathrm{i}(-\mathbf{k})\cdot\mathbf{r}} - \mathbf{e}_{-\mathbf{k}}^{(\eta)} a_{-\mathbf{k}}^{\dagger(\eta)} \mathrm{e}^{-\mathrm{i}(-\mathbf{k})\cdot\mathbf{r}} \right], \tag{1A.4}$$

has odd spatial and even time parity.

The magnetic field operator has the reverse of that:

$$\mathbf{b}(\mathbf{r}) \xrightarrow{P_s} \mathrm{i}\sum_{\mathbf{k},\eta}\sqrt{\frac{\hbar k}{2c\varepsilon_0 V}}\left[\mathbf{b}_{-\mathbf{k}}^{(\eta)}a_{-\mathbf{k}}^{(\eta)}\mathrm{e}^{\mathrm{i}(-\mathbf{k})\cdot(-\mathbf{r})} - \overline{\mathbf{b}}_{-\mathbf{k}}^{(\eta)}a_{-\mathbf{k}}^{\dagger(\eta)}\mathrm{e}^{-\mathrm{i}(-\mathbf{k})\cdot(-\mathbf{r})}\right], \tag{1A.5}$$

$$\mathbf{b}(\mathbf{r}) \xrightarrow{P_t} \mathrm{i}\sum_{\mathbf{k},\eta}\sqrt{\frac{\hbar k}{2c\varepsilon_0 V}}\left[\overline{\mathbf{b}}_{-\mathbf{k}}^{(\eta)}a_{-\mathbf{k}}^{(\eta)}\mathrm{e}^{\mathrm{i}(-\mathbf{k})\cdot\mathbf{r}} - \mathbf{b}_{-\mathbf{k}}^{(\eta)}a_{-\mathbf{k}}^{\dagger(\eta)}\mathrm{e}^{-\mathrm{i}(-\mathbf{k})\cdot\mathbf{r}}\right], \tag{1A.6}$$

thus, displaying even spatial and odd time parity.

With regard to the higher order multipoles, appearing as equations (1.2.17) – (1.2.19), each electric multipole $(\mathrm{E}n)$ follows the pattern of $(-1)^n$ for spatial parity and all are time-even. Although not the subject of this work, the corresponding magnetic multipole $(\mathrm{M}n)$, alternate in spatial parity $(-1)^{n-1}$, when compared with the series for $(\mathrm{E}n)$, again all are time-odd. As such, the overall spatial and temporal parity of the interaction Hamiltonian remains even throughout.

In the case of LG modes, introduced in §1.6, the temporal parity for both the displacement and magnetic field operators, equations (1.7.14) and (1.7.15), remain unchanged. However, in the case of the spatial parity, the former becomes $(-1)^{l+1}$ and $(-1)^l$ for the latter. Moreover, since light without an OAM character is equivalent to saying $l = 0$, the above results hold.

COMPLEMENT 1B: MOLECULAR SYMMETRY

For the purposes of considering the selection rules engaged by a process, any symmetry properties associated with the response tensors must initially be identified. There are two sets of symmetries that will be considered here: the first is where two interactions both involve same radiation mode and invariably the same photon operator; the second arises where two interactions can, to a first approximation, be considered interchangeable. The former set can be found by interrogating the response tensors. Two interaction indices (each connecting any pair of adjacent states) are said to be symmetric, if they are interchanged and the original tensor is regenerated. Moreover, all intermediary states are arbitrarily defined and as such any pair of states can be freely interchanged without altering the regarded system.

To pursue the latter form of symmetry, let's first consider Rayleigh scattering, §1.4A. Here, linear polarisabilities are generated from a product of two electronic transition moments connecting the same pair of states, this is an exceptional case where index symmetry is guaranteed. Now, if we consider Raman scattering, §1.4B, the electronic transition energies dominate over any vibrational constituent and to a strong approximation the vibrational transition can be neglected; this is analogous to the Placzek treatment for single-centre scattering away from resonance. From this we can infer that the interaction indices are therefore symmetric, as such this is an example of the latter group of symmetry introduced.

The most expedient method to home in on the symmetry associated with a process is by resolving the molecular response tensor into irreducible Cartesian tensors, all of which have known symmetry behaviours. Under this method, a response tensor of rank, n, is expressed as a sum of irreducible tensors each holding a number of the total parameters, P, expressible for the system,

$$P = \sum_{j=0}^{n} N_n^{(j)} \left(2j+1\right) . \tag{1B.1}$$

Here, $N_n^{(j)}$ is the multiplicity of weight j, whose natural tensors will always have a number of parameters equal to $2j+1$, where $\left(j \le n\right) \in \mathbb{N}_0$, with transformation properties of a rank j

tensor. It follows that $j = 0$ weights transform as a scalar and therefore always transforms under the totally symmetric representation of the molecular point group. Moreover, $j = n$ weights have the transformation properties of a tensor of rank n that is symmetric and traceless with respect to every pair of indices, and is known as a *natural tensor*. In all instances $N_n^{(n)} \equiv 1$.

A selection of tensors, alongside the number of irreducible tensors they can be decomposed into, are all displayed in Table 2. The list of tensors is not exhaustive, but covers all of the tensor representations considered throughout this work. The rank (n) of the process corresponds to the number of Greek subscripts attached to a tensor and in turn correspond to the number of photon-molecule interactions engaged in the course of the process. The parentheses denote index symmetry across the highlighted indices. This will always represent an increase in the symmetry of the system and therefore correspond to less irreducible weights [89].

Table 2: Selected irreducible weights for an arbitrary Cartesian tensor, $\mathbf{T}$.

	P	$N_n^{(0)}$	$N_n^{(1)}$	$N_n^{(2)}$	$N_n^{(3)}$	$N_n^{(4)}$	$N_n^{(5)}$	$N_n^{(6)}$
T_{λ}	3	0	1					
$T_{\lambda\mu}$	9	1	1	1				
$T_{(\lambda\mu)}$	6	1	0	1				
$T_{\lambda\mu\nu}$	27	1	3	2	1			
$T_{(\lambda\mu)\nu}$	18	0	2	1	1			
$T_{(\lambda\mu)\nu\pi}$	54	2	3	4	2	1		
$T_{(\lambda\mu)(\nu\pi)}$	36	2	1	3	1	1		
$T_{(\lambda\mu)(\nu\pi\rho\sigma)}$	90	2	1	4	2	3	1	1

COMPLEMENT 1C: COHERENCE AND WAVE-VECTOR MATCHING

Nonlinear optical effects, by definition, require more than one photon in the vicinity of an optical centre at one time. An increased dependence on the intensity of the throughput beam then follows. In these nonlinear processes, there are techniques that can be employed to maximise the yield of the scattering process. In the case of coherent processes wave-vector matching can be deployed. A coherent process is defined as one in which the energy and momentum of the radiation states are the same immediately before and following said process. Therefore, the collective wavevector(s), $\mathbf{k}'$, of the output photon(s) must equal the collective wavevector(s), $\mathbf{k}$, of the incident photon(s) engaging in the process.

Let us consider an expression for the rate of a general process,

$$\Gamma = \frac{2\pi}{\hbar}\left|\sum_{\xi}\varepsilon_0^{-n}\chi^{(\xi)}_{\{i,j,\ldots\}}\mathrm{e}^{\mathrm{i}\Delta\mathbf{k}\cdot\mathbf{R}_\xi}\right|^2\rho_F \ , \tag{1C.1}$$

where n is representative of an n-order process, χ is the general response tensor, $\Delta\mathbf{k}$ is the wave-vector mismatch between the input and output photon(s), $\mathbf{R}_\xi$ is the position vector for centre ξ, which is introduced from the phase factor present in the matrix element and contributes to the coherence of the process.

$$\Gamma = \frac{2\pi\rho_F}{\varepsilon_0^{2n}\hbar}\sum_{\xi}\left\{\left|\chi^{(\xi)}_{\{i,j,\ldots\}}\right|^2 + \sum_{\xi'\neq\xi}\chi^{(\xi)}_{\{i,j,\ldots\}}\bar{\chi}^{(\xi')}_{\{i,j,\ldots\}}\mathrm{e}^{\mathrm{i}\Delta\mathbf{k}\cdot\mathbf{R}_{\xi\xi'}}\right\} . \tag{1C.2}$$

The first term in the curly brace will be unique for each constituent centre. It follows that this term depends linearly on the number of scatterers N and is present in all forms of scattering. The second term has a relative position dependence for each of the molecules in the exponent, and has two broad outcomes, in the first case:

$$\Delta\mathbf{k} \neq 0 \ , \tag{1C.3}$$

the matrix element is sensitive to the spatial distribution of the molecules in the assembly and there will be deconstructive interference amongst the different members of the ensemble. This

is non-forward scattering and the first term in equation (1C.2) is the sole contributor. In the second case of,

$$\Delta\mathbf{k} = 0 \ , \tag{1C.4}$$

which is position independent and as such all the scattering amplitude interfere constructively, this is the remit of forward scattering. Here, the matrix element is in fact proportional to the number of scatterers and in turn the rate has a square dependence on the number of independent scattering rates, N^2.

Note, that in equation (1C.2), there is a further way in which the exponent can be reduced to zero and that is when all molecules are lined up perpendicular to the wavevector.

In the case of LG modes, in the case of paraxial beams considered, it has been proven both theoretically and experimentally that the OAM quality is conserved separately by the radiation field [94, 95], equation (1C.1) becomes,

$$\left| \sum_{\xi}^{N} \mathrm{e}^{\mathrm{i}\left(\Delta\mathbf{k}\cdot\mathbf{R}_{\xi} + \Delta l\phi\right)} \right|^2 . \tag{1C.5}$$

When $\Delta\mathbf{k} = \Delta l = 0$, they both satisfy the conditions for wave-vector and OAM matching for both the incident and scattered light and thereby will interfere constructively. Now, considering disordered units in particular, the only term with a ξ-orientational dependence is seen in equation (1C.5). Under the matching stated, the rate will become quadratically dependent on N.

The depth of the substance investigated requires additional consideration and offers a trade-off. The more potential scatterers the light traverses, the greater the probability that the process will occur. However, if several processes occur at various depths through the material, coherence issues can come into play, this is particularly the case with harmonic signals. The phase velocity can differ for different frequencies of light, as such, judicious selection of the frequency and

$$n_{\omega'} = n_{\omega} \ . \tag{1C.6}$$

Of course, the less depth of material the less the chance of a process occurring. But at the lower limit of depth, for example a thin film, surface effects can exhibit interesting results of their own, where bulk symmetry is affected. An obvious example of this is with a material that demonstrates isotropy as a bulk, however, when it is reduced to a single layer, the collective symmetry often does not retain the same degree of symmetry. One interesting result that can exploit this feature is in the case of odd n-ordered processes, the prior requirement of parity conservation is lifted and enables such processes to be observed [63].

COMPLEMENT 1D: ROTATIONAL AVERAGING OF TENSORS

GENERAL STRUCTURE

The rate expressions developed for solid states matter are precise; however, condensed phase media require an extra layer of consideration. A crucial stage of determining the rate for such phases is accounting for the tumbling motion and thereby the range of orientations a process may be carried out. For this, the ergodic theorem can be applied: in a sufficiently large time period, the ensemble average will be equivalent to the time average for the system. The applicability here is that the time averaged result for the system is valid also for the ensemble of randomly oriented optical centres.

To carry out a rotational average, the respective frames of reference and how they are associated with each other, must first be considered. For the field vectors, the axial framework for conventional space is ideally suited, by convention these adopt the Latin indices, i_p. However, when regarding the molecular response tensor, the evolution in orientation of the molecule must be accounted for. With this in mind, it is logical to associate the axial frame with the molecule itself, Greek indices are conventionally used to distinguish these, λ_q. The two frames of reference are connected by the relation,

$$T_{i_p} = I^{(n)}_{i_p;\lambda_q} T_{\lambda_q} \ , \tag{1D.1}$$

where $p,q = \{1,2,3...n\}$. $I^{(n)}_{i_p;\lambda_q}$ takes the cosine of the angle subtending the index where $p = q$ of the space-fixed frame and molecule-fixed frame. $\left(i_p, \lambda_q\right)$ corresponds to the elements of the Euler angle matrix. $I^{(n)}_{i_p;\lambda_q}$ is rotationally invariant and hence can be expressed as a linear combination of two isotropic tensors [96-99]. For 3D space, there are two fundamental isotropic tensors Kronecker delta δ_{ij} and Levi-Civita ε_{ijk}. The parity of n invokes two different sets of linear combinations of these two tensors. Where n is even, isotropic tensors are formed of $n/2$ Kronecker deltas: $\delta_{i_1 i_2}...\delta_{i_{n-1} i_n}$; and where n is odd, the isotropic tensor is formed from one Levi-Civita and $\left(n-3\right)/2$ Kronecker deltas: $\varepsilon_{i_1 i_2 i_3}\delta_{i_4 i_5}...\delta_{i_{n-1} i_n}$.

The isotropic tensor can be split as follows,

$$I^{(n)} = \sum_{p,q} f_p^{(n)} m_{pq}^{(n)} g_q^{(n)} \quad , \tag{1D.2}$$

where f_p is a rank 1 tensor formed from all permutations for the linear combinations of isotropic tensors that acts on the field vectors, m_{pq} is a rank 2 tensor with number weightings for the permutations, finally g_q is the molecular equivalent to f_p acting on the molecular response tensor [100]. Tensor m_{pq} and therefore $I^{(n)}_{i_p;\lambda_q}$ is obtainable from an inversion operation of another matrix;

$$m^{(n)} = \left[s^{(n)} \right]^{-1} \quad , \tag{1D.3}$$

For brevity of notation the space fixed indices, $\{i_1, i_2, i_3, ...\} \to \{i, j, k, ...\}$ and similarly for the molecule-fixed indices $\{\lambda_1, \lambda_2, \lambda_3, ...\} \to \{\lambda, \mu, \nu, ...\}$.

In the introductory chapter, we first consider the rate of a process involving a centre located in a rigid structure, such as a lattice. In this complement, we consider how the ensuing rate is affected by a centre free to tumble. Evidently, not all setups accommodate a centre that abides by these limits of motion. This can occur by two means: either, the centres motion is inhibited; or, the centre is incapable of fully reorienting itself in the time segment. Both cases can be regarded as two sides of the same coin and shall be discussed here.

To begin, we shall assume that the orientation of the system is energetically favourable. The rate of a given process, as the system evolves, will be characterised by a Boltzmann factor and a trigonometric function of the intermolecular vector. In general, the leading contribution will be that of the static form, with successive orders of weightings modifying this result; the end limit will be that of the isotropic form dominating.

RANK 2

For $n = 2$, there is only one isotropic tensor of rank two, that is the Kronecker delta, therefore,

$$s^{(2)} = \delta_{ij}\delta_{ij} = 3 \ , \tag{1D.4}$$

$m^{(2)}$ would then be 3^{-1} and hence,

$$I^{(2)}_{ij;\lambda\mu} = \frac{1}{3}\delta_{ij}\delta_{\lambda\mu} \ . \tag{1D.5}$$

RANK 3

For $n = 3$, as with $n = 2$, there is just one isotropic tensor of this rank, the Levi-Civita antisymmetric tensor, which delivers,

$$s^{(3)} = \varepsilon_{ijk}\varepsilon_{ijk} = 6 \ , \tag{1D.6}$$

and it follows that,

$$I^{(3)}_{ijk;\lambda\mu\nu} = \frac{1}{6}\varepsilon_{ijk}\varepsilon_{\lambda\mu\nu} \ . \tag{1D.7}$$

RANK 4

For $n = 4$ there are three linearly independent isomers:

$$\begin{pmatrix} f_1^{(4)} \\ f_2^{(4)} \\ f_3^{(4)} \end{pmatrix} = \begin{pmatrix} \delta_{ij}\delta_{kl} \\ \delta_{ik}\delta_{jl} \\ \delta_{il}\delta_{jk} \end{pmatrix} , \tag{1D.8}$$

which combine to form the following,

$$s^{(4)} = \begin{pmatrix} 9 & 3 & 3 \\ 3 & 9 & 3 \\ 3 & 3 & 9 \end{pmatrix} , \tag{1D.9}$$

$$I^{(4)}_{ijkl;\lambda\mu\nu\pi} = \frac{1}{30}\begin{pmatrix} \delta_{ij}\delta_{kl} \\ \delta_{ik}\delta_{jl} \\ \delta_{il}\delta_{jk} \end{pmatrix}^{\mathrm{T}} \begin{pmatrix} 4 & -1 & -1 \\ -1 & 4 & -1 \\ -1 & -1 & 4 \end{pmatrix} \begin{pmatrix} \delta_{\lambda\mu}\delta_{\nu\pi} \\ \delta_{\lambda\nu}\delta_{\mu\pi} \\ \delta_{\lambda\pi}\delta_{\mu\nu} \end{pmatrix} . \tag{1D.10}$$

RANK 5

For $n = 5$ there are ten distinct isomers:

$$\begin{pmatrix} f_1'^{(5)} \\ f_2'^{(5)} \\ f_3'^{(5)} \\ f_4'^{(5)} \\ f_5'^{(5)} \\ f_6'^{(5)} \\ f_7'^{(5)} \\ f_8'^{(5)} \\ f_9'^{(5)} \\ f_{10}'^{(5)} \end{pmatrix} = \begin{pmatrix} \varepsilon_{ijk}\delta_{lm} \\ \varepsilon_{ijl}\delta_{km} \\ \varepsilon_{ijm}\delta_{kl} \\ \varepsilon_{ikl}\delta_{jm} \\ \varepsilon_{ikm}\delta_{jl} \\ \varepsilon_{ilm}\delta_{jk} \\ \varepsilon_{jkl}\delta_{im} \\ \varepsilon_{jkm}\delta_{il} \\ \varepsilon_{jlm}\delta_{ik} \\ \varepsilon_{klm}\delta_{ij} \end{pmatrix} . \qquad (1D.11)$$

A prime has been used in this instance, to signify that this is an overcomplete set that can and will be reduced in order to display an irreducible set of linear independent permutations:

$$I^{(5)}_{ijklm;\lambda\mu\nu\pi\rho} = \frac{1}{30} \begin{pmatrix} \varepsilon_{ijk}\delta_{lm} \\ \varepsilon_{ijl}\delta_{km} \\ \varepsilon_{ijm}\delta_{kl} \\ \varepsilon_{ikl}\delta_{jm} \\ \varepsilon_{ikm}\delta_{jl} \\ \varepsilon_{ilm}\delta_{jk} \end{pmatrix}^{\mathrm{T}} \begin{pmatrix} 3 & -1 & -1 & 1 & 1 & 0 \\ -1 & 3 & -1 & -1 & 0 & 1 \\ -1 & -1 & 3 & 0 & -1 & -1 \\ 1 & -1 & 0 & 3 & -1 & 1 \\ 1 & 0 & -1 & -1 & 3 & -1 \\ 0 & 1 & -1 & 1 & -1 & 3 \end{pmatrix} \begin{pmatrix} \varepsilon_{\lambda\mu\nu}\delta_{\pi\rho} \\ \varepsilon_{\lambda\mu\pi}\delta_{\nu\rho} \\ \varepsilon_{\lambda\mu\rho}\delta_{\nu\pi} \\ \varepsilon_{\lambda\nu\pi}\delta_{\mu\rho} \\ \varepsilon_{\lambda\nu\rho}\delta_{\mu\pi} \\ \varepsilon_{\lambda\pi\rho}\delta_{\mu\nu} \end{pmatrix} . \qquad (1D.12)$$

RANK 6

For $n = 6$ there are fifteen distinct isomers that form a linearly independent set:

$$I^{(6)}_{ijklmn;\lambda\mu\nu\pi\rho\sigma} = \frac{1}{210}\begin{pmatrix} \delta_{ij}\delta_{kl}\delta_{mn} \\ \delta_{ij}\delta_{km}\delta_{ln} \\ \delta_{ij}\delta_{kn}\delta_{lm} \\ \delta_{ik}\delta_{jl}\delta_{mn} \\ \delta_{ik}\delta_{jm}\delta_{ln} \\ \delta_{ik}\delta_{jn}\delta_{lm} \\ \delta_{il}\delta_{jk}\delta_{mn} \\ \delta_{il}\delta_{jm}\delta_{kn} \\ \delta_{il}\delta_{jn}\delta_{km} \\ \delta_{im}\delta_{jk}\delta_{ln} \\ \delta_{im}\delta_{jl}\delta_{kn} \\ \delta_{im}\delta_{jn}\delta_{kl} \\ \delta_{in}\delta_{jk}\delta_{lm} \\ \delta_{in}\delta_{jl}\delta_{km} \\ \delta_{in}\delta_{jm}\delta_{kl} \end{pmatrix}^{\mathrm{T}} \begin{pmatrix} 16 & -5 & -5 & -5 & 2 & 2 & -5 & 2 & 2 & 2 & 2 & -5 & 2 & 2 & -5 \\ -5 & 16 & -5 & 2 & -5 & 2 & 2 & 2 & -5 & -5 & 2 & 2 & 2 & -5 & 2 \\ -5 & -5 & 16 & 2 & 2 & -5 & 2 & -5 & 2 & 2 & -5 & 2 & -5 & 2 & 2 \\ -5 & 2 & 2 & 16 & -5 & -5 & -5 & 2 & 2 & 2 & -5 & 2 & 2 & -5 & 2 \\ 2 & -5 & 2 & -5 & 16 & -5 & 2 & -5 & 2 & -5 & 2 & 2 & 2 & 2 & -5 \\ 2 & 2 & -5 & -5 & -5 & 16 & 2 & 2 & -5 & 2 & 2 & -5 & -5 & 2 & 2 \\ -5 & 2 & 2 & -5 & 2 & 2 & 16 & -5 & -5 & -5 & 2 & 2 & -5 & 2 & 2 \\ 2 & 2 & -5 & 2 & -5 & 2 & -5 & 16 & -5 & 2 & -5 & 2 & 2 & 2 & -5 \\ 2 & -5 & 2 & 2 & 2 & -5 & -5 & -5 & 16 & 2 & 2 & -5 & 2 & -5 & 2 \\ 2 & -5 & 2 & 2 & -5 & 2 & -5 & 2 & 2 & 16 & -5 & -5 & -5 & 2 & 2 \\ 2 & 2 & -5 & -5 & 2 & 2 & 2 & -5 & 2 & -5 & 16 & -5 & 2 & -5 & 2 \\ -5 & 2 & 2 & 2 & 2 & -5 & 2 & 2 & -5 & -5 & -5 & 16 & 2 & 2 & -5 \\ 2 & 2 & -5 & 2 & 2 & -5 & -5 & 2 & 2 & -5 & 2 & 2 & 16 & -5 & -5 \\ 2 & -5 & 2 & -5 & 2 & 2 & 2 & 2 & -5 & 2 & -5 & 2 & -5 & 16 & -5 \\ -5 & 2 & 2 & 2 & -5 & 2 & 2 & -5 & 2 & 2 & 2 & -5 & -5 & -5 & 16 \end{pmatrix} \begin{pmatrix} \delta_{\lambda\mu}\delta_{\nu\pi}\delta_{\rho\sigma} \\ \delta_{\lambda\mu}\delta_{\nu\rho}\delta_{\pi\sigma} \\ \delta_{\lambda\mu}\delta_{\nu\sigma}\delta_{\pi\rho} \\ \delta_{\lambda\nu}\delta_{\mu\pi}\delta_{\rho\sigma} \\ \delta_{\lambda\nu}\delta_{\mu\rho}\delta_{\pi\sigma} \\ \delta_{\lambda\nu}\delta_{\mu\sigma}\delta_{\pi\rho} \\ \delta_{\lambda\pi}\delta_{\mu\nu}\delta_{\rho\sigma} \\ \delta_{\lambda\pi}\delta_{\mu\rho}\delta_{\nu\sigma} \\ \delta_{\lambda\pi}\delta_{\mu\sigma}\delta_{\nu\rho} \\ \delta_{\lambda\rho}\delta_{\mu\nu}\delta_{\pi\sigma} \\ \delta_{\lambda\rho}\delta_{\mu\pi}\delta_{\nu\sigma} \\ \delta_{\lambda\rho}\delta_{\mu\sigma}\delta_{\nu\pi} \\ \delta_{\lambda\sigma}\delta_{\mu\nu}\delta_{\pi\rho} \\ \delta_{\lambda\sigma}\delta_{\mu\pi}\delta_{\nu\rho} \\ \delta_{\lambda\sigma}\delta_{\mu\rho}\delta_{\nu\pi} \end{pmatrix} . \qquad (1D.13)$$

RANK 7

For $n=7$ there are 105 isomers and takes the following form,

$$I^{(7)}_{ijklmno;\lambda\mu\nu\pi\rho\sigma\tau} = \frac{1}{840}\begin{pmatrix} \varepsilon_{ijk}\delta_{lm}\delta_{no} \\ \varepsilon_{ijk}\delta_{ln}\delta_{mo} \\ \varepsilon_{ijk}\delta_{lo}\delta_{mn} \\ \varepsilon_{ijl}\delta_{km}\delta_{no} \\ \varepsilon_{ijl}\delta_{kn}\delta_{mo} \\ \cdots \\ \varepsilon_{mno}\delta_{il}\delta_{jk} \end{pmatrix}^{\mathrm{T}} \begin{pmatrix} 6 & -1 & -1 & 0 & 0 & \cdots & 0 \\ -1 & 6 & -1 & 0 & 0 & \cdots & 0 \\ -1 & -1 & 6 & 0 & 0 & \cdots & 0 \\ 0 & 0 & 0 & 6 & -1 & \cdots & 0 \\ 0 & 0 & 0 & -1 & 6 & \cdots & -1 \\ \cdots & \cdots & \cdots & \cdots & \cdots & \cdots & -1 \\ 0 & 0 & 0 & 0 & -1 & -1 & 6 \end{pmatrix} \begin{pmatrix} \varepsilon_{\lambda\mu\nu}\delta_{\pi\rho}\delta_{\sigma\tau} \\ \varepsilon_{\lambda\mu\nu}\delta_{\pi\sigma}\delta_{\rho\tau} \\ \varepsilon_{\lambda\mu\nu}\delta_{\pi\tau}\delta_{\rho\sigma} \\ \varepsilon_{\lambda\mu\pi}\delta_{\nu\rho}\delta_{\sigma\tau} \\ \varepsilon_{\lambda\mu\pi}\delta_{\nu\sigma}\delta_{\rho\tau} \\ \cdots \\ \varepsilon_{\rho\sigma\tau}\delta_{\lambda\pi}\delta_{\mu\nu} \end{pmatrix} . \quad \text{(1D.14)}$$

The full set of 105 permutations of linear combinations of isotropic tensors that appear in the first rank 1 tensor are:

$$\begin{pmatrix} \varepsilon_{ijk}\delta_{lm}\delta_{no} \\ \varepsilon_{ijk}\delta_{ln}\delta_{mo} \\ \varepsilon_{ijk}\delta_{lo}\delta_{mn} \\ \varepsilon_{ijl}\delta_{km}\delta_{no} \\ \varepsilon_{ijl}\delta_{kn}\delta_{mo} \\ \varepsilon_{ijl}\delta_{ko}\delta_{mn} \\ \varepsilon_{ijm}\delta_{kl}\delta_{no} \\ \varepsilon_{ijm}\delta_{kn}\delta_{lo} \\ \varepsilon_{ijm}\delta_{ko}\delta_{ln} \\ \varepsilon_{ijn}\delta_{kl}\delta_{mo} \\ \varepsilon_{ijn}\delta_{km}\delta_{lo} \\ \varepsilon_{ijn}\delta_{ko}\delta_{lm} \\ \varepsilon_{ijo}\delta_{kl}\delta_{mn} \\ \varepsilon_{ijo}\delta_{km}\delta_{ln} \\ \varepsilon_{ijo}\delta_{kn}\delta_{lm} \\ \varepsilon_{ikl}\delta_{jm}\delta_{no} \\ \varepsilon_{ikl}\delta_{jn}\delta_{mo} \\ \varepsilon_{ikl}\delta_{jo}\delta_{mn} \\ \varepsilon_{ikm}\delta_{jl}\delta_{no} \\ \varepsilon_{ikm}\delta_{jn}\delta_{lo} \\ \varepsilon_{ikm}\delta_{jo}\delta_{ln} \\ \cdots \end{pmatrix}^{\mathrm{T}} \begin{pmatrix} \cdots \\ \varepsilon_{ikn}\delta_{jl}\delta_{mo} \\ \varepsilon_{ikn}\delta_{jm}\delta_{lo} \\ \varepsilon_{ikn}\delta_{jo}\delta_{lm} \\ \varepsilon_{iko}\delta_{jl}\delta_{mn} \\ \varepsilon_{iko}\delta_{jm}\delta_{ln} \\ \varepsilon_{iko}\delta_{jn}\delta_{lm} \\ \varepsilon_{ilm}\delta_{jk}\delta_{no} \\ \varepsilon_{ilm}\delta_{jn}\delta_{ko} \\ \varepsilon_{ilm}\delta_{jo}\delta_{kn} \\ \varepsilon_{iln}\delta_{jk}\delta_{mo} \\ \varepsilon_{iln}\delta_{jm}\delta_{ko} \\ \varepsilon_{iln}\delta_{jo}\delta_{km} \\ \varepsilon_{ilo}\delta_{jk}\delta_{mn} \\ \varepsilon_{ilo}\delta_{jm}\delta_{kn} \\ \varepsilon_{ilo}\delta_{jn}\delta_{km} \\ \varepsilon_{imn}\delta_{jk}\delta_{lo} \\ \varepsilon_{imn}\delta_{jl}\delta_{ko} \\ \varepsilon_{imn}\delta_{jo}\delta_{kl} \\ \varepsilon_{imo}\delta_{jk}\delta_{ln} \\ \varepsilon_{imo}\delta_{jl}\delta_{kn} \\ \varepsilon_{imo}\delta_{jn}\delta_{kl} \\ \cdots \end{pmatrix} \begin{pmatrix} \cdots \\ \varepsilon_{ino}\delta_{jk}\delta_{lm} \\ \varepsilon_{ino}\delta_{jl}\delta_{km} \\ \varepsilon_{ino}\delta_{jm}\delta_{kl} \\ \varepsilon_{jkl}\delta_{im}\delta_{no} \\ \varepsilon_{jkl}\delta_{in}\delta_{mo} \\ \varepsilon_{jkl}\delta_{io}\delta_{mn} \\ \varepsilon_{jkm}\delta_{il}\delta_{no} \\ \varepsilon_{jkm}\delta_{in}\delta_{lo} \\ \varepsilon_{jkm}\delta_{io}\delta_{ln} \\ \varepsilon_{jkn}\delta_{il}\delta_{mo} \\ \varepsilon_{jkn}\delta_{im}\delta_{lo} \\ \varepsilon_{jkn}\delta_{io}\delta_{lm} \\ \varepsilon_{jko}\delta_{il}\delta_{mn} \\ \varepsilon_{jko}\delta_{im}\delta_{ln} \\ \varepsilon_{jko}\delta_{in}\delta_{lm} \\ \varepsilon_{jlm}\delta_{ik}\delta_{no} \\ \varepsilon_{jlm}\delta_{in}\delta_{ko} \\ \varepsilon_{jlm}\delta_{io}\delta_{kn} \\ \varepsilon_{jln}\delta_{ik}\delta_{mo} \\ \varepsilon_{jln}\delta_{im}\delta_{ko} \\ \varepsilon_{jln}\delta_{io}\delta_{km} \\ \cdots \end{pmatrix} \begin{pmatrix} \cdots \\ \varepsilon_{jlo}\delta_{ik}\delta_{mn} \\ \varepsilon_{jlo}\delta_{im}\delta_{kn} \\ \varepsilon_{jlo}\delta_{in}\delta_{km} \\ \varepsilon_{jmn}\delta_{ik}\delta_{lo} \\ \varepsilon_{jmn}\delta_{il}\delta_{ko} \\ \varepsilon_{jmn}\delta_{io}\delta_{kl} \\ \varepsilon_{jmo}\delta_{ik}\delta_{ln} \\ \varepsilon_{jmo}\delta_{il}\delta_{kn} \\ \varepsilon_{jmo}\delta_{in}\delta_{kl} \\ \varepsilon_{jno}\delta_{ik}\delta_{lm} \\ \varepsilon_{jno}\delta_{il}\delta_{km} \\ \varepsilon_{jno}\delta_{im}\delta_{kl} \\ \varepsilon_{klm}\delta_{ij}\delta_{no} \\ \varepsilon_{klm}\delta_{in}\delta_{jo} \\ \varepsilon_{klm}\delta_{io}\delta_{jn} \\ \varepsilon_{kln}\delta_{ij}\delta_{mo} \\ \varepsilon_{kln}\delta_{im}\delta_{jo} \\ \varepsilon_{kln}\delta_{io}\delta_{jm} \\ \varepsilon_{klo}\delta_{ij}\delta_{mn} \\ \varepsilon_{klo}\delta_{im}\delta_{jn} \\ \varepsilon_{klo}\delta_{in}\delta_{jm} \\ \cdots \end{pmatrix} \begin{pmatrix} \\ \cdots \\ \varepsilon_{kmn}\delta_{ij}\delta_{lo} \\ \varepsilon_{kmn}\delta_{il}\delta_{jo} \\ \varepsilon_{kmn}\delta_{io}\delta_{jl} \\ \varepsilon_{kmo}\delta_{ij}\delta_{ln} \\ \varepsilon_{kmo}\delta_{il}\delta_{jn} \\ \varepsilon_{kmo}\delta_{in}\delta_{jl} \\ \varepsilon_{kno}\delta_{ij}\delta_{lm} \\ \varepsilon_{kno}\delta_{il}\delta_{jm} \\ \varepsilon_{kno}\delta_{im}\delta_{jl} \\ \varepsilon_{lmn}\delta_{ij}\delta_{ko} \\ \varepsilon_{lmn}\delta_{ik}\delta_{jo} \\ \varepsilon_{lmn}\delta_{io}\delta_{jk} \\ \varepsilon_{lmo}\delta_{ij}\delta_{kn} \\ \varepsilon_{lmo}\delta_{ik}\delta_{jn} \\ \varepsilon_{lmo}\delta_{in}\delta_{jk} \\ \varepsilon_{lno}\delta_{ij}\delta_{km} \\ \varepsilon_{lno}\delta_{ik}\delta_{jm} \\ \varepsilon_{lno}\delta_{im}\delta_{jk} \\ \varepsilon_{mno}\delta_{ij}\delta_{kl} \\ \varepsilon_{mno}\delta_{ik}\delta_{jl} \\ \varepsilon_{mno}\delta_{il}\delta_{jk} \end{pmatrix} . \quad \text{(1D.15)}$$

The rank 2 tensor in equation (1D.14), follows the repeated 3×3 matrix structure down the leading diagonal of the 105×105 matrix. The full set of permutations for the final rank 1 tensor are as follows,

$$\begin{pmatrix}
\varepsilon_{\lambda\mu\nu}\delta_{\pi\rho}\delta_{\sigma\tau}\\
\varepsilon_{\lambda\mu\nu}\delta_{\pi\sigma}\delta_{\rho\tau}\\
\varepsilon_{\lambda\mu\nu}\delta_{\pi\tau}\delta_{\rho\sigma}\\
\varepsilon_{\lambda\mu\pi}\delta_{\nu\rho}\delta_{\sigma\tau}\\
\varepsilon_{\lambda\mu\pi}\delta_{\nu\sigma}\delta_{\rho\tau}\\
\varepsilon_{\lambda\mu\pi}\delta_{\nu\tau}\delta_{\rho\sigma}\\
\varepsilon_{\lambda\mu\rho}\delta_{\nu\pi}\delta_{\sigma\tau}\\
\varepsilon_{\lambda\mu\rho}\delta_{\nu\sigma}\delta_{\pi\tau}\\
\varepsilon_{\lambda\mu\rho}\delta_{\nu\tau}\delta_{\pi\sigma}\\
\varepsilon_{\lambda\mu\sigma}\delta_{\nu\pi}\delta_{\rho\tau}\\
\varepsilon_{\lambda\mu\sigma}\delta_{\nu\rho}\delta_{\pi\tau}\\
\varepsilon_{\lambda\mu\sigma}\delta_{\nu\tau}\delta_{\pi\rho}\\
\varepsilon_{\lambda\mu\tau}\delta_{\nu\pi}\delta_{\rho\sigma}\\
\varepsilon_{\lambda\mu\tau}\delta_{\nu\rho}\delta_{\pi\sigma}\\
\varepsilon_{\lambda\mu\tau}\delta_{\nu\sigma}\delta_{\pi\rho}\\
\varepsilon_{\lambda\nu\pi}\delta_{\mu\rho}\delta_{\sigma\tau}\\
\varepsilon_{\lambda\nu\pi}\delta_{\mu\sigma}\delta_{\rho\tau}\\
\varepsilon_{\lambda\nu\pi}\delta_{\mu\tau}\delta_{\rho\sigma}\\
\varepsilon_{\lambda\nu\rho}\delta_{\mu\pi}\delta_{\sigma\tau}\\
\varepsilon_{\lambda\nu\rho}\delta_{\mu\sigma}\delta_{\pi\tau}\\
\varepsilon_{\lambda\nu\rho}\delta_{\mu\tau}\delta_{\pi\sigma}\\
\ldots
\end{pmatrix}^{\mathrm{T}}
\begin{vmatrix}
\ldots\\
\varepsilon_{\lambda\nu\sigma}\delta_{\mu\pi}\delta_{\rho\tau}\\
\varepsilon_{\lambda\nu\sigma}\delta_{\mu\rho}\delta_{\pi\tau}\\
\varepsilon_{\lambda\nu\sigma}\delta_{\mu\tau}\delta_{\pi\rho}\\
\varepsilon_{\lambda\nu\tau}\delta_{\mu\pi}\delta_{\rho\sigma}\\
\varepsilon_{\lambda\nu\tau}\delta_{\mu\rho}\delta_{\pi\sigma}\\
\varepsilon_{\lambda\nu\tau}\delta_{\mu\sigma}\delta_{\pi\rho}\\
\varepsilon_{\lambda\pi\rho}\delta_{\mu\nu}\delta_{\sigma\tau}\\
\varepsilon_{\lambda\pi\rho}\delta_{\mu\sigma}\delta_{\nu\tau}\\
\varepsilon_{\lambda\pi\rho}\delta_{\mu\tau}\delta_{\nu\sigma}\\
\varepsilon_{\lambda\pi\sigma}\delta_{\mu\nu}\delta_{\rho\tau}\\
\varepsilon_{\lambda\pi\sigma}\delta_{\mu\rho}\delta_{\nu\tau}\\
\varepsilon_{\lambda\pi\sigma}\delta_{\mu\tau}\delta_{\nu\rho}\\
\varepsilon_{\lambda\pi\tau}\delta_{\mu\nu}\delta_{\rho\sigma}\\
\varepsilon_{\lambda\pi\tau}\delta_{\mu\rho}\delta_{\nu\sigma}\\
\varepsilon_{\lambda\pi\tau}\delta_{\mu\sigma}\delta_{\nu\rho}\\
\varepsilon_{\lambda\rho\sigma}\delta_{\mu\nu}\delta_{\pi\tau}\\
\varepsilon_{\lambda\rho\sigma}\delta_{\mu\pi}\delta_{\nu\tau}\\
\varepsilon_{\lambda\rho\sigma}\delta_{\mu\tau}\delta_{\nu\pi}\\
\varepsilon_{\lambda\rho\tau}\delta_{\mu\nu}\delta_{\pi\sigma}\\
\varepsilon_{\lambda\rho\tau}\delta_{\mu\pi}\delta_{\nu\sigma}\\
\varepsilon_{\lambda\rho\tau}\delta_{\mu\sigma}\delta_{\nu\pi}\\
\ldots
\end{vmatrix}
\begin{vmatrix}
\ldots\\
\varepsilon_{\lambda\sigma\tau}\delta_{\mu\nu}\delta_{\pi\rho}\\
\varepsilon_{\lambda\sigma\tau}\delta_{\mu\pi}\delta_{\nu\rho}\\
\varepsilon_{\lambda\sigma\tau}\delta_{\mu\rho}\delta_{\nu\pi}\\
\varepsilon_{\mu\nu\pi}\delta_{\lambda\rho}\delta_{\sigma\tau}\\
\varepsilon_{\mu\nu\pi}\delta_{\lambda\sigma}\delta_{\rho\tau}\\
\varepsilon_{\mu\nu\pi}\delta_{\lambda\tau}\delta_{\rho\sigma}\\
\varepsilon_{\mu\nu\rho}\delta_{\lambda\pi}\delta_{\sigma\tau}\\
\varepsilon_{\mu\nu\rho}\delta_{\lambda\sigma}\delta_{\pi\tau}\\
\varepsilon_{\mu\nu\rho}\delta_{\lambda\tau}\delta_{\pi\sigma}\\
\varepsilon_{\mu\nu\sigma}\delta_{\lambda\pi}\delta_{\rho\tau}\\
\varepsilon_{\mu\nu\sigma}\delta_{\lambda\rho}\delta_{\pi\tau}\\
\varepsilon_{\mu\nu\sigma}\delta_{\lambda\tau}\delta_{\pi\rho}\\
\varepsilon_{\mu\nu\tau}\delta_{\lambda\pi}\delta_{\rho\sigma}\\
\varepsilon_{\mu\nu\tau}\delta_{\lambda\rho}\delta_{\pi\sigma}\\
\varepsilon_{\mu\nu\tau}\delta_{\lambda\sigma}\delta_{\pi\rho}\\
\varepsilon_{\mu\pi\rho}\delta_{\lambda\nu}\delta_{\sigma\tau}\\
\varepsilon_{\mu\pi\rho}\delta_{\lambda\sigma}\delta_{\nu\tau}\\
\varepsilon_{\mu\pi\rho}\delta_{\lambda\tau}\delta_{\nu\sigma}\\
\varepsilon_{\mu\pi\sigma}\delta_{\lambda\nu}\delta_{\rho\tau}\\
\varepsilon_{\mu\pi\sigma}\delta_{\lambda\rho}\delta_{\nu\tau}\\
\varepsilon_{\mu\pi\sigma}\delta_{\lambda\tau}\delta_{\nu\rho}\\
\ldots
\end{vmatrix}
\begin{vmatrix}
\ldots\\
\varepsilon_{\mu\pi\tau}\delta_{\lambda\nu}\delta_{\rho\sigma}\\
\varepsilon_{\mu\pi\tau}\delta_{\lambda\rho}\delta_{\nu\sigma}\\
\varepsilon_{\mu\pi\tau}\delta_{\lambda\sigma}\delta_{\nu\rho}\\
\varepsilon_{\mu\rho\sigma}\delta_{\lambda\nu}\delta_{\pi\tau}\\
\varepsilon_{\mu\rho\sigma}\delta_{\lambda\pi}\delta_{\nu\tau}\\
\varepsilon_{\mu\rho\sigma}\delta_{\lambda\tau}\delta_{\nu\pi}\\
\varepsilon_{\mu\rho\tau}\delta_{\lambda\nu}\delta_{\pi\sigma}\\
\varepsilon_{\mu\rho\tau}\delta_{\lambda\pi}\delta_{\nu\sigma}\\
\varepsilon_{\mu\rho\tau}\delta_{\lambda\sigma}\delta_{\nu\pi}\\
\varepsilon_{\mu\sigma\tau}\delta_{\lambda\nu}\delta_{\pi\rho}\\
\varepsilon_{\mu\sigma\tau}\delta_{\lambda\pi}\delta_{\nu\rho}\\
\varepsilon_{\mu\sigma\tau}\delta_{\lambda\rho}\delta_{\nu\pi}\\
\varepsilon_{\nu\pi\rho}\delta_{\lambda\mu}\delta_{\sigma\tau}\\
\varepsilon_{\nu\pi\rho}\delta_{\lambda\sigma}\delta_{\mu\tau}\\
\varepsilon_{\nu\pi\rho}\delta_{\lambda\tau}\delta_{\mu\sigma}\\
\varepsilon_{\nu\pi\sigma}\delta_{\lambda\mu}\delta_{\rho\tau}\\
\varepsilon_{\nu\pi\sigma}\delta_{\lambda\rho}\delta_{\mu\tau}\\
\varepsilon_{\nu\pi\sigma}\delta_{\lambda\tau}\delta_{\mu\rho}\\
\varepsilon_{\nu\pi\tau}\delta_{\lambda\mu}\delta_{\rho\sigma}\\
\varepsilon_{\nu\pi\tau}\delta_{\lambda\rho}\delta_{\mu\sigma}\\
\varepsilon_{\nu\pi\tau}\delta_{\lambda\sigma}\delta_{\mu\rho}\\
\ldots
\end{vmatrix}
\begin{vmatrix}
\\
\ldots\\
\varepsilon_{\nu\rho\sigma}\delta_{\lambda\mu}\delta_{\pi\tau}\\
\varepsilon_{\nu\rho\sigma}\delta_{\lambda\pi}\delta_{\mu\tau}\\
\varepsilon_{\nu\rho\sigma}\delta_{\lambda\tau}\delta_{\mu\pi}\\
\varepsilon_{\nu\rho\tau}\delta_{\lambda\mu}\delta_{\pi\sigma}\\
\varepsilon_{\nu\rho\tau}\delta_{\lambda\pi}\delta_{\mu\sigma}\\
\varepsilon_{\nu\rho\tau}\delta_{\lambda\sigma}\delta_{\mu\pi}\\
\varepsilon_{\nu\sigma\tau}\delta_{\lambda\mu}\delta_{\pi\rho}\\
\varepsilon_{\nu\sigma\tau}\delta_{\lambda\pi}\delta_{\mu\rho}\\
\varepsilon_{\nu\sigma\tau}\delta_{\lambda\rho}\delta_{\mu\pi}\\
\varepsilon_{\pi\rho\sigma}\delta_{\lambda\mu}\delta_{\nu\tau}\\
\varepsilon_{\pi\rho\sigma}\delta_{\lambda\nu}\delta_{\mu\tau}\\
\varepsilon_{\pi\rho\sigma}\delta_{\lambda\tau}\delta_{\mu\nu}\\
\varepsilon_{\pi\rho\tau}\delta_{\lambda\mu}\delta_{\nu\sigma}\\
\varepsilon_{\pi\rho\tau}\delta_{\lambda\nu}\delta_{\mu\sigma}\\
\varepsilon_{\pi\rho\tau}\delta_{\lambda\sigma}\delta_{\mu\nu}\\
\varepsilon_{\pi\sigma\tau}\delta_{\lambda\mu}\delta_{\nu\rho}\\
\varepsilon_{\pi\sigma\tau}\delta_{\lambda\nu}\delta_{\mu\rho}\\
\varepsilon_{\pi\sigma\tau}\delta_{\lambda\rho}\delta_{\mu\nu}\\
\varepsilon_{\rho\sigma\tau}\delta_{\lambda\mu}\delta_{\nu\pi}\\
\varepsilon_{\rho\sigma\tau}\delta_{\lambda\nu}\delta_{\mu\pi}\\
\varepsilon_{\rho\sigma\tau}\delta_{\lambda\pi}\delta_{\mu\nu}
\end{vmatrix}
\qquad . \text{(1D.16)}$$

Similar to the rank 5 case, this is result is overcomplete and it is possible to choose a set of 36 to form a linearly independent set:

$$
I^{(7)}_{ijklmno;\lambda\mu\nu\pi\rho\sigma\tau} = \frac{1}{420}
\begin{pmatrix}
\varepsilon_{ijk}\delta_{lm}\delta_{no} \\
\varepsilon_{ijk}\delta_{ln}\delta_{mo} \\
\varepsilon_{ijk}\delta_{lo}\delta_{mn} \\
\varepsilon_{ijl}\delta_{kn}\delta_{no} \\
\varepsilon_{ijl}\delta_{kn}\delta_{mo} \\
\varepsilon_{ijl}\delta_{ko}\delta_{mn} \\
\varepsilon_{ijm}\delta_{kl}\delta_{no} \\
\varepsilon_{ijm}\delta_{kn}\delta_{lo} \\
\varepsilon_{ijm}\delta_{ko}\delta_{ln} \\
\varepsilon_{ijn}\delta_{kl}\delta_{mo} \\
\varepsilon_{ijn}\delta_{km}\delta_{lo} \\
\varepsilon_{ijn}\delta_{ko}\delta_{lm} \\
\varepsilon_{ijo}\delta_{kl}\delta_{mn} \\
\varepsilon_{ijo}\delta_{km}\delta_{ln} \\
\varepsilon_{ijo}\delta_{kn}\delta_{lm} \\
\varepsilon_{ikl}\delta_{jm}\delta_{no} \\
\varepsilon_{ikl}\delta_{jn}\delta_{mo} \\
\varepsilon_{ikl}\delta_{jo}\delta_{mn} \\
\varepsilon_{ikm}\delta_{jl}\delta_{no} \\
\varepsilon_{ikm}\delta_{jn}\delta_{lo} \\
\varepsilon_{ikm}\delta_{jo}\delta_{ln} \\
\varepsilon_{ikn}\delta_{jl}\delta_{mo} \\
\varepsilon_{ikn}\delta_{jm}\delta_{lo} \\
\varepsilon_{ikn}\delta_{jo}\delta_{lm} \\
\varepsilon_{iko}\delta_{jl}\delta_{mn} \\
\varepsilon_{iko}\delta_{jm}\delta_{ln} \\
\varepsilon_{iko}\delta_{jn}\delta_{lm} \\
\varepsilon_{ilm}\delta_{jk}\delta_{no} \\
\varepsilon_{ilm}\delta_{jo}\delta_{kn} \\
\varepsilon_{iln}\delta_{jk}\delta_{mo} \\
\varepsilon_{iln}\delta_{jo}\delta_{km} \\
\varepsilon_{ilo}\delta_{jk}\delta_{mn} \\
\varepsilon_{ilo}\delta_{jn}\delta_{km} \\
\varepsilon_{imn}\delta_{jk}\delta_{lo} \\
\varepsilon_{imo}\delta_{jk}\delta_{ln} \\
\varepsilon_{ino}\delta_{jk}\delta_{lm}
\end{pmatrix}^{\mathrm{T}}
\begin{pmatrix}
51 & -28 & -13 & -35 & 22 & 7 & -5 & -8 & 7 & 1 & 16 & -15 & 1 & 16 & -15 & 15 & -16 & -1 & 15 & -1 & -16 & -7 & -7 & 20 & -7 & -7 & 20 & -15 & 15 & 9 & -15 & 9 & -15 & -6 & -6 & 0 \\
-28 & 66 & -28 & 32 & -40 & 6 & -4 & 26 & -16 & -10 & 2 & 6 & 12 & -34 & 12 & -6 & 40 & -32 & -12 & -12 & 34 & 10 & -6 & -2 & 4 & 16 & -26 & 24 & -30 & 0 & 0 & -24 & 30 & 6 & 12 & 6 \\
-13 & -28 & 51 & 1 & 16 & -15 & 7 & -20 & 7 & 7 & -20 & 7 & -15 & 16 & 1 & -7 & -22 & 35 & -1 & 15 & -16 & -1 & 15 & -16 & 5 & -7 & 8 & -9 & 15 & -9 & 15 & 15 & -15 & 0 & -6 & -6 \\
-35 & 32 & 1 & 67 & -42 & -11 & -19 & 28 & -3 & 9 & -28 & 11 & 9 & -28 & 11 & -15 & 24 & -7 & -9 & -7 & 24 & 5 & 7 & -18 & 5 & 7 & -18 & 37 & -31 & -19 & 25 & -19 & 25 & 14 & 14 & 0 \\
22 & -40 & 16 & -42 & 62 & -10 & 14 & -38 & 12 & -14 & 18 & -2 & -2 & 20 & -14 & 4 & -30 & 24 & 10 & 12 & -32 & -4 & -2 & 10 & -6 & -4 & 16 & -34 & 40 & 22 & -16 & 14 & -20 & -14 & -12 & 2 \\
7 & 6 & -15 & -11 & -10 & 27 & 3 & 6 & -9 & 3 & 6 & -9 & -9 & 4 & 3 & 5 & 4 & -15 & -1 & -3 & 6 & -1 & -3 & 6 & 1 & -1 & 0 & -1 & -5 & -1 & -5 & 7 & -1 & 0 & -2 & -2 \\
-5 & -4 & 7 & -19 & 14 & 3 & 27 & -16 & -5 & -9 & 8 & 1 & -9 & 8 & 1 & 1 & -6 & 5 & -5 & 5 & -6 & 1 & -1 & 2 & 1 & -1 & 2 & -17 & 11 & 7 & -5 & 7 & -5 & -6 & -6 & 0 \\
-8 & 26 & -20 & 28 & -38 & 6 & -16 & 50 & -16 & 8 & -22 & 8 & 6 & -6 & -4 & 0 & 16 & -18 & -6 & -16 & 28 & 4 & 2 & -10 & 2 & 0 & -4 & 28 & -34 & -16 & 14 & -10 & 10 & 18 & 6 & 2 \\
7 & -16 & 7 & -3 & 12 & -9 & -5 & -16 & 27 & 1 & 8 & -9 & 3 & -8 & 3 & -1 & -4 & 7 & 5 & 5 & -16 & -3 & -1 & 6 & -1 & 1 & 0 & -5 & 11 & 5 & -5 & -1 & -1 & -6 & 6 & -2 \\
1 & -10 & 7 & 9 & -14 & 3 & -9 & 8 & 1 & 27 & -16 & -5 & -9 & 6 & 3 & -1 & -4 & 5 & 1 & -1 & 2 & -5 & 5 & -6 & 1 & -3 & 4 & 7 & -5 & -17 & 11 & 7 & -5 & 6 & 0 & -6 \\
16 & 2 & -20 & -28 & 18 & 6 & 8 & -22 & 8 & -16 & 50 & -16 & 6 & -14 & 4 & 6 & 10 & -18 & 4 & 2 & -10 & -6 & -16 & 28 & 2 & 6 & -10 & -16 & 14 & 28 & -34 & -10 & 10 & -18 & 2 & 6 \\
-15 & 6 & 7 & 11 & -2 & -9 & 1 & 8 & -9 & -5 & -16 & 27 & 3 & 4 & -9 & -3 & -2 & 7 & -3 & -1 & 6 & 5 & 5 & -16 & -1 & -1 & 2 & 5 & -5 & -5 & 11 & -1 & -1 & 6 & -2 & 6 \\
1 & 12 & -15 & 9 & -2 & -9 & -9 & 6 & 3 & -9 & 6 & 3 & 27 & -16 & -5 & -1 & 10 & -9 & 1 & -3 & 4 & 1 & -3 & 4 & -5 & 5 & -6 & 7 & -5 & 7 & -5 & -17 & 11 & 0 & 6 & 6 \\
16 & -34 & 16 & -28 & 20 & 4 & 8 & -6 & -8 & 6 & -14 & 4 & -16 & 50 & -16 & 6 & -32 & 24 & 4 & 4 & -12 & 2 & 6 & -10 & -6 & -16 & 28 & -16 & 14 & -10 & 10 & 28 & -34 & 2 & -18 & -6 \\
-15 & 12 & 1 & 11 & -14 & 3 & 1 & -4 & 3 & 3 & 4 & -9 & -5 & -16 & 27 & -3 & 12 & -7 & -3 & 1 & 4 & -1 & -1 & 2 & 5 & 5 & -16 & 5 & -5 & -1 & -1 & -5 & 11 & -2 & 6 & -6 \\
15 & -6 & -7 & -15 & 4 & 5 & 1 & 0 & -1 & -1 & 6 & -3 & -1 & 6 & -3 & 27 & -10 & -11 & -9 & 3 & 4 & 3 & -9 & 6 & 3 & -9 & 6 & 7 & -1 & -1 & -5 & -1 & -5 & 2 & 2 & 0 \\
-16 & 40 & -22 & 24 & -30 & 4 & -6 & 16 & -4 & -4 & 10 & -2 & 10 & -32 & 12 & -10 & 62 & -42 & -2 & -14 & 20 & -14 & -2 & 18 & 14 & 12 & -38 & 14 & -20 & 22 & -16 & -34 & 40 & -2 & 12 & 14 \\
-1 & -32 & 35 & -7 & 24 & -15 & 5 & -18 & 7 & 5 & -18 & 7 & -9 & 24 & -7 & -11 & -42 & 67 & 9 & 11 & -28 & 9 & 11 & -28 & -19 & -3 & 28 & -19 & 25 & -19 & 25 & 37 & -31 & 0 & -14 & -14 \\
15 & -12 & -1 & -9 & 10 & -1 & -5 & -6 & 5 & 1 & 4 & -3 & 1 & 4 & -3 & -9 & -2 & 9 & 27 & -5 & -16 & -9 & 3 & 6 & -9 & 3 & 6 & -17 & 11 & 7 & -5 & 7 & -5 & -6 & -6 & 0 \\
-1 & -12 & 15 & -7 & 12 & -3 & 5 & -16 & 5 & -1 & 2 & -1 & -3 & 4 & 1 & 3 & -14 & 11 & -5 & 27 & -16 & 3 & -9 & 4 & 1 & 3 & -4 & -5 & 11 & -1 & -1 & 5 & -5 & 6 & -6 & 2 \\
-16 & 34 & -16 & 24 & -32 & 6 & -6 & 28 & -16 & 2 & -10 & 6 & 4 & -12 & 4 & 4 & 20 & -28 & -16 & -16 & 50 & 6 & 4 & -14 & 8 & -8 & -6 & 28 & -34 & -10 & 10 & -16 & 14 & 6 & 18 & -2 \\
-7 & 10 & -1 & 5 & -4 & -1 & 1 & 4 & -3 & -5 & -6 & 5 & 1 & 2 & -1 & 3 & -14 & 9 & -9 & 3 & 6 & 27 & -5 & -16 & -9 & 1 & 8 & 7 & -5 & -17 & 11 & 7 & -5 & 6 & 0 & -6 \\
-7 & -6 & 15 & 7 & -2 & -3 & -1 & 2 & -1 & 5 & -16 & 5 & -3 & 6 & -1 & -9 & -2 & 11 & 3 & -9 & 4 & -5 & 27 & -16 & 1 & -9 & 8 & -1 & -1 & -5 & 11 & 5 & -5 & -6 & 2 & -6 \\
20 & -2 & -16 & -18 & 10 & 6 & 2 & -10 & 6 & -6 & 28 & -16 & 4 & -10 & 2 & 6 & 18 & -28 & 6 & 4 & -14 & -16 & -16 & 50 & 8 & 8 & -22 & -10 & 10 & 28 & -34 & -16 & 14 & -6 & -2 & 18 \\
-7 & 4 & 5 & 5 & -6 & 1 & 1 & 2 & -1 & 1 & 2 & -1 & -5 & -6 & 5 & 3 & 14 & -19 & -9 & 1 & 8 & -9 & 1 & 8 & 27 & -5 & -16 & 7 & -5 & 7 & -5 & -17 & 11 & 0 & 6 & 6 \\
-7 & 16 & -7 & 7 & -4 & -1 & -1 & 0 & 1 & -3 & 6 & -1 & 5 & -16 & 5 & -9 & 12 & -3 & 3 & 3 & -8 & 1 & -9 & 8 & -5 & 27 & -16 & -1 & -1 & 5 & -5 & -5 & 11 & 2 & -6 & 6 \\
20 & -26 & 8 & -18 & 16 & 0 & 2 & -4 & 0 & 4 & -10 & 2 & -6 & 28 & -16 & 6 & -38 & 28 & 6 & -4 & -6 & 8 & 8 & -22 & -16 & -16 & 50 & -10 & 10 & -16 & 14 & 28 & -34 & -2 & -6 & -18 \\
-15 & 24 & -9 & 37 & -34 & -1 & -17 & 28 & -5 & 7 & -16 & 5 & 7 & -16 & 5 & 7 & 14 & -19 & -17 & -5 & 28 & 7 & -1 & -10 & 7 & -1 & -10 & 51 & -33 & -21 & 15 & -21 & 15 & 18 & 18 & 0 \\
15 & -30 & 15 & -31 & 40 & -5 & 11 & -34 & 11 & -5 & 14 & -5 & -5 & 14 & -5 & -1 & -20 & 25 & 11 & 11 & -34 & -5 & -1 & 10 & -5 & -1 & 10 & -33 & 45 & 15 & -15 & 15 & -15 & -12 & -12 & 0 \\
9 & 0 & -9 & -19 & 22 & -1 & 7 & -16 & 5 & -17 & 28 & -5 & 7 & -10 & -1 & -1 & 22 & -19 & 7 & -1 & -10 & -17 & -5 & 28 & 7 & 5 & -16 & -21 & 15 & 51 & -33 & -21 & 15 & -18 & 0 & 18 \\
-15 & 0 & 15 & 25 & -16 & -5 & -5 & 14 & -5 & 11 & -34 & 11 & -5 & 10 & -1 & -5 & -16 & 25 & -5 & -1 & 10 & 11 & 11 & -34 & -5 & -5 & 14 & 15 & -15 & -33 & 45 & 15 & -15 & 12 & 0 & -12 \\
9 & -24 & 15 & -19 & 14 & 7 & 7 & -10 & -1 & 7 & -10 & -1 & -17 & 28 & -5 & -1 & -34 & 37 & 7 & 5 & -16 & 7 & 5 & -16 & -17 & -5 & 28 & -21 & 15 & -21 & 15 & 51 & -33 & 0 & -18 & -18 \\
-15 & 30 & -15 & 25 & -20 & -1 & -5 & 10 & -1 & -5 & 10 & -1 & 11 & -34 & 11 & -5 & 40 & -31 & -5 & -5 & 14 & -5 & -5 & 14 & 11 & 11 & -34 & 15 & -15 & 15 & -15 & -33 & 45 & 0 & 12 & 12 \\
-6 & 6 & 0 & 14 & -14 & 0 & -6 & 18 & -6 & 6 & -18 & 6 & 0 & 2 & -2 & 2 & -2 & 0 & -6 & 6 & 6 & 6 & -6 & -6 & 0 & 2 & -2 & 18 & -12 & -18 & 12 & 0 & 0 & 30 & -6 & 6 \\
-6 & 12 & -6 & 14 & -12 & -2 & -6 & 6 & 6 & 0 & 2 & -2 & 6 & -18 & 6 & 2 & 12 & -14 & -6 & -6 & 18 & 0 & 2 & -2 & 6 & -6 & -6 & 18 & -12 & 0 & 0 & -18 & 12 & -6 & 30 & -6 \\
0 & 6 & -6 & 0 & 2 & -2 & 0 & 2 & -2 & -6 & 6 & 6 & 6 & -6 & -6 & 0 & 14 & -14 & 0 & 2 & -2 & -6 & -6 & 18 & 6 & 6 & -18 & 0 & 0 & 18 & -12 & -18 & 12 & 6 & -6 & 30
\end{pmatrix}
\begin{pmatrix}
\varepsilon_{\lambda\mu\nu}\delta_{\pi\rho}\delta_{\sigma\tau} \\
\varepsilon_{\lambda\mu\nu}\delta_{\pi\sigma}\delta_{\rho\tau} \\
\varepsilon_{\lambda\mu\nu}\delta_{\pi\tau}\delta_{\rho\sigma} \\
\varepsilon_{\lambda\mu\pi}\delta_{\nu\rho}\delta_{\sigma\tau} \\
\varepsilon_{\lambda\mu\pi}\delta_{\nu\sigma}\delta_{\rho\tau} \\
\varepsilon_{\lambda\mu\pi}\delta_{\nu\tau}\delta_{\rho\sigma} \\
\varepsilon_{\lambda\mu\rho}\delta_{\nu\pi}\delta_{\sigma\tau} \\
\varepsilon_{\lambda\mu\rho}\delta_{\nu\sigma}\delta_{\pi\tau} \\
\varepsilon_{\lambda\mu\rho}\delta_{\nu\tau}\delta_{\pi\sigma} \\
\varepsilon_{\lambda\mu\sigma}\delta_{\nu\pi}\delta_{\rho\tau} \\
\varepsilon_{\lambda\mu\sigma}\delta_{\nu\rho}\delta_{\pi\tau} \\
\varepsilon_{\lambda\mu\sigma}\delta_{\nu\tau}\delta_{\pi\rho} \\
\varepsilon_{\lambda\mu\tau}\delta_{\nu\pi}\delta_{\rho\sigma} \\
\varepsilon_{\lambda\mu\tau}\delta_{\nu\rho}\delta_{\pi\sigma} \\
\varepsilon_{\lambda\mu\tau}\delta_{\nu\sigma}\delta_{\pi\rho} \\
\varepsilon_{\lambda\nu\pi}\delta_{\mu\rho}\delta_{\sigma\tau} \\
\varepsilon_{\lambda\nu\pi}\delta_{\mu\sigma}\delta_{\rho\tau} \\
\varepsilon_{\lambda\nu\pi}\delta_{\mu\tau}\delta_{\rho\sigma} \\
\varepsilon_{\lambda\nu\rho}\delta_{\mu\pi}\delta_{\sigma\tau} \\
\varepsilon_{\lambda\nu\rho}\delta_{\mu\sigma}\delta_{\pi\tau} \\
\varepsilon_{\lambda\nu\rho}\delta_{\mu\tau}\delta_{\pi\sigma} \\
\varepsilon_{\lambda\nu\sigma}\delta_{\mu\pi}\delta_{\rho\tau} \\
\varepsilon_{\lambda\nu\sigma}\delta_{\mu\rho}\delta_{\pi\tau} \\
\varepsilon_{\lambda\nu\sigma}\delta_{\mu\tau}\delta_{\pi\rho} \\
\varepsilon_{\lambda\nu\tau}\delta_{\mu\pi}\delta_{\rho\sigma} \\
\varepsilon_{\lambda\nu\tau}\delta_{\mu\rho}\delta_{\pi\sigma} \\
\varepsilon_{\lambda\nu\tau}\delta_{\mu\sigma}\delta_{\pi\rho} \\
\varepsilon_{\lambda\pi\rho}\delta_{\mu\nu}\delta_{\sigma\tau} \\
\varepsilon_{\lambda\pi\rho}\delta_{\mu\tau}\delta_{\nu\sigma} \\
\varepsilon_{\lambda\pi\sigma}\delta_{\mu\nu}\delta_{\rho\tau} \\
\varepsilon_{\lambda\pi\sigma}\delta_{\mu\tau}\delta_{\nu\rho} \\
\varepsilon_{\lambda\pi\tau}\delta_{\mu\nu}\delta_{\rho\sigma} \\
\varepsilon_{\lambda\pi\tau}\delta_{\mu\sigma}\delta_{\nu\rho} \\
\varepsilon_{\lambda\rho\sigma}\delta_{\mu\nu}\delta_{\pi\tau} \\
\varepsilon_{\lambda\rho\tau}\delta_{\mu\nu}\delta_{\pi\sigma} \\
\varepsilon_{\lambda\sigma\tau}\delta_{\mu\nu}\delta_{\pi\rho}
\end{pmatrix}
\tag{1D.17}
$$

SUCCESSIVE RANKS

Results for isotropic tensors of higher ranks exist [101] and can be deployed in calculations, but due to the complexity, computational techniques are recommended [102]. The results displayed in chapter 3, required the use of rank 8 tensors, these results were carried out by a co-author Jack S. Ford and are included for completeness, but not covered in detail [103].

COMPLEMENT 1E: FIELD VECTORS

Throughout this work, all polarisation products will be analysed in one of four commonly deployed experimental configurations. The first pair will consider plane polarised light detected perpendicular to input, where the electromagnetic field vectors will either be parallel or perpendicular to input. The second pair will consider circularly polarised light, detected forward of the incident of light and with circularity either preserved or reversed. Incident light of left helicity is selected for exemplary purposes.

Table 3: The field vectors for the exemplary experimental setups.

	Linear (right-angled)			Circular (forwards)		
	input	output (′)		input	output (′)	
		$\parallel$	$\perp$	L	L	R
e	$\hat{\mathbf{i}}$	$\hat{\mathbf{i}}$	$\hat{\mathbf{k}}$	$\frac{1}{\sqrt{2}}\left(\hat{\mathbf{i}}+i\hat{\mathbf{j}}\right)$	$\frac{1}{\sqrt{2}}\left(\hat{\mathbf{i}}+i\hat{\mathbf{j}}\right)$	$\frac{1}{\sqrt{2}}\left(\hat{\mathbf{i}}-i\hat{\mathbf{j}}\right)$
$\overline{\mathbf{e}}$	$\hat{\mathbf{i}}$	$\hat{\mathbf{i}}$	$\hat{\mathbf{k}}$	$\frac{1}{\sqrt{2}}\left(\hat{\mathbf{i}}-i\hat{\mathbf{j}}\right)$	$\frac{1}{\sqrt{2}}\left(\hat{\mathbf{i}}-i\hat{\mathbf{j}}\right)$	$\frac{1}{\sqrt{2}}\left(\hat{\mathbf{i}}+i\hat{\mathbf{j}}\right)$
b	$\hat{\mathbf{j}}$	$-\hat{\mathbf{k}}$	$\hat{\mathbf{i}}$	$\frac{1}{i\sqrt{2}}\left(\hat{\mathbf{i}}+i\hat{\mathbf{j}}\right)$	$\frac{1}{i\sqrt{2}}\left(\hat{\mathbf{i}}+i\hat{\mathbf{j}}\right)$	$\frac{i}{\sqrt{2}}\left(\hat{\mathbf{i}}-i\hat{\mathbf{j}}\right)$
$\overline{\mathbf{b}}$	$\hat{\mathbf{j}}$	$-\hat{\mathbf{k}}$	$\hat{\mathbf{i}}$	$\frac{i}{\sqrt{2}}\left(\hat{\mathbf{i}}-i\hat{\mathbf{j}}\right)$	$\frac{i}{\sqrt{2}}\left(\hat{\mathbf{i}}-i\hat{\mathbf{j}}\right)$	$\frac{1}{i\sqrt{2}}\left(\hat{\mathbf{i}}+i\hat{\mathbf{j}}\right)$
k	$\hat{\mathbf{k}}$	$\hat{\mathbf{j}}$	$\hat{\mathbf{j}}$	$\hat{\mathbf{k}}$	$\hat{\mathbf{k}}$	$\hat{\mathbf{k}}$

It is useful to prepare all permutations of product pairings for the field vectors displayed in Table 3, see Table 4 – 7.

Table 4: Field vector products for scattering of *plane polarised* light detected perpendicular to input, with *parallel* oscillations.

	e	$\bar{\mathbf{e}}$	**b**	$\bar{\mathbf{b}}$	**k**	**e′**	$\bar{\mathbf{e}}'$	**b′**	$\bar{\mathbf{b}}'$	**k′**
e	1	1	0	0	0	1	1	0	0	0
$\bar{\mathbf{e}}$	1	1	0	0	0	1	1	0	0	0
b	0	0	1	1	0	0	0	0	0	1
$\bar{\mathbf{b}}$	0	0	1	1	0	0	0	0	0	1
k	0	0	0	0	1	0	0	-1	-1	0
e′	1	1	0	0	0	1	1	0	0	0
$\bar{\mathbf{e}}'$	1	1	0	0	0	1	1	0	0	0
b′	0	0	0	0	-1	0	0	1	1	0
$\bar{\mathbf{b}}'$	0	0	0	0	-1	0	0	1	1	0
k′	0	0	1	1	0	0	0	0	0	1

Table 5: Field vector products for scattering of *plane polarised* light detected perpendicular to input, with *perpendicular* oscillations.

	e	$\bar{\mathbf{e}}$	**b**	$\bar{\mathbf{b}}$	**k**	**e′**	$\bar{\mathbf{e}}'$	**b′**	$\bar{\mathbf{b}}'$	**k′**
e	1	1	0	0	0	0	0	1	1	0
$\bar{\mathbf{e}}$	1	1	0	0	0	0	0	1	1	0
b	0	0	1	1	0	0	0	0	0	1
$\bar{\mathbf{b}}$	0	0	1	1	0	0	0	0	0	1
k	0	0	0	0	1	1	1	0	0	0
e′	0	0	0	0	1	1	1	0	0	0
$\bar{\mathbf{e}}'$	0	0	0	0	1	1	1	0	0	0
b′	1	1	0	0	0	0	0	1	1	0
$\bar{\mathbf{b}}'$	1	1	0	0	0	0	0	1	1	0
k′	0	0	1	1	0	0	0	0	0	1

Table 6: Field vector products for scattering of *forward circularly polarised* light, with *preserved* circularity.

	e	**$\bar{e}$**	**b**	**$\bar{b}$**	**k**	**e′**	**$\bar{e}$′**	**b′**	**$\bar{b}$′**	**k′**
e	0	1	0	i	0	0	1	0	i	0
$\bar{e}$	1	0	-i	0	0	1	0	-i	0	0
b	0	-i	0	1	0	0	-i	0	1	0
$\bar{b}$	i	0	1	0	0	i	0	1	0	0
k	0	0	0	0	1	0	0	0	0	1
e′	0	1	0	i	0	0	1	0	i	0
$\bar{e}$′	1	0	-i	0	0	1	0	-i	0	0
b′	0	-i	0	1	0	0	-i	0	1	0
$\bar{b}$′	i	0	1	0	0	i	0	1	0	0
k′	0	0	0	0	1	0	0	0	0	1

Table 7: Field vector products for scattering of *forward circularly polarised* light, with *reversed* circularity.

	e	**$\bar{e}$**	**b**	**$\bar{b}$**	**k**	**e′**	**$\bar{e}$′**	**b′**	**$\bar{b}$′**	**k′**
e	0	1	0	i	0	1	0	i	0	0
$\bar{e}$	1	0	-i	0	0	0	1	0	-i	0
b	0	-i	0	1	0	-i	0	1	0	0
$\bar{b}$	i	0	1	0	0	0	i	0	1	0
k	0	0	0	0	1	0	0	0	0	1
e′	1	0	-i	0	0	0	1	0	-i	0
$\bar{e}$′	0	1	0	i	0	1	0	i	0	0
b′	i	0	1	0	0	0	i	0	1	0
$\bar{b}$′	0	-i	0	1	0	-i	0	1	0	0
k′	0	0	0	0	1	0	0	0	0	1

COMPLEMENT 1F: RESONANCE EFFECTS

The theory developed in chapter 1 adequately describes the transition rate of any process. In §1.4 we considered a centre engaging in a number of transitions involving its ground state and a virtual excited state. However, additional consideration is required if the input photon energy approaches that of the gap between two real energy levels, for the centre. Under these conditions, an analysis of the denominators associated with the transition energies delivers a zero result, which would correspond to an infinitely intense transition. However, this is not physical and can be addressed by adopting an appropriate substitution that reflects the lifetime of the molecular states,

$$E_r \to \tilde{E}_r - \mathrm{i}\hbar\gamma_r/2 \ , \tag{1F.1}$$

where γ_r is the decay constant for any molecular state, in this case r. Although it should be noted that this is not entirely consistent – by including a damping constant, the energy levels are no longer stationary states and therefore correspond to a Hamiltonian that is non-Hermitian. This can be incorporated into each energy denominator for any given molecular response tensor.

$$\sum_{r,\ldots}\left\{\frac{1}{E_{r0}^{A} - \hbar ck - \mathrm{i}\hbar\gamma_r/2} + \ldots\right\} , \tag{1F.2}$$

this is based on the first term from equation (1.4.1). If, $\hbar ck \approx E_{r0}$, then a given energy denominator will take the form of,

$$\frac{1}{\Delta E - \mathrm{i}\hbar\gamma_r/2} \ , \tag{1F.3}$$

where ΔE is a small energy mismatch. The rate of a process is dependent on the square of the matrix element, from equation (1.3.15), and as such,

$$\Gamma \sim |\chi|^2 = \to \frac{1}{\Delta E^2 + \hbar^2\gamma_r^2/4} \ , \tag{1F.4}$$

which is a Lorentzian form, this defines γ_r for the system, with a linewidth at the half maximum of $\hbar\gamma_r$. Away from resonance, the modification will be negligible when compared to an

electronic transition, however as you approach resonance, this term will serve to more realistic depict the lineshape for optical response.

Although the corrective term introduced in equation (1F.1) does not arise from the perturbative derivation for the system, it does prove to be phenomenological accurate in describing the real evolution of the molecular states [104]. This can be shown by substituting it into the time-dependent Schrödinger equation (1.3.1), which has eigensolutions $e^{-iH_0t/\hbar}$ and associated eigenstates $e^{-iE_rt/\hbar}$. Substituting the corrective term, equation (1F.1), in to produce the modified eigenstates, seen here as a product of exponentials;

$$e^{-iE_rt/\hbar}e^{-\hbar\gamma_rt/2}\ , \tag{1F.5}$$

the first exponential represents a phase factor, often associated with the wavefunction, of more interest is the second exponential, which represents a real exponential decay, the excited state exhibiting a depopulation. Uncertainty in lifetime gives rise to a broadening of the energy level.

At this juncture, it is worth briefly mentioning the two-level approximation. In an effort to simplify calculations it is expedient to limit the sum over an infinite number of molecular states to choice states that are known to contribute most significantly. At the extreme case, a single ground state and excited state may be employed. This is particularly powerful when utilising computational models, in which quantum calculations are often amongst the most resource intensive. The cases exploiting resonance features are particularly suited for such approximations, where the two levels exclusively considered are the ground and resonant levels.

COMPLEMENT 1G: BORN-OPPENHEIMER APPROXIMATION

The majority of this work engages purely electric transitions; however, in processes that engage vibrational transitions, such as with Raman scattering, it is necessary to distinguish between the nuclear and electronic components. Under the Born-Oppenheimer approximation, the molecular states are considered as a product of wavefunctions: $\varphi_r(q)\psi_R^r(Q)$, where the former describes the electronic state r and is dependent on the electronic coordinates q, which is implicitly dependant on the nuclear coordinates of a vibrational mode Q, associated with a vibrational state R. We can justifiably assume that such a transition leaves the energy associated with all other vibrational modes unchanged.

This separation can now be applied to the transition polarizability tensor, equation (1.4.7). Here, the initial, intermediate and final states in each term can thus be cast as $|\varphi_0\rangle|\psi_0^0\rangle$, $|\varphi_r\rangle|\psi_R^r\rangle$ and $|\varphi_0\rangle|\psi_\alpha^0\rangle$, respectively. Moreover, each transition moment component can now be regarded as a Dirac bracket succinctly expressed as $\mu_i^{\alpha r} \Rightarrow \langle\psi_\alpha|\mu_i^{0r}|\psi_0\rangle$. With the associated energy term also separable, *i.e.* $E_{\alpha r} \Rightarrow E_{0r} + E_{\alpha R}$;

$$\alpha_{ij}^{\alpha 0|A} = \sum_{r,R}\left[\frac{\langle\psi_\alpha|\mu_i^{0r}(Q)|\psi_R\rangle\langle\psi_R|\mu_j^{r0}(Q)|\psi_0\rangle}{E_{r0}+E_{R0}-\hbar ck} + \frac{\langle\psi_\alpha|\mu_j^{0r}(Q)|\psi_R\rangle\langle\psi_R|\mu_i^{r0}(Q)|\psi_0\rangle}{E_{r0}+E_{R\alpha}+\hbar ck}\right], \quad (1G.1)$$

Providing that the input optical frequency is far from resonance, the spacing between electronic levels will be much greater than that of vibrational level and hence the following approximation is justifiably exploited:

$$\alpha_{ij}^{\alpha 0|A} \approx \sum_{r,R}\left[\frac{\langle\psi_\alpha|\mu_i^{0r}(Q)|\psi_R\rangle\langle\psi_R|\mu_j^{r0}(Q)|\psi_0\rangle}{E_{r0}-\hbar ck} + \frac{\langle\psi_\alpha|\mu_j^{0r}(Q)|\psi_R\rangle\langle\psi_R|\mu_i^{r0}(Q)|\psi_0\rangle}{E_{r0}+\hbar ck}\right]. \quad (1G.2)$$

Since the denominators in equation (1G.2) do not involve vibrational state energies, the completeness relation, equation (1.4.2), can be invoked, so that;

$$\alpha_{ij}^{\alpha 0|A} \approx \langle\psi_\alpha|\underbrace{\sum_r\left[\frac{\mu_i^{0r}(Q)\mu_j^{r0}(Q)}{E_{r0}-\hbar ck} + \frac{\mu_j^{0r}(Q)\mu_i^{r0}(Q)}{E_{r0}+\hbar ck}\right]}_{\alpha_{ij}^{00}(Q)}|\psi_0\rangle \ . \quad (1G.3)$$

As a result of the nuclear motions producing little variation in the transition moments, a Taylor series expansion can be deployed of the electronic polarisability $\alpha_{ij}^{00|A}$ in terms of the vibrational coordinate Q, about the equilibrium position Q_0;

$$\alpha_{ij}^{00|A}(Q) = \alpha_{ij}^{00}\Big|_{Q_0} + (Q - Q_0)\frac{\partial \alpha_{ij}^{00}}{\partial Q}\Big|_{Q_0} + \ldots . \tag{1G.4}$$

Accordingly, by inserting equation (1G.4) into (1G.3), the leading term of the transition will dominate in any instance where the contained Dirac bracket is non-zero and as such the polarisability emerges in the approximate form:

$$\alpha_{ij}^{\alpha 0|A} \approx \left\langle \psi_\alpha \middle| (Q - Q_0) \middle| \psi_0 \right\rangle \frac{\partial \alpha_{ij}^{00}}{\partial Q}\Big|_{Q_0} + \ldots . \tag{1G.5}$$

The symmetry associated with the right-hand side of this equation determines the criteria for allowing a Raman transition to occur. The elicited irreducible representations correspond with the quadratic terms listed in character tables [105].

COMPLEMENT 1H: LAGUERRE POLYNOMIALS

The main features present, are a product of a Gaussian with an associated Laguerre polynomial, the latter being one of the solutions of the following partial differential equation:

$$x\frac{\partial^2 L_l^p(x)}{\partial x^2}+(p+1-x)\frac{\partial L_l^p(x)}{\partial x}+l\,L_l^p(x)=0\ . \tag{1H.1}$$

Note that it is the $|l|$ of that appears in equation (1.6.10), signifying that optical vortices of opposite topological charge have identical radial distributions; their physical differences arise through their phase factors, considered below.

Orthogonality amongst the associated Laguerre polynomials is usually specified with respect to those of the same index p. The form that is relevant for Laguerre-Gaussian beam applications, which also introduces a weighting factor, is expressible as follows;

$$\int_0^\infty e^{-x}x^p L_l^p(x)L_{l'}^p(x)dx=\frac{(l+p)!}{l!}\delta_{ll'}\ . \tag{1H.2}$$

More generally [106], it may be noted, for the following in terms of hypergeometric functions is found;

$$\begin{aligned}&\int_0^\infty x^\mu \mathrm{e}^{-x}L_l^p(x)L_{l'}^{p'}(x).\mathrm{d}x\\&=\binom{l+p}{l}\binom{l'+p'-\mu-1}{l'}{}_3F_2(-m,\mu+1,\mu-p'+1;p+1,\mu-p'-n+1;1)\Gamma(\mu+1)\ .\end{aligned} \tag{1H.3}$$

2

MULTICENTRE RAMAN SCATTERING

2.1 INTRODUCTION

This chapter will build on two preceding sections: §1.4B and §1.5, by considering the effect of neighbouring molecules on Raman scattering [107, 108]. In the latter section, it was mentioned that a virtual photon exchange between two centres can modify the symmetry of a system, and for these purposes, allow a Raman transition to occur where it might not usually be observable. The evolution of two (or more) centres can be connected by considering virtual photon exchange(s) between the centres concurrent to the Raman scattering event [21-23]. In principle, any number of additional interactions can be rigorously accommodated, however, each virtual photon interaction will increase the order of perturbation theory required to describe the process. This in turn reduces the relative amplitude of contribution.

In §1.4B Raman scattering was introduced as a two-photon process with the $n=2$ leading contributor to the matrix element, as seen in equation (1.3.14), which is fed into the rate of the process too. Each virtual photon exchange will add two photon-molecule interactions (one at each optical centre) and therefore see a corresponding increase in the order of perturbation theory engaged. In this chapter, the leading two contributors to the neighbour mediated Raman scattering will be considered. This involves the one or two virtual photon exchange(s) between a centre undergoing a Raman transition and a neighbouring centre. All relevant quantum interference terms are calculated too.

Figure 9 displays a schematic for this process, with a detector placed perpendicular to the incident beam. In such a setup, the resultant Raman spectrum will display the additionally

permitted transitions as new vibrational frequencies, in addition to modifying the intensities of pre-existing vibrational modes. Despite the higher orders of perturbation theory required to accommodate virtual photon interactions, all degrees of coupling to other centres always utilise just one photon from the laser mode. As such, multicentre Raman scattering mechanisms in this chapter, like the single-centre case, have a linear dependence on the incident laser intensity.

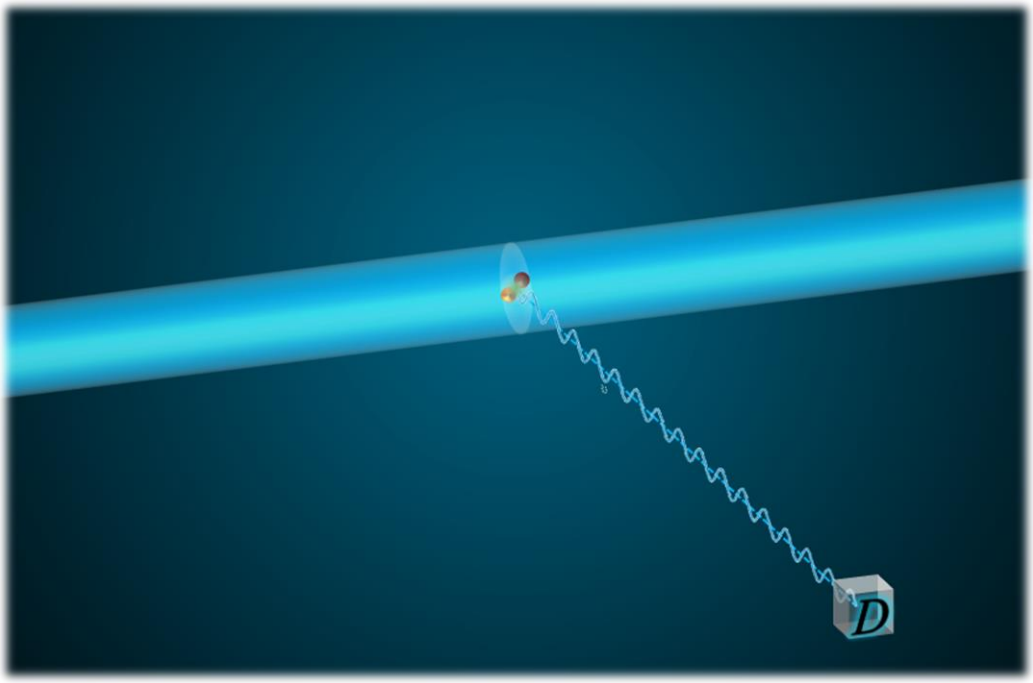

Figure 9: Schematic depiction of a pairwise interaction between two centres in the course of a Raman scattering process, with a detector, D, perpendicular to that of the incident beam.

Previous work has incorporated a second centre for the purposes of bimolecular cooperative Raman excitation [109]. In such a process, the photon annihilation and creation events are split between the two involved centres with a virtual photon coupling the pair. This is one configuration of the photon-molecular interactions that has been included in this work, see §2.2A. However, the previous work specifically considered the excitation to be split across the pair, whereas here the excitation will be localised to the one centre of spectroscopic interest, molecule A. As such, the neighbouring molecule B will always be regarded to enter and leave the process in its ground electronic and vibrational state.

A few realistic parameters have been chosen to carry out the following analysis. Firstly, both centres are considered to be chemically distinct. Secondly, in the course of the process the molecular tumbling is treated to be on a much slower time scale than that which the process evolves at. As such, the orientation of both centres can be regarded as fixed, at a distance R, throughout the process. Moreover, they will be fixed at a distance that satisfies the near-field approximation, equation (1.5.2) [21]. In this region, terms with more negative powers of R will be most readily measurable. Lastly, for demonstrative purposes a Stokes transition has been assumed throughout, although analogous principles hold for the anti-Stokes counterpart.

2.2 GENERAL THEORY

All process involving two or more interaction events have more than one pathway to connect the initial and final state for a process. In cases like these, where there is coupling between two or more centres, there is an additional consideration; not only the temporal order of the interactions can be permuted but also the spatial distribution across the centres. The result of this is that each centre can have a range in number of interactions to contribute to its molecular response. Each molecular response tensor engaged has its own matrix element which contributes to the rate of a process.

The superscript attached to each matrix element will identify the location the photon operators engage with. All will contain A and B, to represent the two molecules, the letter that precedes the other indicates the site of photon annihilation; a prime will be attached to one of the letters to identify the site of the creation event, which may or may not be the same. The number of vertical bars appearing in the superscript will correspond to the number of virtual photon exchanges present between the pair of molecules. Previously, it was introduced that the contribution from both one and two virtual photon exchanges will be included.

In the case of one virtual photon exchange between two centres, there are four unique arrangements that the real photon-molecule interactions can occur. Case *I*, the annihilation at molecule *A* and creation at molecule *B*, $M_{FI}^{A|B'}$. Case *II*, is where the roles of A and B in case

I are interchanged, *i.e.* the radiation mode is annihilated at *B* and created at A, $M_{FI}^{B|A'}$. Case *III*, is a contribution corresponding to the photon annihilation and creation at A, as with conventional Raman, $M_{FI}^{A'|B}$. Case *IV*, is where the radiation modes are both annihilated and created at molecule *B*, $M_{FI}^{B'|A}$. These cases will be covered.

In the case of two virtual photon exchanges between the pair of molecules, there are the same arrangement of real photon-molecule interactions as with cases *I* – *IV*. These will be assigned cases *V* – *VIII*, and will be covered in §2.2E-H, respectively. As an example, case *V* is case *I* with an additional virtual photon exchange. In principle, all occurrences of two virtual photon exchanges are indistinguishable and therefore, similarly to §1.4C, one time-ordering can be considered for both. Although, as will be demonstrated late, further index symmetry is not precluded.

The dipole approximation will be used throughout, to ensure a significant contribution towards the process. This in turn enables the deployment of the V-tensor, introduced in §1.5. In particular, we are interested in the near-zone form, equation (1.5.2). At the static limit, $k = 0$, this can be treated as an instantaneous interaction between the two molecules, usually depicted as a horizontal line connecting the world-lines for the two centres. Consequently, only one additional intermediary state is added for the first virtual photon and two thereafter.

2.2A CASE *I*

The first case considered is where each molecule will engage in a two-photon process: one real and one virtual photon interaction. The real photon events, annihilation and creation, are split across molecules A and B respectively. Moreover, the single virtual photon exchange between the two centres connects the world lines of the two centres and can be regarded as occurring within a single instant. As such, the $n = 3$ from equation (1.3.14) is the leading contributor with two associated intermediary states r and s to be summed over. There are six permutations of time-orderings that are possible, see Figure 10 for one example. Each contributes a single term to the matrix element for the process, which takes the following form,

$$
\begin{aligned}
M_{FI}^{A|B'} = & \frac{1}{\varepsilon_0^2} \times \\
& \sum_{r,s} \Bigg\{ \frac{\left\langle \alpha;0;\mathbf{k}',\eta' \middle| \mu_i^B d_i^{\perp} \middle| \alpha;s;0 \right\rangle \left\langle \alpha;s;0 \middle| \mu_k^A V_{kl}\left(0;R_{AB}\right) \mu_l^B \middle| r;0;0 \right\rangle \left\langle r;0;0 \middle| \mu_j^A d_j^{\perp} \middle| 0;0;\mathbf{k},\eta \right\rangle}{\left[E_{0\alpha}^A + E_{0s}^B + \hbar ck \right] \left[E_{0r}^A + \hbar ck \right]} \\
& + \frac{\left\langle \alpha;0;\mathbf{k}',\eta' \middle| \mu_k^A V_{kl}\left(0;R_{AB}\right) \mu_l^B \middle| r;s;\mathbf{k}',\eta' \right\rangle \left\langle r;s;\mathbf{k}',\eta' \middle| \mu_i^B d_i^{\perp} \middle| r;0;0 \right\rangle \left\langle r;0;0 \middle| \mu_j^A d_j^{\perp} \middle| 0;0;\mathbf{k},\eta \right\rangle}{\left[E_{0r}^A + E_{0s}^B + \hbar ck - \hbar ck' \right] \left[E_{0r}^A + \hbar ck \right]} \\
& + \frac{\left\langle \alpha;0;\mathbf{k}',\eta' \middle| \mu_i^B d_i^{\perp} \middle| \alpha;s;0 \right\rangle \left\langle \alpha;s;0 \middle| \mu_j^A d_j^{\perp} \middle| r;s;\mathbf{k},\eta \right\rangle \left\langle r;s;\mathbf{k},\eta \middle| \mu_k^A V_{kl}\left(0;R_{AB}\right) \mu_l^B \middle| 0;0;\mathbf{k},\eta \right\rangle}{\left[E_{0\alpha}^A + E_{0s}^B + \hbar ck \right] \left[E_{0r}^A + E_{0s}^B \right]} \\
& + \frac{\left\langle \alpha;0;\mathbf{k}',\eta' \middle| \mu_k^A V_{kl}\left(0;R_{AB}\right) \mu_l^B \middle| r;s;\mathbf{k}',\eta' \right\rangle \left\langle r;s;\mathbf{k}',\eta' \middle| \mu_j^A d_j^{\perp} \middle| 0;s;\mathbf{k},\eta;\mathbf{k}',\eta' \right\rangle}{\left[E_{0r}^A + E_{0s}^B + \hbar ck - \hbar ck' \right] \left[E_{0s}^B - \hbar ck' \right]} \\
& \quad \times \left\langle 0;s;\left(\mathbf{k},\eta;\mathbf{k}',\eta'\right) \middle| \mu_i^B d_i^{\perp} \middle| 0;0;\mathbf{k},\eta \right\rangle \\
& + \frac{\left\langle \alpha;0;\mathbf{k}',\eta' \middle| \mu_j^A d_j^{\perp} \middle| r;0;\left(\mathbf{k},\eta;\mathbf{k}',\eta'\right) \right\rangle \left\langle r;0;\left(\mathbf{k},\eta;\mathbf{k}',\eta'\right) \middle| \mu_i^B d_i^{\perp} \middle| r;s;\mathbf{k},\eta \right\rangle}{\left[E_{0r}^A - \hbar ck' \right] \left[E_{0r}^A + E_{0s}^B \right]} \\
& \quad \times \left\langle r;s;\mathbf{k},\eta \middle| \mu_k^A V_{kl}\left(0;R_{AB}\right) \mu_l^B \middle| 0;0;\mathbf{k},\eta \right\rangle \\
& + \frac{\left\langle \alpha;0;\mathbf{k}',\eta' \middle| \mu_j^A d_j^{\perp} \middle| r;0;\left(\mathbf{k},\eta;\mathbf{k}',\eta'\right) \right\rangle \left\langle r;0;\left(\mathbf{k},\eta;\mathbf{k}',\eta'\right) \middle| \mu_k^A V_{kl}\left(0;R_{AB}\right) \mu_l^B \middle| 0;s;\left(\mathbf{k},\eta;\mathbf{k}',\eta'\right) \right\rangle}{\left[E_{0r}^A - \hbar ck' \right] \left[E_{0s}^B - \hbar ck' \right]} \\
& \quad \times \left\langle 0;s;\left(\mathbf{k},\eta;\mathbf{k}',\eta'\right) \middle| \mu_i^B d_i^{\perp} \middle| 0;0;\mathbf{k},\eta \right\rangle \Bigg\} \ . \qquad (2.2.1)
\end{aligned}
$$

The first term corresponds to the contribution from the time ordering displayed in Figure 10. Each of the Dirac brackets above represents the transition between two states of the time series shown up the left-hand-side of the Feynman diagram in Figure 10. Each individual component is the combination of all states present in that interval. Two out of the three instantaneous interactions are real photon transitions, mediated by the interaction Hamiltonian. These can be seen in the heart of the Dirac bracket and modify a single radiation and molecular state, with the ε_0^{-2} extracted as a common factor. The third interaction is handled by the static V-tensor, which is capable of acting on two molecular states. As discussed in the previous chapter, the denominators represent the energy for each intermediate state relative to that contained in the entire system at the inception of (or indeed subsequent to) the process.

Next, the Dirac brackets can be evaluated, in conjunction with completeness relation, equation (1.4.3), the following can be cast,

$$M_{FI}^{A|B'} = \frac{\hbar c\sqrt{kk'n}}{8\varepsilon_0^2\pi R^3 V}\bar{e}_i' e_j \left(\delta_{kl} - 3\hat{R}_k\hat{R}_l\right)\sum_{r,s}\left\{\frac{\mu_k^{\alpha r|A}\mu_j^{r0|A}\mu_i^{0s|B}\mu_l^{s0|B}}{\left[E_{\alpha 0}^A + E_{s0}^B - \hbar ck\right]\left[E_{r0}^A - \hbar ck\right]}\right.$$
$$+\frac{\mu_k^{\alpha r|A}\mu_j^{r0|A}\mu_l^{0s|B}\mu_i^{s0|B}}{\left[E_{r0}^A + E_{s0}^B - \hbar ck + \hbar ck'\right]\left[E_{r0}^A - \hbar ck\right]}$$
$$+\frac{\mu_j^{\alpha r|A}\mu_k^{r0|A}\mu_i^{0s|B}\mu_l^{s0|B}}{\left[E_{\alpha 0}^A + E_{s0}^B - \hbar ck\right]\left[E_{r0}^A + E_{s0}^B\right]}$$
$$+\frac{\mu_k^{\alpha r|A}\mu_j^{r0|A}\mu_l^{0s|B}\mu_i^{s0|B}}{\left[E_{r0}^A + E_{s0}^B - \hbar ck + \hbar ck'\right]\left[E_{s0}^B + \hbar ck'\right]}$$
$$+\frac{\mu_j^{\alpha r|A}\mu_k^{r0|A}\mu_i^{0s|B}\mu_l^{s0|B}}{\left[E_{r0}^A + \hbar ck'\right]\left[E_{r0}^A + E_{s0}^B\right]}$$
$$\left.+\frac{\mu_j^{\alpha r|A}\mu_k^{r0|A}\mu_l^{0s|B}\mu_i^{s0|B}}{\left[E_{r0}^A + \hbar ck'\right]\left[E_{s0}^B + \hbar ck'\right]}\right\}, \qquad (2.2.2)$$

the additional prefactor in parentheses is an orientational weighting, introduced by the V-tensor.

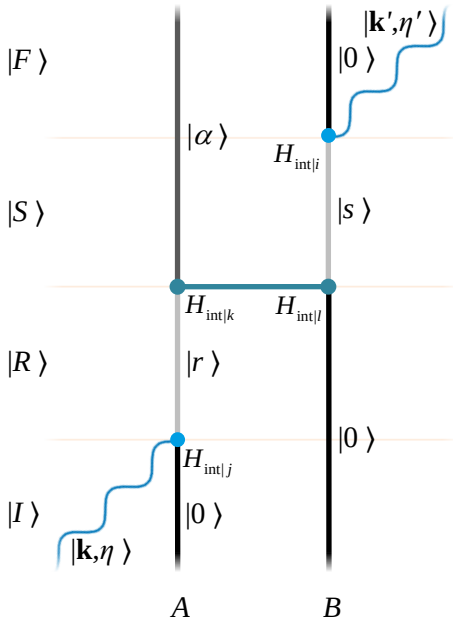

Figure 10: A single representative Feynman diagrams for the time evolution of two molecules *A* and *B*. Prior to the process both centres are in their ground state at a point in time the molecule of spectroscopic interest annihilates a photon and transitions to a virtual intermediate state, *r*. At a subsequent instant, a virtual photon is exchanged between the pair; molecule *A* is left in a vibrationally excited state, while its neighbour transitions to a virtual state, *s*, before immediately creating the scattered photon and returning to its ground state.

Notice that there are two pairs of equivalent numerators, these can be combined by taking common denominators to form four unique contributions. The relation for energy conservation, equation (1.4.16), can also be incorporated to simplify the denominators as follows,

$$M_{FI}^{A|B'} = \frac{\hbar c\sqrt{kk'n}}{8\varepsilon_0^2\pi R^3 V}\bar{e}_i' e_j \left(\delta_{kl} - 3\hat{R}_k\hat{R}_l\right)\sum_{r,s}\left\{\frac{\mu_k^{\alpha r|A}\mu_j^{r0|A}\mu_i^{0s|B}\mu_l^{s0|B}}{\left[E_{r0}^A - \hbar ck\right]\left[E_{s0}^B - \hbar ck'\right]}\right.$$
$$+\frac{\mu_j^{\alpha r|A}\mu_k^{r0|A}\mu_l^{0s|B}\mu_i^{s0|B}}{\left[E_{r\alpha}^A + \hbar ck\right]\left[E_{s0}^B + \hbar ck'\right]}$$
$$+\frac{\mu_k^{\alpha r|A}\mu_j^{r0|A}\mu_l^{0s|B}\mu_i^{s0|B}}{\left[E_{r0}^A - \hbar ck\right]\left[E_{s0}^B + \hbar ck'\right]}$$
$$\left.+\frac{\mu_j^{\alpha r|A}\mu_k^{r0|A}\mu_i^{0s|B}\mu_l^{s0|B}}{\left[E_{r\alpha}^A + \hbar ck\right]\left[E_{s0}^B - \hbar ck'\right]}\right\}, \qquad (2.2.3)$$

Here, the summand can be factorised as a product of two summands over r and s as follows,

$$\alpha_{(jk)}'^{\alpha 0|A} = \sum_r\left\{\frac{\mu_k^{\alpha r|A}\mu_j^{r0|A}}{E_{r0}^A - \hbar ck} + \frac{\mu_j^{\alpha r|A}\mu_k^{r0|A}}{E_{r0}^A + \hbar ck'}\right\}, \qquad (2.2.4)$$

$$\alpha_{(il)}''^{00|B} = \sum_s\left\{\frac{\mu_i^{0s|B}\mu_l^{s0|B}}{E_{s0}^B - \hbar ck'} + \frac{\mu_l^{0s|B}\mu_i^{s0|B}}{E_{s0}^B + \hbar ck'}\right\}. \qquad (2.2.5)$$

These are the familiar polarisability tensors, with one associable to each of the molecules involved in the process. The parenthesis around the subscript indices represent permutable symmetry and always arise in linear polarisability tensors, involving two transition moments connecting the same pair of states [110], see complement 1B. The vibrational transition is not a sufficient difference to break this form of symmetry. The contracted from of the matrix element is now,

$$M_{FI}^{A|B'} = \frac{\hbar c\sqrt{kk'n}}{8\pi\varepsilon_0^2 R^3 V}\bar{e}_i' e_j \left(\delta_{kl} - 3\hat{R}_k\hat{R}_l\right)\alpha_{(jk)}'^{\alpha 0|A}\alpha_{(il)}''^{00|B}. \qquad (2.2.6)$$

Interestingly, one can factorise out Coulomb's constant $\left(4\pi\varepsilon_0\right)^{-1}$ and the distance dependence R^{-3}, to leave a matrix element with identical constant structure and field products as that seen in equation (1.4.14).

2.2B CASE *II*

This case delivers the contribution from the annihilation event on molecule B and the creation event on molecule A, again with a single virtual photon exchanged in the course of the process. Visually, it is very comparable to that of the previous case, as can be seen when you compare the respective figures.

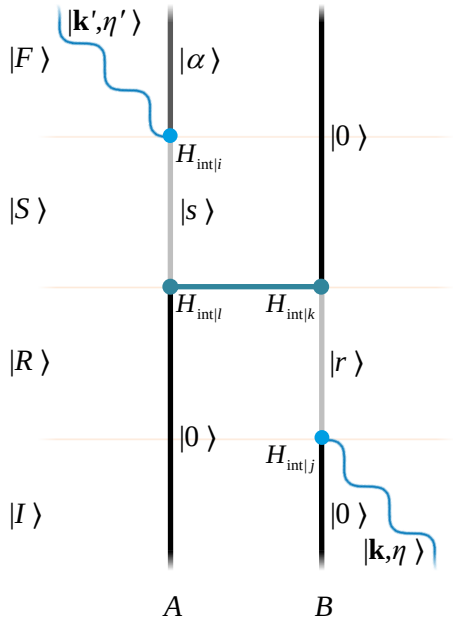

Figure 11: Similar to Figure 10, this is one of six permutations of time orderings for this case, in Feynman diagrammatic representation. The difference here is the sites of the photon operators are interchanged.

The resultant derivation mirrors the visual similarities and has been omitted for that reason, the resulting response tensors are as follows:

$$\alpha_{(il)}^{\prime\prime\prime\alpha 0|A} = \sum_{s}\left\{\frac{\mu_i^{\alpha s|A}\mu_l^{s0|A}}{E_{s0}^{A}-\hbar ck}+\frac{\mu_l^{\alpha s|A}\mu_i^{s0|A}}{E_{s\alpha}^{A}+\hbar ck}\right\}, \tag{2.2.7}$$

$$\alpha_{(jk)}^{\prime\prime\prime r00|B} = \sum_{r}\left\{\frac{\mu_j^{0r|B}\mu_k^{r0|B}}{E_{r0}^{B}+\hbar ck}+\frac{\mu_k^{0r|B}\mu_j^{r0|B}}{E_{r0}^{B}-\hbar ck}\right\}. \tag{2.2.8}$$

The resultant matrix element is almost identical in form too,

$$M_{FI}^{B|A'} = \frac{\hbar c\sqrt{kk'n}}{8\pi\varepsilon_0^2 R^3 V}\bar{e}_i' e_j\left(\delta_{kl}-3\hat{R}_k\hat{R}_l\right)\alpha_{(il)}^{\prime\prime\prime\alpha 0|A}\alpha_{(jk)}^{\prime\prime\prime r00|B}. \tag{2.2.9}$$

2.2C CASE *III*

This is the closest comparable contribution to the single-centre Raman scattering. The two real photon-molecule events are on the molecule of spectroscopic interest, with the single virtual photon the only interaction molecule B engages in.

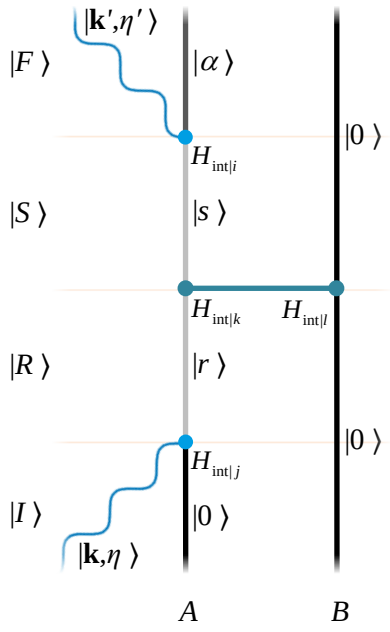

Figure 12: Another example of one time series for this case in Feynman diagrammatic form.

Again, the derivation for this is almost identical to that presented for case *I*, in §2.2A. However, unlike the first two cases, the six permutable orders all have unique numerators and as such it is not possible to take a common denominator to reduce the number of terms in the summand down to four. It is possible to take the transition moment for molecule B as a common factor for all six terms, $\mu_l^{00|B}$, which indicates that this molecule must have a permanent static dipole *i.e.* it must be a polar molecule. With three interactions on molecule A and two virtual states to sum over, the response tensor is displayed as follows,

$$\beta_{(ij)k}^{\alpha 0|A} = \sum_{r,s}\left\{\frac{\mu_i^{\alpha s|A}\mu_k^{sr|A}\mu_j^{r0|A}}{\left[E_{s0}^A-\hbar ck\right]\left[E_{r0}^A-\hbar ck\right]}+\frac{\mu_k^{\alpha s|A}\mu_i^{sr|A}\mu_j^{r0|A}}{E_{s\alpha}^A\left[E_{r0}^A-\hbar ck\right]}+\frac{\mu_i^{\alpha s|A}\mu_j^{sr|A}\mu_k^{r0|A}}{\left[E_{s0}^A-\hbar ck\right]E_{r0}^A}\right.$$
$$\left.+\frac{\mu_k^{\alpha s|A}\mu_j^{sr|A}\mu_i^{r0|A}}{E_{s\alpha}^A\left[E_{r\alpha}^A+\hbar ck\right]}+\frac{\mu_j^{\alpha s|A}\mu_i^{sr|A}\mu_k^{r0|A}}{\left[E_{s\alpha}^A+\hbar ck\right]E_{r0}^A}+\frac{\mu_j^{\alpha s|A}\mu_k^{sr|A}\mu_i^{r0|A}}{\left[E_{s\alpha}^A+\hbar ck\right]\left[E_{r\alpha}^A+\hbar ck\right]}\right\}. \qquad (2.2.10)$$

Note, this is not the same as the hyperpolarisability which appears as equation (1.4.22).

The matrix element is therefore expressible as follow, with a familiar structure,

$$M_{FI}^{A'|B} = \frac{\hbar c\sqrt{kk'n}}{8\pi\varepsilon_0^2 R^3 V}\bar{e}_i' e_j \left(\delta_{kl} - 3\hat{R}_k\hat{R}_l\right)\beta_{(ij)k}^{\alpha 0|A}\mu_l^{00|B} \ . \tag{2.2.11}$$

Note, there is no energy exchange between the two molecules, which is consistent with the requirement of a polar molecule *B*; this does not arise in any of the other cases.

At this stage, it is necessary to consider the nature of this hyperpolarisability response tensor. It is not possible to directly apply the Born-Oppenheimer treatment as cast in complement 1G. However, similar principles still hold by expressing the response tensor as a Taylor series expansion with leading contribution,

$$\beta_{(ij)k}^{\alpha 0} \approx \left\langle \psi_\beta \middle| \left(Q - Q_0\right) \middle| \psi_0 \right\rangle \left.\frac{\partial \beta_{(ij)k}^{00}}{\partial Q}\right|_{Q_0} + \ldots \ . \tag{2.2.12}$$

Symmetry in the interaction indices has been indicated, in this instance, analysis of the tensors is required to assert this, see complement 1B. Index symmetry will arise if any set of indices can be interchanged and in turn the original response tensor is regenerated. If we first identify two interactions that involve two similar radiation modes: the two real photon interactions, i and j in this case. It is known that the states r and s are arbitrary and as such it is possible to interchange them without altering the regarded system. Following these two interchanges the hyperpolarisability tensor takes the following form,

$$\begin{aligned}\beta_{(ji)k}^{\alpha 0|A} = \sum_{s,r}\Bigg\{ & \frac{\mu_j^{\alpha r|A}\mu_k^{rs|A}\mu_i^{s0|A}}{\left[E_{r0}^A - \hbar ck\right]\left[E_{s0}^A - \hbar ck\right]} + \frac{\mu_j^{\alpha r|A}\mu_i^{rs|A}\mu_k^{s0|A}}{\left[E_{r0}^A - \hbar ck\right]E_{s0}^A} + \frac{\mu_k^{\alpha r|A}\mu_j^{rs|A}\mu_i^{s0|A}}{E_{r\alpha}^A\left[E_{s0}^A - \hbar ck\right]} \\ & + \frac{\mu_i^{\alpha r|A}\mu_j^{rs|A}\mu_k^{s0|A}}{\left[E_{r\alpha}^A + \hbar ck\right]E_{s0}^A} + \frac{\mu_k^{\alpha r|A}\mu_i^{rs|A}\mu_j^{s0|A}}{E_{r\alpha}^A\left[E_{s\alpha}^A + \hbar ck\right]} + \frac{\mu_i^{\alpha r|A}\mu_k^{rs|A}\mu_j^{s0|A}}{\left[E_{r\alpha}^A + \hbar ck\right]\left[E_{s\alpha}^A + \hbar ck\right]}\Bigg\} \ .\end{aligned} \tag{2.2.13}$$

With foresight of the end result, terms two and four have switched positions with terms three and five, respectively. It is known that the inner product of two Dirac brackets, where the bra and ket of one are the same as the ket and bra in the other, are identically equal. Under the

notation deployed here, on any given transition moment the superscript indices represent the molecular states, see equation (1.4.2), it follows that,

$$\mu_k^{sr|A} \equiv \mu_k^{rs|A} \ . \tag{2.2.14}$$

As can be seen, this is identical to equation (2.2.10), all apart from the vibrational energies; these are known to be negligible when compared to that of the electronic transitions allowing us to justifiably disregard them.

2.2D CASE *IV*

An interesting quirk of deploying MQED is that it is entirely possible that the molecule of spectroscopic interest doesn't even "interact" with either of the real photons. Explicitly, molecule B both annihilates and creates the real photon with the single virtual photon exchange imparting the vibrational transition on molecule A.

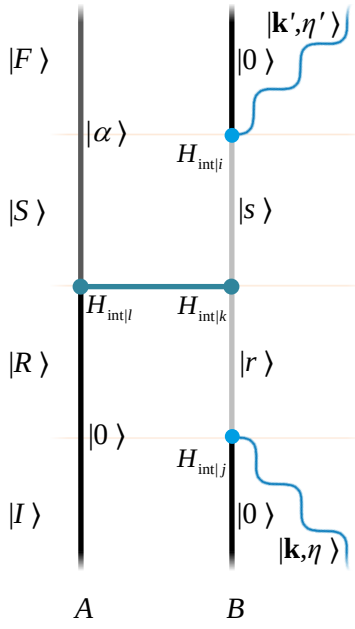

Figure 13: An example time series, in Feynman diagram form, for the final photon-molecule interaction site arrangement.

The derivation of this matrix element is largely the same as that of the previous case,

$$\beta'^{\,00|B}_{ijk} = \sum_{r,s}\left\{ \frac{\mu_i^{0s|B}\mu_k^{sr|B}\mu_j^{r0|B}}{\left[E_{s0}^B - \hbar ck'\right]\left[E_{r0}^B - \hbar ck\right]} + \frac{\mu_k^{0s|B}\mu_i^{sr|B}\mu_j^{r0|B}}{\left[E_{s0}^B - \hbar ck + \hbar ck'\right]\left[E_{r0}^B - \hbar ck\right]} \right.$$
$$+ \frac{\mu_i^{0s|B}\mu_j^{sr|B}\mu_k^{r0|B}}{\left[E_{s0}^B - \hbar ck'\right]\left[E_{r0}^B + \hbar ck - \hbar ck'\right]} + \frac{\mu_k^{0s|B}\mu_j^{sr|B}\mu_i^{r0|B}}{\left[E_{s0}^B - \hbar ck + \hbar ck'\right]\left[E_{r0}^B + \hbar ck'\right]}$$
$$\left. + \frac{\mu_j^{0s|B}\mu_i^{sr|B}\mu_k^{r0|B}}{\left[E_{s0}^B + \hbar ck\right]\left[E_{r0}^B + \hbar ck - \hbar ck'\right]} + \frac{\mu_j^{0s|B}\mu_k^{sr|B}\mu_i^{r0|B}}{\left[E_{s0}^B + \hbar ck\right]\left[E_{r0}^B + \hbar ck'\right]} \right\} . \qquad (2.2.15)$$

There is an immediate visual difference in the denominators. Here, the energy conservation relation, equation (1.4.16), is utilised to replace the presence of molecule A, which demands the presence of more photon energies. It also results in the inability to find any index symmetry in this tensor. The matrix element that seats the above hyperpolarisability tensor is,

$$M_{FI}^{B'|A} = \frac{\sqrt{kk'n}\hbar c}{8\pi\varepsilon_0^2 R^3 V}\bar{e}_i' e_j \left(\delta_{kl} - 3\hat{R}_k\hat{R}_l\right)\beta'^{\,00|B}_{ijk}\mu_l^{\alpha 0|A} \ . \qquad (2.2.16)$$

Here, the transition dipole moment exhibits the vibrational transition, which will in effect have the same selection rules as infrared absorption. The hyperpolarisability tensor here displays symmetry characteristics associated with a three-photon process and has an analogous effect to that of the electro-optic tensor [111], inducing a vibrational displacement onto its neighbour.

2.2E CASE V

This is the first case in which we consider a second virtual photon. In this case, molecule A annihilates the photon and molecule B creates the scattered photon, see Figure 14. As such, each molecule engages in a three-photon process, with two additional pairs of interactions occurring at two separate instants of time. These two events are indistinguishable and as such, interchanging them does not contribute an addition time-ordering. In equation (1.3.14), $n = 5$ term will be the leading contributor with two associated intermediary states r, s, t and u to be summed over. There are twelve possible permutations of time-orderings and again, each contributes one term to the matrix element for the process, as follows,

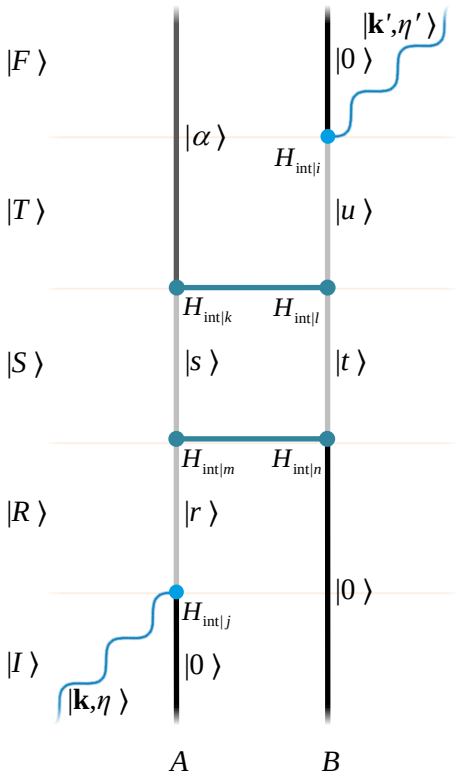

Figure 14: This is very closely related to the Feynman diagram depicted in Figure 10, except a total of two virtual photon exchanges occur between the pair of molecules, making for a total of six interactions, distributed as three interactions at each of the molecules. Two additional intermediary states are required to describe this process t and u. The additional virtual photon exchange doubles the number of possible permutations of time-orderings to twelve.

$$
\begin{aligned}
M_{FI}^{A\|B'} = \frac{1}{\varepsilon_0^2}\sum_{r,s,t,u}\Bigg\{ & \frac{\left\langle \alpha;0;\mathbf{k}',\eta'\middle|\mu_i^B d_i^{\perp}\middle|\alpha;u;0\right\rangle\left\langle \alpha;u;0\middle|\mu_k^A V_{kl}\left(0;R_{AB}\right)\mu_l^B\middle|s;t;0\right\rangle}{\left[E_0^A+E_0^B+\hbar ck-\left(E_\alpha^A+E_u^B\right)\right]\left[E_0^A+E_0^B+\hbar ck-\left(E_s^A+E_t^B\right)\right]} \\
& \times\frac{\left\langle s;t;0\middle|\mu_m^A V_{mn}\left(0;R_{AB}\right)\mu_n^B\middle|r;0;0\right\rangle\left\langle r;0;0\middle|\mu_j^A d_j^{\perp}\middle|0;0;\mathbf{k},\eta\right\rangle}{\left[E_0^A+E_0^B+\hbar ck-\left(E_r^A+E_0^B\right)\right]} \\
& +\frac{\left\langle \alpha;0;\mathbf{k}',\eta'\middle|\mu_k^A V_{kl}\left(0;R_{AB}\right)\mu_l^B\middle|s;u;\mathbf{k}',\eta'\right\rangle\left\langle s;u;\mathbf{k}',\eta'\middle|\mu_i^B d_i^{\perp}\middle|s;t;0\right\rangle}{\left[E_0^A+E_0^B+\hbar ck-\left(E_s^A+E_u^B+\hbar ck'\right)\right]\left[E_0^A+E_0^B+\hbar ck-\left(E_s^A+E_t^B\right)\right]} \\
& \times\frac{\left\langle s;t;0\middle|\mu_m^A V_{mn}\left(0;R_{AB}\right)\mu_n^B\middle|r;0;0\right\rangle\left\langle r;0;0\middle|\mu_j^A d_j^{\perp}\middle|0;0;\mathbf{k},\eta\right\rangle}{\left[E_0^A+E_0^B+\hbar ck-\left(E_r^A+E_0^B\right)\right]} \\
& +\frac{\left\langle \alpha;0;\mathbf{k}',\eta'\middle|\mu_k^A V_{kl}\left(0;R_{AB}\right)\mu_l^B\middle|s;u;\mathbf{k}',\eta'\right\rangle\left\langle s;u;\mathbf{k}',\eta'\middle|\mu_m^A V_{mn}\left(0;R_{AB}\right)\mu_n^B\middle|r;t;\mathbf{k}',\eta'\right\rangle}{\left[E_0^A+E_0^B+\hbar ck-\left(E_s^A+E_u^B+\hbar ck'\right)\right]\left[E_0^A+E_0^B+\hbar ck-\left(E_r^A+E_t^B+\hbar ck'\right)\right]} \\
& \times\frac{\left\langle r;t;\mathbf{k}',\eta'\middle|\mu_i^B d_i^{\perp}\middle|r;0;0\right\rangle\left\langle r;0;0\middle|\mu_j^A d_j^{\perp}\middle|0;0;\mathbf{k},\eta\right\rangle}{\left[E_0^A+E_0^B+\hbar ck-\left(E_r^A+E_0^B\right)\right]} \\
& +\frac{\left\langle \alpha;0;\mathbf{k}',\eta'\middle|\mu_i^B d_i^{\perp}\middle|\alpha;u;0\right\rangle\left\langle \alpha;u;0\middle|\mu_k^A V_{kl}\left(0;R_{AB}\right)\mu_l^B\middle|s;t;0\right\rangle}{\left[E_0^A+E_0^B+\hbar ck-\left(E_\alpha^A+E_u^B\right)\right]\left[E_0^A+E_0^B+\hbar ck-\left(E_s^A+E_t^B\right)\right]} \\
& \times\frac{\left\langle s;t;0\middle|\mu_j^A d_j^{\perp}\middle|r;t;\mathbf{k},\eta\right\rangle\left\langle r;t;\mathbf{k},\eta\middle|\mu_m^A V_{mn}\left(0;R_{AB}\right)\mu_n^B\middle|0;0;\mathbf{k},\eta\right\rangle}{\left[E_0^A+E_0^B+\hbar ck-\left(E_r^A+E_t^B+\hbar ck\right)\right]} \\
& +\frac{\left\langle \alpha;0;\mathbf{k}',\eta'\middle|\mu_k^A V_{kl}\left(0;R_{AB}\right)\mu_l^B\middle|s;u;\mathbf{k},\eta'\right\rangle\left\langle s;u;\mathbf{k},\eta'\middle|\mu_i^B d_i^{\perp}\middle|s;t;0\right\rangle}{\left[E_0^A+E_0^B+\hbar ck-\left(E_s^A+E_u^B+\hbar ck'\right)\right]\left[E_0^A+E_0^B+\hbar ck-\left(E_s^A+E_t^B\right)\right]} \\
& \times\frac{\left\langle s;t;0\middle|\mu_j^A d_j^{\perp}\middle|r;t;\mathbf{k},\eta\right\rangle\left\langle r;t;\mathbf{k},\eta\middle|\mu_m^A V_{mn}\left(0;R_{AB}\right)\mu_n^B\middle|0;0;\mathbf{k},\eta\right\rangle}{\left[E_0^A+E_0^B+\hbar ck-\left(E_r^A+E_t^B+\hbar ck\right)\right]} \\
& +\frac{\left\langle \alpha;0;\mathbf{k}',\eta'\middle|\mu_k^A V_{kl}\left(0;R_{AB}\right)\mu_l^B\middle|s;u;\mathbf{k}',\eta'\right\rangle\left\langle s;u;\mathbf{k}',\eta'\middle|\mu_m^A V_{mn}\left(0;R_{AB}\right)\mu_n^B\middle|r;t;\mathbf{k}',\eta'\right\rangle}{\left[E_0^A+E_0^B+\hbar ck-\left(E_s^A+E_u^B+\hbar ck'\right)\right]\left[E_0^A+E_0^B+\hbar ck-\left(E_r^A+E_t^B+\hbar ck'\right)\right]} \\
& \times\frac{\left\langle r;t;\mathbf{k}',\eta'\middle|\mu_j^A d_j^{\perp}\middle|0;t;(\mathbf{k},\eta;\mathbf{k}',\eta')\right\rangle\left\langle 0;t;(\mathbf{k},\eta;\mathbf{k}',\eta')\middle|\mu_i^B d_i^{\perp}\middle|0;0;\mathbf{k},\eta\right\rangle}{\left[E_0^A+E_0^B+\hbar ck-\left(E_0^A+E_t^B+\hbar ck+\hbar ck'\right)\right]} \\
& +\frac{\left\langle \alpha;0;\mathbf{k}',\eta'\middle|\mu_i^B d_i^{\perp}\middle|\alpha;u;0\right\rangle\left\langle \alpha;u;0\middle|\mu_j^A d_j^{\perp}\middle|s;u;\mathbf{k},\eta\right\rangle}{\left[E_0^A+E_0^B+\hbar ck-\left(E_\alpha^A+E_u^B\right)\right]\left[E_0^A+E_0^B+\hbar ck-\left(E_s^A+E_u^B+\hbar ck\right)\right]} \\
& \times\frac{\left\langle s;u;\mathbf{k},\eta\middle|\mu_k^A V_{kl}\left(0;R_{AB}\right)\mu_l^B\middle|r;t;\mathbf{k},\eta\right\rangle\left\langle r;t;\mathbf{k},\eta\middle|\mu_m^A V_{mn}\left(0;R_{AB}\right)\mu_n^B\middle|0;0;\mathbf{k},\eta\right\rangle}{\left[E_0^A+E_0^B+\hbar ck-\left(E_r^A+E_t^B+\hbar ck\right)\right]} \\
& +\ldots
\end{aligned}
$$

$$
+\frac{\left\langle \alpha;0;\mathbf{k}',\eta'\left|\mu_k^A V_{kl}\left(0;R_{AB}\right)\mu_l^B\right|s;u;\mathbf{k}',\eta'\right\rangle\left\langle s;u;\mathbf{k}',\eta'\left|\mu_j^A d_j^{\perp}\right|r;u;(\mathbf{k},\eta;\mathbf{k}',\eta')\right\rangle}{\left[E_0^A+E_0^B+\hbar ck-\left(E_s^A+E_u^B+\hbar ck'\right)\right]\left[E_0^A+E_0^B+\hbar ck-\left(E_r^A+E_u^B+\hbar ck+\hbar ck'\right)\right]}
$$

$$
\times\frac{\left\langle r;u;(\mathbf{k},\eta;\mathbf{k}',\eta')\left|\mu_i^B d_i^{\perp}\right|r;t;\mathbf{k},\eta\right\rangle\left\langle r;t;\mathbf{k},\eta\left|\mu_m^A V_{mn}\left(0;R_{AB}\right)\mu_n^B\right|0;0;\mathbf{k},\eta\right\rangle}{\left[E_0^A+E_0^B+\hbar ck-\left(E_r^A+E_t^B+\hbar ck\right)\right]}
$$

$$
+\frac{\left\langle \alpha;0;\mathbf{k}',\eta'\left|\mu_k^A V_{kl}\left(0;R_{AB}\right)\mu_l^B\right|s;u;\mathbf{k}',\eta'\right\rangle\left\langle s;u;\mathbf{k}',\eta'\left|\mu_j^A d_j^{\perp}\right|r;u;(\mathbf{k},\eta;\mathbf{k}',\eta')\right\rangle}{\left[E_0^A+E_0^B+\hbar ck-\left(E_s^A+E_u^B+\hbar ck'\right)\right]\left[E_0^A+E_0^B+\hbar ck-\left(E_r^A+E_u^B+\hbar ck+\hbar ck'\right)\right]}
$$

$$
\times\frac{\left\langle r;u;(\mathbf{k},\eta;\mathbf{k}',\eta')\left|\mu_m^A V_{mn}\left(0;R_{AB}\right)\mu_n^B\right|0;t;(\mathbf{k},\eta;\mathbf{k}',\eta')\right\rangle\left\langle 0;t;(\mathbf{k},\eta;\mathbf{k}',\eta')\left|\mu_i^B d_i^{\perp}\right|0;0;\mathbf{k},\eta\right\rangle}{\left[E_0^A+E_0^B+\hbar ck-\left(E_0^A+E_t^B+\hbar ck+\hbar ck'\right)\right]}
$$

$$
+\frac{\left\langle \alpha;0;\mathbf{k}',\eta'\left|\mu_j^A d_j^{\perp}\right|s;0;(\mathbf{k},\eta;\mathbf{k}',\eta')\right\rangle\left\langle s;0;(\mathbf{k},\eta;\mathbf{k}',\eta')\left|\mu_i^B d_i^{\perp}\right|s;u;\mathbf{k},\eta\right\rangle}{\left[E_0^A+E_0^B+\hbar ck-\left(E_s^A+E_0^B+\hbar ck+\hbar ck'\right)\right]\left[E_0^A+E_0^B+\hbar ck-\left(E_s^A+E_u^B+\hbar ck\right)\right]}
$$

$$
\times\frac{\left\langle s;u;\mathbf{k},\eta\left|\mu_k^A V_{kl}\left(0;R_{AB}\right)\mu_l^B\right|r;t;\mathbf{k},\eta\right\rangle\left\langle r;t;\mathbf{k},\eta\left|\mu_m^A V_{mn}\left(0;R_{AB}\right)\mu_n^B\right|0;0;\mathbf{k},\eta\right\rangle}{\left[E_0^A+E_0^B+\hbar ck-\left(E_r^A+E_t^B+\hbar ck\right)\right]}
$$

$$
+\frac{\left\langle \alpha;0;\mathbf{k}',\eta'\left|\mu_j^A d_j^{\perp}\right|s;0;(\mathbf{k},\eta;\mathbf{k}',\eta')\right\rangle\left\langle s;0;(\mathbf{k},\eta;\mathbf{k}',\eta')\left|\mu_k^A V_{kl}\left(0;R_{AB}\right)\mu_l^B\right|r;u;(\mathbf{k},\eta;\mathbf{k}',\eta')\right\rangle}{\left[E_0^A+E_0^B+\hbar ck-\left(E_s^A+E_0^B+\hbar ck+\hbar ck'\right)\right]\left[E_0^A+E_0^B+\hbar ck-\left(E_r^A+E_u^B+\hbar ck+\hbar ck'\right)\right]}
$$

$$
\times\frac{\left\langle r;u;(\mathbf{k},\eta;\mathbf{k}',\eta')\left|\mu_i^B d_i^{\perp}\right|r;t;\mathbf{k},\eta\right\rangle\left\langle r;t;\mathbf{k},\eta\left|\mu_m^A V_{mn}\left(0;R_{AB}\right)\mu_n^B\right|0;0;\mathbf{k},\eta\right\rangle}{\left[E_0^A+E_0^B+\hbar ck-\left(E_r^A+E_t^B+\hbar ck\right)\right]}
$$

$$
+\frac{\left\langle \alpha;0;\mathbf{k}',\eta'\left|\mu_j^A d_j^{\perp}\right|s;0;(\mathbf{k},\eta;\mathbf{k}',\eta')\right\rangle\left\langle s;0;(\mathbf{k},\eta;\mathbf{k}',\eta')\left|\mu_k^A V_{kl}\left(0;R_{AB}\right)\mu_l^B\right|r;u;(\mathbf{k},\eta;\mathbf{k}',\eta')\right\rangle}{\left[E_0^A+E_0^B+\hbar ck-\left(E_s^A+E_0^B+\hbar ck+\hbar ck'\right)\right]\left[E_0^A+E_0^B+\hbar ck-\left(E_r^A+E_u^B+\hbar ck+\hbar ck'\right)\right]}
$$

$$
\times\left.\frac{\left\langle r;u;(\mathbf{k},\eta;\mathbf{k}',\eta')\left|\mu_m^A V_{mn}\left(0;R_{AB}\right)\mu_n^B\right|0;t;(\mathbf{k},\eta;\mathbf{k}',\eta')\right\rangle\left\langle 0;t;(\mathbf{k},\eta;\mathbf{k}',\eta')\left|\mu_i^B d_i^{\perp}\right|0;0;\mathbf{k},\eta\right\rangle}{\left[E_0^A+E_0^B+\hbar ck-\left(E_0^A+E_t^B+\hbar ck+\hbar ck'\right)\right]}\right\}.
$$

(2.2.17)

In all cases, the first term corresponds to the contribution from the time ordering displayed in the figure associated with the case. There are now four Dirac brackets to mediate the transition between states $|I\rangle$, $|R\rangle$, $|S\rangle$, $|T\rangle$ and $|F\rangle$, which each hold information on each of the two molecules and the radiation field. Two out of the four transitions are mediated by the interaction Hamiltonian, seen in the heart of the Dirac bracket and now two are handled by the V-tensor. There are now three terms present in the denominator are the energy for each intermediate state relative to that contained in the whole dynamical system at the inception of the process.

Evaluating all of the Dirac brackets and utilising the completeness relation, equation (1.4.3), the following can be cast,

$$
\begin{aligned}
M_{FI}^{A\|B'} = &-\frac{\hbar c\sqrt{kk'n}}{32\pi^2\varepsilon_0^3 R^6 V}\bar{e}_i' e_j \left(\delta_{kl} - 3\hat{R}_k\hat{R}_l\right)\left(\delta_{mn} - 3\hat{R}_m\hat{R}_n\right) \\
&\times \sum_{r,s,t,u}\left\{ \right. \\
&\frac{\mu_k^{\alpha s|A}\mu_m^{sr|A}\mu_j^{r0|A}\mu_i^{0u|B}\mu_l^{ut|B}\mu_n^{t0|B}}{\left[E_{\alpha 0}^A + E_{u0}^B - \hbar ck\right]\left[E_{s0}^A + E_{t0}^B - \hbar ck\right]\left[E_{r0}^A - \hbar ck\right]} \\
&+\frac{\mu_k^{\alpha s|A}\mu_m^{sr|A}\mu_j^{r0|A}\mu_l^{0u|B}\mu_i^{ut|B}\mu_n^{t0|B}}{\left[E_{s0}^A + E_{u0}^B - \hbar ck + \hbar ck'\right]\left[E_{s0}^A + E_{t0}^B - \hbar ck\right]\left[E_{r0}^A - \hbar ck\right]} \\
&+\frac{\mu_k^{\alpha s|A}\mu_m^{sr|A}\mu_j^{r0|A}\mu_l^{0u|B}\mu_n^{ut|B}\mu_i^{t0|B}}{\left[E_{s0}^A + E_{u0}^B - \hbar ck + \hbar ck'\right]\left[E_{r0}^A + E_{t0}^B - \hbar ck + \hbar ck'\right]\left[E_{r0}^A - \hbar ck\right]} \\
&+\frac{\mu_k^{\alpha s|A}\mu_j^{sr|A}\mu_m^{r0|A}\mu_i^{0u|B}\mu_l^{ut|B}\mu_n^{t0|B}}{\left[E_{\alpha 0}^A + E_{u0}^B - \hbar ck\right]\left[E_{s0}^A + E_{t0}^B - \hbar ck\right]\left[E_{r0}^A + E_{t0}^B\right]} \\
&+\frac{\mu_k^{\alpha s|A}\mu_j^{sr|A}\mu_m^{r0|A}\mu_l^{0u|B}\mu_i^{ut|B}\mu_n^{t0|B}}{\left[E_{s0}^A + E_{u0}^B - \hbar ck + \hbar ck'\right]\left[E_{s0}^A + E_{t0}^B - \hbar ck\right]\left[E_{r0}^A + E_{t0}^B\right]} \\
&+\frac{\mu_k^{\alpha s|A}\mu_m^{sr|A}\mu_j^{r0|A}\mu_l^{0u|B}\mu_n^{ut|B}\mu_i^{t0|B}}{\left[E_{s0}^A + E_{u0}^B - \hbar ck + \hbar ck'\right]\left[E_{r0}^A + E_{t0}^B - \hbar ck + \hbar ck'\right]\left[E_{t0}^B + \hbar ck'\right]} \\
&+\frac{\mu_j^{\alpha s|A}\mu_k^{sr|A}\mu_m^{r0|A}\mu_i^{0u|B}\mu_l^{ut|B}\mu_n^{t0|B}}{\left[E_{\alpha 0}^A + E_{u0}^B - \hbar ck\right]\left[E_{s0}^A + E_{u0}^B\right]\left[E_{r0}^A + E_{t0}^B\right]} \\
&+\frac{\mu_k^{\alpha s|A}\mu_j^{sr|A}\mu_m^{r0|A}\mu_l^{0u|B}\mu_i^{ut|B}\mu_n^{t0|B}}{\left[E_{s0}^A + E_{u0}^B - \hbar ck + \hbar ck'\right]\left[E_{r0}^A + E_{u0}^B + \hbar ck'\right]\left[E_{r0}^A + E_{t0}^B\right]} \\
&+\frac{\mu_k^{\alpha s|A}\mu_j^{sr|A}\mu_m^{r0|A}\mu_l^{0u|B}\mu_n^{ut|B}\mu_i^{t0|B}}{\left[E_{s0}^A + E_{u0}^B - \hbar ck + \hbar ck'\right]\left[E_{r0}^A + E_{u0}^B + \hbar ck'\right]\left[E_{t0}^B + \hbar ck'\right]} \\
&+\frac{\mu_j^{\alpha s|A}\mu_k^{sr|A}\mu_m^{r0|A}\mu_i^{0u|B}\mu_l^{ut|B}\mu_n^{t0|B}}{\left[E_{s0}^A + \hbar ck'\right]\left[E_{s0}^A + E_{u0}^B\right]\left[E_{r0}^A + E_{t0}^B\right]} \\
&+\frac{\mu_j^{\alpha s|A}\mu_k^{sr|A}\mu_m^{r0|A}\mu_l^{0u|B}\mu_i^{ut|B}\mu_n^{t0|B}}{\left[E_{s0}^A + \hbar ck'\right]\left[E_{r0}^A + E_{u0}^B + \hbar ck'\right]\left[E_{r0}^A + E_{t0}^B\right]} \\
&+\frac{\mu_j^{\alpha s|A}\mu_k^{sr|A}\mu_m^{r0|A}\mu_l^{0u|B}\mu_n^{ut|B}\mu_i^{t0|B}}{\left[E_{s0}^A + \hbar ck'\right]\left[E_{r0}^A + E_{u0}^B + \hbar ck'\right]\left[E_{t0}^B + \hbar ck'\right]}\left. \right\}.
\end{aligned}
\tag{2.2.18}
$$

The negative sign is the product of a negative sign from each of the three denominators. For the cases involving two virtual photons, it is not possible to factorise the components relating to each of the molecules and as such, the molecular response tensor is defined as a conglomeration of the pair, such that,

$$\chi'^{\alpha 0|A;00|B}_{jkm;iln} = \sum_{r,s,t,u} \left\{ \frac{\mu_k^{\alpha s|A}\mu_m^{sr|A}\mu_j^{r0|A}\mu_i^{0u|B}\mu_l^{ut|B}\mu_n^{t0|B}}{\left[E^A_{\alpha 0}+E^B_{u0}-\hbar ck\right]\left[E^A_{s0}+E^B_{t0}-\hbar ck\right]\left[E^A_{r0}-\hbar ck\right]} \right.$$
$$+\frac{\mu_k^{\alpha s|A}\mu_m^{sr|A}\mu_j^{r0|A}\mu_l^{0u|B}\mu_i^{ut|B}\mu_n^{t0|B}}{\left[E^A_{s\alpha}+E^B_{u0}\right]\left[E^A_{s0}+E^B_{t0}-\hbar ck\right]\left[E^A_{r0}-\hbar ck\right]}$$
$$+\frac{\mu_k^{\alpha s|A}\mu_m^{sr|A}\mu_j^{r0|A}\mu_l^{0u|B}\mu_n^{ut|B}\mu_i^{t0|B}}{\left[E^A_{s\alpha}+E^B_{u0}\right]\left[E^A_{r\alpha}+E^B_{t0}\right]\left[E^A_{r0}-\hbar ck\right]}$$
$$+\frac{\mu_k^{\alpha s|A}\mu_j^{sr|A}\mu_m^{r0|A}\mu_i^{0u|B}\mu_l^{ut|B}\mu_n^{t0|B}}{\left[E^A_{\alpha 0}+E^B_{u0}-\hbar ck\right]\left[E^A_{s0}+E^B_{t0}-\hbar ck\right]\left[E^A_{r0}+E^B_{t0}\right]}$$
$$+\frac{\mu_k^{\alpha s|A}\mu_j^{sr|A}\mu_m^{r0|A}\mu_l^{0u|B}\mu_i^{ut|B}\mu_n^{t0|B}}{\left[E^A_{s\alpha}+E^B_{u0}\right]\left[E^A_{s0}+E^B_{t0}-\hbar ck\right]\left[E^A_{r0}+E^B_{t0}\right]}$$
$$+\frac{\mu_k^{\alpha s|A}\mu_m^{sr|A}\mu_j^{r0|A}\mu_l^{0u|B}\mu_n^{ut|B}\mu_i^{t0|B}}{\left[E^A_{s\alpha}+E^B_{u0}\right]\left[E^A_{r\alpha}+E^B_{t0}\right]\left[E^A_{0\alpha}+E^B_{t0}+\hbar ck\right]}$$
$$+\frac{\mu_j^{\alpha s|A}\mu_k^{sr|A}\mu_m^{r0|A}\mu_i^{0u|B}\mu_l^{ut|B}\mu_n^{t0|B}}{\left[E^A_{\alpha 0}+E^B_{u0}-\hbar ck\right]\left[E^A_{s0}+E^B_{u0}\right]\left[E^A_{r0}+E^B_{t0}\right]}$$
$$+\frac{\mu_k^{\alpha s|A}\mu_j^{sr|A}\mu_m^{r0|A}\mu_l^{0u|B}\mu_i^{ut|B}\mu_n^{t0|B}}{\left[E^A_{s\alpha}+E^B_{u0}\right]\left[E^A_{r\alpha}+E^B_{u0}+\hbar ck\right]\left[E^A_{r0}+E^B_{t0}\right]}$$
$$+\frac{\mu_k^{\alpha s|A}\mu_j^{sr|A}\mu_m^{r0|A}\mu_n^{0u|B}\mu_l^{ut|B}\mu_i^{t0|B}}{\left[E^A_{s\alpha}+E^B_{u0}\right]\left[E^A_{r\alpha}+E^B_{u0}+\hbar ck\right]\left[E^A_{0\alpha}+E^B_{t0}+\hbar ck\right]}$$
$$+\frac{\mu_j^{\alpha s|A}\mu_k^{sr|A}\mu_m^{r0|A}\mu_i^{0u|B}\mu_l^{ut|B}\mu_n^{t0|B}}{\left[E^A_{s\alpha}+\hbar ck\right]\left[E^A_{s0}+E^B_{u0}\right]\left[E^A_{r0}+E^B_{t0}\right]}$$
$$+\frac{\mu_j^{\alpha s|A}\mu_k^{sr|A}\mu_m^{r0|A}\mu_l^{0u|B}\mu_i^{ut|B}\mu_n^{t0|B}}{\left[E^A_{s\alpha}+\hbar ck\right]\left[E^A_{r\alpha}+E^B_{u0}+\hbar ck\right]\left[E^A_{r0}+E^B_{t0}\right]}$$
$$\left.+\frac{\mu_j^{\alpha s|A}\mu_k^{sr|A}\mu_m^{r0|A}\mu_l^{0u|B}\mu_n^{ut|B}\mu_i^{t0|B}}{\left[E^A_{s\alpha}+\hbar ck\right]\left[E^A_{r\alpha}+E^B_{u0}+\hbar ck\right]\left[E^A_{0\alpha}+E^B_{t0}+\hbar ck\right]}\right\} . \qquad (2.2.19)$$

This is placed in the matrix element as follows,

$$M_{FI}^{A\|B'} = -\frac{\hbar c\sqrt{kk'n}}{32\pi^2\varepsilon_0^3 R^6 V}\bar{e}'_i e_j \left(\delta_{kl}-3\hat{R}_k\hat{R}_l\right)\left(\delta_{mn}-3\hat{R}_m\hat{R}_n\right)\chi'^{\alpha 0|A;00|B}_{jkm;iln} , \qquad (2.2.20)$$

For the cases involving two or more virtual photons, the square of the Coulomb's constant $\left(4\pi\varepsilon_0\right)^{-2}$ as well as a sixth order distance dependence R^{-6} can both be factorised out, to leave a matrix element with identical constant structure and field products as that seen in equation (1.4.14).

Irrespective of whether the molecular responses are separable, the selection rules and symmetry arguments can still be applied to each numerator. It is evident that this process involves three transition dipole moments for each of the molecules in the course of the process, as such both molecules can be said to relate to three-photon selection rules. Take, for example, the transition moments relating to molecule A in the first time-ordering,

$$C_{kmj}^{(1)}(Q) = \mu_k^{\alpha s|A}(Q)\mu_m^{sr|A}(Q)\mu_j^{r0|A}(Q) \ , \tag{2.2.21}$$

the dependence on the vibrational coordinate Q for a specific mode of vibration has been explicitly expressed to emphasise the dependence on three-photon selection rules. The Born-Oppenheimer approximation can be extended to this, in which each term must be considered individually, so the leading contribution from the above example will produce,

$$C_{kmj}^{(1)\alpha 0}(Q) \approx \left\langle \psi_C \middle| (Q - Q_0) \middle| \psi_0 \right\rangle \left. \frac{\partial C_{kmj}^{(1)00}}{\partial Q} \right|_{Q_0} + \ldots \ , \tag{2.2.22}$$

with similar expressions obtainable for each of the twelve terms.

2.2F CASE *VI*

This is the two virtual photon variant on case *II*. Or, case *V* with the photon operator sites interchanged; that is with the annihilation and creation events on molecule B and A, respectively. Satisfyingly, despite the complexity in the derivation, the result agrees with what would be expected of this pathway. The ensuing response tensor again expresses features of both the molecules and takes the following form,

$$
\chi^{\prime\prime\,00|B;\alpha 0|A}_{jkm;iln} = \sum_{r,s,t,u} \left\{ \right.
\frac{\mu_i^{\alpha u|A}\mu_l^{ut|A}\mu_n^{t0|A}\mu_k^{0s|B}\mu_m^{sr|B}\mu_j^{r0|B}}{\left[E_{u0}^A - \hbar ck\right]\left[E_{t0}^A + E_{s0}^B - \hbar ck\right]\left[E_{r0}^B - \hbar ck\right]}
$$

$$
+ \frac{\mu_l^{\alpha u|A}\mu_i^{ut|A}\mu_n^{t0|A}\mu_k^{0s|B}\mu_m^{sr|B}\mu_j^{r0|B}}{\left[E_{u\alpha}^A + E_{s0}^B\right]\left[E_{t0}^A + E_{s0}^B - \hbar ck\right]\left[E_{r0}^B - \hbar ck\right]}
$$

$$
+ \frac{\mu_l^{\alpha u|A}\mu_n^{ut|A}\mu_i^{t0|A}\mu_k^{0s|B}\mu_m^{sr|B}\mu_j^{r0|B}}{\left[E_{u\alpha}^A + E_{s0}^B\right]\left[E_{t\alpha}^A + E_{r0}^B\right]\left[E_{r0}^B - \hbar ck\right]}
$$

$$
+ \frac{\mu_i^{\alpha u|A}\mu_l^{ut|A}\mu_n^{t0|A}\mu_k^{0s|B}\mu_j^{sr|B}\mu_m^{r0|B}}{\left[E_{u0}^A + E_{s0}^B - \hbar ck\right]\left[E_{t0}^A + E_{s0}^B - \hbar ck\right]\left[E_{t0}^A + E_{r0}^B\right]}
$$

$$
+ \frac{\mu_l^{\alpha u|A}\mu_i^{ut|A}\mu_n^{t0|A}\mu_k^{0s|B}\mu_j^{sr|B}\mu_m^{r0|B}}{\left[E_{u\alpha}^A + E_{s0}^B\right]\left[E_{t0}^A + E_{s0}^B - \hbar ck\right]\left[E_{t0}^A + E_{r0}^B\right]}
$$

$$
+ \frac{\mu_l^{\alpha u|A}\mu_n^{ut|A}\mu_i^{t0|A}\mu_k^{0s|B}\mu_m^{sr|B}\mu_j^{r0|B}}{\left[E_{u\alpha}^A + E_{s0}^B\right]\left[E_{t\alpha}^A + E_{r0}^B\right]\left[E_{t\alpha}^A + \hbar ck\right]}
$$

$$
+ \frac{\mu_i^{\alpha u|A}\mu_l^{ut|A}\mu_n^{t0|A}\mu_j^{0s|B}\mu_k^{sr|B}\mu_m^{r0|B}}{\left[E_{u0}^A + \hbar ck\right]\left[E_{u0}^A + E_{s0}^B\right]\left[E_{t0}^A + E_{r0}^B\right]}
$$

$$
+ \frac{\mu_l^{\alpha u|A}\mu_i^{ut|A}\mu_n^{t0|A}\mu_k^{0s|B}\mu_j^{sr|B}\mu_m^{r0|B}}{\left[E_{u\alpha}^A + E_{s0}^B\right]\left[E_{u0}^A + E_{r0}^B + \hbar ck'\right]\left[E_{t0}^A + E_{r0}^B\right]}
$$

$$
+ \frac{\mu_l^{\alpha u|A}\mu_n^{ut|A}\mu_i^{t0|A}\mu_k^{0s|B}\mu_j^{sr|B}\mu_m^{r0|B}}{\left[E_{u\alpha}^A + E_{s0}^B\right]\left[E_{u0}^A + E_{r0}^B + \hbar ck'\right]\left[E_{t\alpha}^A + \hbar ck\right]}
$$

$$
+ \frac{\mu_i^{\alpha u|A}\mu_l^{ut|A}\mu_n^{t0|A}\mu_j^{0s|B}\mu_k^{sr|B}\mu_m^{r0|B}}{\left[E_{s0}^B + \hbar ck\right]\left[E_{u0}^A + E_{s0}^B\right]\left[E_{t0}^A + E_{r0}^B\right]}
$$

$$
+ \frac{\mu_l^{\alpha u|A}\mu_i^{ut|A}\mu_n^{t0|A}\mu_j^{0s|B}\mu_k^{sr|B}\mu_m^{r0|B}}{\left[E_{s0}^B + \hbar ck\right]\left[E_{u\alpha}^A + E_{r0}^B + \hbar ck\right]\left[E_{t0}^A + E_{r0}^B\right]}
$$

$$
\left. + \frac{\mu_l^{\alpha u|A}\mu_n^{ut|A}\mu_i^{t0|A}\mu_j^{0s|B}\mu_k^{sr|B}\mu_m^{r0|B}}{\left[E_{s0}^B + \hbar ck\right]\left[E_{u\alpha}^A + E_{r0}^B + \hbar ck\right]\left[E_{t\alpha}^A + \hbar ck\right]} \right\} . \qquad (2.2.23)
$$

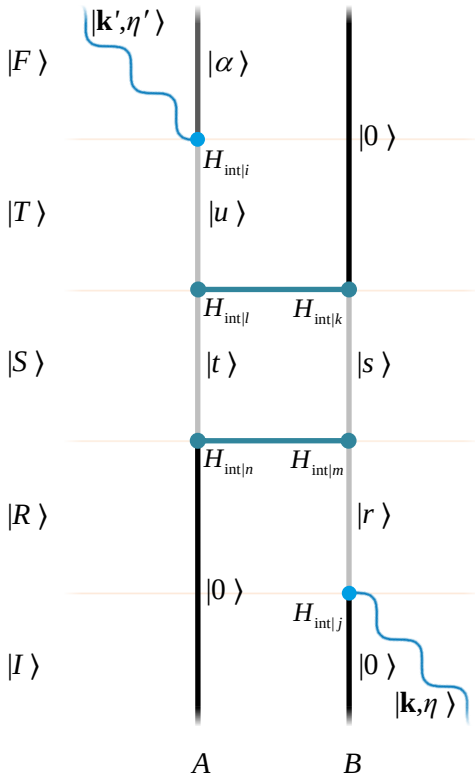

Figure 15: One of twelve Feynman diagrams to represent the photon operator locations. This is comparable in form to that of case *II*, the additional permutations introduced as a result of the second virtual photon.

The very familiar matrix element which contains this response tensor is,

$$M_{FI}^{B||A'} = -\frac{\hbar c\sqrt{kk'n}}{32\pi^2\varepsilon_0^3 R^6 V}\bar{e}_i' e_j \left(\delta_{kl} - 3\hat{R}_k\hat{R}_l\right)\left(\delta_{mn} - 3\hat{R}_m\hat{R}_n\right)\chi'^{\,00|B;\alpha 0|A}_{jkm;iln} \quad . \tag{2.2.24}$$

The only difference in this expression is the interchanging of the superscript attached to the conglomerate molecular response tensor χ, the primes serving to emphasise the difference in tensor structure.

2.2G CASE *VII*

This case produces the highest order of photon process to be considered on the molecule of spectroscopic interest, a four-photon process. For this, both real photon operations in addition to the two virtual photon interactions all occur on molecule A.

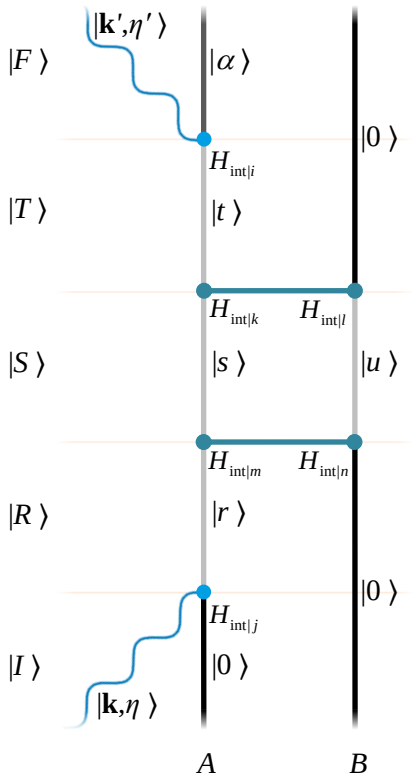

Figure 16: One example Feynman diagrams comparable in form to that of case *III*, where both real photon operators occur at molecule A, the additional permutations introduced as a result of a second virtual photon exchange with molecule B.

There are the same number of interactions and intermediary states as in the previous two cases. The response for each molecule is still inseparable from the other and as such the result is best displayed as a conglomerate of both molecules. In principle, it would be possible to factorise out the transition moments of molecule B; however, a remnant of B would persist in the energy denominator and there would be no real benefit. The collective response tensor is displayed as,

$$\chi^{\alpha 0|A;00|B}_{(ij)(km);(ln)} = \sum_{r,s,t,u} \left\{ \frac{\mu_i^{\alpha t|A}\mu_k^{ts|A}\mu_m^{sr|A}\mu_j^{r0|A}\mu_l^{0u|B}\mu_n^{u0|B}}{\left[E^A_{t0}-\hbar ck\right]\left[E^A_{s0}+E^B_{u0}-\hbar ck\right]\left[E^A_{r0}-\hbar ck\right]} \right.$$
$$+\frac{\mu_k^{\alpha t|A}\mu_i^{ts|A}\mu_m^{sr|A}\mu_j^{r0|A}\mu_l^{0u|B}\mu_n^{u0|B}}{\left[E^A_{t\alpha}+E^B_{u0}\right]\left[E^A_{s0}+E^B_{u0}-\hbar ck\right]\left[E^A_{r0}-\hbar ck\right]}$$
$$+\frac{\mu_k^{\alpha t|A}\mu_m^{ts|A}\mu_i^{sr|A}\mu_j^{r0|A}\mu_l^{0u|B}\mu_n^{u0|B}}{\left[E^A_{t\alpha}+E^B_{u0}\right]E^A_{s\alpha}\left[E^A_{r0}-\hbar ck\right]}$$
$$+\ldots$$

$$
\begin{aligned}
&+\frac{\mu_i^{\alpha t|A}\mu_k^{ts|A}\mu_j^{sr|A}\mu_m^{r0|A}\mu_l^{0u|B}\mu_n^{u0|B}}{\left[E_{t0}^A-\hbar ck\right]\left[E_{s0}^A+E_{u0}^B-\hbar ck\right]\left[E_{r0}^A+E_{u0}^B\right]}\\
&+\frac{\mu_k^{\alpha t|A}\mu_i^{ts|A}\mu_j^{sr|A}\mu_m^{r0|A}\mu_l^{0u|B}\mu_n^{u0|B}}{\left[E_{t\alpha}^A+E_{u0}^B\right]\left[E_{s0}^A+E_{u0}^B-\hbar ck\right]\left[E_{r0}^A+E_{u0}^B\right]}\\
&+\frac{\mu_k^{\alpha t|A}\mu_m^{ts|A}\mu_j^{sr|A}\mu_i^{r0|A}\mu_l^{0u|B}\mu_n^{u0|B}}{\left[E_{t\alpha}^A+E_{u0}^B\right]E_{s\alpha}^A\left[E_{r\alpha}^A+\hbar ck\right]}\\
&+\frac{\mu_i^{\alpha t|A}\mu_j^{ts|A}\mu_k^{sr|A}\mu_m^{r0|A}\mu_l^{0u|B}\mu_n^{u0|B}}{\left[E_{t0}^A-\hbar ck\right]E_{s0}^A\left[E_{r0}^A+E_{u0}^B\right]}\\
&+\frac{\mu_k^{\alpha t|A}\mu_j^{ts|A}\mu_i^{sr|A}\mu_m^{r0|A}\mu_l^{0u|B}\mu_n^{u0|B}}{\left[E_{t\alpha}^A+E_{u0}^B\right]\left[E_{s\alpha}^A+E_{u0}^B+\hbar ck\right]\left[E_{r0}^A+E_{u0}^B\right]}\\
&+\frac{\mu_k^{\alpha t|A}\mu_j^{ts|A}\mu_m^{sr|A}\mu_i^{r0|A}\mu_l^{0u|B}\mu_n^{u0|B}}{\left[E_{t\alpha}^A+E_{u0}^B\right]\left[E_{s\alpha}^A+E_{u0}^B+\hbar ck\right]\left[E_{r\alpha}^A+\hbar ck\right]}\\
&+\frac{\mu_j^{\alpha t|A}\mu_i^{ts|A}\mu_k^{sr|A}\mu_m^{r0|A}\mu_l^{0u|B}\mu_n^{u0|B}}{\left[E_{t\alpha}^A+\hbar ck\right]E_{s0}^A\left[E_{r0}^A+E_{u0}^B\right]}\\
&+\frac{\mu_j^{\alpha t|A}\mu_k^{ts|A}\mu_i^{sr|A}\mu_m^{r0|A}\mu_l^{0u|B}\mu_n^{u0|B}}{\left[E_{t\alpha}^A+\hbar ck\right]\left[E_{s\alpha}^A+E_{u0}^B+\hbar ck\right]\left[E_{r0}^A+E_{u0}^B\right]}\\
&+\frac{\mu_j^{\alpha t|A}\mu_k^{ts|A}\mu_m^{sr|A}\mu_i^{r0|A}\mu_l^{0u|B}\mu_n^{u0|B}}{\left[E_{t\alpha}^A+\hbar ck\right]\left[E_{s\alpha}^A+E_{u0}^B+\hbar ck\right]\left[E_{r\alpha}^A+\hbar ck\right]}\Bigg\},
\end{aligned}
\tag{2.2.25}
$$

which can be found in the matrix element,

$$
M_{FI}^{A'\|B}=-\frac{\hbar c\sqrt{kk'n}}{32\pi^2\varepsilon_0^3R^6V}\bar{e}_i'e_j\left(\delta_{kl}-3\hat{R}_k\hat{R}_l\right)\left(\delta_{mn}-3\hat{R}_m\hat{R}_n\right)\chi_{(ij)(km);(ln)}^{\alpha 0|A;00|B}\ . \tag{2.2.26}
$$

The response tensor indicates the presence of three pairs of index symmetry, this can be shown as follows. Again, we shall try interchanging the indices, i and j, here the two pairs of virtual photon events on each molecule k and m, as well as l and n can be interchanged. Again, the intermediary states are arbitrary and as such r and t are the most likely candidates for symmetry. The result of applying these four operations delivers,

$$\chi^{\alpha 0|A;00|B}_{(ji)(mk);(nl)} = \sum_{t,s,r,u} \left\{ \frac{\mu_j^{\alpha r|A}\mu_m^{rs|A}\mu_k^{st|A}\mu_i^{t0|A}\mu_n^{0u|B}\mu_l^{u0|B}}{\left[E^A_{r0} - \hbar ck\right]\left[E^A_{s0} + E^B_{u0} - \hbar ck\right]\left[E^A_{t0} - \hbar ck\right]} \right.$$
$$+ \frac{\mu_j^{\alpha r|A}\mu_m^{rs|A}\mu_i^{st|A}\mu_k^{t0|A}\mu_n^{0u|B}\mu_l^{u0|B}}{\left[E^A_{r\alpha} - \hbar ck\right]\left[E^A_{s0} + E^B_{u0} - \hbar ck\right]\left[E^A_{t0} + E^B_{u0}\right]}$$
$$+ \frac{\mu_j^{\alpha r|A}\mu_i^{rs|A}\mu_m^{st|A}\mu_k^{t0|A}\mu_n^{0u|B}\mu_l^{u0|B}}{\left[E^A_{r\alpha} - \hbar ck\right]E^A_{s\alpha}\left[E^A_{t0} + E^B_{u0}\right]}$$
$$+ \frac{\mu_m^{\alpha r|A}\mu_j^{rs|A}\mu_k^{st|A}\mu_i^{t0|A}\mu_n^{0u|B}\mu_l^{u0|B}}{\left[E^A_{r0} + E^B_{u0}\right]\left[E^A_{s0} + E^B_{u0} - \hbar ck\right]\left[E^A_{t0} - \hbar ck\right]}$$
$$+ \frac{\mu_m^{\alpha r|A}\mu_j^{rs|A}\mu_i^{st|A}\mu_k^{t0|A}\mu_n^{0u|B}\mu_l^{u0|B}}{\left[E^A_{r\alpha} + E^B_{u0}\right]\left[E^A_{s0} + E^B_{u0} - \hbar ck\right]\left[E^A_{t0} + E^B_{u0}\right]}$$
$$+ \frac{\mu_i^{\alpha r|A}\mu_j^{rs|A}\mu_m^{st|A}\mu_k^{t0|A}\mu_n^{0u|B}\mu_l^{u0|B}}{\left[E^A_{r\alpha} + \hbar ck\right]E^A_{s\alpha}\left[E^A_{t\alpha} + E^B_{u0}\right]}$$
$$+ \frac{\mu_m^{\alpha r|A}\mu_k^{rs|A}\mu_j^{st|A}\mu_i^{t0|A}\mu_n^{0u|B}\mu_l^{u0|B}}{\left[E^A_{r0} + E^B_{u0}\right]E^A_{s0}\left[E^A_{t0} - \hbar ck\right]}$$
$$+ \frac{\mu_m^{\alpha r|A}\mu_i^{rs|A}\mu_j^{st|A}\mu_k^{t0|A}\mu_n^{0u|B}\mu_l^{u0|B}}{\left[E^A_{r\alpha} + E^B_{u0}\right]\left[E^A_{s\alpha} + E^B_{u0} + \hbar ck\right]\left[E^A_{t0} + E^B_{u0}\right]}$$
$$+ \frac{\mu_i^{\alpha r|A}\mu_m^{rs|A}\mu_j^{st|A}\mu_k^{t0|A}\mu_n^{0u|B}\mu_l^{u0|B}}{\left[E^A_{r\alpha} + \hbar ck\right]\left[E^A_{s\alpha} + E^B_{u0} + \hbar ck\right]\left[E^A_{t\alpha} + E^B_{u0}\right]}$$
$$+ \frac{\mu_m^{\alpha r|A}\mu_k^{rs|A}\mu_i^{st|A}\mu_j^{t0|A}\mu_n^{0u|B}\mu_l^{u0|B}}{\left[E^A_{r\alpha} + E^B_{u0}\right]E^A_{s0}\left[E^A_{t0} + \hbar ck\right]}$$
$$+ \frac{\mu_m^{\alpha r|A}\mu_i^{rs|A}\mu_k^{st|A}\mu_j^{t0|A}\mu_n^{0u|B}\mu_l^{u0|B}}{\left[E^A_{r\alpha} + E^B_{u0}\right]\left[E^A_{s\alpha} + E^B_{u0} + \hbar ck\right]\left[E^A_{t0} + \hbar ck\right]}$$
$$\left. + \frac{\mu_i^{\alpha r|A}\mu_m^{rs|A}\mu_k^{st|A}\mu_j^{t0|A}\mu_n^{0u|B}\mu_l^{u0|B}}{\left[E^A_{r\alpha} + \hbar ck\right]\left[E^A_{s\alpha} + E^B_{u0} + \hbar ck\right]\left[E^A_{t\alpha} + \hbar ck\right]} \right\}. \qquad (2.2.27)$$

By comparing the results with the original tensor, terms 1, 5, 8 and 12 have all been kept in the same positions. Whereas terms 2, 3, 6, 9 have been swapped with 4, 7, 10 and 11, respectively. The result is a tensor where each term position connects with that of the original tensor. To best see this, read equation (2.2.27) from right-to-left. Where the identity in equation (2.2.14) still holds here. Again, the vibrational excitations α can be disregarded, when compared to the relative magnitude of the photon energies and associated electronic transitions.

In each of the twelve permutations, molecule A undergoes four photon-molecule interactions and corresponds to the four transition moments that appear in the numerator for each term in

equation (2.2.25). The aspects of each molecule are not separable, similar to case *V*, however, symmetry arguments can be applied to each term. Take the first term, for example,

$$C^{(1)}_{ikmj}(Q) = \mu_i^{\alpha t|A}(Q)\,\mu_k^{ts|A}(Q)\,\mu_m^{sr|A}(Q)\,\mu_j^{r0|A}(Q)\ . \tag{2.2.28}$$

Here, the explicit dependence on the vibrational coordinate Q for a specific mode of vibration has been expressed to emphasise the dependence on four-photon selection rules. Similar expressions obtainable for each of the twelve terms. With an equivalent Born-Oppenheimer treatment as displayed in equation (2.2.22).

2.2H CASE *VIII*

The final case to be considered is where molecule A interacts with neither the beam or the scattered photon, but undergoes a vibrational transition because of a pair of virtual photons exchanged with its neighbour. In keeping with the trend set forth, this is case *IV* with an additional virtual photon and case *VII* with the interaction sites of both molecule A and B interchanged.

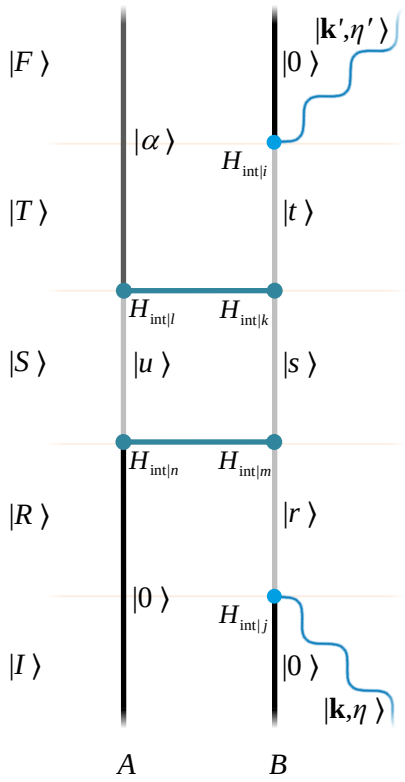

Figure 17: One Feynman diagram to exemplify this mechanism. Both real photon operations occur on molecule B, which is coupled to molecule A by two virtual photons.

The resultant response tensor is again of similar form to that of the previous case. The superscript indices have been interchanged and the primes are present to distinguish this response tensor from the last.

$$\chi''^{\,00|B;\alpha 0|A}_{(ij)(km);(ln)} = \sum_{r,s,t,u}\left\{\frac{\mu_l^{\alpha u|A}\mu_n^{u0|A}\mu_i^{0t|B}\mu_k^{ts|B}\mu_m^{sr|B}\mu_j^{r0|B}}{\left[E^A_{\alpha 0}+E^B_{t0}-\hbar ck\right]\left[E^A_{u0}+E^B_{s0}-\hbar ck\right]\left[E^B_{r0}-\hbar ck\right]}\right.$$
$$+\frac{\mu_l^{\alpha u|A}\mu_n^{u0|A}\mu_k^{0t|B}\mu_i^{ts|B}\mu_m^{sr|B}\mu_j^{r0|B}}{\left[E^A_{u\alpha}+E^B_{t0}\right]\left[E^A_{u0}+E^B_{s0}-\hbar ck\right]\left[E^B_{r0}-\hbar ck\right]}$$
$$+\frac{\mu_l^{\alpha u|A}\mu_n^{u0|A}\mu_k^{0t|B}\mu_m^{ts|B}\mu_i^{sr|B}\mu_j^{r0|B}}{\left[E^A_{u\alpha}+E^B_{t0}\right]\left[E^A_{0\alpha}+E^B_{s0}\right]\left[E^B_{r0}-\hbar ck\right]}$$
$$+\frac{\mu_l^{\alpha u|A}\mu_n^{u0|A}\mu_i^{0t|B}\mu_k^{ts|B}\mu_j^{sr|B}\mu_m^{r0|B}}{\left[E^A_{\alpha 0}+E^B_{t0}-\hbar ck\right]\left[E^A_{u0}+E^B_{s0}-\hbar ck\right]\left[E^A_{u0}+E^B_{r0}\right]}$$
$$+\frac{\mu_l^{\alpha u|A}\mu_n^{u0|A}\mu_k^{0t|B}\mu_i^{ts|B}\mu_j^{sr|B}\mu_m^{r0|B}}{\left[E^A_{u\alpha}+E^B_{t0}\right]\left[E^A_{u0}+E^B_{s0}-\hbar ck\right]\left[E^A_{u0}+E^B_{r0}\right]}$$
$$+\frac{\mu_l^{\alpha u|A}\mu_n^{u0|A}\mu_k^{0t|B}\mu_m^{ts|B}\mu_j^{sr|B}\mu_i^{r0|B}}{\left[E^A_{u\alpha}+E^B_{t0}\right]\left[E^A_{0\alpha}+E^B_{s0}\right]\left[E^A_{0\alpha}+E^B_{r0}+\hbar ck\right]}$$
$$+\frac{\mu_l^{\alpha u|A}\mu_n^{u0|A}\mu_i^{0t|B}\mu_j^{ts|B}\mu_k^{sr|B}\mu_m^{r0|B}}{\left[E^A_{\alpha 0}+E^B_{t0}-\hbar ck\right]\left[E^A_{\alpha 0}+E^B_{s0}\right]\left[E^A_{u0}+E^B_{r0}\right]}$$
$$+\frac{\mu_l^{\alpha u|A}\mu_n^{u0|A}\mu_k^{0t|B}\mu_j^{ts|B}\mu_i^{sr|B}\mu_m^{r0|B}}{\left[E^A_{u\alpha}+E^B_{t0}\right]\left[E^A_{u\alpha}+E^B_{s0}+\hbar ck\right]\left[E^A_{u0}+E^B_{r0}\right]}$$
$$+\frac{\mu_l^{\alpha u|A}\mu_n^{u0|A}\mu_k^{0t|B}\mu_j^{ts|B}\mu_m^{sr|B}\mu_i^{r0|B}}{\left[E^A_{u\alpha}+E^B_{t0}\right]\left[E^A_{u\alpha}+E^B_{s0}+\hbar ck\right]\left[E^A_{0\alpha}+E^B_{r0}+\hbar ck\right]}$$
$$+\frac{\mu_l^{\alpha u|A}\mu_n^{u0|A}\mu_j^{0t|B}\mu_i^{ts|B}\mu_k^{sr|B}\mu_m^{r0|B}}{\left[E^B_{t0}+\hbar ck\right]\left[E^A_{\alpha 0}+E^B_{s0}\right]\left[E^A_{u0}+E^B_{r0}\right]}$$
$$+\frac{\mu_l^{\alpha u|A}\mu_n^{u0|A}\mu_j^{0t|B}\mu_k^{ts|B}\mu_i^{sr|B}\mu_m^{r0|B}}{\left[E^B_{t0}+\hbar ck\right]\left[E^A_{u\alpha}+E^B_{s0}+\hbar ck\right]\left[E^A_{u0}+E^B_{r0}\right]}$$
$$\left.+\frac{\mu_l^{\alpha u|A}\mu_n^{u0|A}\mu_j^{0t|B}\mu_k^{ts|B}\mu_m^{sr|B}\mu_i^{r0|B}}{\left[E^B_{t0}+\hbar ck\right]\left[E^A_{u\alpha}+E^B_{s0}+\hbar ck\right]\left[E^A_{0\alpha}+E^B_{r0}+\hbar ck\right]}\right\}. \qquad (2.2.29)$$

This response tensor also displays index symmetry in the same positions and by the same methods of interchangeability. The matrix element, which houses this conglomerate response tensor is as follows,

$$M_{FI}^{B'\|A} = -\frac{\hbar c\sqrt{kk'n}}{32\pi^2\varepsilon_0^3 R^6 V}\bar{e}_i' e_j\left(\delta_{kl}-3\hat{R}_k\hat{R}_l\right)\left(\delta_{mn}-3\hat{R}_m\hat{R}_n\right)\chi''^{\,00|B;\alpha 0|A}_{(ij)(km);(ln)}\ . \qquad (2.2.30)$$

2.2I SUMMARY OF CASES

Each of the eight cases considered in the preceding subsections represent one pathway that is possible for a Raman transition to occur at a molecule. In contrast to the process introduced in §1.4, there are now several mechanisms that can contribute to the overall rate of a Raman transition occurring for the molecule of spectroscopic interest. This can easily be accommodated additively in the square modulus for the rate of a process. First, it is helpful to scrutinise each of the matrix elements for common factors. Each of the matrix elements, equations (1.4.12), (2.2.6), (2.2.9), (2.2.11), (2.2.16), (2.2.20), (2.2.24), (2.2.26) and (2.2.30), display a common factor, which is also seen in single-centre Raman scattering. The method of substitutions to obtain the radiant intensity have been exposed in §1.4B, as such the common prefactors have already been taken care of. The radiant intensity of the overall process can now be cast incorporating modified matrix elements for each of the mechanism, with the appropriate common factors removed, as follows,

$$I' = \left(\frac{k'^{\,2}}{4\pi\varepsilon_0}\right)^2 I_0 \Bigg| \underset{0}{M_{FI}^{A}} + \underbrace{M_{FI}'^{\,A|B'} + M_{FI}'^{\,B|A'} + M_{FI}'^{\,A'|B} + M_{FI}'^{\,B'|A}}_{1} + \underbrace{M_{FI}'^{\,A\|B'} + M_{FI}'^{\,B\|A'} + M_{FI}'^{\,A'\|B} + M_{FI}'^{\,B'\|A}}_{2} + \ldots \Bigg|^2 . \tag{2.2.31}$$

Each of the modified matrix elements will retain the prefactors relating to the Coulomb's constant, distance dependence and pairwise orientational parentheses. In addition to the field vectors and molecular response tensors, of course. The square modulus produces nine products of the modified matrix elements with their complex conjugates and 36 cross terms by utilising equation (2A.5), the latter are known as the quantum interference between the matrix elements.

As a final note, there is one additional set of Feynman diagrams that also bares the same order of perturbation theory as cases *V*–*VIII*, that is two virtual photons, each connected to two different centres. These have been neglected, with reasonable cause. Although the same order of perturbation would be deployed in both cases, a similar result will be obtained for both. By inspecting the matrix element produced following evaluating the two-photon single-centre case, an R^{-6} dependence is present. As such, any process occurrence of such an exchange will be

hindered in all but the most near-field of cases. As such, two centres present in the immediate vicinity of each other is possible, but probabilistically the instances where a third centre will also coincide with them is far less likely.

2.3 ROTATIONAL AVERAGE

In the preceding section, expressions were cast for the amplitude of transition, where the pair are fixed in orientation, with respect to each other. The radiant intensity, equation (2.2.31), has been cast on the assumption that the pair is also fixed in orientation with the respect to the bulk, this is typically associated with solid phase mixtures. Typically, systems where molecules are free to tumble are of the most interest, such as the case with condensed phase fluids, which is the subject of this section.

To begin, like Raman scattering this is an incoherent process and as such requires an isotropic Cartesian tensor equal to twice the number of real photons, which is another fourth rotational-average, equation (1D.10). As stated in equation (1D.2), this operator is formed of three parts, which can be considered in turn. The first relates to the field vectors, which contracts with the field vectors to produce the same result as in equation (1.4.13). We can apply the field vector products displayed in complement 1E to consider a standard setup of right-angled scattering, two conventional polarization schemes can be chosen: the electric field polarisation of the scattered light is parallel or perpendicular to the incident light, schematics can be seen in Figure 18(a) and Figure 18(b), respectively.

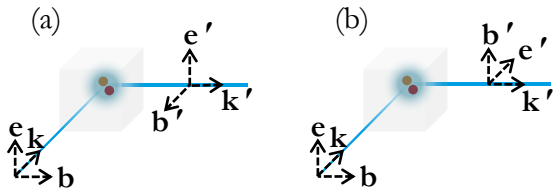

Figure 18: Experimental set-up: (a) parallel plane-polarized light is detected at right angles to the input laser; (b) perpendicularly plane-polarized light also detected at right angles.

By adopting these two polarization schemes, numerical results can be obtained from equation (1.4.13) and contracted with the numerical matrix, $m_{pq}^{(4)}$, in equation (1D.10). Therefore, the parallel configuration produces the expression;

$$\boldsymbol{P} = \frac{1}{15}\begin{pmatrix} 1 & 1 & 1 \end{pmatrix}, \tag{2.3.1}$$

and the perpendicular equivalent yields:

$$\boldsymbol{P} = \frac{1}{30}\begin{pmatrix} -1 & 4 & -1 \end{pmatrix}. \tag{2.3.2}$$

These two configurations are often selected, in turn a ratio can be taken of the two, this quantity is known as the depolarization ratio (DR) [112]. Experimentally, this kind of characterisation can be automated, many technologies exist to observe the process by rapidly switching between polarization states [113].

These expressions are to be contracted with the molecular response tensors formed out of $g_q^{(4)}$ seen in equation (1D.10) along with the molecular response tensors $\{\alpha, \alpha', \alpha'', \alpha''', \alpha'''', \beta, \beta', \chi, \chi', \chi'', \chi'''\}$ from the product of the appropriate matrix elements, to form a new complementary tensor now defined as $\boldsymbol{T}_w$, to appear in the following final result;

$$\langle I' \rangle = \left(\frac{k'^2}{4\pi\varepsilon_0} \right)^2 N I_0 \boldsymbol{P} \sum_{w=0}^{4} \left\{ \boldsymbol{T}_w \left(\frac{-1}{4\pi\varepsilon_0 R^3} \right)^w \prod_{q=1}^{w} \left(\delta_{\rho_q \sigma_q} - 3\hat{R}_{\rho_q} \hat{R}_{\sigma_q} \right) \right\}. \tag{2.3.3}$$

Here, rotational average has several key features. The prefactors are those attributed to all two-real-photon Raman scattering process. The selected polarisation weightings, for example those selected to produce equations (2.3.1) and (2.3.2) above form $\boldsymbol{P}$.

The next series of terms requires a little more consideration. When compared with the single-centre Raman scattering result, it has been shown above that including virtual photon interactions introduces an additional three terms: Coulomb's constant and an R^{-3} distance dependence, each to the power of the number of virtual photons; lastly, a number of parentheses equal to the number of virtual photons with orientational factors connected with the molecular

response tensors. Hence there are contribution from zero to two virtual photons and when this is squared in effect the factors have a power range of zero to four, referred to as w here. The subscript indices on the molecular response tensors have been reassigned a numerological system to connect with the complementary parentheses, the last product in equation (2.3.3). In the above equation, the column vectors $\boldsymbol{T}_{\{0-4\}}$ signify rotational invariants formed from products of the Raman and associated transition tensors. The first of this set comprises the three scalar quantities that arise in conventional Raman scattering;

$$\boldsymbol{T}_0 = \begin{pmatrix} \alpha^{\alpha 0|A}_{\lambda\lambda}\overline{\alpha}^{\alpha 0|A}_{\nu\nu} \\ \alpha^{\alpha 0|A}_{\lambda\mu}\overline{\alpha}^{\alpha 0|A}_{\lambda\mu} \\ \alpha^{\alpha 0|A}_{\lambda\mu}\overline{\alpha}^{\alpha 0|A}_{\mu\lambda} \end{pmatrix} . \tag{2.3.4}$$

The remaining invariants, $\boldsymbol{T}_{\{1-4\}}$, each hold a dependence on $\rho_{q,q+1,\ldots w}$ and $\sigma_{q,q+1,\ldots w}$,

$$\boldsymbol{T}_1 = 2\left\{ \begin{pmatrix} \alpha^{\alpha 0|A}_{\lambda\lambda}\overline{\alpha}'^{\,\alpha 0|A}_{\nu\rho_1}\overline{\alpha}''^{\,00|B}_{\nu\sigma_1} \\ \alpha^{\alpha 0|A}_{\lambda\mu}\overline{\alpha}'^{\,\alpha 0|A}_{\lambda\rho_1}\overline{\alpha}''^{\,00|B}_{\mu\sigma_1} \\ \alpha^{\alpha 0|A}_{\lambda\mu}\overline{\alpha}'^{\,\alpha 0|A}_{\mu\rho_1}\overline{\alpha}''^{\,00|B}_{\lambda\sigma_1} \end{pmatrix} + \begin{pmatrix} \alpha^{\alpha 0|A}_{\lambda\lambda}\overline{\alpha}'''^{\,00|B}_{\nu\rho_1}\overline{\alpha}'''^{\,\alpha 0|A}_{\nu\sigma_1} \\ \alpha^{\alpha 0|A}_{\lambda\mu}\overline{\alpha}'''^{\,00|B}_{\lambda\rho_1}\overline{\alpha}'''^{\,\alpha 0|A}_{\mu\sigma_1} \\ \alpha^{\alpha 0|A}_{\lambda\mu}\overline{\alpha}'''^{\,00|B}_{\mu\rho_1}\overline{\alpha}'''^{\,\alpha 0|A}_{\lambda\sigma_1} \end{pmatrix} + \begin{pmatrix} \alpha^{\alpha 0|A}_{\lambda\lambda}\overline{\beta}^{\alpha 0|A}_{\nu\nu\rho_1}\overline{\mu}^{00|B}_{\sigma_1} \\ \alpha^{\alpha 0|A}_{\lambda\mu}\overline{\beta}^{\alpha 0|A}_{\lambda\mu\rho_1}\overline{\mu}^{00|B}_{\sigma_1} \\ \alpha^{\alpha 0|A}_{\lambda\mu}\overline{\beta}^{\alpha 0|A}_{\mu\lambda\rho_1}\overline{\mu}^{00|B}_{\sigma_1} \end{pmatrix} + \begin{pmatrix} \alpha^{\alpha 0|A}_{\lambda\lambda}\overline{\beta}'^{\,00|B}_{\nu\nu\rho_1}\overline{\mu}^{\alpha 0|A}_{\sigma_1} \\ \alpha^{\alpha 0|A}_{\lambda\mu}\overline{\beta}'^{\,00|B}_{\lambda\mu\rho_1}\overline{\mu}^{\alpha 0|A}_{\sigma_1} \\ \alpha^{\alpha 0|A}_{\lambda\mu}\overline{\beta}'^{\,00|B}_{\mu\lambda\rho_1}\overline{\mu}^{\alpha 0|A}_{\sigma_1} \end{pmatrix} \right\} , \tag{2.3.5}$$

$$\begin{aligned} \boldsymbol{T}_2 = {} & \begin{pmatrix} \alpha'^{\,\alpha 0|A}_{\lambda\rho_1}\alpha''^{\,00|B}_{\lambda\sigma_1}\overline{\alpha}'^{\,\alpha 0|A}_{\nu\rho_2}\overline{\alpha}''^{\,00|B}_{\nu\sigma_2} \\ \alpha'^{\,\alpha 0|A}_{\mu\rho_1}\alpha''^{\,00|B}_{\lambda\sigma_1}\overline{\alpha}'^{\,\alpha 0|A}_{\lambda\rho_2}\overline{\alpha}''^{\,00|B}_{\mu\sigma_2} \\ \alpha'^{\,\alpha 0|A}_{\mu\rho_1}\alpha''^{\,00|B}_{\lambda\sigma_1}\overline{\alpha}'^{\,\alpha 0|A}_{\mu\rho_2}\overline{\alpha}''^{\,00|B}_{\lambda\sigma_2} \end{pmatrix} + \begin{pmatrix} \alpha'''^{\,\alpha 0|A}_{\lambda\sigma_1}\alpha'''^{\,00|B}_{\lambda\rho_1}\overline{\alpha}'''^{\,\alpha 0|A}_{\nu\sigma_2}\overline{\alpha}'''^{\,00|B}_{\nu\rho_2} \\ \alpha'''^{\,\alpha 0|A}_{\lambda\sigma_1}\alpha'''^{\,00|B}_{\mu\rho_1}\overline{\alpha}'''^{\,\alpha 0|A}_{\mu\sigma_2}\overline{\alpha}'''^{\,00|B}_{\lambda\rho_2} \\ \alpha'''^{\,\alpha 0|A}_{\lambda\sigma_1}\alpha'''^{\,00|B}_{\mu\rho_1}\overline{\alpha}'''^{\,\alpha 0|A}_{\lambda\sigma_2}\overline{\alpha}'''^{\,00|B}_{\mu\rho_2} \end{pmatrix} + \begin{pmatrix} \beta^{\alpha 0|A}_{\lambda\lambda\rho_1}\mu^{00|B}_{\sigma_1}\overline{\beta}^{\alpha 0|A}_{\nu\nu\rho_2}\overline{\mu}^{00|B}_{\sigma_2} \\ \beta^{\alpha 0|A}_{\lambda\mu\rho_1}\mu^{00|B}_{\sigma_1}\overline{\beta}^{\alpha 0|A}_{\lambda\mu\rho_2}\overline{\mu}^{00|B}_{\sigma_2} \\ \beta^{\alpha 0|A}_{\lambda\mu\rho_1}\mu^{00|B}_{\sigma_1}\overline{\beta}^{\alpha 0|A}_{\mu\lambda\rho_2}\overline{\mu}^{00|B}_{\sigma_2} \end{pmatrix} \\ & + \begin{pmatrix} \mu^{\alpha 0|A}_{\sigma_1}\beta'^{\,00|B}_{\lambda\lambda\rho_1}\overline{\mu}^{\alpha 0|A}_{\sigma_2}\overline{\beta}'^{\,00|B}_{\nu\nu\rho_2} \\ \mu^{\alpha 0|A}_{\sigma_1}\beta'^{\,00|B}_{\lambda\mu\rho_1}\overline{\mu}^{\alpha 0|A}_{\sigma_2}\overline{\beta}'^{\,00|B}_{\lambda\mu\rho_2} \\ \mu^{\alpha 0|A}_{\sigma_1}\beta'^{\,00|B}_{\lambda\mu\rho_1}\overline{\mu}^{\alpha 0|A}_{\sigma_2}\overline{\beta}'^{\,00|B}_{\mu\lambda\rho_2} \end{pmatrix} + 2\left\{ \begin{pmatrix} \alpha^{\alpha 0|A}_{\lambda\lambda}\overline{\chi}'^{\,\alpha 0|A;00|B}_{\nu\rho_1\rho_2;\nu\sigma_1\sigma_2} \\ \alpha^{\alpha 0|A}_{\lambda\mu}\overline{\chi}'^{\,\alpha 0|A;00|B}_{\mu\rho_1\rho_2;\lambda\sigma_1\sigma_2} \\ \alpha^{\alpha 0|A}_{\lambda\mu}\overline{\chi}'^{\,\alpha 0|A;00|B}_{\lambda\rho_1\rho_2;\mu\sigma_1\sigma_2} \end{pmatrix} + \begin{pmatrix} \alpha^{\alpha 0|A}_{\lambda\lambda}\overline{\chi}'''^{\,00|B;\alpha 0|A}_{\nu\rho_1\rho_2;\nu\sigma_1\sigma_2} \\ \alpha^{\alpha 0|A}_{\lambda\mu}\overline{\chi}'''^{\,00|B;\alpha 0|A}_{\mu\rho_1\rho_2;\lambda\sigma_1\sigma_2} \\ \alpha^{\alpha 0|A}_{\lambda\mu}\overline{\chi}'''^{\,00|B;\alpha 0|A}_{\lambda\rho_1\rho_2;\mu\sigma_1\sigma_2} \end{pmatrix} \right\} \\ & + \begin{pmatrix} \alpha^{\alpha 0|A}_{\lambda\lambda}\overline{\chi}^{\alpha 0|A;00|B}_{\nu\nu\rho_1\rho_2;\sigma_1\sigma_2} \\ \alpha^{\alpha 0|A}_{\lambda\mu}\overline{\chi}^{\alpha 0|A;00|B}_{\lambda\mu\rho_1\rho_2;\sigma_1\sigma_2} \\ \alpha^{\alpha 0|A}_{\lambda\mu}\overline{\chi}^{\alpha 0|A;00|B}_{\mu\lambda\rho_1\rho_2;\sigma_1\sigma_2} \end{pmatrix} + \begin{pmatrix} \alpha^{\alpha 0|A}_{\lambda\lambda}\overline{\chi}'''^{\,00|B;\alpha 0|A}_{\nu\nu\rho_1\rho_2;\sigma_1\sigma_2} \\ \alpha^{\alpha 0|A}_{\lambda\mu}\overline{\chi}'''^{\,00|B;\alpha 0|A}_{\lambda\mu\rho_1\rho_2;\sigma_1\sigma_2} \\ \alpha^{\alpha 0|A}_{\lambda\mu}\overline{\chi}'''^{\,00|B;\alpha 0|A}_{\mu\lambda\rho_1\rho_2;\sigma_1\sigma_2} \end{pmatrix} + \begin{pmatrix} \alpha'^{\,\alpha 0|A}_{\lambda\rho_1}\alpha''^{\,00|B}_{\lambda\sigma_1}\overline{\alpha}'''^{\,\alpha 0|A}_{\nu\sigma_2}\overline{\alpha}'''^{\,00|B}_{\nu\rho_2} \\ \alpha'^{\,\alpha 0|A}_{\mu\rho_1}\alpha''^{\,00|B}_{\lambda\sigma_1}\overline{\alpha}'''^{\,\alpha 0|A}_{\mu\sigma_2}\overline{\alpha}'''^{\,00|B}_{\lambda\rho_2} \\ \alpha'^{\,\alpha 0|A}_{\mu\rho_1}\alpha''^{\,00|B}_{\lambda\sigma_1}\overline{\alpha}'''^{\,\alpha 0|A}_{\lambda\sigma_2}\overline{\alpha}'''^{\,00|B}_{\mu\rho_2} \end{pmatrix} \\ & + \begin{pmatrix} \alpha'^{\,\alpha 0|A}_{\lambda\rho_1}\alpha''^{\,00|B}_{\lambda\sigma_1}\overline{\mu}^{\alpha 0|A}_{\sigma_2}\overline{\beta}'^{\,00|B}_{\nu\nu\rho_2} \\ \alpha'^{\,\alpha 0|A}_{\mu\rho_1}\alpha''^{\,00|B}_{\lambda\sigma_1}\overline{\mu}^{\alpha 0|A}_{\sigma_2}\overline{\beta}'^{\,00|B}_{\lambda\mu\rho_2} \\ \alpha'^{\,\alpha 0|A}_{\mu\rho_1}\alpha''^{\,00|B}_{\lambda\sigma_1}\overline{\mu}^{\alpha 0|A}_{\sigma_2}\overline{\beta}'^{\,00|B}_{\mu\lambda\rho_2} \end{pmatrix} + \begin{pmatrix} \beta^{\alpha 0|A}_{\lambda\lambda\rho_1}\mu^{00|B}_{\sigma_1}\overline{\alpha}'^{\,\alpha 0|A}_{\nu\rho_2}\overline{\alpha}''^{\,00|B}_{\nu\sigma_2} \\ \beta^{\alpha 0|A}_{\lambda\mu\rho_1}\mu^{00|B}_{\sigma_1}\overline{\alpha}'^{\,\alpha 0|A}_{\lambda\rho_2}\overline{\alpha}''^{\,00|B}_{\mu\sigma_2} \\ \beta^{\alpha 0|A}_{\lambda\mu\rho_1}\mu^{00|B}_{\sigma_1}\overline{\alpha}'^{\,\alpha 0|A}_{\mu\rho_2}\overline{\alpha}''^{\,00|B}_{\lambda\sigma_2} \end{pmatrix} + \begin{pmatrix} \beta^{\alpha 0|A}_{\lambda\lambda\rho_1}\mu^{00|B}_{\sigma_1}\overline{\alpha}'''^{\,\alpha 0|A}_{\nu\sigma_2}\overline{\alpha}'''^{\,00|B}_{\nu\rho_2} \\ \beta^{\alpha 0|A}_{\lambda\mu\rho_1}\mu^{00|B}_{\sigma_1}\overline{\alpha}'''^{\,\alpha 0|A}_{\mu\sigma_2}\overline{\alpha}'''^{\,00|B}_{\lambda\rho_2} \\ \beta^{\alpha 0|A}_{\lambda\mu\rho_1}\mu^{00|B}_{\sigma_1}\overline{\alpha}'''^{\,\alpha 0|A}_{\lambda\sigma_2}\overline{\alpha}'''^{\,00|B}_{\mu\rho_2} \end{pmatrix} \\ & + \begin{pmatrix} \beta'^{\,00|B}_{\lambda\lambda\rho_1}\mu^{\alpha 0|A}_{\sigma_1}\overline{\alpha}'''^{\,\alpha 0|A}_{\nu\sigma_2}\overline{\alpha}'''^{\,00|B}_{\nu\rho_2} \\ \beta'^{\,00|B}_{\lambda\mu\rho_1}\mu^{\alpha 0|A}_{\sigma_1}\overline{\alpha}'''^{\,\alpha 0|A}_{\mu\sigma_2}\overline{\alpha}'''^{\,00|B}_{\lambda\rho_2} \\ \beta'^{\,00|B}_{\lambda\mu\rho_1}\mu^{\alpha 0|A}_{\sigma_1}\overline{\alpha}'''^{\,\alpha 0|A}_{\lambda\sigma_2}\overline{\alpha}'''^{\,00|B}_{\mu\rho_2} \end{pmatrix} + \left\{ \begin{pmatrix} \beta^{\alpha 0|A}_{\lambda\lambda\rho_1}\mu^{00|B}_{\sigma_1}\overline{\mu}^{\alpha 0|A}_{\sigma_2}\overline{\beta}'^{\,00|B}_{\nu\nu\rho_2} \\ \beta^{\alpha 0|A}_{\lambda\mu\rho_1}\mu^{00|B}_{\sigma_1}\overline{\mu}^{\alpha 0|A}_{\sigma_2}\overline{\beta}'^{\,00|B}_{\lambda\mu\rho_2} \\ \beta^{\alpha 0|A}_{\lambda\mu\rho_1}\mu^{00|B}_{\sigma_1}\overline{\mu}^{\alpha 0|A}_{\sigma_2}\overline{\beta}'^{\,00|B}_{\mu\lambda\rho_2} \end{pmatrix} \right\} , \end{aligned} \tag{2.3.6}$$

$$\boldsymbol{T}_3 = 2\left\{\begin{pmatrix} \alpha'^{\,\alpha0|A}_{\lambda\rho_1}\alpha''^{\,00|B}_{\lambda\sigma_1}\bar{\chi}'^{\,\alpha0|A;00|B}_{\nu\rho_2\rho_3;\nu\sigma_2\sigma_3} \\ \alpha'^{\,\alpha0|A}_{\mu\rho_1}\alpha''^{\,00|B}_{\lambda\sigma_1}\bar{\chi}'^{\,\alpha0|A;00|B}_{\mu\rho_2\rho_3;\lambda\sigma_2\sigma_3} \\ \alpha'^{\,\alpha0|A}_{\mu\rho_1}\alpha''^{\,00|B}_{\lambda\sigma_1}\bar{\chi}'^{\,\alpha0|A;00|B}_{\lambda\rho_2\rho_3;\mu\sigma_2\sigma_3} \end{pmatrix} + \begin{pmatrix} \alpha'^{\,\alpha0|A}_{\lambda\rho_1}\alpha''^{\,00|B}_{\lambda\sigma_1}\bar{\chi}'''^{\,00|B;\alpha0|A}_{\nu\rho_2\rho_3;\nu\sigma_2\sigma_3} \\ \alpha'^{\,\alpha0|A}_{\mu\rho_1}\alpha''^{\,00|B}_{\lambda\sigma_1}\bar{\chi}'''^{\,00|B;\alpha0|A}_{\mu\rho_2\rho_3;\lambda\sigma_2\sigma_3} \\ \alpha'^{\,\alpha0|A}_{\mu\rho_1}\alpha''^{\,00|B}_{\lambda\sigma_1}\bar{\chi}'''^{\,00|B;\alpha0|A}_{\lambda\rho_2\rho_3;\mu\sigma_2\sigma_3} \end{pmatrix} + \begin{pmatrix} \alpha'^{\,\alpha0|A}_{\lambda\rho_1}\alpha''^{\,00|B}_{\lambda\sigma_1}\bar{\chi}^{\alpha0|A;00|B}_{\nu\nu\rho_2\rho_3;\sigma_2\sigma_3} \\ \alpha'^{\,\alpha0|A}_{\mu\rho_1}\alpha''^{\,00|B}_{\lambda\sigma_1}\bar{\chi}^{\alpha0|A;00|B}_{\lambda\mu\rho_2\rho_3;\sigma_2\sigma_3} \\ \alpha'^{\,\alpha0|A}_{\mu\rho_1}\alpha''^{\,00|B}_{\lambda\sigma_1}\bar{\chi}^{\alpha0|A;00|B}_{\mu\lambda\rho_2\rho_3;\sigma_2\sigma_3} \end{pmatrix}$$
$$+ \begin{pmatrix} \alpha'^{\,\alpha0|A}_{\lambda\rho_1}\alpha''^{\,00|B}_{\lambda\sigma_1}\bar{\chi}''^{\,00|B;\alpha0|A}_{\nu\nu\rho_2\rho_3;\sigma_2\sigma_3} \\ \alpha'^{\,\alpha0|A}_{\mu\rho_1}\alpha''^{\,00|B}_{\lambda\sigma_1}\bar{\chi}''^{\,00|B;\alpha0|A}_{\lambda\mu\rho_2\rho_3;\sigma_2\sigma_3} \\ \alpha'^{\,\alpha0|A}_{\mu\rho_1}\alpha''^{\,00|B}_{\lambda\sigma_1}\bar{\chi}''^{\,00|B;\alpha0|A}_{\mu\lambda\rho_2\rho_3;\sigma_2\sigma_3} \end{pmatrix} + \begin{pmatrix} \chi'^{\,\alpha0|A;00|B}_{\lambda\rho_1\rho_2;\lambda\sigma_1\sigma_2}\bar{\alpha}'''^{\,\alpha0|A}_{\lambda\sigma_1}\bar{\alpha}'''^{\,00|B}_{\lambda\rho_1} \\ \chi'^{\,\alpha0|A;00|B}_{\mu\rho_1\rho_2;\lambda\sigma_1\sigma_2}\bar{\alpha}'''^{\,\alpha0|A}_{\lambda\sigma_1}\bar{\alpha}'''^{\,00|B}_{\mu\rho_1} \\ \chi'^{\,\alpha0|A;00|B}_{\mu\rho_1\rho_2;\lambda\sigma_1\sigma_2}\bar{\alpha}'''^{\,\alpha0|A}_{\lambda\sigma_1}\bar{\alpha}'''^{\,00|B}_{\mu\rho_1} \end{pmatrix} + \begin{pmatrix} \alpha'''^{\,\alpha0|A}_{\lambda\sigma_1}\alpha'''^{\,00|B}_{\lambda\rho_1}\bar{\chi}'''^{\,00|B;\alpha0|A}_{\nu\rho_2\rho_3;\nu\sigma_2\sigma_3} \\ \alpha'''^{\,\alpha0|A}_{\lambda\sigma_1}\alpha'''^{\,00|B}_{\mu\rho_1}\bar{\chi}'''^{\,00|B;\alpha0|A}_{\mu\rho_2\rho_3;\lambda\sigma_2\sigma_3} \\ \alpha'''^{\,\alpha0|A}_{\lambda\sigma_1}\alpha'''^{\,00|B}_{\mu\rho_1}\bar{\chi}'''^{\,00|B;\alpha0|A}_{\lambda\rho_2\rho_3;\mu\sigma_2\sigma_3} \end{pmatrix}$$
$$+ \begin{pmatrix} \chi^{\alpha0|A;00|B}_{\lambda\lambda\rho_1\rho_2;\sigma_1\sigma_2}\bar{\alpha}'''^{\,\alpha0|A}_{\lambda\sigma_1}\bar{\alpha}'''^{\,00|B}_{\lambda\rho_1} \\ \chi^{\alpha0|A;00|B}_{\lambda\mu\rho_1\rho_2;\sigma_1\sigma_2}\bar{\alpha}'''^{\,\alpha0|A}_{\lambda\sigma_1}\bar{\alpha}'''^{\,00|B}_{\mu\rho_1} \\ \chi^{\alpha0|A;00|B}_{\lambda\mu\rho_1\rho_2;\sigma_1\sigma_2}\bar{\alpha}'''^{\,\alpha0|A}_{\lambda\sigma_1}\bar{\alpha}'''^{\,00|B}_{\mu\rho_1} \end{pmatrix} + \begin{pmatrix} \alpha'''^{\,\alpha0|A}_{\lambda\sigma_1}\alpha'''^{\,00|B}_{\lambda\rho_1}\bar{\chi}''^{\,00|B;\alpha0|A}_{\nu\nu\rho_2\rho_3;\sigma_2\sigma_3} \\ \alpha'''^{\,\alpha0|A}_{\lambda\sigma_1}\alpha'''^{\,00|B}_{\mu\rho_1}\bar{\chi}''^{\,00|B;\alpha0|A}_{\lambda\mu\rho_2\rho_3;\sigma_2\sigma_3} \\ \alpha'''^{\,\alpha0|A}_{\lambda\sigma_1}\alpha'''^{\,00|B}_{\mu\rho_1}\bar{\chi}''^{\,00|B;\alpha0|A}_{\mu\lambda\rho_2\rho_3;\sigma_2\sigma_3} \end{pmatrix} + \begin{pmatrix} \beta^{\alpha0|A}_{\lambda\lambda\rho_1}\mu^{\,00|B}_{\sigma_1}\bar{\chi}'^{\,\alpha0|A;00|B}_{\nu\rho_2\rho_3;\nu\sigma_2\sigma_3} \\ \beta^{\alpha0|A}_{\lambda\mu\rho_1}\mu^{\,00|B}_{\sigma_1}\bar{\chi}'^{\,\alpha0|A;00|B}_{\mu\rho_2\rho_3;\lambda\sigma_2\sigma_3} \\ \beta^{\alpha0|A}_{\lambda\mu\rho_1}\mu^{\,00|B}_{\sigma_1}\bar{\chi}'^{\,\alpha0|A;00|B}_{\lambda\rho_2\rho_3;\mu\sigma_2\sigma_3} \end{pmatrix}$$
$$+ \begin{pmatrix} \beta^{\alpha0|A}_{\lambda\lambda\rho_1}\mu^{\,00|B}_{\sigma_1}\bar{\chi}'''^{\,00|B;\alpha0|A}_{\nu\rho_2\rho_3;\nu\sigma_2\sigma_3} \\ \beta^{\alpha0|A}_{\lambda\mu\rho_1}\mu^{\,00|B}_{\sigma_1}\bar{\chi}'''^{\,00|B;\alpha0|A}_{\mu\rho_2\rho_3;\lambda\sigma_2\sigma_3} \\ \beta^{\alpha0|A}_{\lambda\mu\rho_1}\mu^{\,00|B}_{\sigma_1}\bar{\chi}'''^{\,00|B;\alpha0|A}_{\lambda\rho_2\rho_3;\mu\sigma_2\sigma_3} \end{pmatrix} + \begin{pmatrix} \beta^{\alpha0|A}_{\lambda\lambda\rho_1}\mu^{\,00|B}_{\sigma_1}\bar{\chi}^{\alpha0|A;00|B}_{\nu\nu\rho_2\rho_3;\sigma_2\sigma_3} \\ \beta^{\alpha0|A}_{\lambda\mu\rho_1}\mu^{\,00|B}_{\sigma_1}\bar{\chi}^{\alpha0|A;00|B}_{\lambda\mu\rho_2\rho_3;\sigma_2\sigma_3} \\ \beta^{\alpha0|A}_{\lambda\mu\rho_1}\mu^{\,00|B}_{\sigma_1}\bar{\chi}^{\alpha0|A;00|B}_{\mu\lambda\rho_2\rho_3;\sigma_2\sigma_3} \end{pmatrix} + \begin{pmatrix} \beta^{\alpha0|A}_{\lambda\lambda\rho_1}\mu^{\,00|B}_{\sigma_1}\bar{\chi}''^{\,00|B;\alpha0|A}_{\nu\nu\rho_2\rho_3;\sigma_2\sigma_3} \\ \beta^{\alpha0|A}_{\lambda\mu\rho_1}\mu^{\,00|B}_{\sigma_1}\bar{\chi}''^{\,00|B;\alpha0|A}_{\lambda\mu\rho_2\rho_3;\sigma_2\sigma_3} \\ \beta^{\alpha0|A}_{\lambda\mu\rho_1}\mu^{\,00|B}_{\sigma_1}\bar{\chi}''^{\,00|B;\alpha0|A}_{\mu\lambda\rho_2\rho_3;\sigma_2\sigma_3} \end{pmatrix}$$
$$+ \begin{pmatrix} \chi'^{\,\alpha0|A;00|B}_{\lambda\rho_1\rho_2;\lambda\sigma_1\sigma_2}\bar{\mu}^{\alpha0|A}_{\sigma_3}\bar{\beta}'^{\,00|B}_{\nu\nu\rho_3} \\ \chi'^{\,\alpha0|A;00|B}_{\mu\rho_1\rho_2;\lambda\sigma_1\sigma_2}\bar{\mu}^{\alpha0|A}_{\sigma_3}\bar{\beta}'^{\,00|B}_{\lambda\mu\rho_3} \\ \chi'^{\,\alpha0|A;00|B}_{\mu\rho_1\rho_2;\lambda\sigma_1\sigma_2}\bar{\mu}^{\alpha0|A}_{\sigma_3}\bar{\beta}'^{\,00|B}_{\mu\lambda\rho_3} \end{pmatrix} + \begin{pmatrix} \mu^{\alpha0|A}_{\sigma_1}\beta'^{\,00|B}_{\lambda\lambda\rho_1}\bar{\chi}'''^{\,00|B;\alpha0|A}_{\nu\rho_2\rho_3;\nu\sigma_2\sigma_3} \\ \mu^{\alpha0|A}_{\sigma_1}\beta'^{\,00|B}_{\lambda\mu\rho_1}\bar{\chi}'''^{\,00|B;\alpha0|A}_{\mu\rho_2\rho_3;\lambda\sigma_2\sigma_3} \\ \mu^{\alpha0|A}_{\sigma_1}\beta'^{\,00|B}_{\lambda\mu\rho_1}\bar{\chi}'''^{\,00|B;\alpha0|A}_{\lambda\rho_2\rho_3;\mu\sigma_2\sigma_3} \end{pmatrix} + \begin{pmatrix} \chi^{\alpha0|A;00|B}_{\lambda\lambda\rho_1\rho_2;\sigma_1\sigma_2}\bar{\mu}^{\alpha0|A}_{\sigma_3}\bar{\beta}'^{\,00|B}_{\nu\nu\rho_3} \\ \chi^{\alpha0|A;00|B}_{\lambda\mu\rho_1\rho_2;\sigma_1\sigma_2}\bar{\mu}^{\alpha0|A}_{\sigma_3}\bar{\beta}'^{\,00|B}_{\lambda\mu\rho_3} \\ \chi^{\alpha0|A;00|B}_{\lambda\mu\rho_1\rho_2;\sigma_1\sigma_2}\bar{\mu}^{\alpha0|A}_{\sigma_3}\bar{\beta}'^{\,00|B}_{\mu\lambda\rho_3} \end{pmatrix}$$
$$+ \begin{pmatrix} \mu^{\alpha0|A}_{\sigma_1}\beta'^{\,00|B}_{\lambda\lambda\rho_1}\bar{\chi}''^{\,00|B;\alpha0|A}_{\nu\nu\rho_2\rho_3;\sigma_2\sigma_3} \\ \mu^{\alpha0|A}_{\sigma_1}\beta'^{\,00|B}_{\lambda\mu\rho_1}\bar{\chi}''^{\,00|B;\alpha0|A}_{\lambda\mu\rho_2\rho_3;\sigma_2\sigma_3} \\ \mu^{\alpha0|A}_{\sigma_1}\beta'^{\,00|B}_{\lambda\mu\rho_1}\bar{\chi}''^{\,00|B;\alpha0|A}_{\mu\lambda\rho_2\rho_3;\sigma_2\sigma_3} \end{pmatrix}\right\}, \tag{2.3.7}$$

$$\boldsymbol{T}_4 = \begin{pmatrix} \chi'^{\,\alpha0|A;00|B}_{\lambda\rho_1\rho_2;\lambda\sigma_1\sigma_2}\bar{\chi}'^{\,\alpha0|A;00|B}_{\nu\rho_3\rho_4;\nu\sigma_3\sigma_4} \\ \chi'^{\,\alpha0|A;00|B}_{\mu\rho_1\rho_2;\lambda\sigma_1\sigma_2}\bar{\chi}'^{\,\alpha0|A;00|B}_{\mu\rho_3\rho_4;\lambda\sigma_3\sigma_4} \\ \chi'^{\,\alpha0|A;00|B}_{\mu\rho_1\rho_2;\lambda\sigma_1\sigma_2}\bar{\chi}'^{\,\alpha0|A;00|B}_{\lambda\rho_3\rho_4;\mu\sigma_3\sigma_4} \end{pmatrix} + \begin{pmatrix} \chi'''^{\,00|B;\alpha0|A}_{\lambda\rho_1\rho_2;\lambda\sigma_1\sigma_2}\bar{\chi}'''^{\,00|B;\alpha0|A}_{\nu\rho_3\rho_4;\nu\sigma_3\sigma_4} \\ \chi'''^{\,00|B;\alpha0|A}_{\mu\rho_1\rho_2;\lambda\sigma_1\sigma_2}\bar{\chi}'''^{\,00|B;\alpha0|A}_{\mu\rho_3\rho_4;\lambda\sigma_3\sigma_4} \\ \chi'''^{\,00|B;\alpha0|A}_{\mu\rho_1\rho_2;\lambda\sigma_1\sigma_2}\bar{\chi}'''^{\,00|B;\alpha0|A}_{\lambda\rho_3\rho_4;\mu\sigma_3\sigma_4} \end{pmatrix} \begin{pmatrix} \chi^{\alpha0|A;00|B}_{\lambda\lambda\rho_1\rho_2;\sigma_1\sigma_2}\bar{\chi}^{\alpha0|A;00|B}_{\nu\nu\rho_3\rho_4;\sigma_3\sigma_4} \\ \chi^{\alpha0|A;00|B}_{\lambda\mu\rho_1\rho_2;\sigma_1\sigma_2}\bar{\chi}^{\alpha0|A;00|B}_{\lambda\mu\rho_3\rho_4;\sigma_3\sigma_4} \\ \chi^{\alpha0|A;00|B}_{\lambda\mu\rho_1\rho_2;\sigma_1\sigma_2}\bar{\chi}^{\alpha0|A;00|B}_{\mu\lambda\phi\psi;\chi\omega} \end{pmatrix}$$
$$+ \begin{pmatrix} \chi''^{\,00|B;\alpha0|A}_{\lambda\lambda\rho_1\rho_2;\sigma_1\sigma_2}\bar{\chi}''^{\,00|B;\alpha0|A}_{\nu\nu\rho_3\rho_4;\sigma_3\sigma_4} \\ \chi''^{\,00|B;\alpha0|A}_{\lambda\mu\rho_1\rho_2;\sigma_1\sigma_2}\bar{\chi}''^{\,00|B;\alpha0|A}_{\lambda\mu\rho_3\rho_4;\sigma_3\sigma_4} \\ \chi''^{\,00|B;\alpha0|A}_{\lambda\mu\rho_1\rho_2;\sigma_1\sigma_2}\bar{\chi}''^{\,00|B;\alpha0|A}_{\mu\lambda\rho_3\rho_4;\sigma_3\sigma_4} \end{pmatrix} + 2\left\{\begin{pmatrix} \chi'^{\,\alpha0|A;00|B}_{\lambda\rho_1\rho_2;\lambda\sigma_1\sigma_2}\bar{\chi}'''^{\,00|B;\alpha0|A}_{\nu\rho_3\rho_4;\nu\sigma_3\sigma_4} \\ \chi'^{\,\alpha0|A;00|B}_{\mu\rho_1\rho_2;\lambda\sigma_1\sigma_2}\bar{\chi}'''^{\,00|B;\alpha0|A}_{\mu\rho_3\rho_4;\lambda\sigma_3\sigma_4} \\ \chi'^{\,\alpha0|A;00|B}_{\mu\rho_1\rho_2;\lambda\sigma_1\sigma_2}\bar{\chi}'''^{\,00|B;\alpha0|A}_{\lambda\rho_3\rho_4;\mu\sigma_3\sigma_4} \end{pmatrix} + \begin{pmatrix} \chi^{\alpha0|A;00|B}_{\lambda\lambda\rho_1\rho_2;\sigma_1\sigma_2}\bar{\chi}'^{\,\alpha0|A;00|B}_{\nu\rho_3\rho_4;\nu\sigma_3\sigma_4} \\ \chi^{\alpha0|A;00|B}_{\lambda\mu\rho_1\rho_2;\sigma_1\sigma_2}\bar{\chi}'^{\,\alpha0|A;00|B}_{\mu\rho_3\rho_4;\lambda\sigma_3\sigma_4} \\ \chi^{\alpha0|A;00|B}_{\lambda\mu\rho_1\rho_2;\sigma_1\sigma_2}\bar{\chi}'^{\,\alpha0|A;00|B}_{\lambda\rho_3\rho_4;\mu\sigma_3\sigma_4} \end{pmatrix}\right\}$$
$$+ \begin{pmatrix} \chi'^{\,\alpha0|A;00|B}_{\lambda\rho_1\rho_2;\lambda\sigma_1\sigma_2}\bar{\chi}''^{\,00|B;\alpha0|A}_{\nu\nu\rho_3\rho_4;\sigma_3\sigma_4} \\ \chi'^{\,\alpha0|A;00|B}_{\mu\rho_1\rho_2;\lambda\sigma_1\sigma_2}\bar{\chi}''^{\,00|B;\alpha0|A}_{\lambda\mu\rho_3\rho_4;\sigma_3\sigma_4} \\ \chi'^{\,\alpha0|A;00|B}_{\mu\rho_1\rho_2;\lambda\sigma_1\sigma_2}\bar{\chi}''^{\,00|B;\alpha0|A}_{\mu\lambda\rho_3\rho_4;\sigma_3\sigma_4} \end{pmatrix} + \begin{pmatrix} \chi^{\alpha0|A;00|B}_{\lambda\lambda\rho_1\rho_2;\sigma_1\sigma_2}\bar{\chi}'''^{\,00|B;\alpha0|A}_{\nu\rho_3\rho_4;\nu\sigma_3\sigma_4} \\ \chi^{\alpha0|A;00|B}_{\lambda\mu\rho_1\rho_2;\sigma_1\sigma_2}\bar{\chi}'''^{\,00|B;\alpha0|A}_{\mu\rho_3\rho_4;\lambda\sigma_3\sigma_4} \\ \chi^{\alpha0|A;00|B}_{\lambda\mu\rho_1\rho_2;\sigma_1\sigma_2}\bar{\chi}'''^{\,00|B;\alpha0|A}_{\lambda\rho_3\rho_4;\mu\sigma_3\sigma_4} \end{pmatrix} + \begin{pmatrix} \chi''^{\,00|B;\alpha0|A}_{\lambda\lambda\rho_1\rho_2;\sigma_1\sigma_2}\bar{\chi}'''^{\,00|B;\alpha0|A}_{\nu\rho_3\rho_4;\nu\sigma_3\sigma_4} \\ \chi''^{\,00|B;\alpha0|A}_{\lambda\mu\rho_1\rho_2;\sigma_1\sigma_2}\bar{\chi}'''^{\,00|B;\alpha0|A}_{\mu\rho_3\rho_4;\lambda\sigma_3\sigma_4} \\ \chi''^{\,00|B;\alpha0|A}_{\lambda\mu\rho_1\rho_2;\sigma_1\sigma_2}\bar{\chi}'''^{\,00|B;\alpha0|A}_{\lambda\rho_3\rho_4;\mu\sigma_3\sigma_4} \end{pmatrix}$$
$$+ \begin{pmatrix} \chi^{\alpha0|A;00|B}_{\lambda\lambda\rho_1\rho_2;\sigma_1\sigma_2}\bar{\chi}''^{\,00|B;\alpha0|A}_{\nu\nu\rho_3\rho_4;\sigma_3\sigma_4} \\ \chi^{\alpha0|A;00|B}_{\lambda\mu\rho_1\rho_2;\sigma_1\sigma_2}\bar{\chi}''^{\,00|B;\alpha0|A}_{\lambda\mu\rho_3\rho_4;\sigma_3\sigma_4} \\ \chi^{\alpha0|A;00|B}_{\lambda\mu\rho_1\rho_2;\sigma_1\sigma_2}\bar{\chi}''^{\,00|B;\alpha0|A}_{\mu\lambda\rho_3\rho_4;\sigma_3\sigma_4} \end{pmatrix}\right\}. \tag{2.3.8}$$

The tensor brackets merely encapsulate the linear combinations of vectors produced from each matrix element pairing, one for each of the 45.

2.4 SYMMETRY

In this section, we will home in on the symmetry characteristics of each of the molecular response tensors derived in §2.2. We are now equipped to identify the number of photon-molecular interactions present and as such the symmetry rules invoked in each case. Molecule A is the spectroscopic focus and as such the discussion will relate to that, analogous principles hold for molecule B. See Table 8, for a summary of each of the cases sorted by the n-photon selection rules they engage in. A Feynman diagram displaying all of the interactions on molecule A for each case, as well as the associated response tensor. The final column displays the permissible irreducible tensor weights, which builds on principles introduced in complement 1B. The superscript on the rank denotes the parity of the interactions; for this work, each interaction is assumed to engage an electric dipole transition, and thus each additional interaction introduces a change in parity.

The addition of weight 1 for the transition polarisabilities, α , arises from the reduction in symmetry introduced in near-resonance conditions, see complement 1F. In such cases, additional vibrational lines will be observable in the Raman spectra for a given species. The focus of this work is on off-resonance effects. Under this regime, a number of the cases will only be present if single-centre Raman scattering is also permitted, they are cases which involve two-photon process (2^+) with weights of 0 or 2 present, *i.e.* cases *I*, *II* and *VIII*. If this was allowed, such vibrational amplitudes would likely dominate the spectra. It is of interest to consider mechanisms in which new lines are observed of different symmetry. To classify the cases of specific interest, Table 9 introduces a category system referred to as 'type', into which each and every irreducible representation (irrep) will fall, see Table 12 in complement 2B for the complete results.

Table 8: List of molecular response tensors with their corresponding case and world line for molecule A, sorted by number of interactions 'rank'. The permissible weights for the given rank are also displayed. Note, near resonance, linear polarisability tensors α will include weight 1 components.

Rank	Case	Diagram	Tensor	Weights
1^-	*IV*		$\mu_l^{\alpha 0\|A}$	(1)
2^+		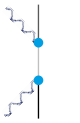	$\alpha_{(ij)}^{\alpha 0}$	(02)
	I	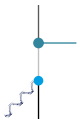	$\alpha'^{\alpha 0\|A}_{(jk)}$	(02)
	II		$\alpha''^{\alpha 0\|A}_{(il)}$	(02)
	VIII	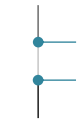	$\chi''^{00\|B';\alpha 0\|A}_{(ij)(km);(ln)}$	(02)
3^-	*III*		$\beta_{(ij)k}^{\alpha 0\|A}$	(123)
	V		$\chi'^{\alpha 0\|A;00\|B'}_{jkm;iln}$	(0123)
	VI		$\chi''^{00\|B;\alpha 0\|A'}_{jkm;iln}$	(0123)
4^+	*VII*	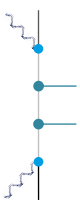	$\chi^{\alpha 0\|A';00\|B}_{(ij)(km);(ln)}$	(01234)

Table 9: Categorizes the irreps for all novel (neighbour-induced) Raman transitions according to the irreducible weights engaged. Columns two – five, are engaged by cases *IV*, *III*, *V*, *VI* and *VII*, respectively.

	Rank 1⁻	Rank 3⁻		Rank 4⁺
Type	(1)[a]	(0123)[b]	(123)[c]	(01234)[d]
I	✓	✓	✓	✓
II	✓	✓	✓	
III	✓			✓
IV		✓	✓	✓
V		✓	✓	
VI			✓	✓
VII			✓	
VIII				✓

2.5 EXAMPLE SYSTEM: BENZENE

At this juncture, an example will be laid out in order to consolidate the principles introduced in this chapter. We shall consider an example where the molecule A undergoing the Raman transition is benzene, whose symmetry is consistent with the point group D_{6h}. Referring to a standard point character table, we can see there are twelve irreps of which three are single-centre Raman active $\left(A_{1g}, E_{1g} \text{ and } E_{2g}\right)$, indicated by the quadratic components. Table 12 lists all irreps that are not single-centre Raman active, but are allowed because of the theory contained within this chapter. The D_{6h} entry lists all nine remaining irreps, indicating that all are active by neighbour coupling.

One can envisage a sample in which the benzene is mixed with low concentrations of an inert molecule, such as naphthalene, where the interaction between the pair should allow for the two centre interactions laid out in this chapter. The three *gerade* irreps listed $\left(A_{2g}, B_{1g} \text{ and } B_{2g}\right)$ would all become allowed by the pathway of case *VII*. $\left(A_{1u}, B_{1u} \text{ and } E_{2u}\right)$ all become allowed by virtue of cases *III*, *V*, *VI*: the complete set of three photon interactions on molecule A. Moreover, A_{2u} and E_{1u} both engage all of cases *III* through *VI*, which are all of the odd ranked processes considered. It is noteworthy that naphthalene mixed with low concentrations of benzene should also exhibit additional Raman active lines. Naphthalene, of D_{2h} symmetry, should then display four additional classes of lines in its Raman vibrational spectra. This example

is, of course, given only to exemplify the mechanisms at work and their potential consequences. Real systems, subjected to this kind of analysis, will need to take account of relative concentrations and avoid any possibility of weak association forces.

By selecting, for example B_{2g}, which involves a planar deformation vibration, we can obtain a specific result for equation (2.3.3):

$$\boldsymbol{T}_0, \boldsymbol{T}_1, \boldsymbol{T}_2 = 0 \ , \tag{2.5.1}$$

$$\begin{aligned} \boldsymbol{T}_3 = & \begin{pmatrix} \beta^{\alpha 0|A}_{\lambda\lambda\rho_1} \mu^{00|B}_{\sigma_1} \overline{\chi}'^{\,\alpha 0|A;00|B}_{\nu\rho_2\rho_3;\nu\sigma_2\sigma_3} \\ \beta^{\alpha 0|A}_{\lambda\mu\rho_1} \mu^{00|B}_{\sigma_1} \overline{\chi}'^{\,\alpha 0|A;00|B}_{\mu\rho_2\rho_3;\lambda\sigma_2\sigma_3} \\ \beta^{\alpha 0|A}_{\lambda\mu\rho_1} \mu^{00|B}_{\sigma_1} \overline{\chi}'^{\,\alpha 0|A;00|B}_{\lambda\rho_2\rho_3;\mu\sigma_2\sigma_3} \end{pmatrix} + \begin{pmatrix} \alpha'^{\alpha 0|A}_{\lambda\rho_1} \alpha''^{00|B}_{\lambda\sigma_1} \overline{\chi}'^{\,\alpha 0|A;00|B}_{\nu\rho_2\rho_3;\nu\sigma_2\sigma_3} \\ \alpha'^{\alpha 0|A}_{\mu\rho_1} \alpha''^{00|B}_{\lambda\sigma_1} \overline{\chi}'^{\,\alpha 0|A;00|B}_{\mu\rho_2\rho_3;\lambda\sigma_2\sigma_3} \\ \alpha'^{\alpha 0|A}_{\mu\rho_1} \alpha''^{00|B}_{\lambda\sigma_1} \overline{\chi}'^{\,\alpha 0|A;00|B}_{\lambda\rho_2\rho_3;\mu\sigma_2\sigma_3} \end{pmatrix} \\ & + \begin{pmatrix} \chi'^{\,\alpha 0|A;00|B}_{\lambda\rho_1\rho_2;\lambda\sigma_1\sigma_2} \overline{\beta}^{00|B}_{\nu\nu\rho_3} \overline{\mu}^{\alpha 0|A}_{\sigma_3} \\ \chi'^{\,\alpha 0|A;00|B}_{\mu\rho_1\rho_2;\lambda\sigma_1\sigma_2} \overline{\beta}^{00|B}_{\lambda\mu\rho_3} \overline{\mu}^{\alpha 0|A}_{\sigma_3} \\ \chi'^{\,\alpha 0|A;00|B}_{\mu\rho_1\rho_2;\lambda\sigma_1\sigma_2} \overline{\beta}^{00|B}_{\mu\lambda\rho_3} \overline{\mu}^{\alpha 0|A}_{\sigma_3} \end{pmatrix} + \begin{pmatrix} \chi'^{\,\alpha 0|A;00|B}_{\lambda\rho_1\rho_2;\lambda\sigma_1\sigma_2} \overline{\alpha}'^{00|B}_{\nu\rho_3} \overline{\alpha}''^{\alpha 0|A}_{\nu\sigma_3} \\ \chi'^{\,\alpha 0|A;00|B}_{\mu\rho_1\rho_2;\lambda\sigma_1\sigma_2} \overline{\alpha}'^{00|B}_{\lambda\rho_3} \overline{\alpha}''^{\alpha 0|A}_{\mu\sigma_3} \\ \chi'^{\,\alpha 0|A;00|B}_{\mu\rho_1\rho_2;\lambda\sigma_1\sigma_2} \overline{\alpha}'^{00|B}_{\mu\rho_3} \overline{\alpha}''^{\alpha 0|A}_{\lambda\sigma_3} \end{pmatrix} , \end{aligned} \tag{2.5.2}$$

$$\begin{aligned} \boldsymbol{T}_4 = & \begin{pmatrix} \chi^{\alpha 0|A;00|B}_{\lambda\lambda\rho_1\rho_2;\sigma_1\sigma_2} \overline{\chi}'^{\,\alpha 0|A;00|B}_{\nu\rho_3\rho_4;\nu\sigma_3\sigma_4} \\ \chi^{\alpha 0|A;00|B}_{\lambda\mu\rho_1\rho_2;\sigma_1\sigma_2} \overline{\chi}'^{\,\alpha 0|A;00|B}_{\mu\rho_3\rho_4;\lambda\sigma_3\sigma_4} \\ \chi^{\alpha 0|A;00|B}_{\lambda\mu\rho_1\rho_2;\sigma_1\sigma_2} \overline{\chi}'^{\,\alpha 0|A;00|B}_{\lambda\rho_3\rho_4;\mu\sigma_3\sigma_4} \end{pmatrix} + \begin{pmatrix} \chi'^{\,\alpha 0|A;00|B}_{\lambda\rho_1\rho_2;\lambda\sigma_1\sigma_2} \overline{\chi}'^{\,\alpha 0|A;00|B}_{\nu\rho_3\rho_4;\nu\sigma_3\sigma_4} \\ \chi'^{\,\alpha 0|A;00|B}_{\mu\rho_1\rho_2;\lambda\sigma_1\sigma_2} \overline{\chi}'^{\,\alpha 0|A;00|B}_{\mu\rho_3\rho_4;\lambda\sigma_3\sigma_4} \\ \chi'^{\,\alpha 0|A;00|B}_{\mu\rho_1\rho_2;\lambda\sigma_1\sigma_2} \overline{\chi}'^{\,\alpha 0|A;00|B}_{\lambda\rho_3\rho_4;\mu\sigma_3\sigma_4} \end{pmatrix} \\ & + \begin{pmatrix} \chi'^{\,\alpha 0|A;00|B}_{\lambda\rho_1\rho_2;\lambda\sigma_1\sigma_2} \overline{\chi}'^{00|B;\alpha 0|A}_{\nu\rho_3\rho_4;\nu\sigma_3\sigma_4} \\ \chi'^{\,\alpha 0|A;00|B}_{\mu\rho_1\rho_2;\lambda\sigma_1\sigma_2} \overline{\chi}'^{00|B;\alpha 0|A}_{\mu\rho_3\rho_4;\lambda\sigma_3\sigma_4} \\ \chi'^{\,\alpha 0|A;00|B}_{\mu\rho_1\rho_2;\lambda\sigma_1\sigma_2} \overline{\chi}'^{00|B;\alpha 0|A}_{\lambda\rho_3\rho_4;\mu\sigma_3\sigma_4} \end{pmatrix} + \begin{pmatrix} \chi'^{\,\alpha 0|A;00|B}_{\lambda\rho_1\rho_2;\lambda\sigma_1\sigma_2} \overline{\chi}^{00|B;\alpha 0|A}_{\nu\nu\rho_3\rho_4;\sigma_3\sigma_4} \\ \chi'^{\,\alpha 0|A;00|B}_{\mu\rho_1\rho_2;\lambda\sigma_1\sigma_2} \overline{\chi}^{00|B;\alpha 0|A}_{\lambda\mu\rho_3\rho_4;\sigma_3\sigma_4} \\ \chi'^{\,\alpha 0|A;00|B}_{\mu\rho_1\rho_2;\lambda\sigma_1\sigma_2} \overline{\chi}^{00|B;\alpha 0|A}_{\mu\lambda\rho_3\rho_4;\sigma_3\sigma_4} \end{pmatrix} . \end{aligned} \tag{2.5.3}$$

Further inspection of the tensor structures in the above non-zero results indicates that terms involving three photon interactions by molecule A, which follow cubic selection rules, will also be forbidden. However, all other terms connected with four photon ('quartic') interactions will be allowed. The result is a weak Raman signal with a depolarisation ratio that is not constrained to the usual [0, ¾] range associated with non-resonant Raman signals [114].

2.6 PRESSURE DEPENDENCE

The mechanisms derived in this chapter exhibit a strong distance dependence, reliant on two centres able to experience near field effects of the other centre. Inevitably, there will be a strong pressure dependence on the likelihood of this occurring, so it warrants consideration. In order to pin down the precise pressure dependence, we must consider the density dependence of the

pair correlation function for the fluid, as well as the dependence on molecular separation R in each contributing mechanism.

It is known that the intensity of scattering signals, in the case of compressible species, exhibit a pressure dependence related to the bulk isothermal compressibility, $\Delta I' \propto \beta_T$. This is a development on the principles introduced in §1.1, the less volume a molecule occupies, the greater the number of scatterers that can be present in the laser beam. It is natural to assume that two-centre scattering should depend quadratically upon the compressibility. The number of centres required is indeed a factor, but the level of electrodynamic coupling also plays a role, with an additional dependence through the R^{-3w} factor in the $\boldsymbol{T}_w$ tensors featured in equation (2.3.3). See Table 10 for the nonlinear compressibility dependence of the line intensities.

Table 10: The range of bulk isothermal compressibilities delivered from the six possible pairings of zero, one and two virtual photons.

	$\lvert M_{FI}\rvert^2$	$\lvert M_{FI}\bar{M}^{\perp}_{FI}\rvert$	$\lvert M_{FI}\bar{M}^{\parallel}_{FI}\rvert$	$\lvert M^{\perp}_{FI}\rvert^2$	$\lvert M^{\perp}_{FI}\bar{M}^{\parallel}_{FI}\rvert$	$\lvert M^{\parallel}_{FI}\rvert^2$
$\Delta I'(\boldsymbol{T}_w)$	R^0	R^{-3}	R^{-6}	R^{-6}	R^{-9}	R^{-12}
β_T^n	β_T	$\beta_T^{2.5}$	$\beta_T^{3.5}$	β_T^4	β_T^5	β_T^6

The sharp nonlinearity should make the detection of such lines through pressure-dependent studies especially identifiable, for example through log-log plots of intensity against pressure.

2.7 DISCUSSION

Raman scattering is a widely deployed spectroscopic technique [115-117] with an ever-increasing range of applications – including surface-enhanced spectroscopy [118-123], sensing [124-126], the detection of environmental pollutants [127, 128] and identification of disease [129]. An advantage it has over similarly deployed techniques such as infra-red absorption, is that the scattering intensity increases with the fourth power of the scattered frequency, see equation (1.4.18) and (2.3.3). Of course, the scattered frequency will be close in frequency to that of the incident light, across the whole spectrum of frequencies. In contrast, infra-red absorption

intensities are proportional to the respective vibration frequency, which is less beneficial in low frequency interrogations, where the low intensities are more difficult to scrutinise.

The theory presented in this chapter offers two distinctive modifications to single-centre Raman spectra. Firstly, there will be a change in the intensities of the well-characterised transition frequencies invoking two-photon symmetry properties. The second is the appearance of entirely new lines in the Raman spectrum, resulting from vibrations that are allowed by different, modified selection rules – those associated with three-photon processes, closely associated with hyper-Raman [130] scattering, or even four photon interactions. This will be of particular value in the identification of molecules of relatively high symmetry that support few or none single-centre vibrational transitions.

It has been commented that the intensity of the two-centre scattering processes, optimally could be within an order of magnitude of that of the more widely known single-centre process, up to an order of magnitude. A rough guide for this can utilise the transition polarisability volume, which is of comparable dimensions to that of the molecular size. This, in turn, suggests that each additional vertex in a pair-interaction time-ordered diagram conveys a correction of the order of molecular size divided by the cube of the pair separation. In species of sufficiently high densities, it may be possible to obtain new lines of comparable intensities to that of single-centre Raman bands. This would increase the possibility of additional centres further altering the electrodynamic environment of the interrogated molecule. However, this would not introduce additional vibrations into the Raman spectra, beyond those arising from the two-centre mechanisms.

COMPLEMENT 2A: PRODUCTS OF MATRIX ELEMENTS

Many processes have a number of possible mechanisms which can contribute to the rate (or intensity) of a process, for example,

$$I' \propto \left| \sum_{i=1}^{n} M_i \right|^2 , \tag{3A.1}$$

where M represents a general matrix element and n is the number of mechanisms contributing to the process. Expressing all the matrix elements as a (rank 1) column matrix,

$$G^{(n)}_{\{1,2,\ldots n\},1} = \begin{pmatrix} M_1 \\ M_2 \\ \ldots \\ M_n \end{pmatrix} , \tag{3A.2}$$

all the products for the matrix elements can be delivered by, $G\bar{G}^{\mathrm{T}}$, this is referred to as the gramian matrix. Mathematically, this can be extracted from the matrix by obtaining the grand sum of the gramian by,

$$A^{\mathrm{T}} G \bar{G}^{\mathrm{T}} A , \tag{3A.3}$$

where A is a column matrix,

$$A^{(n)}_{\{1,2,\ldots n\},1} \equiv 1 . \tag{3A.4}$$

The ensuing number of products to be evaluated can be reduced by exploiting the following identity,

$$\begin{aligned} M_i \bar{M}_j + M_j \bar{M}_i &\equiv 2\,\mathrm{Re}\left[M_i \bar{M}_j \right] \\ &\equiv 2\,\mathrm{Re}\left[M_j \bar{M}_i \right] . \end{aligned} \tag{3A.5}$$

The number of total products is immediately apparent for a given number of mechanisms. In order to identify the number of unique products, the following relation can be utilised,

$$T_n = \frac{n(n+1)}{2} , \tag{3A.6}$$

Table 11 demonstrates the result a process comprising of one, two, three and a general number of mechanisms.

Table 11: The total number of products and number that are uniquely expressible for a given number of mechanisms.

Number of mechanisms	Corresponding matrix elements	Grand sum	Total number of products	Number of *unique* products
1	$\lvert M_1 \rvert^2$	$= M_1^2$	1	1
2	$\lvert M_1 + M_2 \rvert^2$	$= M_1^2 + M_2^2 + M_1\bar{M}_2 + M_2\bar{M}_1$	4	3
3	$\lvert M_1 + M_2 + M_3 \rvert^2$	$= M_1^2 + M_2^2 + M_3^2 + M_1\bar{M}_2 + M_2\bar{M}_3 + M_3\bar{M}_1 + M_2\bar{M}_1 + M_1\bar{M}_3 + M_3\bar{M}_2$	9	6
n		$\left\lvert \sum_{i=1}^{n} M_i \right\rvert^2$	n^2	T_n

The third column in the table above is the equivalent output to equation (3A.3).

In this chapter, a ninth rank instance is considered. Here, there are 81 total products, which is expressible as 45 unique products, nine of which will be products with their own complex conjugates. The remaining 36 terms are known as the quantum interference between the respective pair of matrix elements. In the subsequent chapter, a fifth rank will be introduced, which in turn will be reduced to a fourth. This will result in 16 products, of which ten will be unique, five of which will be products with their own complex conjugate.

COMPLEMENT 2B: COMPLETE SET OF NEWLY RAMAN ACTIVE IRREDUCIBLE REPRESENTATIONS

This complement holds Table 12, designed to display all point groups that are Raman allowed by the additional neighbour interactions contained in chapter 2.

Table 12: A list of irreps (for each point group) that relate to the spectral lines that may feature on a Raman spectrum with neighbour-modified features. Rows which engage the same set of cases are assigned an appropriate 'type'.

Point group	Irrep	Rank 1^-	Rank 3^-	Rank 4^+	Type
C_i	A_u	1	0123		II
C_6	B		3	34	IV
S_6	A_u	1	0123		II
	E_u	1	123		II
S_8	B	1	0123	4	I
	E_1	1	123	34	I
S_{10}	A_u	1	0123		III
	E_{1u}	1	123		II
	E_{2u}		23		V
C_{2h}	A_u	1	0123		II
	B_u	1	123		II
C_{3h}	A''	1	0123	34	I
C_{4h}	A_u	1	0123		II
	B_u		23		V
	E_u	1	123		II
C_{5h}	E_1'	1	123	4	I
	A''	1	0123		II
	E_2''		23	34	IV
C_{6h}	B_g			34	VIII
	A_u	1	0123		II
	B_u		3		V
	E_{1u}	1	123		II
	E_{2u}		23		V
C_{3v}	A_2		023	134	IV

C_{4v}	A_2		02	134	IV
C_{5v}	A_2		02	13	IV
C_{6v}	A_2		02	13	IV
	B_1		3	34	IV
	B_2		3	34	IV
D_3	A_2	1	13	134	I
D_4	A_2	1	13	134	I
D_5	A_2	1	13	13	I
D_6	A_2	1	13	13	I
	B_1		3	34	IV
	B_2		3	34	IV
D_{2h}	A_u		023		V
	B_{1u}	1	123		II
	B_{2u}	1	123		II
	B_{3u}	1	123		II
D_{3h}	A_2'		3	13	IV
	A_1''		02	34	VIII
	A_2''	1	13	34	I
D_{4h}	A_{2g}			134	VIII
	A_{1u}		02		V
	A_{2u}	1	13		II
	B_{1u}		23		V
	B_{2u}		23		V
	E_u	1	123		II
D_{5h}	A_2'			13	VIII
	E_1'	1	123	4	I
	A_1''		02		V
	A_2''	1	13		II
	E_2''		23	34	IV
D_{6h}	A_{2g}			13	VIII
	B_{1g}			34	VIII
	B_{2g}			34	VIII
	A_{1u}		02		V
	A_{2u}	1	13		II
	B_{1u}		3		V
	B_{2u}		3		V

	E_{1u}	1	123		II
	E_{2u}		23		V
D_{2d}	A_2		23	134	IV
D_{3d}	A_{2g}		13	134	IV
	A_{1u}		023		V
	A_{2u}	1	13		II
	E_u	1	123		II
D_{4d}	A_2	1		13	III
	B_1		02	4	IV
	B_2	1	13	4	I
	E_1	1	123	34	I
D_{5d}	A_{2g}			13	VIII
	A_{1u}		02		V
	A_{2u}	1	13		II
	E_{1u}	1	123		II
	E_{2u}		23		V
D_{6d}	A_2			13	VIII
	B_1		02		V
	B_2	1	13		II
	E_1	1	123		II
	E_3		3	34	IV
	E_4		23	4	IV
$C_{\infty v}$	Σ^-		02	13	IV
	Φ		3	34	IV
	Γ			4	VIII
$D_{\infty h}$	Σ_g^-			13	VIII
	Φ_g			34	VIII
	Γ_g			4	VIII
	Σ_u^+	1	13		II
	Σ_u^-		02		V
	Π_u	1	123		II
	Δ_u		23		V
	Φ_u		3		V
T_h	A_u		03		V
	E_u		2		V
	T_u	1	123		II

T_d	A_2		0	3	VI
	T_1		23	134	IV
O	A_2		3	3	IV
	T_1	1	13	134	I
O_h	A_{2g}			3	VIII
	T_{1g}			134	VIII
	A_{1u}		0		VII
	A_{2u}		3		V
	E_u		2		V
	T_{1u}	1	13		II
	T_{2u}		23		V
I	T_1	1	1	1	I
	T_2		3	3	IV
	G		3	34	IV
I_h	T_{1g}			1	VIII
	T_{2g}			3	VIII
	G_g			34	VIII
	A_u		0		VII
	T_{1u}	1	1		II
	T_{2u}		3		V
	G_u		3		V
	H_u		2		V

3

HYPER-RAYLEIGH SCATTERING

3.1 INTRODUCTION

This chapter (as well as the subsequent chapter) will develop the process introduced in §1.4C, second-harmonic generation. Hyper-Rayleigh scattering (HRS) is the incoherent three-photon analogue to SHG, which also comprises of two photon annihilation events and one creation event. Previously, all three of these interactions were treated under the electric dipole approximation *i.e.* they were considered to only interact with the leading contributor to the interaction Hamiltonian, equation (1.2.16).

However, there are instances in which a series of three electric transition dipole moments are not permitted. If we refer to complement 1A, we can see that each electric dipole transition is of odd spatial parity. This in turn requires any E1 transition to result in a parity inversion, often associated with a flip in sign. Any even number of E1 transitions $(-1)^{2n}$ will deliver an equivalent parity to that of the initial state. In contrast, any odd number of E1 transitions, $(-1)^{2n+1}$, will result in a final state of opposite parity to that of the initial state.

If we now consider a system with high symmetry associated with it, a centrosymmetric molecule for example. Any process that engages such a centre is required to reach a final state of equivalent parity to that of the initial state. Each E1 transition is constrained to result in a parity reversal [63]. It follows that any process consisting of an odd number of E1 transitions will therefore be forbidden, second-harmonic generation for example.

Referring back to the interaction Hamiltonian in equation (1.2.16), we can see there are other operators that can be engaged in the course of a transition. In the aforementioned expansion, three terms are included: that of the E1, E2 and M1 operators. At this point we shall reaffirm the relative contributions of each transition moment. The E1 operation is the leading contributor, the E2 and M1 operations are considered the next-most significant contributions and are a factor of the fine structure constant smaller, $\alpha \approx 1/137$. In principle, any number of interactions, in a process, can engage with any combination of these three operators, or indeed the higher order terms. Cross-referencing these with complement 1A, it can be seen that both E2 and M2 transitions are of even spatial parity. This unlocks a pathway to allow processes that are conventionally thought of as forbidden.

Returning to a centrosymmetric system, we can assert that a single-photon process involving an E2 or M1 transition will be allowed, in contrast to that of an E1 transition. In the case of multiphoton processes, for example the three photon SHG: if one or indeed all (but not two) of the interactions engage in an even parity transition, such as E2 or M1, the process is allowed. As mentioned previously, the leading contributors in these cases will be those that engage the fewest number of higher order operators. For our purposes, we shall consider the possibility of one of the three interactions engaging in either an E2 or M1 transition, with the remaining two engaging the E1 operator [103, 131, 132].

The following analysis will consider four possible mechanisms, all of which will be represented by identical Feynman diagrams as those seen for SHG in Figure 4. In case *I*, the creation interaction will engage the M1 operator and the two annihilation events will engage the E1 operator. The notation for this will be $\mathrm{E1^2M1'}$, the prime indicating the transition moment associated with emission. For case *II*, one annihilation event will engage the M1 operator and the other an E1 operator, the creation event will also engage an E1 operator. This is denoted by $\mathrm{E1M1E1'}$. Case *III*, is analogous to that of case *I*, but with an E2 transition taking the place of the M1 transition and is represented by $\mathrm{E1^2E2'}$. Similarly, case *IV* is analogous to case *II*, with an E2 transition in place of and is displayed as $\mathrm{E1E2E1'}$.

3.2 GENERAL THEORY

3.2A CASE *I*

The first case will consider the HRS mechanism where the creation event engages the M1 operator, the two annihilation events will engage the E1 operator. There are three interaction events in this mechanism and so the result for perturbation theory of the same order, $n=3$, can be deployed. The three time orderings, all identical to those displayed in Figure 4 contribute to the matrix element as follows,

$$
\begin{aligned}
M_{FI}^{(\mathrm{E1^2M1'})} = \frac{1}{\varepsilon_0^2}\sum_{r,s}\Bigg\{ & \frac{\langle 0;\mathbf{k}',\eta'|m_i b_i|s;0\rangle\langle s;0|\mu_j d_j^{\perp}|r;\mathbf{k},\eta\rangle\langle r;\mathbf{k},\eta|\mu_k d_k^{\perp}|0;(\mathbf{k},\eta;\mathbf{k},\eta)\rangle}{[E_{0r}+2\hbar ck][E_{0s}+\hbar ck]} \\
& + \frac{\langle 0;\mathbf{k}',\eta'|\mu_j d_j^{\perp}|s;(\mathbf{k},\eta;\mathbf{k}',\eta')\rangle\langle s;(\mathbf{k},\eta;\mathbf{k}',\eta')|m_i b_i|r;\mathbf{k},\eta\rangle}{[E_{0r}+\hbar ck-\hbar ck'][E_{0s}+\hbar ck]} \\
& \times\langle r;\mathbf{k},\eta|\mu_k d_k^{\perp}|0;(\mathbf{k},\eta;\mathbf{k},\eta)\rangle \\
& + \frac{\langle 0;\mathbf{k}',\eta'|\mu_j d_j^{\perp}|s;(\mathbf{k},\eta;\mathbf{k}',\eta')\rangle\langle s;(\mathbf{k},\eta;\mathbf{k}',\eta')|\mu_k d_k^{\perp}|r;(\mathbf{k},\eta;\mathbf{k},\eta;\mathbf{k}',\eta')\rangle}{[E_{0r}+\hbar ck-\hbar ck'][E_{0s}-\hbar ck']} \\
& \times\langle r;(\mathbf{k},\eta;\mathbf{k},\eta;\mathbf{k}',\eta')|m_i b_i|0;(\mathbf{k},\eta;\mathbf{k},\eta)\rangle\Bigg\}\ . \qquad (4.2.1)
\end{aligned}
$$

The superscript attached to the matrix element identifies the mechanism that it represents, $\mathrm{E1^2M1'}$ in this case. This chapter is only concerned with single-centre HRS, for brevity of notation, molecule lettering, adopted in the previous chapter, will therefore be discarded. There are several features of this expression that are like the previously introduced matrix elements: two intermediary states r, s must be summed over; the pair of energy denominators that represent the relative energy of these two states with respect to that of the initial (and final) state. There are a couple of minor changes that are the result of considering a magnetic transition. The prefactor for this matrix element is ε_0^{-2}, unlike ε_0^{-3} seen in the three E1 interaction processes (each contributes a single power). The origin of this difference can be traced to the interaction Hamiltonian, the respective operator displayed in the heart of the Dirac bracket. By scrutinising the M1 operator, it can be readily seen that the power of vacuum permittivity will be restored at the next stage,

$$M_{FI}^{(\mathrm{E1^2M1'})} = -\frac{\mathrm{i}}{c}\left(\frac{\hbar c}{2\varepsilon_0 V}\right)^{3/2}\sqrt{k^2 k'}\sqrt{n(n-1)}\bar{b}_i' e_j e_k \sum_{r,s}\left\{\frac{m_i^{0r}\mu_j^{rs}\mu_k^{s0}}{\left[E_{r0}-2\hbar ck\right]\left[E_{s0}-\hbar ck\right]}\right.$$
$$+\frac{\mu_j^{0r}m_i^{rs}\mu_k^{s0}}{\left[E_{r0}+\hbar ck\right]\left[E_{s0}-\hbar ck\right]}$$
$$\left.+\frac{\mu_j^{0r}\mu_k^{rs}m_i^{s0}}{\left[E_{r0}+\hbar ck\right]\left[E_{s0}+2\hbar ck\right]}\right\}. \qquad (4.2.2)$$

The M1 operator differs from the E1 operator by a factor of c^{-1}, this will be held separate with foresight of the result. Equation (1.4.20) has also been deployed to simplify the denominators. We can now define the molecular response tensor for this mechanism,

$$\boldsymbol{J}'_{i(jk)} = \sum_{r,s}\left\{\frac{m_i^{0s}\mu_j^{sr}\mu_k^{r0}}{\left[E_{s0}-2\hbar ck\right]\left[E_{r0}-\hbar ck\right]}+\frac{\mu_j^{0s}m_i^{sr}\mu_k^{r0}}{\left[E_{s0}+\hbar ck\right]\left[E_{r0}-\hbar ck\right]}+\frac{\mu_j^{0s}\mu_k^{sr}m_i^{r0}}{\left[E_{s0}+\hbar ck\right]\left[E_{r0}+2\hbar ck\right]}\right\}. \qquad (4.2.3)$$

Like SHG, HRS engages a first-order hyperpolarisability tensor [110], this is the microscopic counterpart to a second-order susceptibility tensor, often considered for bulk media [133, 134]. The matrix element can now be cast as,

$$M_{FI}^{(\mathrm{E1^2M1'})} = -\frac{\mathrm{i}}{2c}\left(\frac{\hbar ck}{\varepsilon_0 V}\right)^{3/2}\sqrt{n(n-1)}\bar{b}_i' e_j e_k \boldsymbol{J}'_{i(jk)}\ , \qquad (4.2.4)$$

where the magnitude of the input beam wavevector is preferred, using equation (1.4.20). This expression has an identical structure to that seen in equation (1.4.21), with the anticipated additional c^{-1} prefactor. It can be seen that index symmetry has been chosen in this instance, where the specific index symmetric part of the tensor is defined by,

$$\boldsymbol{J}'_{i(jk)} = \frac{1}{2}\left(\boldsymbol{J}'_{ijk}+\boldsymbol{J}'_{ikj}\right). \qquad (4.2.5)$$

The index symmetry results in a rotational average of a more concise form. This is beneficial when regarding tensors with higher numbers of indices; or indeed, incoherent processes which require the rotational average to be applied to the rate (or radiant intensity) for a process. This is of course a product of two tensors and as such requires a rotational rank of the combined number of indices.

The hyperpolarisability is often simplified by considering the principal components that display a large magnitude shift in charge for a specific optical transition [135-138]. Push-pull chromophores consisting of aromatic structures are often discussed in connection with this [139-141]. In such systems, the excited static dipole moment associated with a molecule display a large optical nonlinearity, specifically an enhanced second harmonic response [142-150]. These methods have been critically analysed in recent years [151-155].

3.2B CASE *II*

This case is the contribution from one of the two annihilation events engaging the M1 operator, with the remaining annihilation event, as well as the creation event both engage the E1 operator. The Feynman diagrams displayed in Figure 4 accurately describe each of the time-orderings for this process, with the ensuing calculation of the matrix element very similar in form to case *I*. The resulting response tensor can be expressed as,

$$\boldsymbol{J}_{ijk} = \sum_{r,s}\left\{\frac{\mu_i^{0s} m_j^{sr} \mu_k^{r0}}{\left[E_{s0}-2\hbar ck\right]\left[E_{r0}-\hbar ck\right]} + \frac{m_j^{0s} \mu_i^{sr} \mu_k^{r0}}{\left[E_{s0}+\hbar ck\right]\left[E_{r0}-\hbar ck\right]} + \frac{m_j^{0s} \mu_k^{sr} \mu_i^{r0}}{\left[E_{s0}+\hbar ck\right]\left[E_{r0}+2\hbar ck\right]}\right.$$
$$\left. \frac{\mu_i^{0s} \mu_j^{sr} m_k^{r0}}{\left[E_{s0}-2\hbar ck\right]\left[E_{r0}-\hbar ck\right]} + \frac{\mu_j^{0s} \mu_i^{sr} m_k^{r0}}{\left[E_{s0}+\hbar ck\right]\left[E_{r0}-\hbar ck\right]} + \frac{\mu_j^{0s} m_k^{sr} \mu_i^{r0}}{\left[E_{s0}+\hbar ck\right]\left[E_{r0}+2\hbar ck\right]}\right\} . \tag{4.2.6}$$

The change seen in the matrix element is that arising from the change in field vectors,

$$M_{FI}^{(\mathrm{E1M1E1'})} = -\frac{\mathrm{i}}{2c}\left(\frac{\hbar ck}{\varepsilon_0 V}\right)^{3/2} \sqrt{n(n-1)}\,\vec{e}_i \vec{b}_j e_k \boldsymbol{J}_{ijk} \ . \tag{4.2.7}$$

This difference undermines the indistinguishability of the two annihilated photons. Each can be derived separately of course; however the same result can be achieved more simply by interchanging the indices j with k in equations (4.2.6) and (4.2.7) above.

3.2C CASE *III*

This mechanism involves an E2 operator at any one of the photon-molecule interactions. In order to do this, we must first obtain the appropriate operator,

$$Q_{il}\nabla_l d_i^{\perp} = \left(\pm \mathrm{i}k_l\right)\mathrm{i}\sum_{\mathbf{k},\eta}\sqrt{\frac{\varepsilon_0\hbar ck}{2V}}\left[\mathbf{e}_{\mathbf{k}}^{(\eta)}a_{\mathbf{k}}^{(\eta)}\mathrm{e}^{\mathrm{i}\mathbf{k}\cdot\mathbf{r}} - \overline{\mathbf{e}}_{\mathbf{k}}^{(\eta)}a_{\mathbf{k}}^{\dagger(\eta)}\mathrm{e}^{-\mathrm{i}\mathbf{k}\cdot\mathbf{r}}\right], \tag{4.2.8}$$

where the sign of this equation corresponds to the form of interaction it engages in. In this case, we will consider the E2 transition on the creation event, and as such the form with a negative sign will be taken. The response tensor can readily be obtained by replacing the appropriate E1 transition in equation (1.4.22) as follows,

$$\boldsymbol{K}'_{i(jk)l} = \sum_{r,s}\left\{\frac{Q_{il}^{0s}\mu_j^{sr}\mu_k^{r0}}{\left[E_{s0}-2\hbar ck\right]\left[E_{r0}-\hbar ck\right]} + \frac{\mu_j^{0s}Q_{il}^{sr}\mu_k^{r0}}{\left[E_{s0}+\hbar ck\right]\left[E_{r0}-\hbar ck\right]} + \frac{\mu_j^{0s}\mu_k^{sr}Q_{il}^{r0}}{\left[E_{s0}+\hbar ck\right]\left[E_{r0}+2\hbar ck\right]}\right\}. \tag{4.2.9}$$

The matrix element can also be cast by accommodating the additional prefactor as follow,

$$M_{FI}^{\left(\mathrm{E1^2E2'}\right)} = -\frac{\mathrm{i}\left(-\mathrm{i}k\right)}{2}\left(\frac{\hbar ck}{\varepsilon_0 V}\right)^{3/2}\sqrt{n\left(n-1\right)}\overline{e}_i' e_j e_k k_l' \boldsymbol{K}'_{i(jk)l}. \tag{4.2.10}$$

Again, with foresight of the result, this is segregated from the prefactors in the $\mathrm{E1}^3$ result.

3.2D CASE *IV*

In this case, we shall consider the mechanism where one of the two annihilation events engage the E2 operator. The additional annihilation event, along with the creation event will both engage the E1 operator. The familiar form of response tensor can be seen as follows,

$$\begin{aligned}\boldsymbol{K}_{i(jk)l} = \sum_{r,s}\Bigg\{&\frac{\mu_i^{0s}Q_{jl}^{sr}\mu_k^{r0}}{\left[E_{s0}-2\hbar ck\right]\left[E_{r0}-\hbar ck\right]} + \frac{Q_{jl}^{0s}\mu_i^{sr}\mu_k^{r0}}{\left[E_{s0}+\hbar ck\right]\left[E_{r0}-\hbar ck\right]} + \frac{Q_{jl}^{0s}\mu_k^{sr}\mu_i^{r0}}{\left[E_{s0}+\hbar ck\right]\left[E_{r0}+2\hbar ck\right]} \\ &\frac{\mu_i^{0s}\mu_j^{sr}Q_{kl}^{r0}}{\left[E_{s0}-2\hbar ck\right]\left[E_{r0}-\hbar ck\right]} + \frac{\mu_j^{0s}\mu_i^{sr}Q_{kl}^{r0}}{\left[E_{s0}+\hbar ck\right]\left[E_{r0}-\hbar ck\right]} + \frac{\mu_j^{0s}Q_{kl}^{sr}\mu_i^{r0}}{\left[E_{s0}+\hbar ck\right]\left[E_{r0}+2\hbar ck\right]}\Bigg\},\end{aligned} \tag{4.2.11}$$

which is found in an even more familiar matrix element,

$$M_{FI}^{(\mathrm{E1E2E1'})} = -\frac{\mathrm{i}(ik)}{2}\left(\frac{\hbar ck}{\varepsilon_0 V}\right)^{3/2}\sqrt{n(n-1)}\vec{e}_i' e_j e_k k_l \boldsymbol{K}_{i(jk)l} \ . \qquad (4.2.12)$$

You can see in this instance the indistinguishability of the two electric field vectors is not undermined by the invocation of an E2 transition.

3.2E SUMMARY OF CASES

Each of these cases represents one possible mechanism by which a second-harmonic emission can be generated. All of these mechanisms will therefore contribute to the radiant intensity of HRS. Care has been taken to retain the prefactors of SHG, which are hence treated as common factors to all of the matrix elements, equations (4.2.4), (4.2.7), (4.2.10) and (4.2.12). Now, equation (1.4.28) can be expanded to accommodate these additional modified matrix elements into the square modulus,

$$I' = \frac{g^{(2)}k^4\overline{I}_0^2}{2c\varepsilon_0^3\pi^2}\left|M_{FI}^{(\mathrm{E1^3})} + M_{FI}'^{(\mathrm{E1^2M1'})} + M_{FI}'^{(\mathrm{E1M1E1'})} + M_{FI}'^{(\mathrm{E1^2E2'})} + M_{FI}'^{(\mathrm{E1E2E1'})}\right|^2 \ . \qquad (4.2.13)$$

The relative strength in contribution of the additional matrix elements has already been noted. It is of interest to consider the series of matrix elements in occasions where additional insights can be delivered, such as systems in which the contribution from the first term is prohibited. If we now regard a centrosymmetric system in which $M_{FI}^{(\mathrm{E1^3})} \equiv 0$; hence, all five products involving the regarded matrix element will not be present. The resulting expansion will correspond to that of $n = 4$ in complement 2A, in which the four products allowed by the HRS mechanism and six the result of quantum interferences between pairs of matrix elements will all become lead contributors to the radiant intensity.

3.3 ROTATIONAL AVERAGE

So far, the system has been considered fixed in orientation with respect to the bulk. To consider a system in which the centres are free to tumble, we shall apply an isotropic average of the molecular response tensors, see complement 1D. HRS is an incoherent process and as such the rotational average will be made on the product of the matrix elements. It can be seen that there is a difference in the number of indices present in cases *I* and *II*, when compared with *III* and

IV. The result is different ranks to be deployed between the two pairs of cases and indeed the interference term requires a different rank again as follows,

$$\begin{aligned}\langle I' \rangle = \frac{g^{(2)} k^4 \bar{I}_0^2}{2c\varepsilon_0^3 \pi^2} \Bigg\{ & \frac{1}{c^2} \Big(\bar{b}_i' e_j e_k b_m' \bar{e}_n \bar{e}_o I^{(6)}_{ijkmno;\lambda\mu\nu\pi\rho\sigma} \boldsymbol{J}'_{\lambda(\mu\nu)} \bar{\boldsymbol{J}}'_{\rho(\sigma\tau)} \\ & + \bar{e}_i' b_j e_k e_m' \bar{b}_n \bar{e}_o I^{(6)}_{ijkmno;\lambda\mu\nu\pi\rho\sigma} \boldsymbol{J}_{\lambda\mu\nu} \bar{\boldsymbol{J}}_{\rho\sigma\tau} \\ & + 2\,\mathrm{Re}\Big[\bar{b}_i' e_j e_k e_m' \bar{b}_n \bar{e}_o I^{(6)}_{ijkmno;\lambda\mu\nu\pi\rho\sigma} \boldsymbol{J}'_{\lambda(\mu\nu)} \bar{\boldsymbol{J}}_{\rho\sigma\tau} \Big] \Big) \\ & + \frac{k}{c} 2\,\mathrm{Re}\Big[\mathrm{i} \Big(\bar{b}_i' e_j e_k e_m' \bar{e}_n \bar{e}_o k_p I^{(7)}_{ijkmnop;\lambda\mu\nu\pi\rho\sigma\tau} \boldsymbol{J}'_{\lambda(\mu\nu)} \bar{\boldsymbol{K}}_{\rho(\sigma\tau)\upsilon} \\ & \quad + \bar{e}_i' b_j e_k e_m' \bar{e}_n \bar{e}_o k_p I^{(7)}_{ijkmnop;\lambda\mu\nu\pi\rho\sigma\tau} \boldsymbol{J}_{\lambda\mu\nu} \bar{\boldsymbol{K}}_{\rho(\sigma\tau)\upsilon} \\ & \quad - \bar{b}_i' e_j e_k e_m' \bar{e}_n \bar{e}_o k_p' I^{(7)}_{ijkmnop;\lambda\mu\nu\pi\rho\sigma\tau} \boldsymbol{J}'_{\lambda(\mu\nu)} \bar{\boldsymbol{K}}'_{\rho(\sigma\tau)\upsilon} \\ & \quad - \bar{e}_i' b_j e_k e_m' \bar{e}_n \bar{e}_o k' I^{(7)}_{ijkmnop;\lambda\mu\nu\pi\rho\sigma\tau} \boldsymbol{J}_{\lambda\mu\nu} \bar{\boldsymbol{K}}'_{\rho(\sigma\tau)\upsilon} \Big) \Big] \\ & + k^2 \Big(2\,\mathrm{Re}\Big[\bar{e}_i' e_j e_k k_l' e_m' \bar{e}_n \bar{e}_o k_p I^{(8)}_{ijkmnopq;\lambda\mu\nu\pi\rho\sigma\tau\upsilon} \boldsymbol{K}'_{\lambda(\mu\nu)\pi} \bar{\boldsymbol{K}}_{\rho(\sigma\tau)\upsilon} \Big] \\ & \quad - \bar{e}_i' e_j e_k k_l e_m' \bar{e}_n \bar{e}_o k_p I^{(8)}_{ijkmnopq;\lambda\mu\nu\pi\rho\sigma\tau\upsilon} \boldsymbol{K}_{\lambda(\mu\nu)\pi} \bar{\boldsymbol{K}}_{\rho(\sigma\tau)\upsilon} \\ & \quad - \bar{e}_i' e_j e_k k_l' e_m' \bar{e}_n \bar{e}_o k_p' I^{(8)}_{ijkmnopq;\lambda\mu\nu\pi\rho\sigma\tau\upsilon} \boldsymbol{K}'_{\lambda(\mu\nu)\pi} \bar{\boldsymbol{K}}'_{\rho(\sigma\tau)\upsilon} \Big) \Bigg\} \,. \end{aligned} \tag{4.3.1}$$

Terms one, two, nine and ten correspond to the matrix element products with their own complex conjugates, cases *I*, *II*, *III* and *IV*, respectively. The first pair require a rotational average equivalent in rank to that of incoherent E1[3] scattering, indicated by the superscript attached to the isotropic tensor, $n = 6$. Any product containing an E2 transition increasing the rank by one, therefore the final pair engage the isotropic tensor of rank $n = 8$. Terms three and eight represent the quantum interference between cases of the same rank of isotropic average and as such engage an average of equivalent rank. It follows that the remaining four products (terms four through seven) each contain just one matrix element with one E2 transition and therefore engage an isotropic tensor of rank $n = 7$. The imaginary prefactor present in these terms contract with the imaginary component of the magnetic operator, $\mathbf{m}$, and as such all four terms have the potential to contribute to the harmonic emission.

3.3A EXAMPLE

Next, we shall evaluate the first term from equation (4.3.1),

$$\left\langle \left| M'^{\left(\mathrm{E1^2M1'}\right)}_{FI} \right|^2 \right\rangle = \bar{b}'_i e_j e_k b'_l \bar{e}_m \bar{e}_n I^{(6)}_{ijkmno;\lambda\mu\nu\pi\rho\sigma} \boldsymbol{J}'_{\lambda(\mu\nu)} \bar{\boldsymbol{J}}'_{o(\pi\rho)}, \tag{4.3.2}$$

at this point the c^{-2} included in the modified matrix element will be neglected, along with those from that form the common factors. Note that all the indices are often referred to as dummy indices, each letter can be adopted in each instance, so long as they are consistent throughout the calculation. The first stage in evaluating the above equation is to retrieve the appropriate (sixth) ranked isotropic average tensor, equation (1D.13). Earlier in this complement it was stated in equation (1D.2) that this can be decomposed into three tensors: a pair of rank 1 tensors evaluated in conjunction with a rank 2 square matrix, where the order is dependent on the number of indices to be permuted, 15 in this case. Each of these three components will be regarded separately.

We shall begin by finding the 15 linear combinations of field vectors,

$$\bar{b}'_i e_j e_k b'_l \bar{e}_m \bar{e}_n \begin{pmatrix} \delta_{ij}\delta_{kl}\delta_{mn} \\ \delta_{ij}\delta_{km}\delta_{ln} \\ \delta_{ij}\delta_{kn}\delta_{lm} \\ \delta_{ik}\delta_{jl}\delta_{mn} \\ \delta_{ik}\delta_{jm}\delta_{ln} \\ \delta_{ik}\delta_{jn}\delta_{lm} \\ \delta_{il}\delta_{jk}\delta_{mn} \\ \delta_{il}\delta_{jm}\delta_{kn} \\ \delta_{il}\delta_{jn}\delta_{km} \\ \delta_{im}\delta_{jk}\delta_{ln} \\ \delta_{im}\delta_{jl}\delta_{kn} \\ \delta_{im}\delta_{jn}\delta_{kl} \\ \delta_{in}\delta_{jk}\delta_{lm} \\ \delta_{in}\delta_{jl}\delta_{km} \\ \delta_{in}\delta_{jm}\delta_{kl} \end{pmatrix}^{\mathrm{T}} = \begin{pmatrix} \bar{b}'_i e_i e_k b'_k \bar{e}_m \bar{e}_m \\ \bar{b}'_i e_i e_k b'_l \bar{e}_k \bar{e}_l \\ \bar{b}'_i e_i e_k b'_l \bar{e}_l \bar{e}_k \\ \bar{b}'_i e_j e_i b'_j \bar{e}_m \bar{e}_m \\ \bar{b}'_i e_j e_i b'_l \bar{e}_j \bar{e}_l \\ \bar{b}'_i e_j e_i b'_l \bar{e}_l \bar{e}_j \\ \bar{b}'_i e_j e_j b'_i \bar{e}_m \bar{e}_m \\ \bar{b}'_i e_j e_k b'_i \bar{e}_j \bar{e}_k \\ \bar{b}'_i e_j e_k b'_i \bar{e}_k \bar{e}_j \\ \bar{b}'_i e_j e_j b'_l \bar{e}_i \bar{e}_l \\ \bar{b}'_i e_j e_k b'_j \bar{e}_i \bar{e}_k \\ \bar{b}'_i e_j e_k b'_k \bar{e}_i \bar{e}_j \\ \bar{b}'_i e_j e_j b'_l \bar{e}_l \bar{e}_i \\ \bar{b}'_i e_j e_k b'_j \bar{e}_k \bar{e}_i \\ \bar{b}'_i e_j e_k b'_k \bar{e}_j \bar{e}_i \end{pmatrix}^{\mathrm{T}} = \begin{pmatrix} (\bar{\mathbf{b}}'.\mathbf{e})(\mathbf{e}.\mathbf{b}')(\bar{\mathbf{e}}.\bar{\mathbf{e}}) \\ (\bar{\mathbf{b}}'.\mathbf{e})(\mathbf{e}.\bar{\mathbf{e}})(\mathbf{b}'.\bar{\mathbf{e}}) \\ (\bar{\mathbf{b}}'.\mathbf{e})(\mathbf{e}.\bar{\mathbf{e}})(\mathbf{b}'.\bar{\mathbf{e}}) \\ (\bar{\mathbf{b}}'.\mathbf{e})(\mathbf{e}.\mathbf{b}')(\bar{\mathbf{e}}.\bar{\mathbf{e}}) \\ (\bar{\mathbf{b}}'.\mathbf{e})(\mathbf{e}.\bar{\mathbf{e}})(\mathbf{b}'.\bar{\mathbf{e}}) \\ (\bar{\mathbf{b}}'.\mathbf{e})(\mathbf{e}.\bar{\mathbf{e}})(\mathbf{b}'.\bar{\mathbf{e}}) \\ (\bar{\mathbf{b}}'.\mathbf{b}')(\mathbf{e}.\mathbf{e})(\bar{\mathbf{e}}.\bar{\mathbf{e}}) \\ (\bar{\mathbf{b}}'.\mathbf{b}')(\mathbf{e}.\bar{\mathbf{e}})(\mathbf{e}.\bar{\mathbf{e}}) \\ (\bar{\mathbf{b}}'.\mathbf{b}')(\mathbf{e}.\bar{\mathbf{e}})(\mathbf{e}.\bar{\mathbf{e}}) \\ (\bar{\mathbf{b}}'.\bar{\mathbf{e}})(\mathbf{e}.\mathbf{e})(\mathbf{b}'.\bar{\mathbf{e}}) \\ (\bar{\mathbf{b}}'.\bar{\mathbf{e}})(\mathbf{e}.\mathbf{b}')(\mathbf{e}.\bar{\mathbf{e}}) \\ (\bar{\mathbf{b}}'.\bar{\mathbf{e}})(\mathbf{e}.\bar{\mathbf{e}})(\mathbf{e}.\mathbf{b}') \\ (\bar{\mathbf{b}}'.\bar{\mathbf{e}})(\mathbf{e}.\mathbf{e})(\mathbf{b}'.\bar{\mathbf{e}}) \\ (\bar{\mathbf{b}}'.\bar{\mathbf{e}})(\mathbf{e}.\mathbf{b}')(\mathbf{e}.\bar{\mathbf{e}}) \\ (\bar{\mathbf{b}}'.\bar{\mathbf{e}})(\mathbf{e}.\bar{\mathbf{e}})(\mathbf{e}.\mathbf{b}') \end{pmatrix}^{\mathrm{T}} . \tag{4.3.3}$$

Here, the dirac delta selects the appropriate pairings of field vectors, which is displayed on the far right of the above equation. Here, there are in fact only six out of the fifteen unique combinations of field vectors in this rotational average, to be identified at the next stage.

The other rank 1 tensor to be evaluated is the one that will be contracted with the molecular response tensor,

$$\begin{pmatrix} \delta_{\lambda\mu}\delta_{\nu o}\delta_{\pi\rho} \\ \delta_{\lambda\mu}\delta_{\nu\pi}\delta_{o\rho} \\ \delta_{\lambda\mu}\delta_{\nu\rho}\delta_{o\pi} \\ \delta_{\lambda\nu}\delta_{\mu o}\delta_{\pi\rho} \\ \delta_{\lambda\nu}\delta_{\mu\pi}\delta_{o\rho} \\ \delta_{\lambda\nu}\delta_{\mu\rho}\delta_{o\pi} \\ \delta_{\lambda o}\delta_{\mu\nu}\delta_{\pi\rho} \\ \delta_{\lambda o}\delta_{\mu\pi}\delta_{\nu\rho} \\ \delta_{\lambda o}\delta_{\mu\rho}\delta_{\nu\pi} \\ \delta_{\lambda\pi}\delta_{\mu\nu}\delta_{o\rho} \\ \delta_{\lambda\pi}\delta_{\mu o}\delta_{\nu\rho} \\ \delta_{\lambda\pi}\delta_{\mu\rho}\delta_{\nu o} \\ \delta_{\lambda\rho}\delta_{\mu\nu}\delta_{o\pi} \\ \delta_{\lambda\rho}\delta_{\mu o}\delta_{\nu\pi} \\ \delta_{\lambda\rho}\delta_{\mu\pi}\delta_{\nu o} \end{pmatrix} \boldsymbol{J}'_{\lambda(\mu\nu)}\bar{\boldsymbol{J}}'_{o(\pi\rho)} = \begin{pmatrix} \boldsymbol{J}'_{\lambda(\lambda\mu)}\bar{\boldsymbol{J}}'_{\mu(\nu\nu)} \\ \boldsymbol{J}'_{\lambda(\lambda\mu)}\bar{\boldsymbol{J}}'_{\nu(\nu\mu)} \\ \boldsymbol{J}'_{\lambda(\lambda\mu)}\bar{\boldsymbol{J}}'_{\nu(\nu\mu)} \\ \boldsymbol{J}'_{\lambda(\lambda\mu)}\bar{\boldsymbol{J}}'_{\mu(\nu\nu)} \\ \boldsymbol{J}'_{\lambda(\lambda\mu)}\bar{\boldsymbol{J}}'_{\nu(\nu\mu)} \\ \boldsymbol{J}'_{\lambda(\lambda\mu)}\bar{\boldsymbol{J}}'_{\nu(\nu\mu)} \\ \boldsymbol{J}'_{\lambda(\mu\mu)}\bar{\boldsymbol{J}}'_{\lambda(\nu\nu)} \\ \boldsymbol{J}'_{\lambda(\mu\nu)}\bar{\boldsymbol{J}}'_{\lambda(\mu\nu)} \\ \boldsymbol{J}'_{\lambda(\mu\nu)}\bar{\boldsymbol{J}}'_{\lambda(\mu\nu)} \\ \boldsymbol{J}'_{\lambda(\mu\mu)}\bar{\boldsymbol{J}}'_{\nu(\nu\lambda)} \\ \boldsymbol{J}'_{\lambda(\mu\nu)}\bar{\boldsymbol{J}}'_{\mu(\lambda\nu)} \\ \boldsymbol{J}'_{\lambda(\mu\nu)}\bar{\boldsymbol{J}}'_{\mu(\lambda\nu)} \\ \boldsymbol{J}'_{\lambda(\mu\mu)}\bar{\boldsymbol{J}}'_{\nu(\nu\lambda)} \\ \boldsymbol{J}'_{\lambda(\mu\nu)}\bar{\boldsymbol{J}}'_{\mu(\lambda\nu)} \\ \boldsymbol{J}'_{\lambda(\mu\nu)}\bar{\boldsymbol{J}}'_{\mu(\lambda\nu)} \end{pmatrix} . \tag{4.3.4}$$

Similarly to the result for equation (4.3.3), there are six unique arrangements of indices for the tensors. It is convenient to combine the respective rows and columns of the two rank 1 tensor results above. In turn the square matrix, which applies the appropriate weightings to each of the terms can also have the appropriate rows and columns combined to display the result in the following form,

$$\left\langle \left| M'^{(\mathrm{E1^2M1'})}_{FI} \right|^2 \right\rangle = \frac{1}{210} \begin{pmatrix} \left(\bar{\mathbf{b}}'.\mathbf{e}\right)\left(\mathbf{e}.\mathbf{b}'\right)\left(\bar{\mathbf{e}}.\bar{\mathbf{e}}\right) \\ \left(\mathbf{e}.\bar{\mathbf{e}}\right)\left|\left(\mathbf{b}'.\bar{\mathbf{e}}\right)\right|^2 \\ \left(\bar{\mathbf{b}}'.\mathbf{b}'\right)\left|\left(\mathbf{e}.\mathbf{e}\right)\right|^2 \\ \left(\bar{\mathbf{b}}'.\mathbf{b}'\right)\left(\mathbf{e}.\bar{\mathbf{e}}\right)^2 \\ \left(\bar{\mathbf{b}}'.\bar{\mathbf{e}}\right)\left(\mathbf{e}.\mathbf{e}\right)\left(\mathbf{b}'.\bar{\mathbf{e}}\right) \\ \left(\mathbf{e}.\bar{\mathbf{e}}\right)\left|\left(\mathbf{e}.\mathbf{b}'\right)\right|^2 \end{pmatrix}^{\mathrm{T}} \begin{pmatrix} 22 & -12 & -10 & 8 & 8 & -12 \\ -12 & 32 & 8 & -12 & -12 & 4 \\ -10 & 8 & 16 & -10 & -10 & 8 \\ 8 & -12 & -10 & 22 & 8 & -12 \\ 8 & -12 & -10 & 8 & 22 & -12 \\ -12 & 4 & 8 & -12 & -12 & 32 \end{pmatrix} \begin{pmatrix} \boldsymbol{J}'_{\lambda(\lambda\mu)}\bar{\boldsymbol{J}}'_{\mu(\nu\nu)} \\ \boldsymbol{J}'_{\lambda(\lambda\mu)}\bar{\boldsymbol{J}}'_{\nu(\nu\mu)} \\ \boldsymbol{J}'_{\lambda(\mu\mu)}\bar{\boldsymbol{J}}'_{\lambda(\nu\nu)} \\ \boldsymbol{J}'_{\lambda(\mu\nu)}\bar{\boldsymbol{J}}'_{\lambda(\mu\nu)} \\ \boldsymbol{J}'_{\lambda(\mu\mu)}\bar{\boldsymbol{J}}'_{\nu(\nu\lambda)} \\ \boldsymbol{J}'_{\lambda(\mu\nu)}\bar{\boldsymbol{J}}'_{\mu(\lambda\nu)} \end{pmatrix} . \tag{4.3.5}$$

Here is the rotational average of the first product of matrix elements in equation (4.3.1). Each of the parameters are determinable for a given specimen based on the laser input and polarisation. The field vector products in complement 1E can be used to evaluate this result for experimental setups displayed in Figure 19. In principle, each of the material parameters are unique and also determinable, for a set of specific conditions. This should be achievable by computational means, but under experimental conditions, it would likely be too sensitive to changes in environmental conditions. Having said that, obtaining a collective response does seem plausible, delivering a fingerprint for the specimen.

3.4 EXPERIMENTAL APPLICATION

By considering the four experimental setups displayed in Figure 19, it is possible to obtain a DR for the perpendicular and parallel light polarizations. As well as a comparable measurement for circular polarizations, known as the reversal ratio (RR) [156]. This relates the relative intensities of emission between the reversed and preserved circularities: $(c \to c^*)/(c \to c)$. The tables displayed in complement 1E are where c stands for L and the star denotes a reversal in helicity. Analogous results can be obtained for where c represents R.

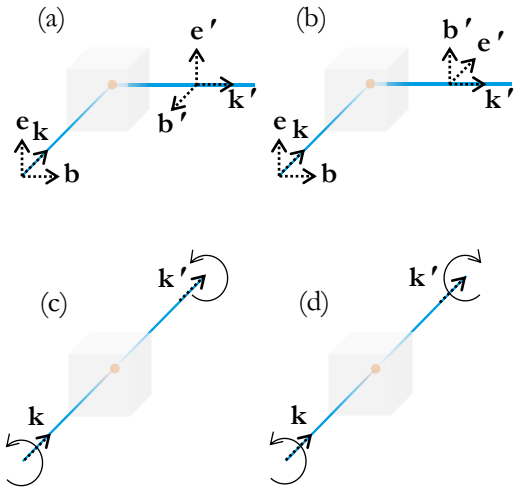

Figure 19: Experimental set-up: (a) parallel plane-polarised light is detected at right angles to the input laser; (b) perpendicularly plane-polarised light detected also detected at right angles; (c) forward scattered circular-polarised light with preserved circularity; (d) forward scattered circular-polarised light of reversed circularity.

3.4A EXAMPLE (CONTINUED)

Returning to our example rotational average, we will now display numerical results for the four regimes displayed in Figure 19. Beginning with (a) plane-polarised light detected at right angles to the input laser with parallel field vectors,

$$\begin{pmatrix} 0 & 0 & 1 & 1 & 0 & 0 \end{pmatrix}, \tag{4.4.1}$$

see Figure 18(a) for a schematic depiction of this. Contracting all the tensors in equation (4.3.5), we obtain the following weightings for each of the tensors,

$$\frac{-2\boldsymbol{J}_{\lambda(\lambda\nu)}\bar{\boldsymbol{J}}'_{\mu(\nu\nu)} - 4\boldsymbol{J}_{\lambda(\lambda\mu)}\bar{\boldsymbol{J}}'_{\nu(\nu\mu)} + 6\boldsymbol{J}_{\lambda(\mu\mu)}\bar{\boldsymbol{J}}'_{\lambda(\nu\nu)} + 12\boldsymbol{J}_{\lambda(\mu\nu)}\bar{\boldsymbol{J}}'_{\lambda(\mu\nu)} - 2\boldsymbol{J}_{\lambda(\mu\mu)}\bar{\boldsymbol{J}}'_{\nu(\nu\lambda)} - 4\boldsymbol{J}_{\lambda(\mu\nu)}\bar{\boldsymbol{J}}'_{\mu(\lambda\nu)}}{210}. \tag{4.4.2}$$

Next, we shall consider (b), where the emergent field vectors are perpendicular to that of the input laser,

$$\begin{pmatrix} 1 & 1 & 1 & 1 & 1 & 1 \end{pmatrix}. \tag{4.4.3}$$

The subsequent tensor weightings in this setup are,

$$\frac{4\boldsymbol{J}_{\lambda(\lambda\nu)}\bar{\boldsymbol{J}}'_{\mu(\nu\nu)} + 8\boldsymbol{J}_{\lambda(\lambda\mu)}\bar{\boldsymbol{J}}'_{\nu(\nu\mu)} + 2\boldsymbol{J}_{\lambda(\mu\mu)}\bar{\boldsymbol{J}}'_{\lambda(\nu\nu)} + 4\boldsymbol{J}_{\lambda(\mu\nu)}\bar{\boldsymbol{J}}'_{\lambda(\mu\nu)} + 4\boldsymbol{J}_{\lambda(\mu\mu)}\bar{\boldsymbol{J}}'_{\nu(\nu\lambda)} + 8\boldsymbol{J}_{\lambda(\mu\nu)}\bar{\boldsymbol{J}}'_{\mu(\lambda\nu)}}{210}. \tag{4.4.4}$$

The next pair of setups are for forward scattered circularly-polarised light and in the case of (c) preserved circularity,

$$\begin{pmatrix} 0 & 1 & 0 & 1 & 0 & 0 \end{pmatrix}. \tag{4.4.5}$$

The resulting weightings of the molecular response tensors are as follows,

$$\frac{-4\boldsymbol{J}_{\lambda(\lambda\nu)}\bar{\boldsymbol{J}}'_{\mu(\nu\nu)} + 20\boldsymbol{J}_{\lambda(\lambda\mu)}\bar{\boldsymbol{J}}'_{\nu(\nu\mu)} - 2\boldsymbol{J}_{\lambda(\mu\mu)}\bar{\boldsymbol{J}}'_{\lambda(\nu\nu)} + 10\boldsymbol{J}_{\lambda(\mu\nu)}\bar{\boldsymbol{J}}'_{\lambda(\mu\nu)} - 4\boldsymbol{J}_{\lambda(\mu\mu)}\bar{\boldsymbol{J}}'_{\nu(\nu\lambda)} - 8\boldsymbol{J}_{\lambda(\mu\nu)}\bar{\boldsymbol{J}}'_{\mu(\lambda\nu)}}{210}. \tag{4.4.6}$$

The final setup (d) is where the circularity is reversed,

$$\begin{pmatrix} 0 & 0 & 0 & 1 & 0 & 1 \end{pmatrix}. \tag{4.4.7}$$

The final result for this rotational average and the fourth and final contraction delivers the tensor weightings,

$$\frac{-4\boldsymbol{J}_{\lambda(\lambda\nu)}\bar{\boldsymbol{J}}'_{\mu(\nu\nu)} - 8\boldsymbol{J}_{\lambda(\lambda\mu)}\bar{\boldsymbol{J}}'_{\nu(\nu\mu)} - 2\boldsymbol{J}_{\lambda(\mu\mu)}\bar{\boldsymbol{J}}'_{\lambda(\nu\nu)} + 10\boldsymbol{J}_{\lambda(\mu\nu)}\bar{\boldsymbol{J}}'_{\lambda(\mu\nu)} - 4\boldsymbol{J}_{\lambda(\mu\mu)}\bar{\boldsymbol{J}}'_{\nu(\nu\lambda)} + 20\boldsymbol{J}_{\lambda(\mu\nu)}\bar{\boldsymbol{J}}'_{\mu(\lambda\nu)}}{210}. \tag{4.4.8}$$

All of these weightings are displayed in complement 3A, alongside a full set of results for all of the product pairings under each setup. It will be of little surprise that the averages which require the evaluation of much higher order tensor cannot be expressed quite so succinctly, hence a tabulated format was selected. These higher ranked averages are intricate to carry out and as such are seldom deployed [102, 157, 158].

3.5 SUMMARISED RESULTS

Continuing the directive towards experimental applications, we shall now entertain approximations that can still indicate the relative magnitudes of each term contributing to observations of HRS. We shall achieve this by suggesting that all tensors with identical matrix element product pairings, irrespective of the indices, will provide a similar contribution to the overall intensity of the process. At the end of each set of results there is an additional row which corresponds to the same tensor product but discards any indices attached to it. The entries in that row represent the summed contribution for all the arrangements of indices for that product pairing. This is a shorthand notation for a representative inner tensor product of the two respective tensors. These results are summarised in Table 13**Error! Reference source not found.** below.

Table 13: Summary of the results from Table 14, for each of the experimental setups in Figure 19(a) – (d).

Pre-factor	Tensor product	(a)	(b)	(c)	(d)
1/105	$\boldsymbol{J}'\bar{\boldsymbol{J}}'$	-2	15	6	6
1/105	$\boldsymbol{J}'\bar{\boldsymbol{J}}$	0	0	-12	12
1/105	$\boldsymbol{J}\bar{\boldsymbol{J}}$	3	1	6	6
1/105	$\boldsymbol{K}'\bar{\boldsymbol{J}}'$	0	0	6	-28
1/105	$\boldsymbol{K}\bar{\boldsymbol{J}}'$	3	-1	6	0
1/105	$\boldsymbol{K}'\bar{\boldsymbol{J}}$	-3	1	-6	-44
1/105	$\boldsymbol{K}\bar{\boldsymbol{J}}$	0	0	6	0
1/315	$\boldsymbol{K}'\bar{\boldsymbol{K}}'$	5	1	2	2
1/315	$\boldsymbol{K}'\bar{\boldsymbol{K}}$	0	0	4	4
1/315	$\boldsymbol{K}\bar{\boldsymbol{K}}$	5	3	2	2

From this table, it can be seen that not all of the tensor inner products contribute to the radiant intensity of all polarisation setups. For example, under the plane polarised there are a handful of tensor inner products that do not contribute to the intensity of either sought polarisation output. In the case of the circular polarisations, a couple of instances contribute to only one of the output helicities: the preserved circularity and not the reversed circularity.

Better still, we can transform this back into expressions, which are of a more familiar form. By incorporating the relative magnitudes of the transition moments, we recall that the regarded transition moments can be expected to be weaker by a factor in the order of the fine structure constant, α. This is compared to the E1 moment of the same transition, where all the transitions would be allowed. Now, if we include this assumption into a constant containing the common factors for all the mechanisms, we have,

$$C_0 = \frac{\alpha^2 g^{(2)} k^4 \bar{I}_0^2}{2c\varepsilon_0^3 \pi^2} \ . \tag{4.5.1}$$

Introducing further constants $C_1 = c^{-2}$, $C_2 = ikc^{-1}$, $C_3 = k^2$ we can produce the following intensities of radiant emission in given directions:

(a) Parallel plane-polarized light detected orthogonal to the input laser:

$$I'^{(\parallel\rightarrow\parallel)} = C_0\left[3C_1\left\{3\boldsymbol{J}\bar{\boldsymbol{J}} - 2\boldsymbol{J}'\bar{\boldsymbol{J}}'\right\} + 9C_2\left\{\boldsymbol{K}\bar{\boldsymbol{J}}' - \boldsymbol{K}'\bar{\boldsymbol{J}}\right\} + 5C_3\left\{\boldsymbol{K}\bar{\boldsymbol{K}} + \boldsymbol{K}'\bar{\boldsymbol{K}}'\right\}\right]. \qquad (4.5.2)$$

(b) Perpendicular plane-polarized light detected orthogonal to the input laser:

$$I'^{(\parallel\rightarrow\perp)} = C_0\left[3C_1\left\{15\boldsymbol{J}'\bar{\boldsymbol{J}}' + \boldsymbol{J}\bar{\boldsymbol{J}}\right\} + 3C_2\left\{\boldsymbol{K}'\bar{\boldsymbol{J}} - \boldsymbol{K}\bar{\boldsymbol{J}}'\right\} + C_3\left\{3\boldsymbol{K}\bar{\boldsymbol{K}} + \boldsymbol{K}'\bar{\boldsymbol{K}}'\right\}\right]. \qquad (4.5.3)$$

It can be seen that obtaining the DR from the preceding two equations (4.5.2) and (4.5.3), the prefactor C_0 will explicitly cancel.

(c) Forward scattered circular-polarized light with preserved left circularity:

$$\begin{aligned} I'^{(\mathrm{L}\rightarrow\mathrm{L})} = 2C_0\Big[&9C_1\left\{\boldsymbol{J}'\bar{\boldsymbol{J}}' - 2\boldsymbol{J}'\bar{\boldsymbol{J}} + \boldsymbol{J}\bar{\boldsymbol{J}}\right\} + 9C_2\left\{\boldsymbol{K}\bar{\boldsymbol{J}}' + \boldsymbol{K}\bar{\boldsymbol{J}} + \boldsymbol{K}'\bar{\boldsymbol{J}}' - \boldsymbol{K}'\bar{\boldsymbol{J}}\right\} \\ &+C_3\left\{\boldsymbol{K}\bar{\boldsymbol{K}} + 2\boldsymbol{K}'\bar{\boldsymbol{K}} + \boldsymbol{K}'\bar{\boldsymbol{K}}'\right\}\Big]. \end{aligned} \qquad (4.5.4)$$

(d) Forward scattered circular-polarized light with reversed (left to right) circularity:

$$\begin{aligned} I'^{(\mathrm{L}\rightarrow\mathrm{R})} = 2C_0\Big[&9C_1\left\{\boldsymbol{J}'\bar{\boldsymbol{J}}' + 2\boldsymbol{J}'\bar{\boldsymbol{J}} + \boldsymbol{J}\bar{\boldsymbol{J}}\right\} - 6C_2\left\{7\boldsymbol{K}'\bar{\boldsymbol{J}}' + 11\boldsymbol{K}'\bar{\boldsymbol{J}}\right\} \\ &+C_3\left\{\boldsymbol{K}\bar{\boldsymbol{K}} + 2\boldsymbol{K}'\bar{\boldsymbol{K}} + \boldsymbol{K}'\bar{\boldsymbol{K}}'\right\}\Big]. \end{aligned} \qquad (4.5.5)$$

Similar to the DR, the sought RR delivered from equations (4.5.4) and (4.5.5), results in a cancellation of the prefactor, C_0. Inspecting the above equations, it can be seen that in a case where the molecular response tensors resulting from an E2 transitions dominate over those of M1 transitions, the reversal ratio delivers a value of precisely 1. This corresponds to a complete reversal of circularity in the forward second-harmonic emission. The corresponding terms in each equation (term 3) also display the highest dependence on k and as such will be most noticeable at short wavelengths.

3.6 DISCUSSION

All four of the cases considered in this chapter should contribute to all second-harmonic signals where HRS is permitted. Moreover, by deploying DR and RR techniques, it is anticipated that a unique fingerprint of all response action for a molecule would enable the characterisation of that molecule. The signal strengths will of course be lower than that of second harmonic generation engaging in a series of three E1 transitions. It is anticipated that the mechanisms considered here will display a comparative reduction by α^2, this equates to a reduction in the region of 10^{-4} to 10^{-5} smaller than the signals from the more familiar E1 transitions.

These signals can be bolstered or be made more dominant by deploying reasonable experimental conditions. The particular application to centrosymmetric systems has been suggested, where the $E1^3$ contribution will not be present and as such the mechanisms derived in this chapter will be the leading contributors. Explicitly, the inclusion of either an E2 or M1 transition subverts the standard selection rules [159]. It is worthy of note that a judiciously selected input beam, in which the pair of photons concurrently encountering the centre are endowed with a combined energy approaching that of a real electronic excited state, such that resonance conditions are met, the $\boldsymbol{J}$ and $\boldsymbol{K}$ tensor components will be magnified to a comparable level of the $\boldsymbol{\beta}$ tensor [160]. In a setup exploiting either (or both) techniques, HRS should be a measurable optical property of every material. Incoherent second harmonic generation is therefore a unique technical application in the optical characterization of minerals [161], and recently has been exploited in the analysis of liquid suspensions – in particular with regard to nanoparticles and nanorods [162, 163].

COMPLEMENT 3A: RESULTS TABLE FOR THE ROTATIONAL AVERAGES

The results displayed in Table 14, supplement those that appear in the chapter. Here the complete results for all the rotational averages, for each of the ten matrix element products, are laid out. The four right-most column headings correspond to the experimental setups that appear in Figure 19: (a) parallel plane-polarized light detected orthogonal to the input laser; (b) perpendicular plane-polarized light detected orthogonal to the input laser; (c) forward scattered circular-polarized light of preserved left circularity; (d) forward scattered circular-polarized light of reversed (left to right) circularity. The table is partitioned for each of the ten products, with the first line for each block displaying the relative weighting arising from the rotational averaging and the last row is a sum of all comparable tensor products. A special thank you should be made to Jack S. Ford for evaluating the eighth rank isotropic averages required for the matrix element products eight through ten in equation (3.2.13).

Table 14: Complete results for each of the experimental setups in Figure 2(a) – (d).

Tensor product	(a)	(b)	(c)	(d)
1/210				
$\boldsymbol{J}'_{\lambda(\lambda\mu)}\overline{\boldsymbol{J}}'_{\mu(\nu\nu)}$	-2	4	-4	-4
$\boldsymbol{J}'_{\lambda(\lambda\mu)}\overline{\boldsymbol{J}}'_{\nu(\nu\mu)}$	-4	8	20	-8
$\boldsymbol{J}'_{\lambda(\mu\mu)}\overline{\boldsymbol{J}}'_{\lambda(\nu\nu)}$	6	2	-2	-2
$\boldsymbol{J}'_{\lambda(\mu\nu)}\overline{\boldsymbol{J}}'_{\lambda(\mu\nu)}$	12	4	10	10
$\boldsymbol{J}'_{\lambda(\mu\mu)}\overline{\boldsymbol{J}}'_{\nu(\nu\lambda)}$	-2	4	-4	-4
$\boldsymbol{J}'_{\lambda(\mu\nu)}\overline{\boldsymbol{J}}'_{\mu(\lambda\nu)}$	-4	8	-8	20
$\boldsymbol{J}'\overline{\boldsymbol{J}}'$	-4	30	12	12
1/105				
$\boldsymbol{J}'_{\lambda(\lambda\mu)}\overline{\boldsymbol{J}}_{\mu\nu\nu}$	0	0	4	-4
$\boldsymbol{J}'_{\lambda(\lambda\mu)}\overline{\boldsymbol{J}}_{\nu\mu\nu}$	0	0	-10	-4
$\boldsymbol{J}'_{\lambda(\lambda\mu)}\overline{\boldsymbol{J}}_{\nu\nu\mu}$	0	0	-10	-4
$\boldsymbol{J}'_{\lambda(\mu\mu)}\overline{\boldsymbol{J}}_{\lambda\nu\nu}$	0	0	2	-2
$\boldsymbol{J}'_{\lambda(\mu\nu)}\overline{\boldsymbol{J}}_{\lambda\mu\nu}$	0	0	-10	10
$\boldsymbol{J}'_{\lambda(\mu\mu)}\overline{\boldsymbol{J}}_{\nu\lambda\nu}$	0	0	2	-2
$\boldsymbol{J}'_{\lambda(\mu\nu)}\overline{\boldsymbol{J}}_{\mu\lambda\nu}$	0	0	4	10
$\boldsymbol{J}'_{\lambda(\mu\mu)}\overline{\boldsymbol{J}}_{\nu\nu\lambda}$	0	0	2	-2
$\boldsymbol{J}'_{\lambda(\mu\nu)}\overline{\boldsymbol{J}}_{\mu\nu\lambda}$	0	0	4	10
$\boldsymbol{J}'\overline{\boldsymbol{J}}$	0	0	-12	12
1/210				
$\boldsymbol{J}_{\lambda\lambda\mu}\overline{\boldsymbol{J}}_{\mu\nu\nu}$	-1	2	-2	-2
$\boldsymbol{J}_{\lambda\lambda\mu}\overline{\boldsymbol{J}}_{\nu\mu\nu}$	-1	2	5	-2
$\boldsymbol{J}_{\lambda\lambda\mu}\overline{\boldsymbol{J}}_{\nu\nu\mu}$	6	-5	5	-2
$\boldsymbol{J}_{\lambda\mu\lambda}\overline{\boldsymbol{J}}_{\mu\nu\nu}$	-1	2	-2	-2
$\boldsymbol{J}_{\lambda\mu\lambda}\overline{\boldsymbol{J}}_{\nu\mu\nu}$	-1	-5	5	-2
$\boldsymbol{J}_{\lambda\mu\lambda}\overline{\boldsymbol{J}}_{\nu\nu\mu}$	-1	2	5	-2
$\boldsymbol{J}_{\lambda\mu\mu}\overline{\boldsymbol{J}}_{\lambda\nu\nu}$	-1	-5	-2	-2
$\boldsymbol{J}_{\lambda\mu\nu}\overline{\boldsymbol{J}}_{\lambda\mu\nu}$	6	16	5	5
$\boldsymbol{J}_{\lambda\mu\nu}\overline{\boldsymbol{J}}_{\lambda\nu\mu}$	-1	-5	5	5
$\boldsymbol{J}_{\lambda\mu\nu}\overline{\boldsymbol{J}}_{\nu\lambda\mu}$	-1	2	-2	-2
$\boldsymbol{J}_{\lambda\mu\mu}\overline{\boldsymbol{J}}_{\mu\lambda\nu}$	6	-5	-2	5
$\boldsymbol{J}_{\lambda\mu\nu}\overline{\boldsymbol{J}}_{\nu\lambda\mu}$	-1	2	-2	5
$\boldsymbol{J}_{\lambda\mu\mu}\overline{\boldsymbol{J}}_{\nu\nu\lambda}$	-1	2	-2	-2
$\boldsymbol{J}_{\lambda\mu\nu}\overline{\boldsymbol{J}}_{\mu\nu\lambda}$	-1	2	-2	5
$\boldsymbol{J}_{\lambda\mu\nu}\overline{\boldsymbol{J}}_{\nu\mu\lambda}$	-1	-5	-2	5
$\boldsymbol{J}\overline{\boldsymbol{J}}$	6	2	12	12
1/420				
$\boldsymbol{K}'_{\lambda(\mu o)\nu}\overline{\boldsymbol{J}}'_{o(\pi\pi)}$	0	0	-4	0
$\boldsymbol{K}'_{\lambda(\mu o)\nu}\overline{\boldsymbol{J}}'_{\pi(o\pi)}$	0	0	20	0
$\boldsymbol{K}'_{\lambda(oo)\mu}\overline{\boldsymbol{J}}'_{\nu(\pi\pi)}$	0	0	2	0
$\boldsymbol{K}'_{\lambda(o\pi)\mu}\overline{\boldsymbol{J}}'_{\nu(o\pi)}$	0	0	-10	0
$\boldsymbol{K}'_{o(\lambda o)\mu}\overline{\boldsymbol{J}}'_{\pi(\nu\pi)}$	0	0	20	-16

$K'_{o(\lambda\pi)\mu}\,\bar{J}'_{o(\nu\pi)}$	0	0	20	-16
$K'_{o(\lambda\pi)\mu}\,\bar{J}'_{\pi(\nu o)}$	0	0	-8	-16
$K'_{o(o\pi)\lambda}\,\bar{J}'_{\mu(\nu\pi)}$	0	0	-20	-8
$K'_{o(\pi\pi)\lambda}\,\bar{J}'_{\mu(\nu o)}$	0	0	4	-4
$K'_{o(\lambda o)\mu}\,\bar{J}'_{\nu(\pi\pi)}$	0	0	0	-4
$K'_{o(\lambda\pi)\mu}\,\bar{J}'_{\nu(o\pi)}$	0	0	0	-8
$K'_{o(\lambda o)\pi}\,\bar{J}'_{\mu(\nu\pi)}$	0	0	0	-8
$K'_{o(\lambda\mu)o}\,\bar{J}'_{\mu(\nu\pi)}$	0	0	0	-8
$K'_{o(\lambda\pi)\pi}\,\bar{J}'_{\mu(\nu o)}$	0	0	0	-8
$K'_{o(\lambda o)\pi}\,\bar{J}'_{\pi(\mu\nu)}$	0	0	0	-4
$K'_{o(\lambda\pi)o}\,\bar{J}'_{\pi(\mu\nu)}$	0	0	0	-4
$K'_{o(\lambda\pi)\pi}\,\bar{J}'_{o(\mu\nu)}$	0	0	0	-4
$K'_{o(o\pi)\lambda}\,\bar{J}'_{\pi(\mu\nu)}$	0	0	0	-5
$K'_{o(\pi\pi)\lambda}\,\bar{J}'_{o(\mu\nu)}$	0	0	0	1
$K'\bar{J}'$	0	0	24	-112
1/420				
$K_{\lambda(oo)\mu}\,\bar{J}'_{\pi(\nu\pi)}$	4	0	0	0
$K_{\lambda(o\pi)\mu}\,\bar{J}'_{o(\nu\pi)}$	8	0	0	0
$K_{o(\lambda o)\mu}\,\bar{J}'_{\pi(\nu\pi)}$	8	-3	20	0
$K_{o(\lambda\pi)\mu}\,\bar{J}'_{o(\nu\pi)}$	8	18	20	0
$K_{o(\lambda\pi)\mu}\,\bar{J}'_{\pi(\nu o)}$	8	-3	-8	0
$K_{o(o\pi)\lambda}\,\bar{J}'_{\mu(\nu\pi)}$	-8	0	-20	0
$K_{o(\pi\pi)\lambda}\,\bar{J}'_{\mu(\nu o)}$	-4	0	4	0
$K_{o(o\pi)\lambda}\,\bar{J}'_{\pi(\mu\nu)}$	-8	2	0	0
$K_{o(\pi\pi)\lambda}\,\bar{J}'_{o(\mu\nu)}$	-4	-6	0	0
$K_{\lambda(\mu o)o}\,\bar{J}'_{\pi(\nu\pi)}$	0	2	0	0
	0	2	0	0
$K_{\lambda(\mu o)\pi}\,\bar{J}'_{\pi(\nu o)}$	0	-12	0	0
$K_{\lambda(oo)\pi}\,\bar{J}'_{\pi(\mu\nu)}$	0	-6	0	0
$K_{\lambda(o\pi)o}\,\bar{J}'_{\pi(\mu\nu)}$	0	2	0	0
$K_{o(\lambda o)\pi}\,\bar{J}'_{\mu(\nu\pi)}$	0	-1	0	0
$K_{o(\lambda\mu)o}\,\bar{J}'_{\mu(\nu\pi)}$	0	6	0	0
$K_{o(\lambda\pi)\pi}\,\bar{J}'_{\mu(\nu o)}$	0	-1	0	0
$K_{o(o\pi)\pi}\,\bar{J}'_{\lambda(\mu\nu)}$	0	2	0	0
$K_{o(\pi\pi)o}\,\bar{J}'_{\lambda(\mu\nu)}$	0	-6	0	0
$K_{\lambda(\mu o)\nu}\,\bar{J}'_{o(\pi\pi)}$	0	0	-4	0
$K_{\lambda(\mu o)\nu}\,\bar{J}'_{\pi(o\pi)}$	0	0	20	0
$K_{\lambda(oo)\mu}\,\bar{J}'_{\nu(\pi\pi)}$	0	0	2	0
$K_{\lambda(o\pi)\mu}\,\bar{J}'_{\nu(o\pi)}$	0	0	-10	0
$K\bar{J}'$	12	-4	24	0
1/420				
$K'_{\lambda(oo)\mu}\,\bar{J}_{\pi\pi\nu}$	-4	0	0	-6
$K'_{\lambda(o\pi)\mu}\,\bar{J}_{o\pi\nu}$	-8	0	0	2
$K'_{o(\lambda o)\mu}\,\bar{J}_{\pi\pi\nu}$	-8	2	-10	-10
$K'_{o(\lambda\pi)\mu}\,\bar{J}_{o\pi\nu}$	-8	-12	-10	-3
$K'_{o(\lambda\pi)\mu}\,\bar{J}_{\pi o\nu}$	-8	2	4	-3
$K'_{o(o\pi)\lambda}\,\bar{J}_{\mu\pi\nu}$	8	0	10	-8
$K'_{o(\pi\pi)\lambda}\,\bar{J}_{\mu o\nu}$	4	0	-2	-4
$K'_{o(o\pi)\lambda}\,\bar{J}_{\pi\mu\nu}$	8	-2	0	-5
$K'_{o(\pi\pi)\lambda}\,\bar{J}_{o\mu\nu}$	4	6	0	1
$K'_{\lambda(\mu o)o}\,\bar{J}_{\pi\pi\nu}$	0	-2	0	-6
$K'_{\lambda(\mu o)\pi}\,\bar{J}_{o\pi\nu}$	0	-2	0	1
$K'_{\lambda(\mu o)\pi}\,\bar{J}_{\pi o\nu}$	0	12	0	1
$K'_{\lambda(oo)\pi}\,\bar{J}_{\pi\mu\nu}$	0	6	0	0
$K'_{\lambda(o\pi)o}\,\bar{J}_{\pi\mu\nu}$	0	-2	0	0
$K'_{\lambda(o\pi)\pi}\,\bar{J}_{\mu\pi\nu}$	0	2	0	-6
$K'_{o(\lambda\pi)o}\,\bar{J}_{\mu\pi\nu}$	0	-12	0	1
$K'_{o(\lambda\pi)\pi}\,\bar{J}_{\mu o\nu}$	0	2	0	1
$K'_{o(o\pi)\pi}\,\bar{J}_{\lambda\mu\nu}$	0	-2	0	0
$K'_{o(\pi\pi)o}\,\bar{J}_{\lambda\mu\nu}$	0	6	0	0
$K'_{\lambda(\mu o)\nu}\,\bar{J}_{o\pi\pi}$	0	0	4	-6
$K'_{\lambda(\mu o)\nu}\,\bar{J}_{\pi o\pi}$	0	0	-10	1
$K'_{\lambda(\mu o)\nu}\,\bar{J}_{\pi\pi o}$	0	0	-10	1
$K'_{\lambda(oo)\mu}\,\bar{J}_{\nu\pi\pi}$	0	0	-2	0
$K'_{\lambda(o\pi)\mu}\,\bar{J}_{\nu o\pi}$	0	0	10	0
$K'_{o(\lambda o)\mu}\,\bar{J}_{\pi\nu\pi}$	0	0	-10	-4
$K'_{o(\lambda\pi)\mu}\,\bar{J}_{o\nu\pi}$	0	0	-10	-4
$K'_{o(\lambda\pi)\mu}\,\bar{J}_{\pi\nu o}$	0	0	4	-4
$K'_{o(o\pi)\lambda}\,\bar{J}_{\mu\nu\pi}$	0	0	10	-5
$K'_{o(\pi\pi)\lambda}\,\bar{J}_{\mu\nu o}$	0	0	-2	1
$K'_{\lambda(\mu\nu)o}\,\bar{J}_{o\pi\pi}$	0	0	0	-4
$K'_{\lambda(\mu\nu)o}\,\bar{J}_{\pi o\pi}$	0	0	0	-4
$K'_{\lambda(\mu\nu)o}\,\bar{J}_{\pi\pi o}$	0	0	0	-4
$K'_{\lambda(\mu o)o}\,\bar{J}_{\nu\pi\pi}$	0	0	0	-4
$K'_{\lambda(\mu o)\pi}\,\bar{J}_{\nu o\pi}$	0	0	0	-4
$K'_{\lambda(\mu o)\pi}\,\bar{J}_{\nu\pi o}$	0	0	0	-4
$K'_{\lambda(\mu o)o}\,\bar{J}_{\pi\nu\pi}$	0	0	0	-10
$K'_{\lambda(\mu o)\pi}\,\bar{J}_{o\nu\pi}$	0	0	0	-3
$K'_{\lambda(\mu o)\pi}\,\bar{J}_{\pi\nu o}$	0	0	0	-3
$K'_{\lambda(oo)\mu}\,\bar{J}_{\pi\nu\pi}$	0	0	0	-4
$K'_{\lambda(o\pi)\mu}\,\bar{J}_{o\nu\pi}$	0	0	0	-8
$K'_{\lambda(oo)\pi}\,\bar{J}_{\mu\nu\pi}$	0	0	0	-4
$K'_{\lambda(o\pi)o}\,\bar{J}_{\mu\nu\pi}$	0	0	0	-8
$K'_{\lambda(oo)\pi}\,\bar{J}_{\mu\pi\nu}$	0	0	0	-6

$K'_{\lambda(o\pi)o}\,\bar{J}_{\mu\pi\nu}$	0	0	0	2
$K'_{o(\lambda\mu)o}\,\bar{J}_{\pi\nu\pi}$	0	0	0	-4
$K'_{o(\lambda\mu)\pi}\,\bar{J}_{o\nu\pi}$	0	0	0	-4
$K'_{o(\lambda\mu)\pi}\,\bar{J}_{\pi\nu o}$	0	0	0	-4
$K'_{o(\lambda\mu)o}\,\bar{J}_{\pi\pi\nu}$	0	0	0	-6
$K'_{o(\lambda\mu)\pi}\,\bar{J}_{o\pi\nu}$	0	0	0	1
$K'_{o(\lambda\mu)\pi}\,\bar{J}_{\pi o\nu}$	0	0	0	1
$K'_{o(\lambda o)\pi}\,\bar{J}_{\mu\nu\pi}$	0	0	0	-10
$K'_{o(\lambda\mu)o}\,\bar{J}_{\mu\nu\pi}$	0	0	0	-3
$K'_{o(\lambda\pi)\pi}\,\bar{J}_{\mu\nu o}$	0	0	0	-3
$K'_{o(\lambda o)\pi}\,\bar{J}_{\pi\mu\nu}$	0	0	0	-4
$K'_{o(\lambda\pi)o}\,\bar{J}_{\pi\mu\nu}$	0	0	0	-4
$K'_{o(\lambda\pi)\pi}\,\bar{J}_{o\mu\nu}$	0	0	0	-4
$K'\bar{J}$	-12	4	-24	-176
1/420				
$K_{\lambda(\mu o)\nu}\,\bar{J}_{o\pi\pi}$	0	0	-4	0
$K_{\lambda(\mu o)\nu}\,\bar{J}_{\pi o\pi}$	0	0	10	0
$K_{\lambda(\mu o)\nu}\,\bar{J}_{\pi\pi o}$	0	0	10	0
$K_{\lambda(oo)\mu}\,\bar{J}_{\nu\pi\pi}$	0	0	2	0
$K_{\lambda(o\pi)\mu}\,\bar{J}_{\nu o\pi}$	0	0	-10	0
$K_{o(\lambda o)\mu}\,\bar{J}_{\pi\nu\pi}$	0	0	10	0
$K_{o(\lambda\pi)\mu}\,\bar{J}_{o\nu\pi}$	0	0	10	0
$K_{o(\lambda\pi)\mu}\,\bar{J}_{\pi\nu o}$	0	0	-4	0
$K_{o(\lambda o)\mu}\,\bar{J}_{\pi\pi\nu}$	0	0	10	0
$K_{o(\lambda\pi)\mu}\,\bar{J}_{o\pi\nu}$	0	0	10	0
$K_{o(\lambda\pi)\mu}\,\bar{J}_{\pi o\nu}$	0	0	-4	0
$K_{o(o\pi)\lambda}\,\bar{J}_{\mu\nu\pi}$	0	0	-10	0
$K_{o(\pi\pi)\lambda}\,\bar{J}_{\mu\nu o}$	0	0	2	0
$K_{o(o\pi)\lambda}\,\bar{J}_{\mu\pi\nu}$	0	0	-10	0
$K_{o(\pi\pi)\lambda}\,\bar{J}_{\mu o\nu}$	0	0	2	0
$K\bar{J}$	0	0	24	0
1/7560				
$K'_{\lambda(\lambda\mu)\mu}\,\bar{K}'_{\nu(\nu o)o}$	-16	4	-100	8
$K'_{\lambda(\lambda\mu)\mu}\,\bar{K}'_{\nu(oo)\nu}$	-8	20	40	4
$K'_{\lambda(\lambda\mu)\nu}\,\bar{K}'_{\mu(\nu o)o}$	-16	4	80	80
$K'_{\lambda(\lambda\mu)\nu}\,\bar{K}'_{\mu(oo)\nu}$	64	-52	-104	-104
$K'_{\lambda(\lambda\mu)\nu}\,\bar{K}'_{\nu(\mu o)o}$	-16	40	-100	80
$K'_{\lambda(\lambda\mu)\nu}\,\bar{K}'_{o(\mu\nu)o}$	-16	40	-100	80
$K'_{\lambda(\lambda\mu)\nu}\,\bar{K}'_{o(\mu o)\nu}$	128	-104	440	-208
$K'_{\lambda(\lambda\mu)\nu}\,\bar{K}'_{\nu(oo)\mu}$	-8	20	40	4
$K'_{\lambda(\lambda\mu)\nu}\,\bar{K}'_{o(\nu o)\mu}$	-16	4	-100	8
$K'_{\lambda(\mu\mu)\lambda}\,\bar{K}'_{\nu(\nu o)o}$	-8	20	40	4
$K'_{\lambda(\mu\mu)\lambda}\,\bar{K}'_{\nu(oo)\nu}$	-4	-44	2	2
$K'_{\lambda(\mu\nu)\lambda}\,\bar{K}'_{\mu(\nu o)o}$	-16	40	80	-100
$K'_{\lambda(\mu\nu)\lambda}\,\bar{K}'_{\mu(oo)\nu}$	-8	20	4	40
$K'_{\lambda(\mu\nu)\lambda}\,\bar{K}'_{o(\mu\nu)o}$	-8	-88	-50	-50
$K'_{\lambda(\mu\nu)\lambda}\,\bar{K}'_{o(\mu o)\nu}$	-16	40	-100	80
$K'_{\lambda(\mu\mu)\nu}\,\bar{K}'_{\lambda(\nu o)o}$	-8	-52	40	40
$K'_{\lambda(\mu\mu)\nu}\,\bar{K}'_{\lambda(oo)\nu}$	32	136	-52	-52
$K'_{\lambda(\mu\nu)\mu}\,\bar{K}'_{\lambda(\nu o)o}$	-16	-104	-100	-100
$K'_{\lambda(\mu\nu)\mu}\,\bar{K}'_{\lambda(oo)\nu}$	-8	-52	40	40
$K'_{\lambda(\mu\nu)o}\,\bar{K}'_{\lambda(\mu\nu)o}$	64	272	220	220
$K'_{\lambda(\mu\nu)o}\,\bar{K}'_{\lambda(\mu o)\nu}$	-16	-104	-100	-100
$K'_{\lambda(\mu\mu)\nu}\,\bar{K}'_{\nu(\lambda o)o}$	-8	20	4	40
$K'_{\lambda(\mu\mu)\nu}\,\bar{K}'_{o(\lambda\nu)o}$	-8	20	4	40
$K'_{\lambda(\mu\mu)\nu}\,\bar{K}'_{o(\lambda o)\nu}$	64	-52	-104	-104
$K'_{\lambda(\mu\nu)\mu}\,\bar{K}'_{\nu(\lambda o)o}$	-16	4	8	-100
$K'_{\lambda(\mu\nu)\mu}\,\bar{K}'_{o(\lambda\nu)o}$	-16	40	80	-100
$K'_{\lambda(\mu\nu)\mu}\,\bar{K}'_{o(\lambda o)\nu}$	-16	4	80	80
$K'_{\lambda(\mu\nu)o}\,\bar{K}'_{\mu(\lambda\nu)o}$	128	-104	-208	440
$K'_{\lambda(\mu\nu)o}\,\bar{K}'_{\mu(\lambda o)\nu}$	-16	4	8	-100
$K'_{\lambda(\mu\nu)o}\,\bar{K}'_{o(\lambda\mu)\nu}$	-16	40	80	-100
$K'_{\lambda(\mu\mu)\nu}\,\bar{K}'_{\nu(oo)\lambda}$	-4	-44	2	2
$K'_{\lambda(\mu\mu)\nu}\,\bar{K}'_{o(\nu o)\lambda}$	-8	20	40	4
$K'_{\lambda(\mu\nu)\mu}\,\bar{K}'_{\nu(oo)\lambda}$	-8	20	4	40
$K'_{\lambda(\mu\nu)\mu}\,\bar{K}'_{o(\nu o)\lambda}$	-16	40	-100	80
$K'_{\lambda(\mu\nu)o}\,\bar{K}'_{\mu(\nu o)\lambda}$	-16	40	80	-100
$K'_{\lambda(\mu\nu)o}\,\bar{K}'_{o(\mu\nu)\lambda}$	-8	-88	-50	-50
$K'\bar{K}'$	120	24	48	48
1/3780				
$K'_{\lambda(\lambda\mu)\mu}\,\bar{K}_{\nu(\nu o)o}$	0	0	-100	8
$K'_{\lambda(\lambda\mu)\mu}\,\bar{K}_{\nu(oo)\nu}$	0	0	40	4
$K'_{\lambda(\lambda\mu)\nu}\,\bar{K}_{\mu(\nu o)o}$	0	0	80	80
$K'_{\lambda(\lambda\mu)\nu}\,\bar{K}_{\mu(oo)\nu}$	0	0	-104	-104
$K'_{\lambda(\lambda\mu)\nu}\,\bar{K}_{\nu(\mu o)o}$	0	0	-100	80
$K'_{\lambda(\lambda\mu)\nu}\,\bar{K}_{o(\mu\nu)o}$	0	0	-100	80
$K'_{\lambda(\lambda\mu)\nu}\,\bar{K}_{o(\mu o)\nu}$	0	0	440	-208
$K'_{\lambda(\lambda\mu)\nu}\,\bar{K}_{\nu(oo)\mu}$	0	0	40	4
$K'_{\lambda(\lambda\mu)\nu}\,\bar{K}_{o(\nu o)\mu}$	0	0	-100	8
$K'_{\lambda(\mu\mu)\lambda}\,\bar{K}_{\nu(\nu o)o}$	0	0	40	4
$K'_{\lambda(\mu\mu)\lambda}\,\bar{K}_{\nu(oo)\nu}$	0	0	2	2
$K'_{\lambda(\mu\nu)\lambda}\,\bar{K}_{\mu(\nu o)o}$	0	0	80	-100
$K'_{\lambda(\mu\nu)\lambda}\,\bar{K}_{\mu(oo)\nu}$	0	0	4	40
$K'_{\lambda(\mu\nu)\lambda}\,\bar{K}_{o(\mu\nu)o}$	0	0	-50	-50

$K'_{\lambda(\mu\nu)\lambda}\,\bar{K}_{o(\mu o)\nu}$	0	0	-100	80
$K'_{\lambda(\mu\mu)\nu}\,\bar{K}_{\lambda(\nu o)o}$	0	0	40	40
$K'_{\lambda(\mu\mu)\nu}\,\bar{K}_{\lambda(oo)\nu}$	0	0	-52	-52
$K'_{\lambda(\mu\nu)\mu}\,\bar{K}_{\lambda(\nu o)o}$	0	0	-100	-100
$K'_{\lambda(\mu\nu)\mu}\,\bar{K}_{\lambda(oo)\nu}$	0	0	40	40
$K'_{\lambda(\mu\nu)o}\,\bar{K}_{\lambda(\mu\nu)o}$	0	0	220	220
$K'_{\lambda(\mu\nu)o}\,\bar{K}_{\lambda(\mu o)\nu}$	0	0	-100	-100
$K'_{\lambda(\mu\mu)\nu}\,\bar{K}_{\nu(\lambda o)o}$	0	0	4	40
$K'_{\lambda(\mu\mu)\nu}\,\bar{K}_{o(\lambda\nu)o}$	0	0	4	40
$K'_{\lambda(\mu\mu)\nu}\,\bar{K}_{o(\lambda o)\nu}$	0	0	-104	-104
$K'_{\lambda(\mu\nu)\mu}\,\bar{K}_{\nu(\lambda o)o}$	0	0	8	-100
$K'_{\lambda(\mu\nu)\mu}\,\bar{K}_{o(\lambda\nu)o}$	0	0	80	-100
$K'_{\lambda(\mu\nu)\mu}\,\bar{K}_{o(\lambda o)\nu}$	0	0	80	80
$K'_{\lambda(\mu\nu)o}\,\bar{K}_{\mu(\lambda\nu)o}$	0	0	-208	440
$K'_{\lambda(\mu\nu)o}\,\bar{K}_{\mu(\lambda o)\nu}$	0	0	8	-100
$K'_{\lambda(\mu\nu)o}\,\bar{K}_{o(\lambda\mu)\nu}$	0	0	80	-100
$K'_{\lambda(\mu\mu)\nu}\,\bar{K}_{\nu(oo)\lambda}$	0	0	2	2
$K'_{\lambda(\mu\mu)\nu}\,\bar{K}_{o(\nu o)\lambda}$	0	0	40	4
$K'_{\lambda(\mu\nu)\mu}\,\bar{K}_{\nu(oo)\lambda}$	0	0	4	40
$K'_{\lambda(\mu\nu)\mu}\,\bar{K}_{o(\nu o)\lambda}$	0	0	-100	80
$K'_{\lambda(\mu\nu)o}\,\bar{K}_{\mu(\nu o)\lambda}$	0	0	80	-100
$K'_{\lambda(\mu\nu)o}\,\bar{K}_{o(\mu\nu)\lambda}$	0	0	-50	-50
$K'\bar{K}$	0	0	48	48
1/7560				
$K_{\lambda(\lambda\mu)\mu}\,\bar{K}_{\nu(\nu o)o}$	-16	12	-100	8
$K_{\lambda(\lambda\mu)\mu}\,\bar{K}_{\nu(oo)\nu}$	-8	-12	40	4
$K_{\lambda(\lambda\mu)\nu}\,\bar{K}_{\mu(\nu o)o}$	-16	12	80	80
$K_{\lambda(\lambda\mu)\nu}\,\bar{K}_{\mu(oo)\nu}$	64	-12	-104	-104
$K_{\lambda(\lambda\mu)\nu}\,\bar{K}_{\nu(\mu o)o}$	-16	-24	-100	80
$K_{\lambda(\lambda\mu)\nu}\,\bar{K}_{o(\mu\nu)o}$	-16	-24	-100	80
$K_{\lambda(\lambda\mu)\nu}\,\bar{K}_{o(\mu o)\nu}$	128	-24	440	-208
$K_{\lambda(\lambda\mu)\nu}\,\bar{K}_{\nu(oo)\mu}$	-8	-12	40	4
$K_{\lambda(\lambda\mu)\nu}\,\bar{K}_{o(\nu o)\mu}$	-16	12	-100	8
$K_{\lambda(\mu\mu)\lambda}\,\bar{K}_{\nu(\nu o)o}$	-8	-12	40	4
$K_{\lambda(\mu\mu)\lambda}\,\bar{K}_{\nu(oo)\nu}$	-4	48	2	2
$K_{\lambda(\mu\nu)\lambda}\,\bar{K}_{\mu(\nu o)o}$	-16	-24	80	-100
$K_{\lambda(\mu\nu)\lambda}\,\bar{K}_{\mu(oo)\nu}$	-8	-12	4	40
$K_{\lambda(\mu\nu)\lambda}\,\bar{K}_{o(\mu\nu)o}$	-8	96	-50	-50
$K_{\lambda(\mu\nu)\lambda}\,\bar{K}_{o(\mu o)\nu}$	-16	-24	-100	80
$K_{\lambda(\mu\mu)\nu}\,\bar{K}_{\lambda(\nu o)o}$	-8	-12	40	40
$K_{\lambda(\mu\mu)\nu}\,\bar{K}_{\lambda(oo)\nu}$	32	48	-52	-52
$K_{\lambda(\mu\nu)\mu}\,\bar{K}_{\lambda(\nu o)o}$	-16	-24	-100	-100
$K_{\lambda(\mu\nu)\mu}\,\bar{K}_{\lambda(oo)\nu}$	-8	-12	40	40
$K_{\lambda(\mu\nu)o}\,\bar{K}_{\lambda(\mu\nu)o}$	64	96	220	220
$K_{\lambda(\mu\nu)o}\,\bar{K}_{\lambda(\mu o)\nu}$	-16	-24	-100	-100
$K_{\lambda(\mu\mu)\nu}\,\bar{K}_{\nu(\lambda o)o}$	-8	-12	4	40
$K_{\lambda(\mu\mu)\nu}\,\bar{K}_{o(\lambda\nu)o}$	-8	-12	4	40
$K_{\lambda(\mu\mu)\nu}\,\bar{K}_{o(\lambda o)\nu}$	64	-12	-104	-104
$K_{\lambda(\mu\nu)\mu}\,\bar{K}_{\nu(\lambda o)o}$	-16	12	8	-100
$K_{\lambda(\mu\nu)\mu}\,\bar{K}_{o(\lambda\nu)o}$	-16	-24	80	-100
$K_{\lambda(\mu\nu)\mu}\,\bar{K}_{o(\lambda o)\nu}$	-16	12	80	80
$K_{\lambda(\mu\nu)o}\,\bar{K}_{\mu(\lambda\nu)o}$	128	-24	-208	440
$K_{\lambda(\mu\nu)o}\,\bar{K}_{\mu(\lambda o)\nu}$	-16	12	8	-100
$K_{\lambda(\mu\nu)o}\,\bar{K}_{o(\lambda\mu)\nu}$	-16	-24	80	-100
$K_{\lambda(\mu\mu)\nu}\,\bar{K}_{\nu(oo)\lambda}$	-4	48	2	2
$K_{\lambda(\mu\mu)\nu}\,\bar{K}_{o(\nu o)\lambda}$	-8	-12	40	4
$K_{\lambda(\mu\nu)\mu}\,\bar{K}_{\nu(oo)\lambda}$	-8	-12	4	40
$K_{\lambda(\mu\nu)\mu}\,\bar{K}_{o(\nu o)\lambda}$	-16	-24	-100	80
$K_{\lambda(\mu\nu)o}\,\bar{K}_{\mu(\nu o)\lambda}$	-16	-24	80	-100
$K_{\lambda(\mu\nu)o}\,\bar{K}_{o(\mu\nu)\lambda}$	-8	96	-50	-50
$K\bar{K}$	120	72	48	48

4

SIX-WAVE SECOND HARMONIC GENERATION WITH STRUCTURED LIGHT

4.1 INTRODUCTION

In the previous chapter a series of mechanisms were introduced, by which a second-harmonic signal in media of high symmetry, such as centrosymmetric media, could be detected. In this chapter, another method of subverting the standard selection rules will be presented [164]. If we recall the selection rules prohibiting coherent SHG are governed by the relative parity of the initial and final states of a process: explicitly, they must both be equivalent. It was a suggested that by adopting a transition that conforms to even spatial parity, in contrast to the commonly considered odd inversion arising from an E1 transition, that this would then adhere to the requisite parity equivalence.

There is a more immediately apparent method of reaching a final state of the same parity of the initial state, that is by identically doubling each photon interaction engaged in the process [165]. This results in a six-photon process, where each interaction engages in an odd parity E1 transition. The six photon-molecule interactions each engage in an odd parity transform, which results in an overall even parity process, which will be allowed. By ensuring all the interactions engage an E1 operator, we can be confident that a significant harmonic signal strength will be achieved. Having said that, the process requires four photons to concurrently arrive at an optical centre, which means that this process has a higher degree of nonlinearity than its three-wave counterpart. In order to maximise the intensity of second-harmonic emission, the lasers with the levels of high irradiance mentioned in the introduction offer the best chance of observing processes such as these.

4.2 GENERAL THEORY

4.2A VACUUM FORMULATION

To begin, we shall consider the general process of six-wave second harmonic generation. In such a process, four photons of radiation mode $\mathbf{k},\eta$ are concurrently annihilated at an optical centre, each event raises the optical centre to a virtual excited state. In the span of the process, the centre relaxes to its ground state, by emitting two photons $(\mathbf{k}',\eta'$ and $\mathbf{k}'',\eta'')$, such that,

$$\hbar ck' + \hbar ck'' = 4\hbar ck \ . \tag{5.2.1}$$

One example time-ordering of this is displayed in Figure 4.

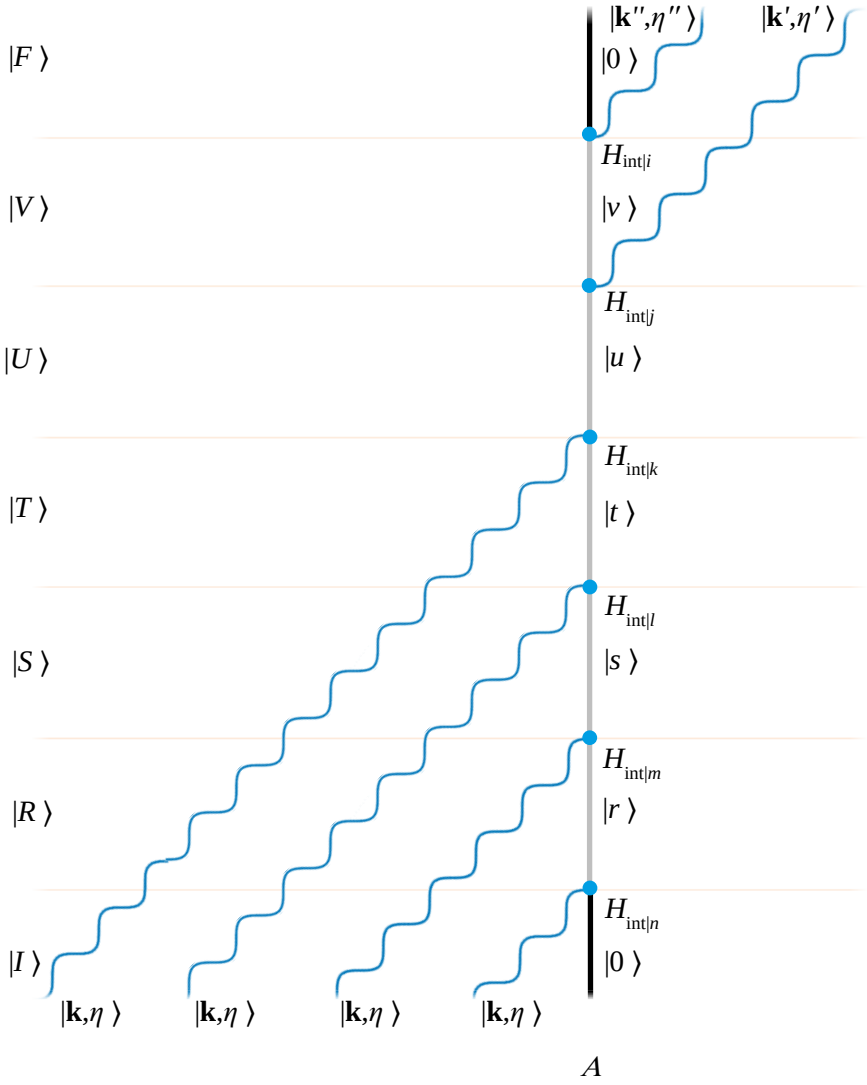

Figure 20: An example Feynman diagram for six-wave second harmonic generation. The photon annihilation operators k, l, m, n precede the photon creation i and j. At the time of the process resolves, the scatterer reaches the state in which it began, the ground state 0, subsequent to traversing five intermediary states, r, s, t, u and v.

Generally, any six independent events can be expected to occur in any of 720 forms. However, in §1.4C it was introduced that indistinguishability of photon interaction truncates the number of unique representations. In this process, we have four photons of identical radiation mode annihilated, all engaging the same photon operator; in regard to the annihilation events, 24 time-orderings will appear identical. Moreover, the two created photons engage the same photon operators and as such half of the 30 remaining time-orderings will also appear identical, with respect to the photon creation events. The fifteen remaining unique time-orderings can be displayed most succinctly in the form of a state sequence method [14], which is based on the Hasse combinatorial diagram [15]. Figure 21, displays a modified form of this form of diagram in which the Fock states of equal number of photons are displayed in a given row. Each pathway from the initial to final state represents one of the fifteen unique time-orderings. The pathway associated with that of Figure 4 is that of the bottom-most path and is highlighted for clarity.

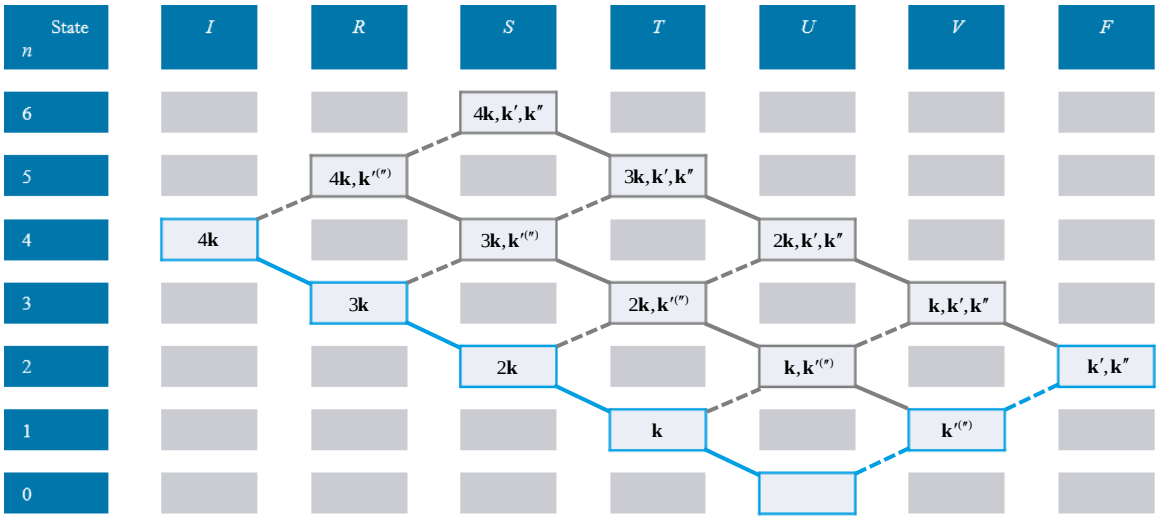

Figure 21: In this tabular state sequence diagram, each row represents a state of consecutive photon occupying number, n. Columns denote successive system states. Each vacant column and row, which also contains a connector represents an interaction. The solid lines with a declination representing a photon annihilation event and the inclined dashed lines represent a photon creation event. In the more widely known Feynman diagrams, these correspond to nodes, such as those displayed in Figure 4. In the central line of catawampus cells, the wavevector of either output mode has been accommodated, with both modes populated in the upper set.

The six photon-molecule interactions will result in a leading contribution from the $n=6$ term in equation (1.3.14), with all fifteen time-orderings contributing unique terms to the matrix element. Here is the first time-ordering exemplified in Figure 4,

$$M_{FI}=\frac{1}{\varepsilon_0^6}\sum_{\substack{r,s,t,\\u,v}}\left\{\frac{\left\langle 0;(\mathbf{k}',\eta';\mathbf{k}'',\eta'')\left|\mu_i d_i^{\perp}\right|v;\mathbf{k}',\eta'\right\rangle\left\langle v;\mathbf{k}',\eta'\left|\mu_j d_j^{\perp}\right|u;0\right\rangle\left\langle u;0\left|\mu_k d_k^{\perp}\right|t;\mathbf{k},\eta\right\rangle}{\left[\left(E_0+4\hbar ck\right)-\left(E_v+\hbar ck'\right)\right]\left[\left(E_0+4\hbar ck\right)-E_u\right]\left[\left(E_0+4\hbar ck\right)-\left(E_t+\hbar ck\right)\right]}\right.$$
$$\times\frac{\left\langle t;\mathbf{k},\eta\left|\mu_l d_l^{\perp}\right|s;(\mathbf{k},\eta)_2\right\rangle\left\langle s;(\mathbf{k},\eta)_2\left|\mu_m d_m^{\perp}\right|r;(\mathbf{k},\eta)_3\right\rangle\left\langle r;(\mathbf{k},\eta)_3\left|\mu_n d_n^{\perp}\right|0;(\mathbf{k},\eta)_4\right\rangle}{\left[\left(E_0+4\hbar ck\right)-\left(E_s+2\hbar ck\right)\right]\left[\left(E_0+4\hbar ck\right)-\left(E_r+3\hbar ck\right)\right]}$$
$$\left.+...\right\}\ . \qquad (5.2.2)$$

There are five intermediary states all to be summed over: r, s, t, u and v. The power of the prefactor corresponds to the number of E1 operators engaged in the process. For brevity of notation, any radiation states that exist in multiples are listed once and a subscript number corresponds to the number of such occurrences there are. There are now five energy denominators all representing the total energy of the intermediary state relative to that of the initial (and final) state, which can be simplified by adopting the relation in equation (1.4.20). The complete molecular response tensor can be expressed as follows,

$$\chi^{(5)}_{(ij)(klmn)}=\frac{1}{48}\sum_{r,s,t,u,v}\left\{\frac{\mu_i^{0v}\mu_j^{vu}\mu_k^{ut}\mu_l^{ts}\mu_m^{sr}\mu_n^{r0}}{\left[E_{v0}-2\hbar ck\right]\left[E_{u0}-4\hbar ck\right]\left[E_{t0}-3\hbar ck\right]\left[E_{s0}-2\hbar ck\right]\left[E_{r0}-\hbar ck\right]}\right.$$
$$+\frac{\mu_i^{0v}\mu_k^{vu}\mu_j^{ut}\mu_l^{ts}\mu_m^{sr}\mu_n^{r0}}{\left[E_{v0}-2\hbar ck\right]\left[E_{u0}-\hbar ck\right]\left[E_{t0}-3\hbar ck\right]\left[E_{s0}-2\hbar ck\right]\left[E_{r0}-\hbar ck\right]}$$
$$+\frac{\mu_i^{0v}\mu_k^{vu}\mu_l^{ut}\mu_j^{ts}\mu_m^{sr}\mu_n^{r0}}{\left[E_{v0}-2\hbar ck\right]\left[E_{u0}-\hbar ck\right]\left[E_{t0}\right]\left[E_{s0}-2\hbar ck\right]\left[E_{r0}-\hbar ck\right]}$$
$$+\frac{\mu_i^{0v}\mu_k^{vu}\mu_l^{ut}\mu_m^{ts}\mu_j^{sr}\mu_n^{r0}}{\left[E_{v0}-2\hbar ck\right]\left[E_{u0}-\hbar ck\right]\left[E_{t0}\right]\left[E_{s0}+\hbar ck\right]\left[E_{r0}-\hbar ck\right]}$$
$$+\frac{\mu_i^{0v}\mu_k^{vu}\mu_l^{ut}\mu_m^{ts}\mu_n^{sr}\mu_j^{r0}}{\left[E_{v0}-2\hbar ck\right]\left[E_{u0}-\hbar ck\right]\left[E_{t0}\right]\left[E_{s0}+\hbar ck\right]\left[E_{r0}+2\hbar ck\right]}$$
$$+\frac{\mu_k^{0v}\mu_i^{vu}\mu_l^{ut}\mu_m^{ts}\mu_n^{sr}\mu_j^{r0}}{\left[E_{v0}+\hbar ck\right]\left[E_{u0}-\hbar ck\right]\left[E_{t0}\right]\left[E_{s0}+\hbar ck\right]\left[E_{r0}+2\hbar ck\right]}$$
$$+\frac{\mu_k^{0v}\mu_l^{vu}\mu_i^{ut}\mu_m^{ts}\mu_n^{sr}\mu_j^{r0}}{\left[E_{v0}+\hbar ck\right]\left[E_{u0}+2\hbar ck\right]\left[E_{t0}\right]\left[E_{s0}+\hbar ck\right]\left[E_{r0}+2\hbar ck\right]}$$
$$+\frac{\mu_k^{0v}\mu_l^{vu}\mu_m^{ut}\mu_i^{ts}\mu_n^{sr}\mu_j^{r0}}{\left[E_{v0}+\hbar ck\right]\left[E_{u0}+2\hbar ck\right]\left[E_{t0}+3\hbar ck\right]\left[E_{s0}+\hbar ck\right]\left[E_{r0}+2\hbar ck\right]}$$
$$+\frac{\mu_k^{0v}\mu_l^{vu}\mu_m^{ut}\mu_n^{ts}\mu_i^{sr}\mu_j^{r0}}{\left[E_{v0}+\hbar ck\right]\left[E_{u0}+2\hbar ck\right]\left[E_{t0}+3\hbar ck\right]\left[E_{s0}+4\hbar ck\right]\left[E_{r0}+2\hbar ck\right]}$$
$$+...$$

$$
\begin{aligned}
&+\frac{\mu_k^{0v}\mu_l^{vu}\mu_m^{ut}\mu_i^{ts}\mu_j^{sr}\mu_n^{r0}}{[E_{v0}+\hbar ck][E_{u0}+2\hbar ck][E_{t0}+3\hbar ck][E_{s0}+\hbar ck][E_{r0}-\hbar ck]}\\
&+\frac{\mu_k^{0v}\mu_l^{vu}\mu_i^{ut}\mu_m^{ts}\mu_j^{sr}\mu_n^{r0}}{[E_{v0}+\hbar ck][E_{u0}+2\hbar ck][E_{t0}][E_{s0}+\hbar ck][E_{r0}-\hbar ck]}\\
&+\frac{\mu_k^{0v}\mu_i^{vu}\mu_l^{ut}\mu_m^{ts}\mu_j^{sr}\mu_n^{r0}}{[E_{v0}+\hbar ck][E_{u0}-\hbar ck][E_{t0}][E_{s0}+\hbar ck][E_{r0}-\hbar ck]}\\
&+\frac{\mu_k^{0v}\mu_i^{vu}\mu_l^{ut}\mu_j^{ts}\mu_m^{sr}\mu_n^{r0}}{[E_{v0}+\hbar ck][E_{u0}-\hbar ck][E_{t0}][E_{s0}-2\hbar ck][E_{r0}-\hbar ck]}\\
&+\frac{\mu_k^{0v}\mu_i^{vu}\mu_j^{ut}\mu_l^{ts}\mu_m^{sr}\mu_n^{r0}}{[E_{v0}+\hbar ck][E_{u0}-\hbar ck][E_{t0}-3\hbar ck][E_{s0}-2\hbar ck][E_{r0}-\hbar ck]}\\
&+\frac{\mu_k^{0v}\mu_l^{vu}\mu_i^{ut}\mu_j^{ts}\mu_m^{sr}\mu_n^{r0}}{[E_{v0}+\hbar ck][E_{u0}+2\hbar ck][E_{t0}][E_{s0}-2\hbar ck][E_{r0}-\hbar ck]}\Bigg\}\,.
\end{aligned}
\tag{5.2.3}
$$

The superscript attached to the response tensor identifies this as the fifth order molecular susceptibility. The factor of the whole tensor corresponds to the number of indistinguishable time-orderings represented by each term. Following this definition, the matrix element can be much more simply expressed as,

$$
M_{FI}=\left(\frac{\hbar c}{2\varepsilon_0 V}\right)^3 k^2\sqrt{k'k''}\sqrt{n(n-1)(n-2)(n-3)}\,\vec{e}_i''\vec{e}_j' e_k e_l e_m e_n \chi^{(5)}_{(ij)(klmn)}\,, \tag{5.2.4}
$$

Hence, we can now write the rate of a transition in a scatterer of fixed orientation as,

$$
\Gamma=\frac{\pi\hbar^5 c^6 k^6}{8\varepsilon_0^6 V^6}\,n(n-1)(n-2)(n-3)\left|\vec{e}_i''\vec{e}_j' e_k e_l e_m e_n \chi^{(5)}_{(ij)(klmn)}\right|^2 \rho_F\,. \tag{5.2.5}
$$

Note, this is in fact the vacuum formulation for the rate. We will now briefly discuss the affect a medium can have on this result.

4.2B MEDIA EFFECTS

In this subsection, we shall develop the principles introduced in complement 1C and in the course of the previous processes. It is well known that different frequencies of light traverse a medium at different velocities, you need look no further than a simple prism to demonstrate this. The refractive index is, as the name eludes to, an index to relate the velocity light travels through a given medium to that it would travel through a vacuum,

$$n_{\omega} = \frac{ck}{\omega} \ . \tag{5.2.6}$$

Importantly, it can be seen that it holds a dependence on the frequency. In the case of second harmonic generation, we are considering a pair of photons emitted at twice the frequency, $\omega'^{(\prime)} = 2\omega$ of the input beam. Each harmonic photon therefore may have a different refractive index $n_{\omega'}$ and $n_{\omega''}$. If this is the case, the wavevector relation in equation (1.4.20) isn't strictly true. This discrepancy in the magnitude of the wavevector associated with the emitted photons can be displayed in a diagram such as the one in Figure 22.

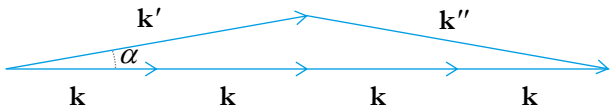

Figure 22: Schematic for the wavevector matching condition, the sum of the wavevectors **k** for the annihilated photons from the input beam is equal to the sum the two harmonic photons of wavevectors **k′** and **k″** at a conical angle, α. Here, $\alpha = 10^{o}$ is depicted.

This is formed under the knowledge that we are considering a parametric process, in which the momenta in the system must be conserved. It follows that the wave-vector matching condition specific to six-wave coherent SHG is,

$$4\mathbf{k} = \mathbf{k}' + \mathbf{k}'' \ . \tag{5.2.7}$$

With this, the refractive indices of all photons can be related with a single dependency on the conical emission angle, α ,

$$\alpha = \arccos\left(\frac{2k}{k'}\right) \ . \tag{5.2.8}$$

As the name suggests each process can deliver any pair of diametrically opposed $\mathbf{k}'^{(\prime)}$ such that they deviate from **k** by an equivalent angle α . The desired relation for the refractive indices is as follows,

$$2n_{\omega} = \left(n_{\omega'} + n_{\omega''}\right)\cos\alpha \ . \tag{5.2.9}$$

4.3 ROTATIONAL AVERAGE

Equation (5.2.5) is perfectly suitable for any solid-phase process. At this juncture, we will consider the effects of molecular motion in condensed-phase specimens. Consistent with previous methods we will perform a rotational average to obtain a result for such species,

$$\langle \Gamma \rangle = \frac{\pi \hbar^5 c^6 k^6}{8\varepsilon_0^6 V^6} n(n-1)(n-2)(n-3)\left| \bar{e}_i'' \bar{e}_j' e_k e_l e_m e_n I^{(6)}_{ijklmn;\lambda\mu\nu o\pi\rho} \chi^{(5)}_{(\lambda\mu)(\nu o\pi\rho)} \right|^2 \rho_F \; . \qquad (5.3.1)$$

As a parametric process, equation (5.2.7), the matrix element associated with each centre adds constructively to the ensemble; as such, we can perform the rotational average on the contents of the square modulus [100], see complement 1C for more details. In contrast to the processes considered in the previous two chapters, which required evaluation of the square modulus prior to performing the rotational average. The obvious benefit is that a rotational average of the same order as that for (three-wave) hyper-Rayleigh scattering can be applied.

It is worth noting that although a condensed-phase system is of interest here and will be seen to deliver interesting results. In the case of a solid-phase system, a distributional average should still be performed to accommodate the various orientations each centre can assume within the material. Of course, bulk isotropy would then be assumed to benefit from the theory deployed herein. To begin, we first refer to the sixth rank isotropic tensor, equation (1D.13), and contract the field vectors with the full set of fifteen linear combinations of isotropic tensors,

$$\bar{e}_i' \bar{e}_j' e_k e_l e_m e_n \begin{pmatrix} \delta_{ij}\delta_{kl}\delta_{mn} \\ \delta_{ij}\delta_{km}\delta_{ln} \\ \delta_{ij}\delta_{kn}\delta_{lm} \\ \delta_{ik}\delta_{jl}\delta_{mn} \\ \delta_{ik}\delta_{jm}\delta_{ln} \\ \delta_{ik}\delta_{jn}\delta_{lm} \\ \delta_{il}\delta_{jk}\delta_{mn} \\ \delta_{il}\delta_{jm}\delta_{kn} \\ \delta_{il}\delta_{jn}\delta_{km} \\ \delta_{im}\delta_{jk}\delta_{ln} \\ \delta_{im}\delta_{jl}\delta_{kn} \\ \delta_{im}\delta_{jn}\delta_{kl} \\ \delta_{in}\delta_{jk}\delta_{lm} \\ \delta_{in}\delta_{jl}\delta_{km} \\ \delta_{in}\delta_{jm}\delta_{kl} \end{pmatrix}^{\mathrm{T}} = \begin{pmatrix} \bar{e}_i''\bar{e}_i' e_k e_k e_m e_m \\ \bar{e}_i''\bar{e}_i' e_k e_l e_k e_l \\ \bar{e}_i''\bar{e}_i' e_k e_l e_l e_k \\ \bar{e}_i''\bar{e}_j' e_i e_j e_m e_m \\ \bar{e}_i''\bar{e}_j' e_i e_l e_j e_l \\ \bar{e}_i''\bar{e}_j' e_i e_l e_l e_j \\ \bar{e}_i''\bar{e}_j' e_j e_i e_m e_m \\ \bar{e}_i''\bar{e}_j' e_k e_i e_j e_k \\ \bar{e}_i''\bar{e}_j' e_k e_i e_k e_j \\ \bar{e}_i''\bar{e}_j' e_j e_l e_i e_l \\ \bar{e}_i''\bar{e}_j' e_k e_j e_i e_k \\ \bar{e}_i''\bar{e}_j' e_k e_k e_i e_j \\ \bar{e}_i''\bar{e}_j' e_j e_l e_l e_i \\ \bar{e}_i''\bar{e}_j' e_k e_j e_k e_i \\ \bar{e}_i''\bar{e}_j' e_k e_k e_j e_i \end{pmatrix}^{\mathrm{T}} = \begin{pmatrix} (\bar{\mathbf{e}}'' \cdot \bar{\mathbf{e}}')(\mathbf{e}\cdot\mathbf{e})^2 \\ (\bar{\mathbf{e}}'' \cdot \bar{\mathbf{e}}')(\mathbf{e}\cdot\mathbf{e})^2 \\ (\bar{\mathbf{e}}'' \cdot \bar{\mathbf{e}}')(\mathbf{e}\cdot\mathbf{e})^2 \\ (\bar{\mathbf{e}}''\cdot\bar{\mathbf{e}})(\bar{\mathbf{e}}'\cdot\mathbf{e})(\mathbf{e}\cdot\mathbf{e}) \\ (\bar{\mathbf{e}}''\cdot\bar{\mathbf{e}})(\bar{\mathbf{e}}'\cdot\mathbf{e})(\mathbf{e}\cdot\mathbf{e}) \\ (\bar{\mathbf{e}}''\cdot\bar{\mathbf{e}})(\bar{\mathbf{e}}'\cdot\mathbf{e})(\mathbf{e}\cdot\mathbf{e}) \\ (\bar{\mathbf{e}}''\cdot\bar{\mathbf{e}})(\bar{\mathbf{e}}'\cdot\mathbf{e})(\mathbf{e}\cdot\mathbf{e}) \\ (\bar{\mathbf{e}}''\cdot\bar{\mathbf{e}})(\bar{\mathbf{e}}'\cdot\mathbf{e})(\mathbf{e}\cdot\mathbf{e}) \\ (\bar{\mathbf{e}}''\cdot\bar{\mathbf{e}})(\bar{\mathbf{e}}'\cdot\mathbf{e})(\mathbf{e}\cdot\mathbf{e}) \\ (\bar{\mathbf{e}}''\cdot\bar{\mathbf{e}})(\bar{\mathbf{e}}'\cdot\mathbf{e})(\mathbf{e}\cdot\mathbf{e}) \\ (\bar{\mathbf{e}}''\cdot\bar{\mathbf{e}})(\bar{\mathbf{e}}'\cdot\mathbf{e})(\mathbf{e}\cdot\mathbf{e}) \\ (\bar{\mathbf{e}}''\cdot\bar{\mathbf{e}})(\bar{\mathbf{e}}'\cdot\mathbf{e})(\mathbf{e}\cdot\mathbf{e}) \\ (\bar{\mathbf{e}}''\cdot\bar{\mathbf{e}})(\bar{\mathbf{e}}'\cdot\mathbf{e})(\mathbf{e}\cdot\mathbf{e}) \\ (\bar{\mathbf{e}}''\cdot\bar{\mathbf{e}})(\bar{\mathbf{e}}'\cdot\mathbf{e})(\mathbf{e}\cdot\mathbf{e}) \\ (\bar{\mathbf{e}}''\cdot\bar{\mathbf{e}})(\bar{\mathbf{e}}'\cdot\mathbf{e})(\mathbf{e}\cdot\mathbf{e}) \end{pmatrix}^{\mathrm{T}} . \qquad (5.3.2)$$

It is immediately apparent that with a set of field vectors that has little variation, there are few unique combinations of the field vectors. There are in fact just two, which will be displayed at the next stage.

Next, we will contract the response tensor with the rank 1 tensor formed of the molecular linear combinations,

$$\begin{pmatrix} \delta_{\lambda\mu}\delta_{\nu o}\delta_{\pi\rho} \\ \delta_{\lambda\mu}\delta_{\nu\pi}\delta_{o\rho} \\ \delta_{\lambda\mu}\delta_{\nu\rho}\delta_{o\pi} \\ \delta_{\lambda\nu}\delta_{\mu o}\delta_{\pi\rho} \\ \delta_{\lambda\nu}\delta_{\mu\pi}\delta_{o\rho} \\ \delta_{\lambda\nu}\delta_{\mu\rho}\delta_{o\pi} \\ \delta_{\lambda o}\delta_{\mu\nu}\delta_{\pi\rho} \\ \delta_{\lambda o}\delta_{\mu\pi}\delta_{\nu\rho} \\ \delta_{\lambda o}\delta_{\mu\rho}\delta_{\nu\pi} \\ \delta_{\lambda\pi}\delta_{\mu\nu}\delta_{o\rho} \\ \delta_{\lambda\pi}\delta_{\mu o}\delta_{\nu\rho} \\ \delta_{\lambda\pi}\delta_{\mu\rho}\delta_{\nu o} \\ \delta_{\lambda\rho}\delta_{\mu\nu}\delta_{o\pi} \\ \delta_{\lambda\rho}\delta_{\mu o}\delta_{\nu\pi} \\ \delta_{\lambda\rho}\delta_{\mu\pi}\delta_{\nu o} \end{pmatrix} \chi^{(5)}_{(\lambda\mu)(\nu o\pi\rho)} = \begin{pmatrix} \chi^{(5)}_{(\lambda\lambda)(\mu\mu\nu\nu)} \\ \chi^{(5)}_{(\lambda\lambda)(\mu\mu\nu\nu)} \\ \chi^{(5)}_{(\lambda\lambda)(\mu\mu\nu\nu)} \\ \chi^{(5)}_{(\lambda\mu)(\lambda\mu\nu\nu)} \\ \chi^{(5)}_{(\lambda\mu)(\lambda\mu\nu\nu)} \\ \chi^{(5)}_{(\lambda\mu)(\lambda\mu\nu\nu)} \\ \chi^{(5)}_{(\lambda\mu)(\lambda\mu\nu\nu)} \\ \chi^{(5)}_{(\lambda\mu)(\lambda\mu\nu\nu)} \\ \chi^{(5)}_{(\lambda\mu)(\lambda\mu\nu\nu)} \\ \chi^{(5)}_{(\lambda\mu)(\lambda\mu\nu\nu)} \\ \chi^{(5)}_{(\lambda\mu)(\lambda\mu\nu\nu)} \\ \chi^{(5)}_{(\lambda\mu)(\lambda\mu\nu\nu)} \\ \chi^{(5)}_{(\lambda\mu)(\lambda\mu\nu\nu)} \\ \chi^{(5)}_{(\lambda\mu)(\lambda\mu\nu\nu)} \\ \chi^{(5)}_{(\lambda\mu)(\lambda\mu\nu\nu)} \end{pmatrix} . \tag{5.3.3}$$

The result is consistent with that of equation (5.3.2), with just two distinct linear combinations appearing. Note, the indices associated with any one of the response tensors can be replaced with any Greek index that does not already appear; this is consistent with their epithet, dummy indices.

The final step is summing the appropriate elements from the weighting tensor to deliver the following result [166],

$$\langle\Gamma\rangle = \frac{\pi\hbar^5 c^6 k^6}{260\varepsilon_0^6 V^6} n(n-1)(n-2)(n-3)\left|\begin{pmatrix} (\bar{\mathbf{e}}''\cdot\bar{\mathbf{e}}')(\mathbf{e}\cdot\mathbf{e})^2 \\ (\bar{\mathbf{e}}''\cdot\bar{\mathbf{e}})(\bar{\mathbf{e}}'\cdot\mathbf{e})(\mathbf{e}\cdot\mathbf{e}) \end{pmatrix}^{\mathrm{T}} \begin{pmatrix} 3 & -4 \\ -4 & 12 \end{pmatrix} \begin{pmatrix} \chi^{(5)}_{(\lambda\lambda)(\mu\mu\nu\nu)} \\ \chi^{(5)}_{(\lambda\mu)(\lambda\mu\nu\nu)} \end{pmatrix}\right|^2 \rho_F \ .$$

(5.3.4)

The resulting tensor of field vectors both hold a vector product consisting of at least one $(\mathbf{e}\cdot\mathbf{e})$. If we refer to the vector products in complement 1F, we can see that in any setup adopting a circular polarised basis would deliver a vanishing result. However, both setups utilising plane polarised light, seen in Figure 18(a) and (b), deliver a nonzero result. The polarisation tensor for orthogonal detection with parallel field vectors is,

$$\begin{pmatrix} 1 & 1 \end{pmatrix}, \tag{5.3.5}$$

by substituting this into equation (4.3.4) we obtain,

$$\langle\Gamma\rangle \sim \left|-1\chi^{(5)}_{(\lambda\lambda)(\mu\mu\nu\nu)} + 8\chi^{(5)}_{(\lambda\mu)(\lambda\mu\nu\nu)}\right|^2 . \tag{5.3.6}$$

For orthogonal detection, where the field vectors are detected perpendicular to input, the polarisation tensor becomes,

$$\begin{pmatrix} 1 & 0 \end{pmatrix}, \tag{5.3.7}$$

and the corresponding quantum amplitude in the rate expression becomes,

$$\langle\Gamma\rangle \sim \left|3\chi^{(5)}_{(\lambda\lambda)(\mu\mu\nu\nu)} - 4\chi^{(5)}_{(\lambda\mu)(\lambda\mu\nu\nu)}\right|^2 . \tag{5.3.8}$$

From this setup, we can expect the emergent radiation to be primarily polarised parallel to the input, provided the materials have tensor components of comparable magnitude and sign. Furthermore, the following expression for DR can be succinctly expressed,

$$\rho_\perp = \left|\frac{3\chi^{(5)}_{(\lambda\lambda)(\mu\mu\nu\nu)} - 4\chi^{(5)}_{(\lambda\mu)(\lambda\mu\nu\nu)}}{-1\chi^{(5)}_{(\lambda\lambda)(\mu\mu\nu\nu)} + 8\chi^{(5)}_{(\lambda\mu)(\lambda\mu\nu\nu)}}\right|^2 . \tag{5.3.9}$$

The molecular responses displayed in this expression are scalar quantities that are not known. However, it is possible to determine the boundary values to which the DR can assume. These

are produced in the cases where either response term dominates over the other. It therefore follows that,

$$\frac{1}{4} \leq \rho_{\perp} \leq 9 \ . \tag{5.3.10}$$

4.4 STRUCTURED LIGHT

Experimental results from nonlinear optical processes in isotropic materials indicate $\alpha < 12^{o}$ [167]. For processes involving structured light, the equations delivered from the paraxial approximation are the most widely deployed, see §1.6. This approximation applies the small angle approximations to all angles deviating from the propagation axis. The conical emission can therefore expect to have an absolute error of less than 2% even at the upper limit conical emission angle.

This regime is consistent with the paraxial approximation commonly deployed for OAM light. Referring now to §1.6 where the corresponding field vectors are cast we can simply consider the matrix element, equation (5.2.4), as a product of the existing terms and the separable radial and azimuthal components of the beam,

$$f^{4}_{l,p}(\mathbf{r})\, \overline{f}_{l',p'}(\mathbf{r})\, \overline{f}_{l'',p''}(\mathbf{r})\, \mathrm{e}^{\mathrm{i}\left[(4\mathbf{k}-\mathbf{k}'-\mathbf{k}'')\cdot\mathbf{z}-(l-l'-l'')\phi\right]} \ . \tag{5.4.1}$$

Here, the absence of a prime relates the function to an input photon, with the single and double prime each correspond to one of the two emergent photons. The exponential term is the combined phase factor introduced in equation (1C.5). The first collection of functions, defined in equation (1.6.10), hold all radial distribution dependence of the respective photons of azimuthal and radial indices l and p, respectively. Both of these indices will also be included in the summation, they each represent one additional degree of freedom in the light. It is also noteworthy that the index p is often regarded to be 0, for the purposes of our investigation, this is a legitimate assumption. In the cases where $p > 0$ the radial intensity profile is split by p nodes, displayed in Figure 6; this splitting results in successively smaller contributions to the intensity profile. The maximum magnitude contribution is what we are concerned with, which is delivered by $p = 0$ [168]. Having said that, it is still included purely for generality and

completeness of the modal decomposition [169]. Recent work has even indicated that the radial index may have more significance than previously thought [170, 171].

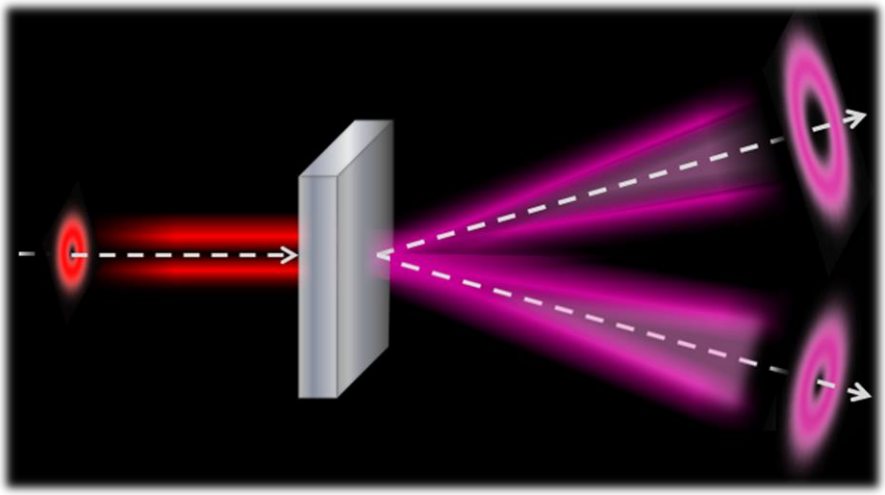

Figure 23: A schematic depiction of the regarded process. From left-to-right, the input beam of intercepts a nonlinear isotropic media and a single centre creates two photons of $l' = 3$ (top) and $l'' = 1$ (bottom). The cone can be envisaged tracing a shaved pencil tip pressed against the media, with $\mathbf{k}'$ and $\mathbf{k}''$ emerging along two diametrically opposed axes.

We will now consider a system where conservation arguments extend to the OAM parameters. Hence, for six-wave SHG we can say,

$$l' + l'' = 4l \ . \tag{5.4.2}$$

If we first consider an input beam comprising purely of a mode $l = 1$, it follows that $l' + l'' = 4$. By selecting $l' \geq l''$ we can see that there are three possible pairings for the emergent photons (l', l''): $(4,0)$, $(3,1)$ and $(2,2)$. Figure 24(a) displays cross sections for the relative magnitudes of the three outputs, as produced by equation (5.4.1). As can be seen there is no difference in displacement from the input beam axis, *i.e.* the conical angle is equivalent for each output pairing. The uniform transverse cross section of the intensity distribution of the conical emission is displayed in Figure 24(b). I would like to thank Matt M. Coles for providing these simulations [172]. They were performed in a region well removed from that of the conversion material. Experimentally, the closer any measurements are made to the conversion centre, the greater the influence of uncertainty in the angle-angular momentum quantum uncertainty [173-176].

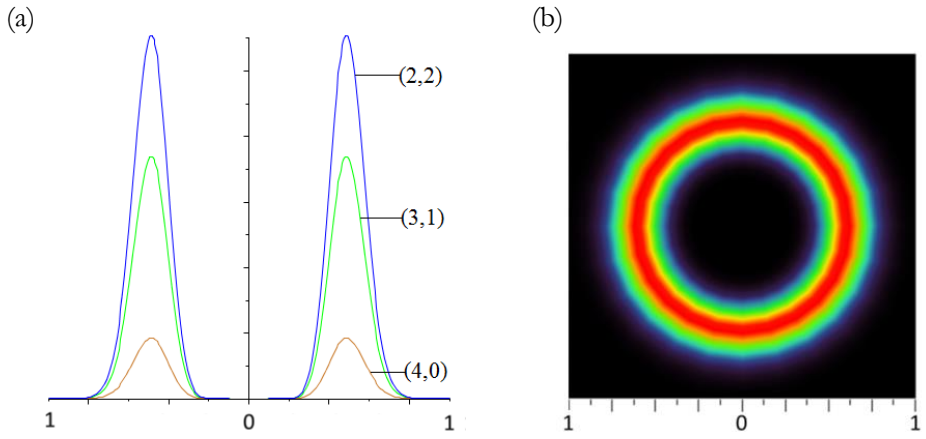

Figure 24: (a) A cross section of magnitude distribution, where the y-axis is aligned with the input axis. It demonstrates the relative magnitude in output of the three permitted pairings of topological charges, (l',l''). (b) A transverse intensity distribution around the input beam axis. The (2,2) output has been selected in this case, where red indicates high intensity, through to black where there is zero intensity. The calculations have been performed at a distance of 100 wavelengths from the conversion material, adopting a source laser of wavelength of 800 nm.

Upon inspecting the relative maximum magnitudes in Figure 24(a), a familiar structure is seen. The three permissible OAM pairings of the harmonic photons appear to follow the series for the binomial coefficients of order equal to the sum topological charge. If we cast the emergent photons as a product of states $|l'\rangle_{k'}|4-l'\rangle_{k''}$ and acknowledge the arbitrary distinction between l' and l'', the product of states can be expressed more simply as, $|l':4-l'\rangle$. The relative weightings for each product of states are summarised in Table 15. Note that when $l'\neq l''$, there are two possible products of states, $|l':l''\rangle=|l'':l'\rangle$, this results in double the contribution to the resultant field.

Table 15: Relative magnitudes of the intensities for permitted combinations of OAM output for the harmonic photons.

Product of states	$\|4:0\rangle$	$\|3:1\rangle$	$\|2:2\rangle$
Relative magnitude	1	4	3

The Pascalian distribution arising without any combinatorial dependence introduced in the establishing of the theory is interesting in itself. Although, of a potentially wider interest may be the interdependence of the topological charge for the two photons. By detecting either photon, the knowledge of the topological charge of its harmonic pair is instantly known. This is indicative of quantum entanglement between the pair of photons, which is a feature of quantum mechanics that is of experimentally widespread interest [177-180]. In this regard, parallels to parametric down-conversion can be drawn, however, the distribution of harmonic emission is unique to six-wave mixing.

4.5 DISCUSSION

The process considered in this chapter combines two far reaching fields: nonlinear and structured optics. The intersection of these two fields has been of growing interest in recent years [181, 182], most often concerned with four-wave parametric processes [183, 184]. Six-wave mixing is a useful technique to subvert the selection rules of SHG in materials of high symmetry; moreover, by considering the addition of structured light, it can be seen as an up-conversion counterpart to processes such as parametric down-conversion. Recent methods of detection are found to be able to scrutinise OAM modes to near perfect efficiency [26, 185-187]. These innovations will be particularly valuable as efforts are made to secure the conservation laws governing parametric processes. Here, the preferential emission of a specific topological charge in the harmonic-emission was observed, which has not been demonstrate in any conversion process.

In this chapter and the proceeding chapter methods for second-harmonic emission were discussed. One additional method that is commonly deployed to subvert the symmetry rules is that of SHG in a static electric field. This adds an additional interaction, which results in the requisite even number of interaction events; the additional interaction not imparting any change in energy to the system. In principle, a second centre could serve the same purpose, by deploying the static V-tensor, equation (1.5.2). This would be an analogous mechanism to that covered in §2.2.3.

5

DIRECT GENERATION OF STRUCTURED LIGHT

5.1 INTRODUCTION

Since the inception of vortex light, the interest in the field has grown rapidly. The key developments seek to perfect the purity and detection of vortex modes. Such advances hold promise in data transmissions and novel manipulation techniques. Despite all the developments, one limitation has held back the application of such forms of light. Up until recently, the only way of creating OAM modes of light has been by deploying optical elements to modify the wavefront of a pre-existing beam. This in turn imparts the characteristic helical progression in wavefront, which conveys units of topological charge, introduced in §1.6. However, such methods are reliant on equipment to not only generate but also transform the light to the desired structure. The additional stage of production requires additional parts and this in turn demands more space. In the current arena of perpetually slimmer and more compact technologies, there is not the capacity for such inefficiencies.

For this reason, the prospect of direct generation of vortex light is particularly pivotal to the ongoing success of this field. In particular, with commercial applications in mind. This chapter introduces one method theorised to fill this gap [188-190] and at the time of writing, it is the only solution to be found in the literature. The proposed mechanism relies on a series of chromophores equally spaced on a ring. By orienting them such that they can support a delocalised excitation (exciton) across an array with tailored symmetry characteristics, the ensuing results indicate that a vortex emission can be produced directly.

5.2 ARRAY CONFIGURATION

There are stringent conditions that must be met to elicit an emission with a non-zero topological charge. Due consideration must be taken over the characteristics of the produced light and how that can be married by the structure of the emitters. Figure 25 provides an impression of a system satisfying these requirements. To begin, we must consider the structure of the desired emission, namely the characteristic azimuthal variation in phase it displays. Next, we can consider a structure that can manifest this azimuthal 2π progression in phase. It has been shown that one lone emitter is not capable of producing such a structure, to any level of multipolar structure [191, 192]. The next logical step is to consider a pair of emitters that attempt to enforce the desired phase structure by being π out of phase with the other. Although this is part way towards the solution, it can be seen that we are not quite there. The phase at the two positions is indeed as desired, however, careful consideration must also be taken over the phase of the intervening space. Namely the azimuthal progression in phase, with just two emitters there is no means to dictate the direction that the phase progression asserts and as such neither is favoured and a planar discontinuity in phase bisects the pair of emitters [193].

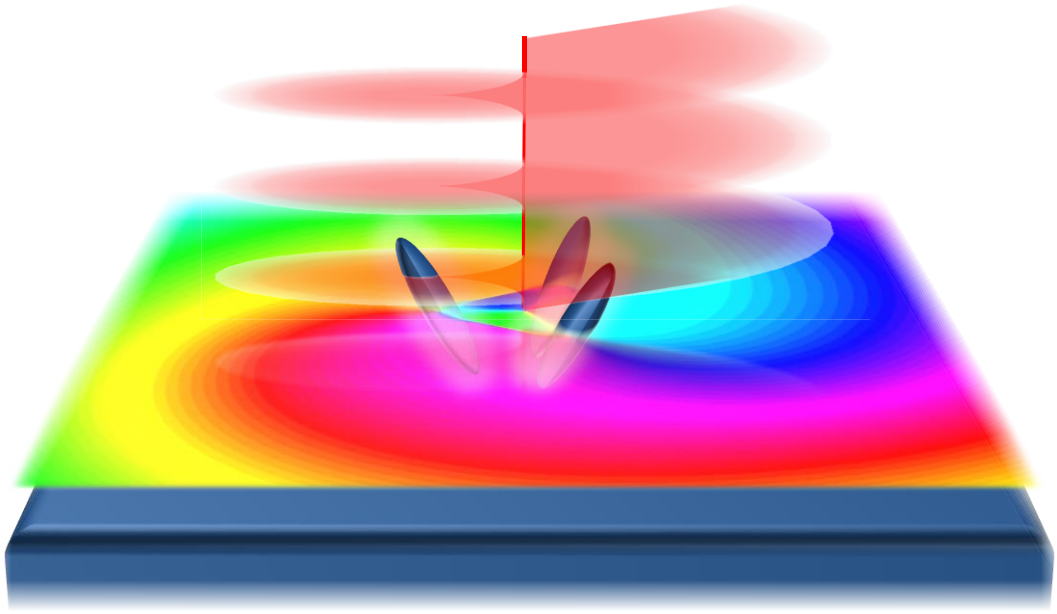

Figure 25: An impression of a permissible structure conforming to point group C_3 to support an exciton of phase cross-section displayed, which in turn relaxes to produce a helical emission of $l=1$.

In contrast, an array consisting of three emitters does not suffer such limitations. Specifying the phase at three coordinates not only enforces a phase progression but also a directionality. There are in fact two circularities that can be achieved from such an array and these correspond to the two handednesses of helicity light can manifest. Importantly, this indicates that each array is not limited to a single functionalised emission, but in fact any number of different excitonic structures, which will be shown to be dictated by the number of centres in the array. Another consideration are the conditions to which each emitter must satisfy. To achieve an excitation with directionality, non-spherical emitters are required. For the purposes of this work, we will discuss the most familiar option of molecules. However, the theory detailed in this chapter can readily be applied to other forms of emitter, such as planar chiral metamaterials [194-198].

Increasing the number of points with a dictated phase, introduced by an additional emitter each time, enables increasingly complex topologies of phase; this will be shown later. Moreover, by considering more than three emitters an array can escape the confines of a single planar arrangement. However, the planar arrangements offer a uniform increase in maximum topological charge supported and are the focus of this work.

The many structural considerations for the array of emitters can be met by a number of the symmetry groups in the Schoenflies point group tables [105, 199]. Specifically, we require a biaxial degeneracy in the array plane, with no mirror symmetry down the emission axis. The reasoning for this is analogous to why an array of two emitters was not capable of supporting the directionality in phase progression. Inspecting the tables for these conditions, the following symmetry groups prove suitable: C_n, $C_{n\mathrm{h}}$, S_n, T and T_h, where n directly corresponds to the number of emitters in the array.

The desired delocalised electronic excitation is generally associated with the doubly degenerate irreps, hence it is the radiative decay of the corresponding states that is of interest here [200]. We must assume that any excitation returns the entire array to its ground state, which conforms to its totally symmetric representation. This ensures that the product of the representations for the excited state and the radiative dipolar emission both include totally symmetric

representations. Table 1 compiles the complete set of members of each family of symmetry groups that permit integer values of OAM for an array of up to $n = 12$. Moreover, it concludes with an expression to predict the supported range of OAM values for any given symmetry group.

Table 16**:** Summary of the allowed topological charge l, for OAM outputs based on arrays of the allowed symmetry groups. For the S_n groups, $m = 0$ if $i \notin \{S_n\}$; $m = 1$ if $i \in \{S_n\}$. The entries in the last row, for the general case, express the necessary conditions incorporating a *floor function* [201]. All point groups that do not exist are greyed out and the ones with dashes indicate they exist but do not support any non-zero topological emission. Note, T and T_h also support an emission of a single unit of topological charge, $|l| \leq 1$.

n	C_n	C_{nh}	S_n
1	-		
2	-	-	
3	1	1	
4	1	1	1
5	1, 2	1, 2	
6	1, 2	1, 2	1
7	1, 2, 3	1, 2, 3	
8	1, 2, 3	1, 2, 3	1, 2, 3
9	1, 2, 3, 4	1, 2, 3, 4	
10	1, 2, 3, 4	1, 2, 3, 4	1, 2
11	1, 2, 3, 4, 5	1, 2, 3, 4, 5	
12	1, 2, 3, 4, 5	1, 2, 3, 4, 5	1, 2, 3, 4, 5
General expression	$\lvert l\rvert \leq \left\lfloor \frac{n-1}{2} \right\rfloor$		$\lvert l\rvert \leq \left\lfloor \left(\frac{1}{2}\right)^m \frac{n-2}{2} \right\rfloor$

Cross-referencing Table 16 with Figure 25, we can see that a C_3 is capable of supporting a maximum magnitude of topological charge of 1, which agrees with what has been said previously. It follows that for an array of such geometry, the supported emissions are that of $l = \{-1, 0, 1\}$. To proceed further we will now consider the set of coordinates that describe a general array conforming to one of either of point groups C_n or C_{nh}. All systems based on these symmetry groups are planar arrangements of the constituent molecules. Each array is formed of n emitters equally dispersed on a ring with Figure 26 displaying one example where $n = 7$.

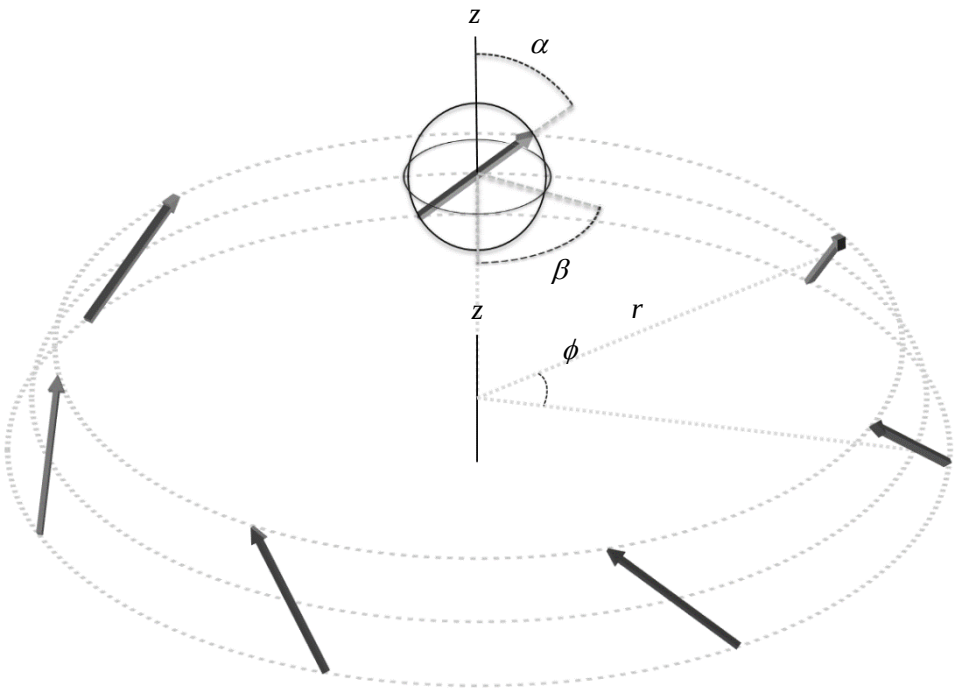

Figure 26: Schematic depiction of the array of seven emitters. The emission axis is that of the z-axis in the centre of the plane. The angles α and β dictate the local orientation of each and every emitter. The angle ϕ designates the azimuthal position in the array. Here, $\alpha = \beta = \pi/4$ and $\phi = 2\pi/7$. The circumferential dotted lines serve as visual guides only.

The figure above can be seen to conform to the point group C_7. From here, it is easy to envisage a collection of arrangements consistent with C_{7h} symmetry, which requires a plane of mirror symmetry perpendicular to the emission axis. To achieve this $\alpha = \pi/2$. Notice that several emitter arrangements would result in C_{7v}, namely: $\alpha = 0$ and $\beta = 0$ or π. These arrangements are undesirable for the aforementioned addition of mirror planes of symmetry along the emission axis.

5.3 EXCITON HAMILTONIAN AND WAVEFUNCTIONS

Now an appropriate set of structures have been determined, let us regard the delocalised excitonic state they can support and the associated energies. In such a system, any number of emitters can potentially be excited at once; however, for analogous reasons that have been mentioned with previous chapters, a single excitation is most probable and will be developed further. As such, all other centres will be in their ground state dispersed by a distance such that

the most dominant interaction will be that with each neighbour. This can be modelled by utilising the V-tensor, equation (1.5.1), to determine the electrodynamic coupling between neighbouring transitions. We will use a modified form here to specify which emitters are coupled,

$$\mathbf{V}(\mathbf{R}_{rs}) \equiv V_{r,(r+1)\bmod n}\left(k_u, \mathbf{R}_{r,(r+1)\bmod n}\right), \tag{5.3.1}$$

Here, $k_u = E_u/\hbar c$ and E_u is the energy of an isolated centre in its excited state u. The resulting energy of the interaction between two neighbouring centres can be obtained by,

$$U = \boldsymbol{\mu}_r \cdot \mathbf{V}(\mathbf{R}_{rs}) \cdot \boldsymbol{\mu}_s \equiv \frac{\mathrm{e}^{\mathrm{i}k_u R}}{4\pi\varepsilon_0 R^3}\Big[\left\{1 - \mathrm{i}k_u R - (k_u R)^2\right\}\left(\boldsymbol{\mu}_1^{0u} \cdot \boldsymbol{\mu}_2^{0u}\right) - \left\{3 - 3\mathrm{i}k_u R - (k_u R)^2\right\}\left\{\left(\boldsymbol{\mu}_1^{0u} \cdot \hat{\mathbf{R}}_{12}\right)\left(\boldsymbol{\mu}_2^{0u} \cdot \hat{\mathbf{R}}_{12}\right)\right\}\Big]. \tag{5.3.2}$$

The presence of pairwise coupling across the system indicates that a stationary state is not immediately achieved. To discover the stationary state that will be reached, let us consider a block diagonalised form of the appropriate Hamiltonian for such an array. The stationary states follow, in the form of superpositions of the basis states with normalised coefficients [202]. In general, the above system will have a Hamiltonian that may be expressed in matrix form as follows:

$$H_{rs} = E_u \delta_{rs} + U\left\{\delta_{r-1,s(\bmod n)} + \delta_{r(\bmod n),s-1}\right\}, \tag{5.3.3}$$

where each element of the n-square matrix relates to a pair of emitters $\{r,s\} \in \mathbb{N}$. The contents of the curly braces only engage adjacent centres corresponding to off-diagonal positions of the matrix as well as connecting the end of the cycle back to that of the first. By diagonalising the Hamiltonian,

$$\begin{aligned} 0 &= \det\left[H_{rs} - \lambda I\right] \\ &= \det\left[\left(E_u - \lambda\right)\delta_{rs} + V\left(\delta_{r-1,s(\bmod n)} + \delta_{r(\bmod n),s-1}\right)\right], \end{aligned} \tag{5.3.4}$$

we can obtain the eigenstates corresponding to the splitting in the excited states (see §5.4). The normalised eigenfunction associated with the exciton for a general array consisting of n centres can be cast as follows,

$$\left|\psi_p\right\rangle = \frac{1}{\sqrt{n}}\sum_{r=1}^{n}\left\{\varepsilon_n^{(r-1)p}\left|\xi^{r;u}\right\rangle\prod_{s\neq r}\left|\xi^{s;0}\right\rangle\right\}, \tag{5.3.5}$$

where $p \in \mathbb{N}$. In this linear combination, $\left|\xi^{r;u}\right\rangle$ is a state function corresponding to an emitter r in electronic state u, and $\varepsilon_n = \exp\left(2\mathrm{i}\pi/n\right)$, which is the difference in phase for each of the emitters. Each summand contains one centre is in an electronically excited state u, while the others remain in their ground states. The energy eigenvalues associated with the above exciton states are generally expressible in the form;

$$E_p = E_u + 2U\cos\left(2pq/n\right), \tag{5.3.6}$$

with $-\lfloor(n-1)/2\rfloor < q \leq \lfloor n/2\rfloor$ and with this index q related to p in equation (5.3.5) through:

$$q = \begin{cases} p \mid p \leq \lfloor n/2\rfloor \\ p-n \mid p > \lfloor n/2\rfloor \end{cases}. \tag{5.3.7}$$

Table 17, summarises the relationships between the indexes p, q for arrays comprising of three to nine emitters. The irreducible representation of the corresponding family of point groups C_n, which are associated with each excitonic state are also displayed. In this table, a strong correlation can be seen between the permitted l-values and the index q. This is the case for all instances, except when p is even and an antisymmetric representation, B, is present. The subsequent section will scrutinise the q values and each of their associated energies of the excitonic states.

Table 17: The irreps of the C_n excited states for $n = \{3:9\}$.

n	p	1	2	3	4	5	6	7	8	9
3	q	1	-1	0						
	Irrep	E_1	E_1	A						
4	q	1	2	-1	0					
	Irrep	E_1	B	E_1	A					
5	q	1	2	-2	-1	0				
	Irrep	E_1	E_2	E_2	E_1	A				
6	q	1	2	3	-2	-1	0			
	Irrep	E_1	E_2	B	E_2	E_1	A			
7	q	1	2	3	-3	-2	-1	0		
	Irrep	E_1	E_2	E_3	E_3	E_2	E_1	A		
8	q	1	2	3	4	-3	-2	-1	0	
	Irrep	E_1	E_2	E_3	B	E_3	E_2	E_1	A	
9	q	1	2	3	4	-4	-3	-2	-1	0
	Irrep	E_1	E_2	E_3	E_4	E_4	E_3	E_2	E_1	A

5.4 STRUCTURE OF THE EXCITONIC ENERGY LEVELS

Each exciton structure has been shown to display different symmetry characteristics, represented by E_q, A (and also B, if present). Each unique form of symmetry for a given array will have a corresponding unique energy level, which will manifest as a fine line splitting, centred on the frequency of an isolated emitter. If we first consider the simplest case displayed in Table 17, where an array comprises of $n = 3$ emitters. Substituting the appropriate values for p and q into equation (5.3.6), we obtain the energies for the three exciton levels: one non-degenerate state, which conforms to the totally symmetric representation A, and energy $E_u - 2U$; the other two form a doubly degenerate E_q representation, with energies $E_u + U$.

In principle, the difference in energies between irreps should enable the preferential selection of one symmetry type and thus associated form of emission [202]. The decay of the doubly degenerate E_q excitons should have a characteristic wavelength of emission, relative to the array structure and initial excitation level. The degeneracy of the E_q excitons is a satisfying result, which is consistent with expectation for the two handednesses of two vortex emissions of equivalent $|l|$. Furthermore, incorporating the desired transition dipole moment vectors, such as those displayed in Figure 26, into equation (5.3.2) the sign of U is readily shown to be positive for all $n \geq 3$. This is also encouraging, if we refer to Kasha's rule, which usually is applied to vibrational sublevels, we can see there is a preferential emission from the lowest-lying energy sublevel, for these purposes this corresponds to the emission of highest $|l|$. These principles have now been applied to the $n = 9$ case from Table 17 and the resultant energy level splitting is displayed in Figure 27.

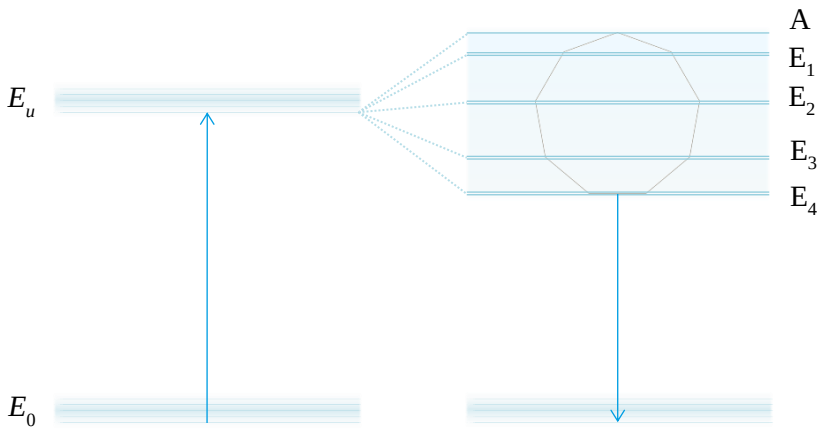

Figure 27: Excitonic irreducible representations and corresponding Davydov energy level splitting of for an array of C_9 point group symmetry. The regular nonagon has been displayed to emphasise the relative displacement in line splitting. $\mathrm{A} = E_u + 2U$, $\mathrm{E}_1 = E_u + 1{\cdot}532U$, $\mathrm{E}_2 = E_u + 0{\cdot}347U$, $\mathrm{E}_3 = E_u - U$ and $\mathrm{E}_4 = E_u - 1{\cdot}879U$. The excitation considered is by a red-edge laser and the magnitude of splitting has been exaggerated for visibility.

5.5 EXCITON PHASE STRUCTURE

To corroborate the assignment of vortex emission from the specified array structures and irreps, an analysis of the phase structure of each excitonic state can be made and so too the radiative emission. The electric field $\mathcal{E}_p(\mathbf{R}_D)$ from each constituent emitter is given by,

$$\mathcal{E}_p(\mathbf{R}_D) = \sum_r^n \frac{e^{ikR_{Dr}}\varepsilon_n^{(r-1)p}}{4\pi\varepsilon_0 R_{Dr}^3}\left\{\left[\left(\hat{\mathbf{R}}_{Dr}\times\boldsymbol{\mu}_r^{0u}\right)\times\hat{\mathbf{R}}_{Dr}\right]k^2R_{Dr}^2 + \left[3\hat{\mathbf{R}}_{Dr}\left(\hat{\mathbf{R}}_{Dr}\cdot\boldsymbol{\mu}_r^{0u}\right)-\boldsymbol{\mu}_r^{0u}\right](1-ikR_{Dr})\right\}, \tag{5.5.1}$$

where $\mathbf{R}_D$ signifies the position of the detector with respect to the ring centre. Notably, in this equation the phase factor, $\varepsilon_n^{(r-1)p}$, corresponds to that of the emitter component in equation (5.3.5) and thus delivers the sought progression in phase around the ring. The phase of the emission can be determined by taking the complex argument of the electric field vector,

$$\theta_i(\mathbf{R}) = \arg\left\{\mathcal{E}_{p;i}(\mathbf{R}_D)\right\}. \tag{5.5.2}$$

The electric field is decomposable into its Cartesian components, which in turn allows us to scrutinise the phase of each of the three orthogonal planes. The displayed phase simulations are produced by first establishing a series of emitters with vectors representing the respective transition moments that conform to a permitted symmetry group. The desired $2p\pi/n$ phase progression is then imposed on each of the centres. With all that done, the expression for the electric field can be called on and a grid produced with the associated phase of each point. Note, that due care needs to be taken around the singular axis. The phase simulations display the characteristic azimuthally varying phase structure associated with LG light. The spiral structure seen here, is describable as a linear superposition of the more commonly seen radially symmetric lines of constant phase, for example those seen in Figure 7.

Figure 28 displays a collection of results for the electromagnetic phase variation centred on an array conforming to the C_n family of point groups. The first plot (top-left) displays the two-emitter case, reinforcing the earlier assertion that two emitters can indeed not support a non-zero topological charge. The next panel (top-right) displays five emitters supporting an excitonic phase consistent with $l = 1$. Moving to the next row (bottom-left) five emitters are displayed again, this time with $l = -1$; this also has an intensity weighting incorporated, which displays a sharp reduction in intensity once the phase spirals through $2\pi^{c}$ and repeats this cycle outwards. The final panel displays the simulation from $n = 21$, $l = 10$ and demonstrates the more complex phase structures that such an array can support.

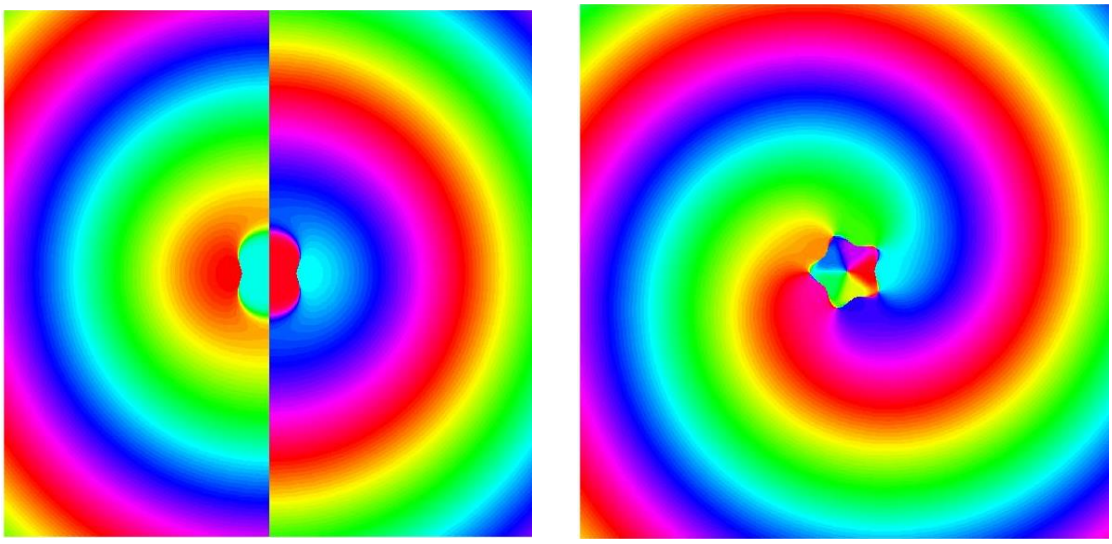

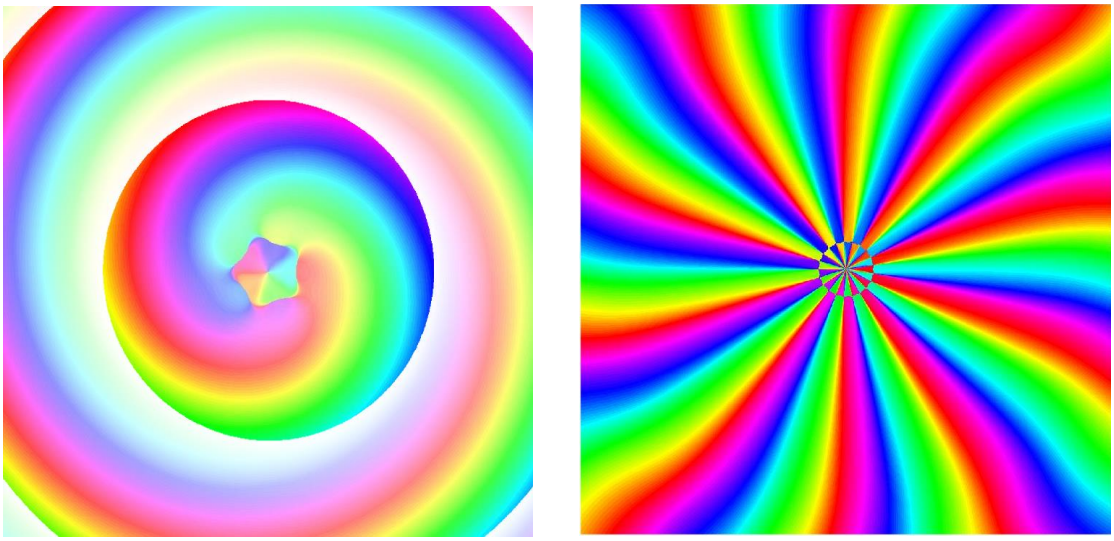

Figure 28: Phase cross-sections perpendicular to the emission axis. From left-to-right and top-to-bottom, they display: $n=2$ with no topological charge supported; $n=5,\ l=1$; $n=5,\ l=-1$ with an intensity weighting introduced; $n=21,\ l=10$. Each colour represents a different phase, with each diagram displaying a $2l\pi^{c}$ azimuthal progression. For these simulations $\alpha=\beta=\pi/4$ and hence each of the arrays conform to the respective C_n point group. In these plots the radius of the array is $\lambda/200\pi$, where λ is the optical wavelength of emission. The simulation cross-section has a length of $\lambda/20\pi$.

5.6 Discussion

In this chapter, a novel mechanism for the direct generation of vortex light is proposed. To achieve an emission of this sought character, the symmetry properties of a delocalised excitonic state are exploited; which can be of a more complex multipolar form than that which is a single emitter is capable of. The phase of the excitonic field is simulated and displays the characteristic azimuthally variation, most commonly associated with that of LG light. There are many advantages of implementing such a method, which will be discussed.

Here, a series of optical centres dispersed on a surface was considered. This would require the manufacture of bespoke arrays to provide pairwise nanoscale coupling [203, 204]. However, there may be alternate more amenable means. Arrays of quantum dots may be capable of eliciting the desired emission [205], especially following work displaying directional emission [206]. The emitters could be formed by deposition techniques [207, 208], such as those utilised

in chiral layered structures [209]. Metamaterial structures could be manufactured [210, 211], where analogous symmetry principles have been deployed to produce OAM modes [212, 213]. Or indeed lithographic techniques to etch such a structure out of a suitable substrate [214-216]. Lastly, a multi-chromophore array [217, 218] could be capable of supporting an emission of the sought character. To ensure their suitability, all electronic transitions in each chromophore would have to be optically distinct from the other centres.

The drive for miniaturisation in technology would suggest that this mechanism would be more desirable than the current alternatives, particularly in a commercial setting. By incorporating any of the above techniques this mechanism would offer a means of generating vortex modes benefiting from fewer parts. For example, the most widely deployed method for generation OAM modes is that of a spatial light modulator, which are collections of optical elements that are about the same size as a portable computer. Compared to rival devices, they benefit from the dynamic production of a range of OAM modes by passing light through an appropriate hologram for the desired phase structure [187]. It has also been demonstrated that the arrays described herein can support a range of topological charges dictated by the number of emitters it comprises of. Importantly, the full set of l-values are supported up to and including $\lfloor (n-1)/2 \rfloor$ for a given number of emitters. Although this work has not yet been implemented experimentally, it has led to several developments utilising spatial light modulators to sample a hologram in a fashion analogous to the phase progression in an array [219, 220].

Each excitonic state will relax to produce a single quanta of light with a corresponding phase structure. The production of single structured photon is particularly interesting for data transmission applications, where topological charge represents a degree of freedom with a range of values much greater than that of binary spin polarisation basis [185, 221-223]. Although, there is a quantum uncertainty associated with photon number-phase [224, 225]; moreover, the true information conveyable by a photon is recently coming under growing scrutiny [226, 227]. It is conceivable that the emission could also be tuneable, with the wavelength of emission unique for a given l-value for a particular array. This also holds promise in the detection and identification of topological charges. Consider an array that has had the energies for each of its

OAM modes characterised, the detection of a specific frequency could then be tied to the associated mode.

There are many instances, for example the processes introduced in the preceding chapters, where higher intensities of light are desired. In principle, multiple arrays could be distributed to produce a laser-like emission. If this could be achieved, there would be no reduction in intensity that is present in current technologies that exploit optical elements to modify a beam [228]. A collection of arrays could conceivably undergo a population inversion, with suitable phase-matching across the system, which would result in a stimulated emission perpendicular to the array plane. Many of the methods previously mentioned could be exploited to manufacture such a vortex laser.

POSTLUDE

This thesis has drawn on fundamental molecular quantum electrodynamical theory to tackle interactions involving both nonlinear and structured light with matter; in particular, systems with high degrees of symmetry. To round off this thesis, we shall consider how each project might continue to evolve.

The first novel research project, chapter 2, discussed the modifications to a Raman spectrum, for a molecule of interest, resulting from neighbour interactions. The obvious next step was to identify the predicted modifications in computed and experimental systems. An ongoing collaboration with researchers at the Université Paris-Saclay seeks to achieve this.

The subsequent project, chapter 3, considered a mechanism that subverts conventional symmetry laws and accommodates a second harmonic signal to be detected from a centrosymmetric system. The ensuing results are in anticipation of sophisticated experiments, in which the tensor coefficients could be registered and used to characterise minerals.

The penultimate project, chapter 4, advanced the theory for nonlinear optics and structured light, with obvious scope to explore other, more exotic, forms of structured light. The results indicate an emission with a preferential topological charge, which could be scrutinised experimentally to exploit the entanglement between the emitted photons.

The final project, chapter 5, introduced a method for the *direct* generation of photons with an intrinsic topological charge. This work has attracted significant attention and is a nexus for several fields of keen interest, such as quantum informatics. The prospect of direct generation holds several advantages over currently employed wavefront modification techniques; particularly, with the view to commercialising vortex light technologies, in which miniaturisation is paramount. An obvious next step is to investigate the emission from several adjacent arrays. Moreover, it would be of particular interest to explore more complex structures, such as a series of stacked arrays, which could provide the basis for a vortex laser.

REFERENCES

1. "Measurement of Sunshine Duration," in *Guide to Meteorological Instruments and Methods of Observation* (World Meteorological Organization, 2008).
2. F. Dollar, P. Cummings, V. Chvykov, L. Willingale, M. Vargas, V. Yanovsky, C. Zulick, A. Maksimchuk, A. G. R. Thomas, and K. Krushelnick, "Scaling High-Order Harmonic Generation from Laser-Solid Interactions to Ultrahigh Intensity," Phys. Rev. Lett. **110**, 175002 (2013).
3. D. P. Craig and T. Thirunamachandran, *Molecular Quantum Electrodynamics: An Introduction to Radiation-Molecule Interactions* (Dover Publications, Mineola, NY, 1998).
4. V. Chernyak and S. Mukamel, "Path integral formulation of retardation effects in nonlinear optics," J. Chem. Phys. **100**, 2953 (1994).
5. J. C. Maxwell, "A dynamical theory of the electromagnetic field," Philosophical Transactions of the Royal Society of London **155**, 459 (1865).
6. W. E. Lamb and R. C. Retherford, "Fine structure of the hydrogen atom by a microwave method," Phys. Rev. **72**, 241 (1947).
7. J. Schwinger, "On quantum-electrodynamics and the magnetic moment of the electron," Phys. Rev. **73**, 416 (1948).
8. H. B. G. Casimir, "On the attraction between two perfectly conducting plates," Proc. Kon. Ned. Akad. Wetensch. **51**, 793 (1948).
9. H. B. G. Casimir and D. Polder, "The influence of retardation on the London-van der Waals forces," Phys. Rev. **73**, 360 (1948).
10. E. A. Power and T. Thirunamachandran, "The multipolar Hamiltonian in radiation theory," Proc. R. Soc. A **372**, 265 (1980).
11. A. Einstein, "Die Grundlage der allgemeinen Relativitätstheorie," Ann. Phys. (Berlin) **354**, 769 (1916).
12. E. Fermi, "Quantum theory of radiation," Rev. Mod. Phys. **4**, 87 (1932).
13. R. P. Feynman, "Space-time approach to quantum electrodynamics," Phys. Rev. **76**, 769 (1949).

14. R. D. Jenkins, D. L. Andrews, and L. C. Dávila Romero, "A new diagrammatic methodology for non-relativistic quantum electrodynamics," J. Phys. B: At. Mol. Opt. Phys. **35**, 445 (2002).
15. D. R. Mazur, *Combinatorics: A Guided Tour* (Mathematical Association of America, Washington, DC, 2010).
16. D. M. Bishop, "Molecular vibrational and rotational motion in static and dynamic electric fields," Rev. Mod. Phys. **62**, 343 (1990).
17. D. M. Bishop and B. Kirtman, "A perturbation method for calculating vibrational dynamic dipole polarizabilities and hyperpolarizabilities," J. Chem. Phys. **95**, 2646 (1991).
18. D. L. Andrews, "Harmonic generation in free molecules," J. Phys. B: At. Mol. Opt. Phys. **13**, 4091 (1980).
19. D. L. Andrews, "The role of longitudinal polarization in surface second-harmonic generation," J. Mod. Opt. **40**, 939 (1993).
20. D. C. Rodenberger, J. R. Heflin, and A. F. Garrto, "Excited-state enhancement of optical nonlinearities in linear conjugated molecules," Nature **359**, 309 (1992).
21. D. L. Andrews and D. S. Bradshaw, "Virtual photons, dipole fields and energy transfer: a quantum electrodynamical approach," Eur. J. Phys. **25**, 845 (2004).
22. A. Salam, *Molecular Quantum Electrodynamics: Long-Range Intermolecular Interactions* (Wiley, Hoboken, NJ, 2010).
23. D. L. Andrews and D. S. Bradshaw, "The role of virtual photons in nanoscale photonics," Ann. Phys. (Berlin) **526**, 173 (2014).
24. L. Mandel and E. Wolf, *Optical Coherence and Quantum Optics* (Cambridge University Press, Cambridge, NY, 1995).
25. N. Sonine, "Recherches sur les fonctions cylindriques et le développement des fonctions continues en séries," Mathematische Annalen **16**.
26. G. C. Berkhout, M. P. Lavery, J. Courtial, M. W. Beijersbergen, and M. J. Padgett, "Efficient sorting of orbital angular momentum states of light," Phys. Rev. Lett. **105**, 153601 (2010).

27. M. Mirhosseini, O. S. Magaña-Loaiza, M. N. O'Sullivan, B. Rodenburg, M. Malik, M. P. J. Lavery, M. J. Padgett, D. J. Gauthier, and R. W. Boyd, "High-dimensional quantum cryptography with twisted light," New J. Phys. **17**, 033033 (2015).
28. V. Potoček, F. M. Miatto, M. Mirhosseini, O. S. Magaña-Loaiza, A. C. Liapis, D. K. L. Oi, R. W. Boyd, and J. Jeffers, "Quantum Hilbert Hotel," Phys. Rev. Lett. **115**, 160505 (2015).
29. H. He, M. E. J. Friese, N. R. Heckenberg, and H. Rubinsztein-Dunlop, "Direct observation of transfer of angular-momentum to absorptive particles from a laser-beam with a phase singularity," Phys. Rev. Lett. **75**, 826 (1995).
30. M. E. J. Friese, H. Rubinsztein-Dunlop, J. Gold, P. Hagberg, and D. Hanstorp, "Optically driven micromachine elements," Appl. Phys. Lett. **78**, 547 (2001).
31. D. G. Grier, "A revolution in optical manipulation," Nature **424**, 810 (2003).
32. T. A. Nieminen, J. Higuet, G. G. Knöner, V. L. Loke, S. Parkin, W. Singer, N. R. Heckenberg, and H. Rubinsztein-Dunlop, "Optically driven micromachines: progress and prospects," Microelectronics, MEMS, and Nanotechnology (2005).
33. M. J. Padgett, "Light in a twist: optical angular momentum," Proc. SPIE **8637**, 863702 (2013).
34. N. B. Simpson, L. Allen, and M. J. Padgett, "Optical tweezers and optical spanners with Laguerre-Gaussian modes," J. Mod. Opt. **43**, 2485 (1996).
35. N. B. Simpson, K. Dholakia, L. Allen, and M. J. Padgett, "Mechanical equivalence of spin and orbital angular momentum of light: An optical spanner," Opt. Lett. **22**, 52 (1997).
36. T. A. Nieminen, N. R. Heckenberg, and H. Rubinsztein-Dunlop, "Optical measurement of microscopic torques," J. Mod. Opt. **48**, 405 (2001).
37. L. Chen, G. Zheng, and W. She, "Electrically and magnetically controlled optical spanner based on the transfer of spin angular momentum of light in an optically active medium," Phys. Rev. A **75**, 061403 (2007).
38. S. Furhapter, A. Jesacher, S. Bernet, and M. Ritsch-Marte, "Spiral phase contrast imaging in microscopy," Opt. Express **13**, 689 (2005).

39. M. W. Beijersbergen, L. Allen, H. E. L. O. Vanderveen, and J. P. Woerdman, "Astigmatic laser mode converters and transfer of orbital angular-momentum," Opt. Commun. **96**, 123 (1993).
40. V. Y. Bazhenov, M. Vasnetsov, and M. Soskin, "Laser beams with screw dislocations in their wavefronts," Jetp Lett **52**, 429 (1990).
41. V. Y. Bazhenov, M. Soskin, and M. Vasnetsov, "Screw dislocations in light wavefronts," J. Mod. Opt. **39**, 985 (1992).
42. L. Marrucci, C. Manzo, and D. Paparo, "Optical spin-to-orbital angular momentum conversion in inhomogeneous anisotropic media," Phys. Rev. Lett. **96**, 163905 (2006).
43. J. Sun, J. Zeng, and N. M. Litchinitser, "Twisting light with hyperbolic metamaterials," Opt. Express **21**, 14975 (2013).
44. M. W. Beijersbergen, R. P. C. Coerwinkel, M. Kristensen, and J. P. Woerdman, "Helical-wave-front laser-beams produced with a spiral phaseplate," Opt. Commun. **112**, 321 (1994).
45. N. R. Heckenberg, R. McDuff, C. P. Smith, and A. G. White, "Generation of optical-phase singularities by computer-generated holograms," Opt. Lett. **17**, 221 (1992).
46. A. S. Ostrovsky, C. Rickenstorff-Parrao, and V. Arrizón, "Generation of the "perfect" optical vortex using a liquid-crystal spatial light modulator," Opt. Lett. **38**, 534 (2013).
47. M. J. Padgett and L. Allen, "The Poynting vector in Laguerre-Gaussian laser modes," Opt. Commun. **121**, 36 (1995).
48. I. Newton, *Philosophiæ Naturalis Principia Mathematica* (London, 1687).
49. J. L. Lagrange, *Mécanique analytique* (Ve Courcier, 1811).
50. H. C. Oersted, "Experiments on the effect of a current of electricity on the magnetic needle," Annals of Philosophy **16**, 273 (1820).
51. M. Faraday, "Experimental researches in electricity," Philos. Trans. R. Soc. A **122**, 125 (1832).
52. W. R. Hamilton, "On a general method of expressing the paths of light and of the planets by the coefficients of a characteristic function," Dublin University Review **1**, 795 (1833).

53. J. H. Poynting, "On the transfer of energy in the electromagnetic field," Philosophical Transactions of the Royal Society of London **175**, 343 (1884).
54. H. Hertz, "Ueber die Einwirkung einer geradlinigen electrischen Schwingung auf eine benachbarte Strombahn," Ann. Phys. (Berlin) **270**, 155 (1888).
55. P. Lebedew, "Untersuchungen über die Druckkräfte des Lichtes," Ann. Phys. (Berlin) **311**, 433 (1901).
56. M. Planck, "Über das Gesetz der Energieverteilung im Normalspektrum," Ann. Phys. (Berlin) **309** (1901).
57. A. Einstein, "Über einen die Erzeugung und Verwandlung des Lichtes betreffenden heuristischen Gesichtspunkt," Ann. Phys. (Berlin) **17**, 132 (1905).
58. A. Einstein, "Zur Elektrodynamik bewegter Körper," Ann. Phys. (Berlin) **322**, 891 (1905).
59. A. Einstein, "Über die Entwicklung unserer Anschauungen über das Wesen und die Konstitution der Strahlung," Physik Journal **25**, 386 (1969).
60. G. I. Taylor, "Interference fringes with feeble light," Proceedings of Cambridge Philosophical Society **15**, 114 (1909).
61. J. H. Poynting, "The wave motion of a revolving shaft, and a suggestion as to the angular momentum in a beam of circularly polarised light," Proc. R. Soc. A **82**, 560 (1909).
62. E. Noether, "Invariante variationsprobleme," Nachrichten von der Gesellschaft der Wissenschaften zu Göttingen, Mathematisch-Physikalische Klasse **1918**, 235 (1918).
63. O. Laporte and W. F. Meggers, "Some rules of spectral structure," J. Opt. Soc. Am. **11**, 459 (1925).
64. G. N. Lewis, "The conservation of photons," Nature **118**, 874 (1926).
65. E. Schrödinger, "An undulatory theory of the mechanics of atoms and molecules," Phys. Rev. **28**, 1049 (1926).
66. P. A. M. Dirac, "The quantum theory of the emission and absorption of radiation," Proc. R. Soc. A **114**, 767 (1927).
67. J. R. Oppenheimer, "Note on the theory of the interaction of field and matter," Phys. Rev. **35**, 461 (1930).

68. C. Darwin, "Notes on the theory of radiation," Proc. R. Soc. A **136**, 36 (1932).
69. R. A. Beth, "Mechanical detection and measurement of the angular momentum of light," Phys. Rev. **50**, 115 (1936).
70. F. Bloch and A. Nordsieck, "Note on the radiation field of the electron," Phys. Rev. **52**, 54 (1937).
71. V. F. Weisskopf, "On the self-energy and the electromagnetic field of the electron," Phys. Rev. **56**, 72 (1939).
72. D. Gabor, "Theory of communication. Part 1: The analysis of information," Electrical Engineers-Part III: Radio and Communication Engineering, Journal of the Institution of **93**, 429 (1946).
73. S. Tomonaga, "On a relativistically invariant formulation of the quantum theory of wave fields," Progr. of Theor. Phys. **1**, 27 (1946).
74. H. A. Bethe, "The electromagnetic shift of energy levels," Phys. Rev. **72**, 339 (1947).
75. J. Schwinger, "Quantum electrodynamics. I. A covariant formulation," Phys. Rev. **74**, 1439 (1948).
76. F. J. Dyson, "The Radiation Theories of Tomonaga, Schwinger, and Feynman," Phys. Rev. **75**, 486 (1949).
77. E. A. Power and S. Zienau, "Coulomb gauge in non-relativistic quantum electro-dynamics and the shape of spectral lines," Philos. Trans. R. Soc. A **251**, 427 (1959).
78. E. P. Wigner, *Group Theory: And its Application to the Quantum Mechanics of Atomic Spectra* (Academic Press, New York, 1959).
79. T. Maiman, "Stimulated optical radiation in ruby masers," Nature **187**, 493 (1960).
80. P. A. Franken, G. Weinreich, C. W. Peters, and A. E. Hill, "Generation of optical harmonics," Phys. Rev. Lett. **7**, 118 (1961).
81. R. W. Terhune, P. D. Maker, and C. M. Savage, "Optical harmonic generation in calcite," Phys. Rev. Lett. **8**, 404 (1962).
82. R. J. Glauber, "Coherent and incoherent states of the radiation field," Phys. Rev. **131**, 2766 (1963).
83. J. Nye and M. Berry, "Dislocations in wave trains," Proc. R. Soc. A **336**, 165 (1974).

84. E. A. Power and T. Thirunamachandran, "Quantum electrodynamics with non-relativistic sources. I. Transformation to the multipolar formalism for second-quantized electron and Maxwell interacting fields," Phys. Rev. A **28**, 2649 (1983).

85. E. A. Power and T. Thirunamachandran, "Quantum electrodynamics with non-relativistic sources. II. Maxwell fields in the vicinity of a molecule," Phys. Rev. A **28**, 2663 (1983).

86. E. A. Power and T. Thirunamachandran, "Quantum electrodynamics with non-relativistic sources. III. Intermolecular interactions," Phys. Rev. A **28**, 2671 (1983).

87. E. Power and T. Thirunamachandran, "Quantum electrodynamics with nonrelativistic sources. IV. Poynting vector, energy densities, and other quadratic operators of the electromagnetic field," Phys. Rev. A **45**, 54 (1992).

88. E. Power and T. Thirunamachandran, "Quantum electrodynamics with nonrelativistic sources. V. Electromagnetic field correlations and intermolecular interactions between molecules in either ground or excited states," Phys. Rev. A **47**, 2539 (1993).

89. D. L. Andrews, "Symmetry characterization in molecular multiphoton spectroscopy," Spectrochim. Acta, Part A **46**, 871 (1990).

90. L. Allen, M. W. Beijersbergen, R. J. C. Spreeuw, and J. P. Woerdman, "Orbital angular momentum of light and the transformation of Laguerre-Gaussian laser modes," Phys. Rev. A **45**, 8185 (1992).

91. I. V. Basistiy, V. Y. Bazhenov, M. S. Soskin, and M. V. Vasnetsov, "Optics of light beams with screw dislocations," Opt. Commun. **103**, 422 (1993).

92. K. Dholakia, N. B. Simpson, M. J. Padgett, and L. Allen, "Second-harmonic generation and the orbital angular momentum of light," Phys. Rev. A **54**, R3742 (1996).

93. D. Bouwmeester, J.-W. Pan, K. Mattle, M. Eibl, H. Weinfurter, and A. Zeilinger, "Experimental quantum teleportation," Nature **390**, 575 (1997).

94. L. C. Dávila Romero, D. L. Andrews, and M. Babiker, "A quantum electrodynamics framework for the nonlinear optics of twisted beams," J. Opt. B: Quantum Semiclassical Opt. **4**, S66 (2002).

95. J. Courtial, K. Dholakia, L. Allen, and M. J. Padgett, "Second-harmonic generation and the conservation of orbital angular momentum with high-order Laguerre-Gaussian modes," Phys. Rev. A **56**, 4193 (1997).
96. J. A. R. Coope, R. F. Snider, and F. R. McCourt, "Irreducible cartesian tensors," J. Chem. Phys. **43**, 2269 (1965).
97. J. A. R. Coope and R. F. Snider, "Irreducible cartesian tensors. II. General formulation," J. Math. Phys. **11**, 1003 (1970).
98. E. A. Kearsley and J. Fong, "Linearly independent sets of isotropic Cartesian tensors of ranks up to eight," J. Res. Natl Bureau of Standards Part B: Math. Sci. B **79**, 49 (1975).
99. H. Jeffreys, "On isotropic tensors," Math. Proc. Camb. Phil. Soc. **73**, 173 (1973).
100. D. L. Andrews and T. Thirunamachandran, "On three-dimensional rotational averages," J. Chem. Phys. **67**, 5026 (1977).
101. D. L. Andrews and W. A. Ghoul, "Eighth rank isotropic tensors and rotational averages," J. Phys. A: Math. Gen. **14**, 1281 (1981).
102. D. H. Friese, M. T. P. Beerepoot, and K. Ruud, "Rotational averaging of multiphoton absorption cross sections," J. Chem. Phys. **141**, 204103 (2014).
103. M. D. Williams, J. S. Ford, and D. L. Andrews, "Hyper-Rayleigh scattering in centrosymmetric systems," J. Chem. Phys. **143**, 124301 (2015).
104. W. Heitler, *The Quantum Theory of Radiation* (Oxford University Press, Oxford, 1954).
105. J. A. Salthouse and M. J. Ware, *Point Group Character Tables and Related Data* (Cambridge University Press, London, 1972).
106. H. A. Mavromatis, "An interesting new result involving associated Laguerre polynomials," International journal of computer mathematics **36**, 257 (1990).
107. M. D. Williams, D. S. Bradshaw, and D. L. Andrews, "Raman scattering mediated by neighboring molecules," J. Chem. Phys. **144**, 174304 (2016).
108. M. D. Williams, D. S. Bradshaw, and D. L. Andrews, "On the emergence of Raman signals characterizing multicenter nanoscale interactions," Proc. SPIE **9884**, 98840N (2016).

109. D. L. Andrews and N. P. Blake, "Quantum electrodynamic study of bimolecular scattering effects in Raman-spectroscopy," Phys. Rev. A **41**, 2547 (1990).

110. D. L. Andrews and P. Allcock, *Optical Harmonics in Molecular Systems* (Wiley-VCH, Weinheim, 2002).

111. L. C. Dávila Romero, S. Naguleswaran, G. E. Stedman, and D. L. Andrews, "Electro-optic response in isotropic media " Nonlinear Opt. **23**, 191 (2000).

112. C. D. Allemand, "Depolarization Ratio Measurements in Raman Spectrometry," Appl. Spectrosc. **24**, 348 (1970).

113. D. P. Shelton, "Accurate hyper-Rayleigh scattering polarization measurements," Rev. Sci. Instrum. **82**, 113103 (2011).

114. D. A. Long, *The Raman Effect: A Unified Treatment of the Theory of Raman Scattering by Molecules* (Wiley, Chichester; New York, 2002).

115. A. F. Chrimes, K. Khoshmanesh, P. R. Stoddart, A. Mitchell, and K. Kalantar-zadeh, "Microfluidics and Raman microscopy: current applications and future challenges," Chem. Soc. Rev. **42**, 5880 (2013).

116. A. F. Palonpon, M. Sodeoka, and K. Fujita, "Molecular imaging of live cells by Raman microscopy," Curr. Opin. Chem. Biol. **17**, 708 (2013).

117. K. A. Antonio and Z. D. Schultz, "Advances in Biomedical Raman Microscopy," Anal. Chem. **86**, 30 (2014).

118. D. Cialla, A. März, R. Böhme, F. Theil, K. Weber, M. Schmitt, and J. Popp, "Surface-enhanced Raman spectroscopy (SERS): progress and trends," Anal. Bioanal. Chem. **403**, 27 (2011).

119. E. C. L. Ru and P. G. Etchegoin, "Single-Molecule Surface-Enhanced Raman Spectroscopy," Annu. Rev. Phys. Chem. **63**, 65 (2012).

120. Z. H. Kim, "Single-molecule surface-enhanced Raman scattering: Current status and future perspective," Front. Phys. **9**, 25 (2013).

121. S. Schlücker, "Surface-enhanced Raman spectroscopy: Concepts and chemical applications," Angew. Chem. Int. Ed. **53**, 4756 (2014).

122. Y. S. Yamamoto, Y. Ozaki, and T. Itoh, "Recent progress and frontiers in the electromagnetic mechanism of surface-enhanced Raman scattering," J. Photochem. Photobiol. C **21**, 81 (2014).

123. E. L. Keller, N. C. Brandt, A. A. Cassabaum, and R. R. Frontiera, "Ultrafast surface-enhanced Raman spectroscopy," Analyst **140**, 4922 (2015).

124. L. Rodriguez-Lorenzo, L. Fabris, and R. A. Alvarez-Puebla, "Multiplex optical sensing with surface-enhanced Raman scattering: A critical review," Anal. Chim. Acta **745**, 10 (2012).

125. H. Wang, X. Jiang, S.-T. Lee, and Y. He, "Silicon Nanohybrid-based Surface-enhanced Raman Scattering Sensors," Small **10**, 4455 (2014).

126. L. Yang, P. Li, and J. Liu, "Progress in multifunctional surface-enhanced Raman scattering substrate for detection," RSC Advances **4**, 49635 (2014).

127. D.-W. Li, W.-L. Zhai, Y.-T. Li, and Y.-T. Long, "Recent progress in surface enhanced Raman spectroscopy for the detection of environmental pollutants," Microchim. Acta **181**, 23 (2013).

128. Z. Li, M. J. Deen, S. Kumar, and P. R. Selvaganapathy, "Raman spectroscopy for in-line water quality monitoring—Instrumentation and potential," Sensors **14**, 17275 (2014).

129. S. McAughtrie, K. Faulds, and D. Graham, "Surface enhanced Raman spectroscopy (SERS): Potential applications for disease detection and treatment," J. Photochem. Photobiol. C **21**, 40 (2014).

130. D. L. Andrews and T. Thirunamachandran, "The hyper-Raman effect: A new approach to vibrational mode classification and assignment of spectral-lines," J. Chem. Phys. **68**, 2941 (1978).

131. D. Epperlein, B. Dick, G. Marowsky, and G. Reider, "Second-harmonic generation in centro-symmetric media," Appl. Phys. B **44**, 5 (1987).

132. M. D. Williams, J. S. Ford, and D. L. Andrews, "Mechanisms universally permitting hyper-Rayleigh scattering," Proc. SPIE **9347**, 934711 (2015).

133. D. M. Bishop, "Explicit Nondivergent Formulas for Atomic and Molecular Dynamic Hyperpolarizabilities," J. Chem. Phys. **100**, 6535 (1994).

134. S. Brasselet and J. Zyss, "Multipolar molecules and multipolar fields: probing and controlling the tensorial nature of nonlinear molecular media," J. Opt. B: Quantum Semiclassical Opt. **15**, 257 (1998).

135. T. Verbiest, L. Derhaeg, E. Kelderman, J. F. J. Engbersen, W. Verboom, D. N. Reinhoudt, K. Clays, and A. Persoons, "Determination of molecular hyperpolarizabilities by hyper Rayleigh scattering," in *Organic Materials for Non-linear Optics III* (Royal Society of Chemistry, Cambridge, 1994), pp. 326-331.

136. E. Hendrickx, K. Clays, and A. Persoons, "Hyper-Rayleigh Scattering in Isotropic Solution," Acc. Chem. Res. **31**, 675 (1998).

137. K. Clays and B. J. Coe, "Design strategies versus limiting theory for engineering large second-order nonlinear optical polarizabilities in charged organic molecules," Chem. Mater. **15**, 642 (2003).

138. S. Van Cleuvenbergen, I. Asselberghs, W. Vanormelingen, T. Verbiest, E. Franz, K. Clays, M. G. Kuzyk, and G. Koeckelberghs, "Record-high hyperpolarizabilities in conjugated polymers," J. Mater. Chem. C **2**, 4533 (2014).

139. M. Barzoukas, C. Runser, A. Fort, and M. Blanchard Desce, "A two-state description of (hyper) polarizabilities of push- pull molecules based on a two-form model," Chem. Phys. Lett. **257**, 531 (1996).

140. S. K. Yang, H. C. Ahn, S.-J. Jeon, I. Asselberghs, K. Clays, A. Persoons, and B. R. Cho, "First hyperpolarizabilities of dipolar, bis-dipolar, and octupolar molecules," Chem. Phys. Lett. **403**, 68 (2005).

141. P. C. Ray, "Size and Shape Dependent Second Order Nonlinear Optical Properties of Nanomaterials and Their Application in Biological and Chemical Sensing," Chem. Rev. **110**, 5332 (2010).

142. K. S. Suslick, C. T. Chen, G. R. Meredith, and L. T. Cheng, "Push-pull porphyrins as nonlinear optical materials," J. Am. Chem. Soc. **114**, 6928 (1992).

143. S. M. LeCours, H.-W. Guan, S. G. DiMagno, C. Wang, and M. J. Therien, "Push-pull arylethynyl porphyrins: new chromophores that exhibit large molecular first-order hyperpolarizabilities," J. Am. Chem. Soc. **118**, 1497 (1996).

144. I. D. Albert, T. J. Marks, and M. A. Ratner, "Large molecular hyperpolarizabilities in "push-pull" porphyrins. Molecular planarity and auxiliary donor-acceptor effects," Chem. Mater. **10**, 753 (1998).

145. M. Yeung, A. C. Ng, M. G. Drew, E. Vorpagel, E. M. Breitung, R. J. McMahon, and D. K. Ng, "Facile synthesis and nonlinear optical properties of push-pull 5, 15-diphenylporphyrins," The Journal of organic chemistry **63**, 7143 (1998).

146. T.-G. Zhang, Y. Zhao, I. Asselberghs, A. Persoons, K. Clays, and M. J. Therien, "Design, synthesis, linear, and nonlinear optical properties of conjugated (porphinato) zinc (II)-based donor-acceptor chromophores featuring nitrothiophenyl and nitrooligothiophenyl electron-accepting moieties," J. Am. Chem. Soc. **127**, 9710 (2005).

147. T. Verbiest, K. Clays, and V. Rodriguez, *Second-order nonlinear optical characterization techniques: an introduction* (CRC press, 2009).

148. T. Ishizuka, L. E. Sinks, K. Song, S.-T. Hung, A. Nayak, K. Clays, and M. J. Therien, "The roles of molecular structure and effective optical symmetry in evolving dipolar chromophoric building blocks to potent octopolar nonlinear optical chromophores," J. Am. Chem. Soc. **133**, 2884 (2011).

149. N. Jiang, G. r. Zuber, S. Keinan, A. Nayak, W. Yang, M. J. Therien, and D. N. Beratan, "Design of coupled porphyrin chromophores with unusually large hyperpolarizabilities," J. Phys. Chem. C **116**, 9724 (2012).

150. I. López-Duarte, J. E. Reeve, J. Pérez-Moreno, I. Boczarow, G. Depotter, J. Fleischhauer, K. Clays, and H. L. Anderson, ""Push-no-pull" porphyrins for second harmonic generation imaging," Chem. Sci. **4**, 2024 (2013).

151. M. G. Kuzyk, "Quantum limits of the hyper-Rayleigh scattering susceptibility," IEEE J. Sel. Top. Quant. Electron. **7**, 774 (2001).

152. D. L. Andrews, D. S. Bradshaw, and M. M. Coles, "Limitations and improvements upon the two-level approximation for molecular nonlinear optics," Proc. SPIE **7917**, 79171K (2011).

153. D. S. Bradshaw and D. L. Andrews, "Mechanisms of light energy harvesting in dendrimers and hyperbranched polymers," Polymers **3**, 2053 (2011).

154. J. Perez-Moreno, K. Clays, and M. G. Kuzyk, "Why do we need three levels to understand the molecular optical response?," Proc. SPIE **8113**, 81130L (2011).

155. M. G. Kuzyk, J. Pérez-Moreno, and S. Shafei, "Sum rules and scaling in nonlinear optics," Phys. Rep. **529**, 297 (2013).

156. S. Kielich and Z. Ożgo, "Reversal ratio of double-photon scattering by noncentro-symmetric molecules," Opt. Commun. **8**, 417 (1973).

157. D. L. Andrews and T. Thirunamachandran, "Polarization effects in nonlinear scattering," Opt. Commun. **22**, 312 (1977).

158. D. L. Andrews and W. A. Ghoul, "Polarization studies in multi-photon absorption-spectroscopy," J. Chem. Phys. **75**, 530 (1981).

159. Y. Zhang, X. Wang, D. Fu, J. Cheng, Y. Shen, J. Liu, and Z. Lu, "Second-order optical nonlinearity study of CdS nanoparticles via hyper-Rayleigh scattering," J. Phys. Chem. Solids **62**, 903 (2001).

160. D. A. Long and L. Stanton, "Studies of Nonlinear Phenomena. I. Theory of the Hyper Raman Effect," Proc. R. Soc. A **318**, 441 (1970).

161. D. B. Hollis, "Review of hyper-Rayleigh and second-harmonic scattering in minerals and other inorganic solids," Am. Mineral. **73**, 701 (1988).

162. G. Revillod, J. Duboisset, I. Russier-Antoine, E. Benichou, G. Bachelier, C. Jonin, and P.-F. Brevet, "Multipolar contributions to the second harmonic response from mixed DiA−SDS molecular aggregates," J. Phys. Chem. C **112**, 2716 (2008).

163. S. Roke and G. Gonella, "Nonlinear light scattering and spectroscopy of particles and droplets in liquids," Annu. Rev. Phys. Chem. **63**, 353 (2012).

164. M. M. Coles, M. D. Williams, and D. L. Andrews, "Second harmonic generation in isotropic media: six-wave mixing of optical vortices," Opt. Express **21**, 12783 (2013).

165. P. Allcock and D. L. Andrews, "Six-wave mixing: secular resonances in a higher-order mechanism for second-harmonic generation," J. Phys. B: At. Mol. Opt. Phys. **30**, 3731 (1997).

166. M. M. Coles, M. D. Williams, and D. L. Andrews, "Second harmonic generation in isotropic media: six-wave mixing of optical vortices: erratum," Opt. Express **22**, 17478 (2014).

167. K. D. Moll, D. Homoelle, A. L. Gaeta, and R. W. Boyd, "Conical Harmonic Generation in Isotropic Materials," Phys. Rev. Lett. **88**, 153901 (2002).

168. B. Sephton, A. Dudley, and A. Forbes, "Revealing the radial modes in vortex beams," Applied Optics **55**, 7830 (2016).

169. S. Christian, D. Angela, F. Daniel, D. Michael, and F. Andrew, "Measurement of the orbital angular momentum density of light by modal decomposition," New J. Phys. **15**, 073025 (2013).

170. E. Karimi, R. W. Boyd, P. de la Hoz, H. de Guise, J. Řeháček, Z. Hradil, A. Aiello, G. Leuchs, and L. L. Sánchez-Soto, "Radial quantum number of Laguerre-Gauss modes," Phys. Rev. A **89**, 063813 (2014).

171. W. N. Plick and M. Krenn, "Physical meaning of the radial index of Laguerre-Gauss beams," Phys. Rev. A **92**, 063841 (2015).

172. M. M. Coles, M. D. Williams, and D. L. Andrews, "Optical vortices in six-wave mixing," Proc. SPIE **8999**, 89990Y (2014).

173. S. Franke and S. M. Barnett, "Angular momentum in spontaneous emission," J. Phys. B: At. Mol. Opt. Phys. **29**, 2141 (1996).

174. H. H. Arnaut and G. A. Barbosa, "Orbital and intrinsic angular momentum of single photons and entangled pairs of photons generated by parametric down- conversion," Phys. Rev. Lett. **85**, 286 (2000).

175. S. Franke-Arnold, S. M. Barnett, E. Yao, J. Leach, J. Courtial, and M. Padgett, "Uncertainty principle for angular position and angular momentum," New J. Phys. **6**, 103 (2004).

176. G. Gibson, J. Courtial, M. Padgett, M. Vasnetsov, V. Pas'ko, S. Barnett, and S. Franke-Arnold, "Free-space information transfer using light beams carrying orbital angular momentum," Opt. Express **12**, 5448 (2004).

177. S. Franke-Arnold, S. M. Barnett, M. J. Padgett, and L. Allen, "Two-photon entanglement of orbital angular momentum states," Phys. Rev. A **65**, 033823 (2002).

178. J. Romero, D. Giovannini, S. Franke-Arnold, S. M. Barnett, and M. J. Padgett, "Increasing the dimension in high-dimensional two-photon orbital angular momentum entanglement," Phys. Rev. A **86**, 012334 (2012).

179. A. Mair, A. Vaziri, G. Weihs, and A. Zeilinger, "Entanglement of the orbital angular momentum states of photons," Nature **412**, 313 (2001).

180. M. Malik, M. Erhard, M. Huber, M. Krenn, R. Fickler, and A. Zeilinger, "Multi-photon entanglement in high dimensions," Nat. Photonics **10**, 248 (2016).

181. D. Shwa, E. Shtranvasser, Y. Shalibo, and N. Katz, "Controllable motion of optical vortex arrays using electromagnetically induced transparency," Opt. Express **20**, 24835 (2012).

182. K. S. Grigoriev, V. A. Makarov, and I. A. Perezhogin, "Formation of the lines of circular polarization in a second harmonic beam generated from the surface of an isotropic medium with nonlocal nonlinear response in the case of normal incidence," J. Opt. **18**, 014004 (2016).

183. N. Olivier, D. Débarre, P. Mahou, and E. Beaurepaire, "Third-harmonic generation microscopy with Bessel beams: a numerical study," Opt. Express **20**, 24886 (2012).

184. M. T. Cao, L. Han, R. F. Liu, H. Liu, D. Wei, P. Zhang, Y. Zhou, W. G. Guo, S. G. Zhang, H. Gao, and F. L. Li, "Deutsch's algorithm with topological charges of optical vortices via non-degenerate four-wave mixing," Opt. Express **20**, 24263 (2012).

185. M. N. O'Sullivan, M. Mirhosseini, M. Malik, and R. W. Boyd, "Near-perfect sorting of orbital angular momentum and angular position states of light," Opt. Express **20**, 24444 (2012).

186. M. Mirhosseini, M. Malik, Z. Shi, and R. Boyd, "Efficient separation of the orbital angular momentum eigenstates of light," Nat. Commun. **4**, 2781 (2013).

187. A. Forbes, A. Dudley, and M. McLaren, "Creation and detection of optical modes with spatial light modulators," Adv. Opt. Photon. **8**, 200 (2016).

188. M. M. Coles, M. D. Williams, K. Saadi, D. S. Bradshaw, and D. L. Andrews, "Chiral nanoemitter array: A launchpad for optical vortices," Laser & Photon. Rev. **7**, 1088 (2013).

189. M. D. Williams, M. M. Coles, K. Saadi, D. S. Bradshaw, and D. L. Andrews, "Optical vortex generation from molecular chromophore arrays," Phys. Rev. Lett. **111**, 153603 (2013).

190. M. D. Williams, M. M. Coles, D. S. Bradshaw, and D. L. Andrews, "Direct generation of optical vortices," Phys. Rev. A **89**, 033837 (2014).

191. D. L. Andrews, "Optical angular momentum: Multipole transitions and photonics," Phys. Rev. A **81**, 033825 (2010).

192. D. L. Andrews, "On the conveyance of angular momentum in electronic energy transfer," Phys. Chem. Chem. Phys. **12**, 7409 (2010).

193. J. S. Ford, D. S. Bradshaw, and D. L. Andrews, "Signatures of exciton coupling in paired nanoemitters," J. Phys. Chem. C **117**, 1293 (2013).

194. B. Bai, Y. Svirko, J. Turunen, and T. Vallius, "Optical activity in planar chiral metamaterials: Theoretical study," Phys. Rev. A **76**, 023811 (2007).

195. V. A. Fedotov, A. S. Schwanecke, N. I. Zheludev, V. V. Khardikov, and S. L. Prosvirnin, "Asymmetric transmission of light and enantiomerically sensitive plasmon resonance in planar chiral nanostructures," Nano Lett. **7**, 1996 (2007).

196. E. Plum, X. X. Liu, V. A. Fedotov, Y. Chen, D. P. Tsai, and N. I. Zheludev, "Metamaterials: Optical activity without chirality," Phys. Rev. Lett. **102**, 113902 (2009).

197. N. A. Abdulrahman, Z. Fan, T. Tonooka, S. M. Kelly, N. Gadegaard, E. Hendry, A. O. Govorov, and M. Kadodwala, "Induced chirality through electromagnetic coupling between chiral molecular layers and plasmonic nanostructures," Nano Lett. **12**, 977 (2012).

198. N. Shitrit, S. Maayani, D. Veksler, V. Kleiner, and E. Hasman, "Rashba-type plasmonic metasurface," Opt. Lett. **38**, 4358 (2013).

199. R. L. Carter, *Molecular Symmetry and Group Theory* (J. Wiley, New York, 1998).

200. L. Valkunas, D. Abramavicius, and T. Mancal, *Molecular excitation dynamics and relaxation: quantum theory and spectroscopy* (Wiley-VCH, Weinheim, 2013).

201. E. W. Weisstein, *CRC concise encyclopedia of mathematics* (Chapman & Hall/CRC, Boca Raton, 2003).

202. R. D. Jenkins and D. L. Andrews, "Multichromophore excitons and resonance energy transfer: Molecular quantum electrodynamics," J. Chem. Phys. **118**, 3470 (2003).

203. B. D. Gates, Q. B. Xu, M. Stewart, D. Ryan, C. G. Willson, and G. M. Whitesides, "New approaches to nanofabrication: Molding, printing, and other techniques," Chem. Rev. **105**, 1171 (2005).

204. J. V. Barth, G. Costantini, and K. Kern, "Engineering atomic and molecular nanostructures at surfaces," Nature **437**, 671 (2005).

205. J. Abramson, M. Palma, S. J. Wind, and J. Hone, "Quantum dot nanoarrays: Self-assembly with single-particle control and resolution," Adv. Mater. **24**, 2207 (2012).

206. A. Lundskog, C.-W. Hsu, K. Fredrik Karlsson, S. Amloy, D. Nilsson, U. Forsberg, P. Olof Holtz, and E. Janzen, "Direct generation of linearly polarized photon emission with designated orientations from site-controlled InGaN quantum dots," Light Sci. Appl. **3**, e139 (2014).

207. M. Knez, K. Nielsch, and L. Niinistö, "Synthesis and surface engineering of complex nanostructures by atomic layer deposition," Adv. Mater. **19**, 3425 (2007).

208. W. F. van Dorp and C. W. Hagen, "A critical literature review of focused electron beam induced deposition," J. Appl. Phys. **104**, 081301 (2008).

209. I. J. Hodgkinson, A. Lakhtakia, Q. H. Wu, L. De Silva, and M. W. McCall, "Ambichiral, equichiral and finely chiral layered structures," Opt. Commun. **239**, 353 (2004).

210. A. Papakostas, A. Potts, D. M. Bagnall, S. L. Prosvirnin, H. J. Coles, and N. I. Zheludev, "Optical manifestations of planar chirality," Phys. Rev. Lett. **90**, 107404 (2003).

211. E. Plum, J. Zhou, J. Dong, V. A. Fedotov, T. Koschny, C. M. Soukoulis, and N. I. Zheludev, "Metamaterial with negative index due to chirality," Phys. Rev. B **79**, 035407 (2009).

212. B. Terhalle, T. Richter, A. S. Desyatnikov, D. N. Neshev, W. Krolikowski, F. Kaiser, C. Denz, and Y. S. Kivshar, "Observation of Multivortex Solitons in Photonic Lattices," Phys. Rev. Lett. **101**, 013903 (2008).

213. B. Terhalle, T. Richter, K. J. H. Law, D. Göries, P. Rose, T. J. Alexander, P. G. Kevrekidis, A. S. Desyatnikov, W. Krolikowski, F. Kaiser, C. Denz, and Y. S. Kivshar, "Observation of double-charge discrete vortex solitons in hexagonal photonic lattices," Phys. Rev. A **79**, 043821 (2009).

214. F. Watt, A. A. Bettiol, J. A. Van Kan, E. J. Teo, and M. B. H. Breese, "Ion beam lithography and nanofabrication: A review," Int. J. Nanosci. **04**, 269 (2005).

215. L. J. Guo, "Nanoimprint lithography: Methods and material requirements," Adv. Mater. **19**, 495 (2007).

216. Z. Xie, W. Yu, T. Wang, H. Zhang, Y. Fu, H. Liu, F. Li, Z. Lu, and Q. Sun, "Plasmonic Nanolithography: A Review," Plasmonics **6**, 565 (2011).

217. J. Brunel, O. Mongin, A. Jutand, I. Ledoux, J. Zyss, and M. Blanchard-Desce, "Propeller-shaped octupolar molecules derived from triphenylbenzene for nonlinear optics: Synthesis and optical Studies," Chem. Mater. **15**, 4139 (2003).

218. C. Rouxel, C. Le Droumaguet, Y. Macé, S. Clift, O. Mongin, E. Magnier, and M. Blanchard-Desce, "Octupolar derivatives functionalized with superacceptor peripheral groups: Synthesis and evaluation of the electron-withdrawing ability of potent unusual groups," Chem. Eur. J. **18**, 12487 (2012).

219. D. L. Andrews, M. D. Williams, D. S. Bradshaw, R. Lui, D. B. Phillips, S. Franke-Arnold, and M. J. Padgett, "Nanoarrays for the generation of complex optical wave-forms," Proc. SPIE **9160**, 91601L (2014).

220. R. Liu, D. B. Phillips, F. Li, M. D. Williams, D. L. Andrews, and M. J. Padgett, "Discrete emitters as a source of orbital angular momentum," J. Opt. **17**, 045608 (2015).

221. B. G. C. G., M. P. Lavery, J. Courtial, M. W. Beijersbergen, and M. J. Padgett, "Efficient Sorting of Orbital Angular Momentum States of Light," Phys. Rev. Lett. **105**, 153601 (2010).

222. A.-P. Liu, X. Xiong, X.-F. Ren, Y.-J. Cai, G.-H. Rui, Q.-W. Zhan, G.-C. Guo, and G.-P. Guo, "Detecting orbital angular momentum through division-of-amplitude interference with a circular plasmonic lens," Sci. Rep. **3**, 2402 (2013).

223. A. Dudley, C. Schulze, I. Litvin, M. Duparré, and A. Forbes, "Quantitatively measuring the orbital angular momentum density of light," Proc. SPIE, 88100E (2013).

224. D. T. Pegg and S. M. Barnett, "Unitary phase operator in quantum mechanics," Europhys. Lett. **6**, 483 (1988).

225. S. M. Barnett and D. T. Pegg, "On the Hermitian optical phase operator," J. Mod. Opt. **36**, 7 (1989).

226. J. T. Barreiro, T.-C. Wei, and P. G. Kwiat, "Remote preparation of single-photon 'hybrid' entangled and vector-polarization states," Phys. Rev. Lett. **105**, 030407 (2010).

227. M. D. Williams, D. S. Bradshaw, and D. L. Andrews, "Quantum issues with structured light," Proc. SPIE **9764**, 976407 (2016).

228. H. Yu, M. Xu, Y. Zhao, Y. Wang, S. Han, H. Zhang, Z. Wang, and J. Wang, "Dual-wavelength laser with topological charge," AIP Advances **3**, 092129 (2013).